Dissertation
submitted to the
Combined Faculty of Mathematics, Engineering and Natural Sciences
of Heidelberg University, Germany
for the degree of
Doctor of Natural Sciences

Put forward by
Nils Hoyer
born in: Wuppertal, Germany
Oral examination: July 2nd, 2025

The Assembly of Nuclear Star Clusters

Referees: Dr. Nadine Neumayer
Prof. Dr. Michela Mapelli

Abstract

The evolution of galaxies represents a hitherto unsolved area of modern astrophysics. Various dynamical effects play an important role in shaping galaxy centres making them extremely interesting to study in detail. Nuclear star clusters are often a key element of galaxy centres and feature both diverse and complex formation histories as well as extremely high stellar densities. Many aspects of nuclear star cluster formation are still uncertain and require new constraints to make full use of their ability as ideal laboratories for studying galaxy evolution and the growth of massive black holes that are located in their centres. An improved knowledge of nuclear star cluster assembly is especially relevant today in order to properly interpret the vast amount of upcoming data produced with all-sky surveys. I present in this dissertation various analyses of high-resolution observational data sets from space-based missions ranging between the X-ray and mid-infrared regimes and a new computer simulation of the assembly of massive star cluster populations. The first analysis reveals tight correlations between the properties of nuclear star clusters and old globular star clusters in the Milky Way indicating a potential common formation mechanism of the two cluster types. In a second analysis I identify nuclear star clusters with variable accretion signatures from massive black holes within them and provide upper limits for lower-mass systems in case of non-detections. I demonstrate in a third project that analysing the spectral energy distribution of the nuclear star cluster in the nearby massive spiral galaxy Messier 74 constrains the assembly history of both the host galaxy and a potential massive black hole in the star cluster's centre. In addition to the projects that rely on observational data sets, I introduce a new simulation that is based on a dark matter-only computation and considers the co-formation of galaxies and massive star clusters. I show that my simulation can reproduce a number of observational quantities such as the mass function of young massive star clusters or the metallicity distribution of old globular clusters, both in nearby galaxies. I conclude by summarising the contents of this dissertation and by presenting future efforts that build on the presented observational and numerical approaches.

Zusammenfassung

Die Entwicklung von Galaxien stellt einen bislang ungelösten Teilbereich der modernen Astrophysik dar. Verschiedene dynamische Effekte beeinflussen die Entstehung von Galaxienzentren, was diese besonders interessant macht. Oftmals sind Kernsternhaufen ein Hauptelement von Galaxienzentren und zeichnen sich durch diverse und komplexe Entstehungsgeschichten und extrem hohe stellare Dichten aus. Viele Aspekte der Entstehung von Kernsternhaufen blieben bislang verborgen und wir benötigen neue Erkentnisse, damit man sie als ideale Umgebungen zur Eingrenzung von Galaxienentwicklungsmodellen und dem Wachsen von massereichen Schwarzen Löchern, welche sich in ihren Zentren befinden, nutzen kann. Das verbesserte Verständnis von der Entstehungsgeschichte von Kernsternhaufen ist zu diesem Zeitpunkt besonders relevant, um neue und umfangreiche Datensätze, die mit Hilfe von flächendeckenden Himmelsvermessungen gewonnen werden, korrekt interpretieren zu können. In dieser Dissertation präsentiere ich verschiedene Analysen von Beobachtungsdaten, die Daten aus dem Wellenlängenbereich zwischen dem Röntgen- und mittleren Infrarotbereich nutzen und von hochauflösenden Weltraumteleskopen aufgenommen wurden, sowie eine neue Computersimulation, welche die Entstehung von Populationen von massereichen Sternhaufen betrachtet. Die erste Analyse enthüllt eine enge Verbindung zwischen den Eigenschaften von Kernsternhaufen und alten Kugelsternhaufen der Michstraße und lässt einen vergleichbaren Entstehungsprozess zwischen beiden Sternhaufentypen vermuten. In einer zweiten Analyse nutze ich Röntgendaten und identifiziere Kernsternhaufen, die variable Akkretionssignale von massereichen Schwarzen Löchern aufweisen und präsentiere maximale Akkretionsflüsse für andere Systeme in masseärmeren Galaxien. In einem dritten Projekt demonstriere ich, dass sich durch die Analyse einer spektralen Energieverteilung eines Kernsternhaufens in der nahegelegenden massereichen Spiralgalaxie Messier 74 die Entwicklungsgeschichte der Galaxie, sowie eines potentiell vorhandenen massereichen Schwarzen Lochs, eingrenzen lässt. Zusätzlich zu den verschiedenen Analysen der Beobachtungsdaten führe ich ein neues Modell von Galaxienentstehung ein, welches, basierend auf einer Berechnung der Verteilung von dunkler Materie, analytische Gleichungen nutzt, um die Entstehung von Galaxien und massereichen Sternhaufen zu simulieren. Ich zeige, dass mein Modell bereits in der Lage ist die Eigenschaften von Kernsternhaufen in benachbarten Galaxien, wie zum Beispiel die Massefunktion von jungen Sternhaufen oder die durchschnittliche Verteilung der Metallizitäten von alten Kugelsternhaufen als Funktion der Galaxienmasse zu erklären. Der Abschluß dieser Dissertation beinhaltet eine Zusammenfassung der eingeführten Arbeiten und gibt einen Ausblick auf zukünftige Projekte, die durch neue Beobachtungsdaten und numerische Ansätze erkundet werden können.

Contents

List of Figures

List of Tables

Acknowledgments

I am fortunate enough to say that many dear friends and colleagues supported me throughout this incredible journey. My accomplishments would have been impossible without you.

I sincerely thank my two advisors Silvia Bonoli and Nadine Neumayer. You have been two wonderful colleagues and guiding figures throughout the last couple of years and gave me the chance to pursue my doctoral studies when others doubted my abilities. I'm very much grateful for your openness to new project ideas that enabled me to tackle interesting problems. Furthermore, thank you for introducing me to many excellent scientists and for providing me the opportunity to attend many conferences, visit other countries and continents, and work with you and your research teams. I thoroughly enjoyed spending time with you.

Next I want to highlight the importance of my various conversations with Nate Bastian, Thorsten Böker, and Anil Seth. You provided critical feedback for my research projects and scientific practice that enabled the success of all projects. Thank you for all the "behind-the-scenes" information and honesty about academic research.

In addition to the above people, I acknowledge the helpful advice provided by Wolfgang Brandtner, Tom Herbst, Ralf Klessen, Ralf Lauenhardt, and Annalisa Pillepich during our thesis and PhD advisory committee meetings. Your guidance and feedback for my research ideas and long-term survival in academia were quite helpful to me. I really appreciate the time and effort you invested into these meetings.

I want to thank Michela Mapelli and Nadine Neumayer for agreeing to referee this dissertation as well as Luca Amendola and Eva Grebel for making room in their busy schedules to join my PhD examination committee later this year.

It was a great pleasure to work with the members of the Galactic Nuclei group in Heidelberg and the Galaxy Evolution group in Donostia. Your support, engaging conversations, and overall incredible working atmosphere significantly contributed to my ability to perform this research. I thoroughly enjoyed spending time with you, both in- and outside the institutes.

Finally, I need to thank my family and friends for their continued support in my endeavours. I allocate a lot of time to research and study, and I know that you respect this choice, which is not to be taken for granted. Thank you for giving me the possibility to develop my interest in academic research and sharing my results with you.

I acknowledge support from the International Max Planck Research School for Astronomy and Cosmic Physics at the University of Heidelberg (IMPRS-HD). I thank the Latin-American Chinese European Galaxy Formation Network LACEGAL via the European Union's HORIZON-MSCA-2021-SE-01 Research and Innovation programme under the Marie Sklodowska-Curie grant agreement number 101 086 388 for giving me the opportunity to travel to Chile.

Chapter 1

Introduction

A principal astrophysical research line revolves around how baryons assemble within dark matter halos to eventually form the magnificent galaxies that we observe today. This process of galaxy assembly involves a large range of energy-, time-, and physical scales, which makes galaxies extremely complex objects. Galaxies are a result of the combined action of a plethora of astrophysical phenomena that work simultaneously, which makes it difficult to distinguish between the different processes and understand galaxy formation as a whole. This complexity is directly revealed by, for example, the occurrence of warps, triaxial components, halos with shell-like structures, clumps, tidal tails, other (arbitrary) irregularities, and many galaxy constituents such as bars, bulges, disks, or rings, both in nearby and distant galaxies.

One noteworthy galaxy constituent are massive star clusters, self-gravitating spheres that contain more than a million individual stars, and have long survival times. By analysing the properties of their stars, their internal kinematics, their trajectories within their host galaxy, and their abundance, one can directly probe the properties of the host galaxy itself, both today and at the time when these star clusters formed, which is typically many billion years ago. This makes star clusters a suitable tracer for galaxy evolution.

A special type of a massive star cluster is located in galaxy centres. These objects are referred to as "nuclear star clusters" and frequently interact with their environment, accrete cold molecular gas that forms stars within them, merge with other star clusters that either formed in their proximity or migrated towards the galaxy's centre, and interact with massive black holes that are located within them. These processes are believed to be absent for any other type of star cluster, making nuclear star clusters unique and an interesting laboratory to study many astrophysical processes.

In order to use nuclear star clusters as probes of galaxy evolution it is essential to understand how they relate to other types of star clusters and how they co-evolve with massive black holes (or not). Many of these issues remain not fully constrained and new results on nuclear star cluster evolution are necessary in light of the large increase in observational data from large-scale surveys and big telescopes. For example, we find high-redshift galaxies with many star clusters that contain a significant fraction of the galaxy's mass within a small volume and directly affect how the galaxy evolves until today. Upcoming all-sky surveys will rapidly increase the number of transient events, such as the tidal disruption of stars by a black hole or gravitational wave mergers from (stellar mass) black holes. Both a high fraction of stars bound in star clusters and the tidal disruption of stars by massive black holes benefit from dense environments, and nuclear star clusters exhibit the highest stellar densities observed. Therefore, it is important to address open questions around nuclear star cluster assembly as soon as possible.

The goal of this dissertation is to advance our knowledge of nuclear star cluster assembly across a large galaxy mass range. I will demonstrate that high-resolution imaging data across a large wavelength range is important for this goal and present a new semi-analytical galaxy formation model for the build-up of star cluster populations that may contribute to the build-up of a nuclear star cluster.

Chapter 2

Nuclear Star Clusters

Some of the earliest work that specifically focussed on galaxy centres was conducted many decades ago but did not detect any separate components from extended galaxy bulges that have been known for a few centuries. The first detections of distinct nuclear components stem from Becklin and Neugebauer (1968) for the Milky Way and Light et al. (1974) for Messier 31, the most massive galaxy in the Local Group. After these initial discoveries it was found that other nearby galaxies contain such a separate nucleus as well, both in nearby massive (e.g. Gallagher et al., 1982; Nieto & Auriere, 1982; O'Connell, 1983; Kormendy, 1985; Lauer, 1985) and lower-mass dwarf galaxies in the Virgo galaxy cluster (e.g. Caldwell, 1983; Reaves, 1983; Binggeli et al., 1985). It took another few years until the term "nuclear star cluster" (NSC hereafter) was first used (Kormendy & Djorgovski, 1989), which is the common reference for the "separate nucleus" in modern-day astronomy.

Definitions of NSCs face the same challenges as for globular clusters (GCs hereafter) in that their properties overlap with other systems (Renaud, 2018). For example, some NSCs clearly show similar star formation histories as GCs (such as KKs 58; Fahrion et al., 2020b) and others are located at up to 10 % for the host galaxy's half-light radius (e.g. Poulain et al., 2021). This issue directly reveals an important question: *what differentiates NSCs from GCs?* While there exist different definitions in the literature, in this dissertation I classify a star cluster that formed within the galaxy as an NSC if one of three conditions is met:

1. the star cluster experienced at least one merger event with another massive star cluster, or
2. the star cluster contains multiple stellar populations of different metallicity *and* age, or
3. the star cluster formed in the kinematic centre of its host galaxy and has a long survival time.

The next sections outline the basic properties of NSCs and how they relate to other systems, such as GCs, nuclear disks, or massive black holes within a galaxy. We will raise different questions about NSC assembly whose answers are important for galaxy evolution as a whole and may assist in solving related issues to the seeding and growth mechanisms of massive black holes, tidal disruptions of stars, or gravitational wave events. Current and future facilities will investigate and constrain these phenomena, thus, motivating my detailed investigation of galaxy centres.

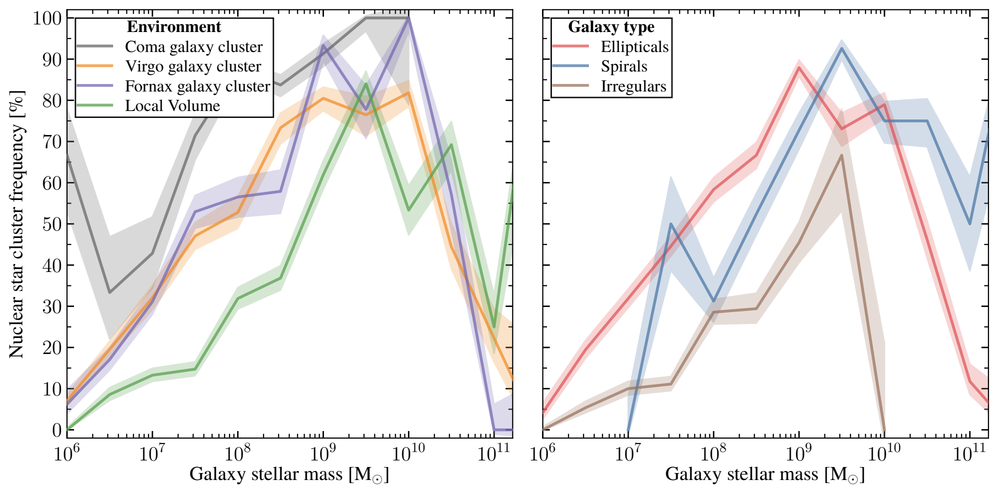

Figure 2.1. Nuclear star cluster frequency (or "occupation fraction") as a function of host galaxy stellar mass. Coloured lines in the *left panel* separate galaxies within different environments with the Local Volume (distance $\lesssim 11$ Mpc) being the least- and the Coma galaxy cluster the most dense surrounding. The *right panel* separates galaxies by their morphological Hubble T-type where ellipticals have $T \leq 0$, spirals $0 < T \leq 8$, and irregulars $T > 8$. The shaded regions give the 1-σ uncertainty. The data are taken from Hoyer et al. (2021).

2.1 Properties

2.1.1 Frequency

NSCs are basically ubiquitous objects in galaxies of different types and masses. They have already been detected in dwarf ellipticals (e.g. Binggeli et al., 1987) and irregulars (e.g. Georgiev et al., 2009a), massive ellipticals (e.g. Côté et al., 2006) and spirals (e.g. Carollo et al., 2002), and ultra-diffuse galaxies (e.g. Lambert et al., 2024; Khim et al., 2025). NSCs occupy some of the least massive galaxies, such as Eridanus 2 with a stellar mass of $M_\star \approx 10^5\,\mathrm{M}_\odot$ (Contenta et al., 2018) to some of the most massive galaxies such as IC 2006 with $M_\star \approx 3 \times 10^{10}\,\mathrm{M}_\odot$ (Turner et al., 2012). Despite their presence at all mass- and morphological type scales, the NSC frequency depends on several global quantities.

Figure 2.1 shows the NSC frequency (or "occupation fraction") as a function of host galaxy stellar mass, separated by galaxy environment and morphological type. In galaxies up to a few times $10^9\,\mathrm{M}_\odot$ the frequency increases up to a maximum of approximately 80 % before declining for the most massive objects. The initial increase in the dwarf galaxy regime shows a secondary dependency in that elliptical galaxies in dense environments host NSCs more frequently than their irregular counterparts in galaxy voids. The dependence on environment has mostly been attributed to a difference in both the frequency (Sánchez-Janssen et al., 2019a) and number (Carlsten et al., 2022) of GCs. This argument was used to explain the discrepancy between elliptical and irregular galaxies of the same stellar mass as the former has a higher GC specific frequency (a quantity for "GC richness") than the latter (Jordán et al., 2007a; Miller & Lotz, 2007; Peng et al., 2008).

Assessing the NSC frequency in disk-dominated and irregular galaxies is influenced by the presence of dust and star forming regions. These features often make it challenging to both detect the NSC and to identify the location of the galaxy centre. Additionally, while NSCs in more massive galaxies often reside in or close to the kinematic centre of their host galaxy (Böker et al., 2002; Neumayer et al., 2011), this is not necessarily the case for dwarf galaxies where NSCs can be located outside the photometric centre by up to 10 % of the half-mass radius (Poulain et al., 2021; Khim et al., 2024). This offset is also present in irregular dwarf galaxies (Fahrion et al., 2022a) and further complicates detection. Furthermore, dense bulges in more massive ellipticals can make a photometric detection of NSCs challenging, especially in distant galaxies and lower-resolution imaging data. Therefore, the presented NSC frequencies in Figure 2.1 mark lower limits.

At the massive galaxy end the NSC frequency decreases and is independent of galaxy environment. One commonly referred to explanation is that these galaxies previously contained NSCs that were eventually destroyed during a galaxy merger. During this process the two NSCs would migrate towards each other due to dynamical friction, a process that can be seen in NGC 7727 (Voggel et al., 2022), until they come into contact with each other. Afterwards, during the coalescence of the two star clusters the two massive black holes at their centres continue to sink towards each other, injecting energy into surrounding stars and heating the clusters. This may eventually result in the destruction of the cluster and lead the two black holes to enter the gravitational wave regime at sub-parsec scales (e.g. Quinlan & Hernquist, 1997; Milosavljević & Merritt, 2001; Merritt et al., 2007; Sesana et al., 2008; Bekki & Graham, 2010).

Notice that the decline in NSC frequency is not as clear for massive spiral galaxies. Instead of a rapid decline the occupation fraction shows a slower decline and may even remain constant (Ashok et al., 2023). This observation could corroborate the theory that mergers of massive black holes predominantly destroy NSCs in elliptical galaxies, as outlined above. It remains unclear, however, why the NSC occupation fraction does not reach 100 % if major galaxy mergers are absent: *which physical mechanisms prevent NSCs to assemble?*

2.1.2 Masses and Sizes

Early studies with the *Hubble Space Telescope* already revealed that NSCs feature a variety of luminosities (or masses) and half-light radii (e.g. Carollo et al., 1998; Böker et al., 2002): while some fraction of these objects have similar sizes to typical GCs (approximately 3 pc) others are more massive and extended. By now many more NSCs were studied with high-resolution imaging data, leading to the compiled data sets presented in Figure 2.2. Typical NSCs have masses of the order of $10^6\,\mathrm{M}_\odot$ and half-light radii of a few parsec, i.e. they are more massive but similarly sized as GCs. However, some of the lowest-mass NSCs compare well to typical GC masses suggesting a potential common origin and evolution of both star cluster types.

There are two factors that separate NSCs from GCs in the size-mass plane: (1) The most massive NSCs are up to two orders of magnitude more massive than the most massive (old) GCs, and (2) there exists a positive relationship between the half-light radius and mass of NSCs that is absent in the presented GC sample.

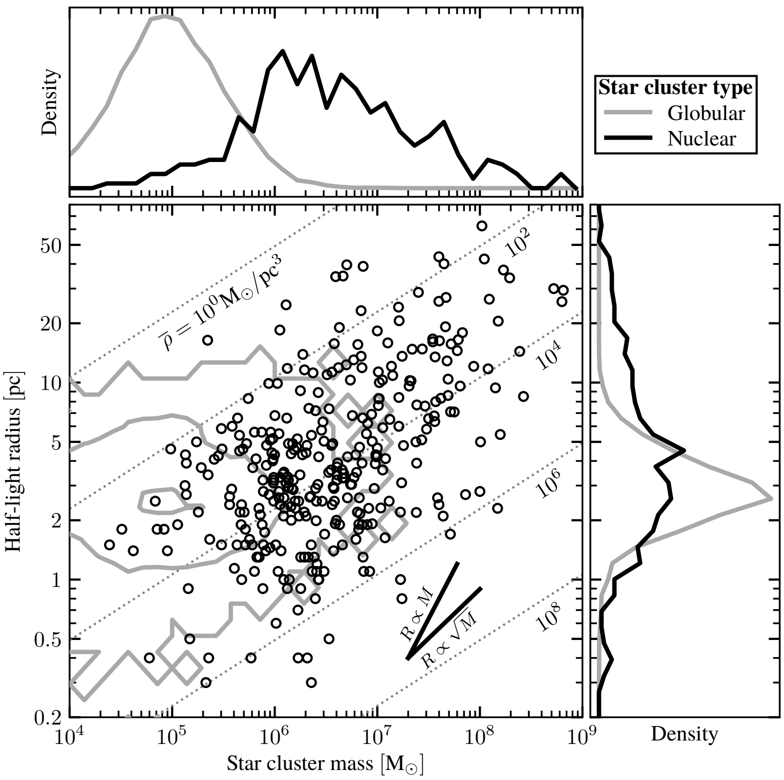

Figure 2.2. Distribution of half-light radii and masses of nuclear (black; various galaxy environments) and globular star clusters (gray; 1-, 2-, and 3-σ contours; Virgo galaxy cluster). Dotted lines give the average density within the half-mass radius. The data for nuclear star clusters are compiled from Côté et al. (2006), Georgiev et al. (2009a), Georgiev and Böker (2014), Georgiev et al. (2016), Spengler et al. (2017), Pechetti et al. (2020), and Ashok et al. (2023). The data for globular clusters come from the *ACSVCS* survey (https://www.acsvcs.org; Côté et al., 2004; Jordán et al., 2005; Peng et al., 2006).

The first observation indicates that the most massive NSCs do not assemble in similar ways compared to GCs but receive additional mass contributions. As we discuss in Section 2.2, an NSC may grow through star formation *in-situ* and via merging star clusters. The contribution of both processes may be required at least for the most massive NSCs as they exceed the upper mass limit for star cluster formation (of the order of 10^8 M$_\odot$; Norris et al., 2019).

The positive correlation between half-light radius and mass has been observed in young massive clusters (e.g. Bastian et al., 2012; Ryon et al., 2015) and, thus, may be related to their birth environments. Giant molecular clouds in the Milky Way, that may eventually form star clusters, show roughly constant surface densities (i.e. $R \propto \sqrt{M}$; Larson, 1981) and may contribute to the positive correlation. For NSCs, however, the data indicate a more complex behaviour than both a constant density or constant surface mass, potentially as high as $R \propto M$, but clearly with significant scatter at all mass scales.

Other factors that play a role in setting the relationship between the half-light radius and mass include the NSC's assembly history. On the one hand, if an NSC and a migrating GC have similar mass one expects $R \propto \sqrt{M}$ after a single merger whereas $R \propto M$ in the limit of many GC mergers (Antonini et al., 2012). On the other hand, *in-situ* star formation can occur in the centre of the NSC (e.g. Hannah et al., 2021), thus increasing its central density and mass but not necessarily the half-mass radius. If the star formation occurs outside the NSC's centre the observed half-mass radius may increase. Both effects become visible in UV- and optical filterbands where the half-light radius and axis ratio of the NSC changes with wavelength (e.g. Carson et al., 2015) and viewing angle (Seth et al., 2008a).

The NSC mass also increases as a function of host galaxy mass, which I show in Figure 2.3. The scaling relation is not constant across the whole mass range and displays a transition region around $M_\star \approx 10^{9.5}\,\mathrm{M}_\odot$ where the relationship becomes steeper. A simple linear regression to galaxies below this mass threshold yields

$$\log_{10}(M_{\mathrm{NSC}}/\mathrm{M}_\odot) = 0.54 \times \log_{10}(M_\star/10^9\,\mathrm{M}_\odot) + 6.55\ . \tag{2.1}$$

NSCs in more massive galaxies have typical masses above this relationship, which indicates either an additional mass-contributing factor or a more efficient build-up of the cluster. We discuss this observation again in Section 2.2.

Notice that the slope of the correlation is below unity, i.e. NSCs loose importance for the mass budget of galaxies with increasing stellar mass. Therefore, it is important to study the assembly of NSCs especially in dwarf galaxies to better understand dwarf galaxy assembly itself. However, the (structural) properties of NSCs in this mass regime are still relatively unexplored (*c.f.* Figure 2.2).

2.1.3 Stellar Populations

Many NSCs assemble in a complex way and contain multiple stellar populations with different metallicities, ages, and kinematics. This is fundamentally different from GCs that contain multiple stellar populations of the same age and comparable metallicities and kinematics (but with other element variations; see Bastian & Lardo, 2018, and references therein). For example, M 54, the NSC of the Sagittarius dwarf galaxy that is currently in a merger process with the Milky Way, contains distinct stellar populations with metallicities and ages differing by ≈ 2 dex and ≈ 12 Gyr, respectively (Alfaro-Cuello et al., 2019).

I show examples of estimates for the metallicity and age of the main stellar population of NSCs as well as three examples for NSC star formation histories in Figure 2.4. While most NSCs have dominant stellar populations with $\tau \approx 10$ Gyr there exist other systems with significantly younger ages, going down to $\tau \approx 100$ Myr. Similarly, the spread in metallicity extends from $[\mathrm{M/H}] \approx -2.5$ to 0.5, thus, NSCs show a great diversity in their dominant stellar populations.

There exists a secondary dependence on galaxy stellar mass (and, thus, NSC mass as per Figure 2.3) in that NSCs in more massive galaxies have higher metallicity values. At these high metallicity values the age spread is larger than for NSCs in lower-mass galaxies. This mass dependence indicates that self-enrichment might play an important role in NSC formation and that this process already occurs at the earliest stages of galaxy formation.

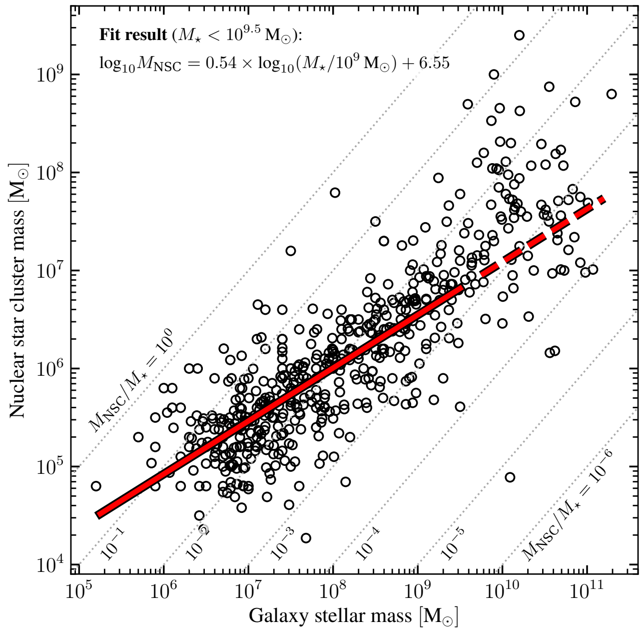

Figure 2.3. Nuclear star cluster versus host galaxy stellar mass. The correlation below a galaxy stellar mass of $10^{9.5}$ M$_\odot$ is described well by a linear relationship, as indicated in the top left corner. The data represent galaxies in a variety of environments and were collected from Georgiev et al. (2016), Spengler et al. (2017), Eigenthaler et al. (2018), Ordenes-Briceño et al. (2018), Sánchez-Janssen et al. (2019a), Pechetti et al. (2020), Carlsten et al. (2022), Ashok et al. (2023), and Khim et al. (2024).

Another observation is that some "uncertainties" of individual data points are larger than for others. The magnitudes of the error bars do not reflect statistical but systematic uncertainties from the modelling procedure. All spectra were fit with single stellar populations, thus, a larger uncertainty correlates with a more prominent subpopulation. This is exemplified for NGC 247, 3621, and 5102 in the right panel of Figure 2.4 where their star formation histories vary greatly but their (mass-weighted) age estimates do not.

Another evidence for the presence of multiple stellar populations in NSCs come from kinematic analyses. As mentioned in the previous subsection, structural changes in NSCs appear at different wavelength ranges. Such changes are captured by kinematic analysis and reveal a great variety in rotation signatures (e.g. Seth et al., 2008a; Seth et al., 2010; Lyubenova et al., 2013; Nguyen et al., 2018; Lyubenova & Tsatsi, 2019; Pinna et al., 2021). In some cases the overall rotation of the NSC can also be off-axis compared to the host galaxy's rotation axis, indicative of an *ex-situ* origin from a galaxy merger (Fahrion et al., 2019).

Detailed analyses of individual NSCs reveal differential rotation of stellar populations. For example, the old and young stellar populations of M 54 show unequal rates of rotation, which indicates separate formation mechanisms (Alfaro-Cuello et al., 2020). Such complexity is present in the Milky Way's NSC as well with a rotating substructure perpendicular to the Galactic plane (Feldmeier et al., 2014).

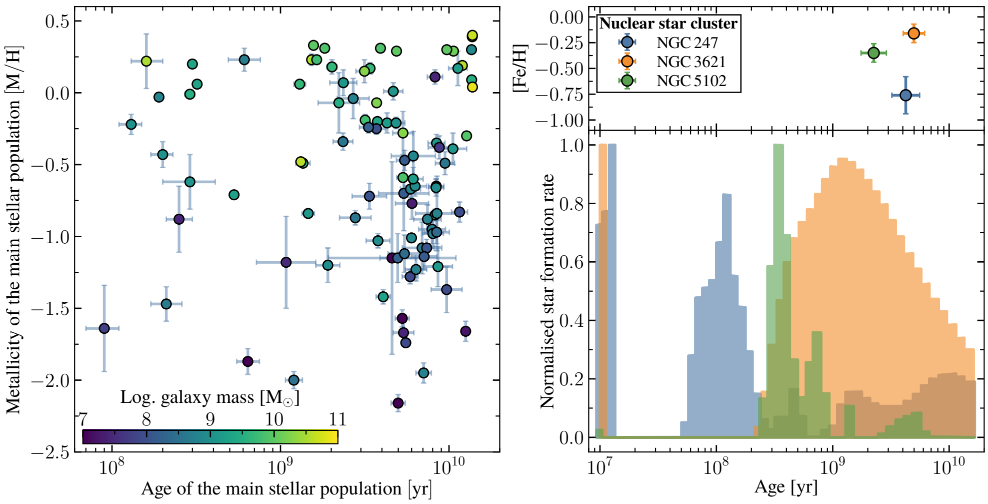

Figure 2.4. *Left panel: Light*-weighted metallicity of the main stellar population of a nuclear star cluster versus its *light*-weighted age, colour-coded by the host galaxy's stellar mass. The data are taken from Lyu et al. (2025). *Right panel:* Normalised star formation rate versus age of nuclear star clusters in NGC 247, 3621, and 5102. The top panel provides the *mass*-weighted estimates of the iron-abundance and age. The data are taken from Kacharov et al. (2018).

Overall, the presence of a wide metallicity and age distributions as well as kinematic signatures of different stellar populations show that NSCs have a complex and variable formation history. It is unclear if this complexity (e.g. the presence of individual stellar populations) directly reflects galaxy-wide events, such as galaxy mergers or disk instabilities, or whether most of the NSC's evolution is distinct from large-scale galaxy dynamics.

2.2 Formation Scenarios

All of the above mentioned properties point towards a complex formation history of most NSCs. A majority of approaches that try to explain the assembly of NSCs can be separated into two categories: accreted GCs (*c.f.* Section 2.2.1) and star formation in galaxy centres (*c.f.* Section 2.2.2).

Note that the different formation scenarios are *not* mutually exclusive. Instead, it is believed that both GC migration and central star formation contributes to NSCs at basically all galaxy mass scales, although perhaps in different relative amounts. We will discuss this point towards the end of this section.

2.2.1 *Ex-situ* Origin

The idea that a GC migrates towards a galaxy centre where it would transition to an NSC was born shortly after the discovery of distinct nuclear components in nearby galaxies (Tremaine et al., 1975). This scenario assumes that massive star clusters form in the galaxy's disk at larger radii of typically a few kpc and migrate towards the centre due to an exchange of energy with nearby individual bodies (stars and dark matter particles) as well as gas, i.e. via dynamical friction. The star clusters loose mass during their in-spiral, which is why only the most massive objects would not disrupt, thus, potentially explaining why NSCs are often the most massive star cluster in a galaxy (see e.g. Figure 2 in Neumayer et al., 2020).

Observational evidence suggests that this formation scenario is important and may dominate in the dwarf galaxy regime, i.e. at galaxy stellar masses below $M_\star \lesssim 10^9\,\mathrm{M}_\odot$. For example, some galaxies show a deficit of GCs in their inner regions (e.g. Lotz et al., 2001; Capuzzo-Dolcetta & Mastrobuono-Battisti, 2009) suggesting that they migrated inwards and merged with each other. Other systems like UGC 7346 feature multiple centrally-concentrated GCs that will likely merge with each other, resulting both in the formation of an NSC and a lack of massive GCs in the galaxy's central region (Román et al., 2023). While these authors argue for dwarf galaxy mergers, Poulain et al. (2021) do not detect any "shell"-like features, which could then suggest (1) a biased formation of massive GCs in galaxy centres, or (2) a stalling of migrating GCs due to too shallow slopes of the underlying density distribution. More examples of multiple centrally concentrated star clusters are presented in Georgiev and Böker (2014), Pak et al. (2016), and Euclid Collaboration (2024a) but the cause of this concentration of GCs is unclear. Finally, most recently Poulain et al. (2025) disovered multiple NSCs that feature tidal tails, which is indicative of recent star cluster mergers.

Some NSCs feature similar metallicities and ages compared to typical GCs (see Section 2.1.3 and Fahrion et al., 2020b) and the presence of more metal-rich stars in their direct surrounding (within the galactic body) indicate that the NSCs formed outside the centre (Fahrion et al., 2021). From a statistical perspective, there exists a tight correlation between the fraction of galaxies that host at least one GC and an NSC (Sánchez-Janssen et al., 2019a; Carlsten et al., 2022). This demonstrates a tight link between the two types of star clusters.

The dynamical friction-driven merger scenario of GCs has received great attention in numerical studies as well, suggesting that massive GCs reach a galaxy's centre within a Hubble time (e.g. Capuzzo-Dolcetta, 1993; Oh & Lin, 2000; Agarwal & Milosavljević, 2011; Neumayer et al., 2011; Antonini et al., 2012; Arca Sedda & Capuzzo-Dolcetta, 2014; Gnedin et al., 2014; Abbate et al., 2018; Arca Sedda et al., 2020; Leaman & van de Ven, 2022; Leveque et al., 2022). By using N-body similations, Hartmann et al. (2011) argue that NSCs, which result from repeated GC mergers, exhibit a large variety of structural properties, including masses, sizes, and rotation signatures that result in a flattening of the light profiles (see also Tsatsi et al., 2017). As mentioned previously (*c.f.* Section 2.1.3), such signatures are observed in NSCs, including the Milky Way's NSC (Feldmeier et al., 2014; Feldmeier-Krause et al., 2017b).

Other works also consider the γ-ray excess in galaxy centres. As argued by Gao et al. (2024), migrating GCs will merge with the NSC (or get tidally disrupted) and place millisecond pulsars in the galaxy centre region. This process may then account for observational constraints for the galaxy centres of the Milky Way (Abazajian et al., 2014) and M 31 (Ackermann et al., 2017) when considering up to 100 GC merger events (see also Arca Sedda et al., 2018; Fragione et al., 2018).

In summary, a great number of numerical works and observational studies support the GC merger-driven scenario for the build-up of NSCs.

2.2.2 *In-situ* Origin

One of the strongest arguments in favour of *in-situ* star formation is the presence of young ($\tau \lesssim 100\,\mathrm{Myr}$) stellar populations within NSCs. These populations have been detected in massive galaxies (e.g. Loose et al., 1982; Rossa et al., 2006; Seth et al., 2006; Walcher et al., 2006; Kacharov et al., 2018), including ellipticals (e.g. Nguyen et al., 2017, 2019). More recent studies reveal that *in-situ* star formation contributes to the mass budget of NSCs in dwarf irregulars (Fahrion et al., 2022a; Lyu et al., 2025) and sometimes ellipticals (Paudel & Yoon, 2020) as well. As mentioned previously, young populations are often detected in the centres of NSCs resulting in a more centrally concentrated light emission in far-ultraviolet bands (Bender et al., 2005; Georgiev & Böker, 2014; Carson et al., 2015; Hannah et al., 2021), including the Milky Way's NSC (Paumard et al., 2006; Feldmeier-Krause et al., 2015; Chen et al., 2023). This shows that, overall, *in-situ* star formation is an important contributor to the build-up of NSCs, potentially at all galaxy masses.

Using a hydrodynamical simulation, Guillard et al. (2016) discuss a hybrid scenario where a star cluster that still retained some cold gas from its birth environment merges with an NSC. The competing time scales of gas expulsion and migration require that these young star clusters form in the NSC's vicinity, diffusing the picture between *in-situ* formation and an *ex-situ* origin. Observations indicate that this scenario may still be at play in forming NSCs today. The nearby dwarf galaxy Henize 2-10 shows signs for centrally concentrated massive star clusters (Johnson et al., 2000; Cresci et al., 2010, 2017; Costa et al., 2021) that will merge with each other to form a yet absent NSC (Nguyen et al., 2014; Arca-Sedda et al., 2015). More recently, Fahrion et al. (2024) finds two young clusters in the vicinity of the NSC in NGC 4654 that may merge with and contribute to the NSCs mass.

Cold gas in galaxy centres is required for central star formation to occur. Various mechanisms have been proposed to fuel a galaxy's centre with new cold gas, including angular momentum-loss due to non-axisymmetric potentials like bars (Shlosman et al., 1990), dynamical friction of star forming clumps (Bekki et al., 2006; Bekki, 2007), supernovae-driven turbulence (Sormani et al., 2020; Tress et al., 2020), rotational instabilities within a disk (Milosavljević, 2004), tidal compression in shallow density profiles (Emsellem & van de Ven, 2008), and galaxy-merger induced in-spiral (Mihos & Hernquist, 1994; Gray et al., 2024). The relative importance of the different fuelling channels is unclear and numerical experiments that probe simultaneously the different channels are challenging because of the multi-scale structure of the problem (but see van Donkelaar et al., 2024, for a recent zoom-in simulation). Individual studies already investigated gas in-flows (Hopkins & Quataert, 2010), self-regulation (McLaughlin et al., 2006), or two-body relaxation (Aharon & Perets, 2015) but an emerging picture is still missing.

The currently most-promising approach is to use semi-analytical models. Antonini et al. (2015) simulate the co-formation of galaxies, massive black holes, and NSCs based on dark matter-only merger trees and find that *in-situ* star formation plays an important role in NSC assembly, especially in massive galaxies. In a similar vein, Leaman and van de Ven (2022) consider GCs in an elliptical host galaxy and determine the mass fraction of in-spiralling GCs that contribute to the build-up of an NSC. In

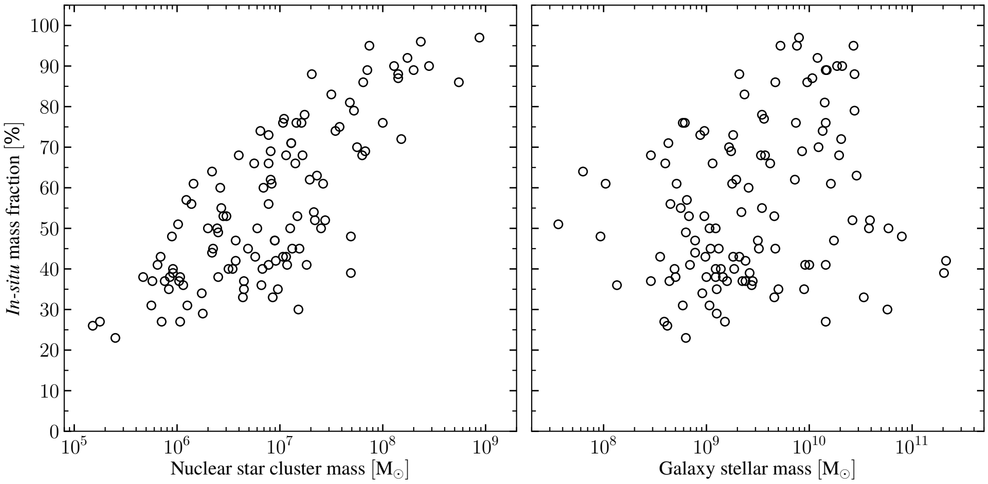

Figure 2.5. Estimated fraction of mass that formed *in-situ* versus nuclear star cluster (*left*) and host galaxy stellar mass (*right panel*). The determination of the *in-situ* fraction is based on the expected mass contribution from migrating globular clusters (Leaman & van de Ven, 2022). The data are taken from Fahrion et al. (2022b).

turn, the residual mass between the expected value from the NSC to host galaxy stellar mass relationship (*c.f.* Figure 2.3) and the merger-driven scenario should form *in-situ*.

The latter model by Leaman and van de Ven (2022) was applied to a compilation of nearby galaxies to determine the *in-situ* fraction as a function of NSC and host galaxy mass (Fahrion et al., 2022b). As I show in Figure 2.5, the *in-situ* fraction positively correlates with NSC mass increasing from $f_{in-situ} \approx 20\,\%$ at $M_{\rm NSC} \approx 10^5\,\mathrm{M}_\odot$ to $f_{in-situ} \approx 100\,\%$ at $M_{\rm NSC} \approx 10^9\,\mathrm{M}_\odot$. At a given NSC mass the scatter in the correlation can be quite significant, except for the lowest- and highest-mass NSCs, which is a result of both the set-up of the theoretical model and the variety in galaxy systems. Given the scaling relation between NSC and host galaxy stellar mass it is somewhat surprising to find that the correlation between *in-situ* fraction and host galaxy stellar mass disappears. This issue is likely related to the model assumptions of an isolated elliptical galaxy where both secular and galaxy-merger driven gas migration are missing.

Overall, both *in-situ* star formation and migrating star clusters contribute to the present-day properties of NSCs. While many specific details about e.g. the dominant process for gas migration or the total number of GC mergers remain elusive, observations indicate that the relative contributions significantly vary with mass and that *in-situ* star formation becomes more important in massive NSCs.

2.3 Relation to Other Systems

2.3.1 Nuclear Disks

Nuclear stellar disks (NSDs) are disk-like structures with typical scale-lengths of $\lesssim 200\,\mathrm{pc}$ and occupy some galaxy centres, including the Milky Way (e.g. Launhardt et al., 2002; Schödel et al., 2014a). One may expect them to be related to NSCs given that they form stars and star clusters (e.g. Barth et al., 1995; Pérez et al., 2000; de Grijs et al., 2017) with the latter potentially contributing to the build-up of the NSC if they survive for significant times (but see counter-arguments in Portegies Zwart et al., 2001, 2002). For the best studied case, the Milky Way, Nogueras-Lara et al. (2020), Schödel et al. (2020), and Schultheis et al. (2021) find that the NSC and NSD may differ in that they host intermediate-age populations of different ages, which are absent from the other nuclear type (Nogueras-Lara et al., 2019). However, Nogueras-Lara et al. (2023) point out that both kinematic and metallicity gradients in the Milky Way centre point towards a common origin of both structures.

NSDs are present in a number of external galaxies as well (e.g. Pizzella et al., 2002; Gadotti et al., 2019), however, not always accompanied by an NSC. The formation scenarios of NSDs are tightly linked to the above mentioned *in-situ* scenario for NSCs, i.e. gas funnelling via bar structures (e.g. Binney et al., 1991; Knapen et al., 1999; Fragkoudi et al., 2016) or galaxy mergers (Downes & Solomon, 1998; Mayer et al., 2008). Additionally, van Donkelaar et al. (2024) find that gas-rich star clusters can contribute both to the build-up of the NSC and NSD, directly linking both systems. Finally, as pointed out in Trani et al. (2018), the presence of a massive black hole and the properties of the NSC can directly influence the shape of circum-nuclear rings that may shape the NSD.

2.3.2 Massive Black Holes

NSCs are directly related to MBHs by providing seeding mechanisms, influencing their growth rate, and increasing the probability of transients. This makes NSCs a powerful laboratory to study the assembly of MBHs, especially with upcoming surveys from the *Large Synoptic Survey Telescope*, the *Einstein Telescope*, and the *Laser Interferometer Space Antenna*.

The co-existence of MBHs and NSCs has been known for many decades, starting with the Milky Way (Becklin & Neugebauer, 1968; Balick & Brown, 1974; Genzel et al., 1997; Ghez et al., 1998). Detections and measurements of black hole masses in NSCs in other galaxies come from modelling the velocity dispersion towards the NSC's centre, determining the enclosed mass and constraining the mass of black holes to $M_{\rm BH} \gtrsim 10^5\,{\rm M}_\odot$ (e.g. Bacon et al., 1994; Bender et al., 2005; Seth et al., 2010; Nguyen et al., 2017, 2018, 2019, 2022; Thater et al., 2023). A separate approach is to detect electromagnetic accretion signatures from a MBH across various wavelength regimes (Filippenko & Ho, 2003; Seth et al., 2008a; Shields et al., 2012; Foord et al., 2017; Baldassare et al., 2022; Dullo et al., 2024). However, for this approach to work one generally requires that the optical light emission is at most comparable to NSC in order to be able to detect and characterise the star cluster.

Central densities of the order of $10^8\,{\rm M}_\odot\,{\rm pc}^{-3}$ (Kritos et al., 2023) that are sometimes present in nearby NSCs (Stone et al., 2017) may provide ideal conditions to generate initial black holes masses (or "black hole seeds") that could potentially explain the observations of high-redshift quasars with inferred black hole masses of a billion solar masses (e.g. Bañados et al., 2018; Zhang et al., 2024). The high stellar densities allow for a collisional mass-growth of a very massive star that collapses to an intermediate-mass black hole after a few million years (e.g. Katz et al., 2015; Sakurai et al., 2017;

Schleicher et al., 2022) or via the merger of a cluster of black holes within the star clusters centre (e.g. Gaete et al., 2024). Afterwards, the intermediate-mass black holes in dense star clusters can merge with each other during cluster mergers to form even higher-mass black holes, reaching the "super-massive black hole" range (e.g. Mapelli et al., 2021; Fragione, 2022; Fragione et al., 2022; Mukherjee et al., 2023; Liu et al., 2024; Torniamenti et al., 2024). These signatures can be traced by their emission of gravitational waves (e.g. Liu & Bromm, 2021) and it appears likely that many detected and future signals come from distant NSCs.

Once formed, the MBH can grow through multiple channels, which are influenced by the NSC's presence. For example, the high stellar densities can cause the (partial) tidal disruption (Rees, 1988; Somalwar et al., 2024) or even direct plunge-ins of star cluster members or stellar mass black holes (e.g. Atallah et al., 2023; Kıroğlu et al., 2025). Other interesting phenomena include quasi-periodic eruptions (Evans et al., 2023; Arcodia et al., 2024a; Guolo et al., 2024; Linial & Metzger, 2024a, 2024b; Linial & Quataert, 2024) and extreme-mass-ratio in-spirals (see an overview in Rom & Sari, 2025). In some cases electromagnetic signals can be detected (e.g. Yao et al., 2023) if the collisional body is not a black hole or if the star does not directly plunge into the MBH. However, in case of a merger event with a compact object one may expect to detect gravitational waves (e.g. Liu & Bromm, 2021). According to the numerical study of Polkas et al. (2024), NSCs are a more important contributor to tidal disruption event rates than bulges because of their higher densities and *in-situ* star formation that may re-fill the loss-cone region. If true, this observation makes NSCs an important environment for high-energy astrophysical phenomena.

Another channel for MBH growth is via the accretion of gas. The NSC can assist in this growth channel as well by providing a deeper gravitational potential. As discussed in Partmann et al. (2024), the deep potential wells of NSCs are important for black hole growth in dwarf galaxies. In turn, this suggests that MBHs outside of NSCs (but within dwarf galaxies) retain roughly their seeding mass and could be used to constrain the initial MBH mass function (Greene et al., 2020). For more massive systems Naiman et al. (2015) point out the importance of NSCs in galaxy-galaxy mergers resulting in enhanced accretion rates of MBHs. Overall, NSCs are likely an important ingredient in MBH growth.

Given their similarities it was speculated about 20 years ago that NSCs and MBHs are more tightly linked and potentially belong to the same class of object, leading to the creation of the term "central massive object". This attempt at unifying the two types of central objects had the idea that NSCs occupy the centres of dwarf and MBHs more massive galaxies (e.g. Côté et al., 2006; Ferrarese et al., 2006; Wehner & Harris, 2006). However, this idea was eventually refuted by Graham (2012), Leigh et al. (2012), and Scott and Graham (2013). They argued that these two classes show distinct scaling relations that could indicate different assembly channels. In general, though, it is clear that both NSCs and MBHs interact with each other and influence their evolution. Improving our understanding of NSC assembly can, therefore, improve our knowledge of the assembly of MBHs and potentially constrain the mass distribution of black hole seeds, a yet unsolved quantity.

2.3.3 Ultra-Compact Dwarf Galaxies

Tidal stripping of galaxies during galaxy-galaxy interactions can disrupt the lower-mass constituent while preserving its NSC. Depending on the initial conditions of the interaction, the accreted nucleus can orbit its new host resulting in a phenomenon called "ultra-compact dwarf galaxy" (UCD). These objects were first discovered in the nearby Fornax galaxy cluster (Hilker et al., 1999; Drinkwater et al., 2000; Phillipps et al., 2001) and have similar masses and sizes as massive star clusters and dwarf elliptical galaxies, shaping their name (Norris et al., 2014).

One of the theories for the formation of UCD is the birth of young massive star cluster outside of galaxy disks during galaxy-galaxy interactions (e.g. Fellhauer & Kroupa, 2002). However, this scenario fails at explaining features of many UCDs, such as extended star formation histories (Norris et al., 2015) with multiple stellar populations (Janz et al., 2016), MBHs (Mieske et al., 2013; Seth et al., 2014; Ahn et al., 2017, 2018; Taylor et al., 2025), and elevated mass-to-light ratios compared to GCs (Dumont et al., 2022), and masses that exceed the speculated upper mass end of GCs of $M_{\mathrm{GC}}^{\mathrm{max}} \approx 5 \times 10^7\,\mathrm{M}_\odot$ (Norris et al., 2019). Additionally, tidal streams around UCDs, which could show the remnant of the stripped host galaxy, have been detected strengthening the connection between NSCs and UCDs (Jennings et al., 2015; Voggel et al., 2016; Paudel et al., 2023).

Some of the most massive GCs may be accreted NSCs as well. This includes M 54 that shows multiple stellar populations (Alfaro-Cuello et al., 2019, 2020), ω Cen that has a large metallicity and age spread (see Clontz et al., 2024; Nitschai et al., 2024, and references therein) as well as an intermediate-mass black hole (Häberle et al., 2024), and B23-G78, the most massive GC in M 31 that contains an MBH (Pechetti et al., 2022).

Overall, UCDs are interesting objects that may assist in solving the riddle of NSC formation and co-evolution of MBHs. This is especially true in the most massive galaxies that lack an NSC (*c.f.* Figure 2.1) but are expected to harbour many UCDs (Mieske et al., 2012).

2.4 Thesis Goals

There still exist many open questions about the formation of NSCs and how they interact with MBHs and their host galaxies. For example, in the dwarf galaxy regime it is unclear if NSCs share the same structural parameters as GCs, whether they contain any MBHs or are responsible for the detection of off-centre AGN (e.g. Mezcua & Domínguez Sánchez, 2020), or how their frequency is affected by the host galaxy environment. It also needs to be explicitly demonstrated that the properties of an NSC help to constrain the evolution of its host galaxy.

The goal of this dissertation is to make progress on these issues. First, in Chapter 3, we investigate the properties of NSCs in dwarf galaxies. This work significantly expands on the structural parameters in the low-mass regime, which is important for constraints on e.g. tidal disruption events (as outlined in Hannah et al., 2024). Afterwards, we probe the properties of the NSC of Messier 74 in Chapter 4, utilising imaging data from the far-ultraviolet to the mid-infrared regime. The data will prove useful to constrain the metallicity and age of the NSC and, in turn, the assembly history of the host galaxy itself and a potential MBH within the star cluster. In Chapter 5, we search for new signatures of low-luminosity AGN in dwarf galaxies that host an NSC using soft X-ray data from the *eROSITA*/SRG mission. Finally, in Chapter 6, we discuss the details of a newly developed semi-analytical galaxy formation model that takes into account the formation of massive star clusters. The chapter outlines the first results of the model, focussing on the present-day star cluster populations in disk- and bulge-dominated galaxies. In the last part (Chapter 7) I summarise the contents of this dissertation and present an outline for future projects.

2.5 Chapter Summary

- ▹ Nuclear star clusters (NSCs) occupy many galaxy centres and are tightly linked to globular clusters (GCs), massive black holes (MBHs), and ultra-compact dwarf galaxies.
- ▹ A typical NSC has a similar size but is more massive (and, thus, denser) than a typical GC.
- ▹ NSCs often show extended star formation histories with wide metallicity ranges.
- ▹ A correlation between NSC and host galaxy stellar mass indicates a co-evolution of both systems.
- ▹ NSCs form either via *in-situ* star formation or via the accretion of migrating GCs. These formation channels directly impact the seeding and growth of MBHs within NSCs.
- ▹ Interactions between star cluster members and an MBH result in electromagnetic and gravitational wave emission that can be detected over cosmological distances. The high central stellar densities and repeated *in-situ* star formation favour NSCs as ideal laboratories to study such high-energy phenomena.
- ▹ The projects discussed in this dissertation tackles multiple open questions about NSC assembly and presents a basis for future investigations.

Chapter 3

Nuclear Star Clusters in Nearby Dwarf Galaxies

Declaration

The contents of this chapter were previously published in Hoyer et al. (2023a). All co-authors provided commentary that improved the published work.

Abstract

We use high-resolution *Hubble Space Telescope* imaging data of dwarf galaxies in the Local Volume ($\lesssim 11\,\mathrm{Mpc}$) to parameterise 19 newly discovered nuclear star clusters (NSCs). Most of the clusters have stellar masses of $M_\star^{\mathrm{nsc}} \lesssim 10^6\,\mathrm{M}_\odot$ and compare to Galactic globular clusters in terms of ellipticity, effective radius, stellar mass, and surface density. The clusters are modelled with a Sérsic profile and their surface brightness evaluated at the effective radius reveals a tight positive correlation to the host galaxy stellar mass. Our data also indicate an increase in slope of the density profiles with increasing mass, perhaps indicating an increasing role for *in-situ* star formation in more massive hosts. We evaluate the scaling relation between the clusters and their host galaxy stellar mass to find an environmental dependence: for NSCs in field galaxies, the slope of the relation is $\alpha = 0.82^{+0.08}_{-0.08}$ whereas $\alpha = 0.55^{+0.06}_{-0.05}$ for dwarfs in the core of the Virgo cluster. Restricting the fit for the cluster to $M_\star^{\mathrm{gal}} \geq 10^{6.5}\,\mathrm{M}_\odot$ yields $\alpha = 0.70^{+0.08}_{-0.07}$, in agreement with the field environment within the 1σ interval. The environmental dependence is due to the lowest-mass nucleated galaxies and we speculate that this is either due to an increased number of progenitor globular clusters merging to become an NSC, or due to the formation of more massive globular clusters in dense environments, depending on the initial globular cluster mass function. Our results clearly corroborate recent results in that there exists a tight connection between NSCs and globular clusters in dwarf galaxies.

3.1 Introduction

The central regions of galaxies are interesting because of the extreme objects they host. Besides supermassive black holes (SMBHs), which are believed to be common in high-mass galaxies (Kormendy & Ho, 2013), nuclear star clusters (NSCs) often occupy the centers of low- to intermediate-mass galaxies[1]. Their size of typically a few parsecs (e.g. Georgiev & Böker, 2014; Carson et al., 2015; Pechetti et al., 2020) and high stellar mass ($M_\star^{\rm nsc} \sim 10^7\,{\rm M}_\odot$; e.g. Georgiev et al., 2016) make NSCs the densest stellar systems known (see Neumayer et al., 2020, for a review). Similarities between these objects and globular clusters (GCs) have led to the hypothesis that NSCs are formed by the consecutive migration of GCs (Tremaine et al., 1975). However, not all NSC properties can be explained by this formation scenario alone [e.g. young stellar populations in the central regions both in the Milky Way (e.g. Lu et al., 2009; Feldmeier-Krause et al., 2015) and other nearby galaxies (e.g. Bender et al., 2005; Seth et al., 2006; Walcher et al., 2006; Carson et al., 2015; Nguyen et al., 2017; Kacharov et al., 2018; Nguyen et al., 2019)]. Therefore, a second formation scenario, *in-situ* star formation, was proposed (e.g. Milosavljević, 2004; Agarwal & Milosavljević, 2011). Neumayer et al. (2020) established the idea that the relative importance of the two scenarios changes as a function of galaxy mass: in dwarf galaxies ($M_\star^{\rm gal} \lesssim 10^9\,{\rm M}_\odot$) GC migration is the dominant formation scenario, whereas in high-mass galaxies ($M_\star^{\rm gal} \gtrsim 10^9\,{\rm M}_\odot$) the majority of the NSC stellar mass is build-up *in-situ*. Most recently, this transition was observed in dwarf early-type galaxies (Fahrion et al., 2020b, 2021). In addition, using the theoretical framework of Leaman and van de Ven (2022) of the build-up of NSCs through GC migration, Fahrion et al. (2022b) quantified the *in-situ* fraction of NSCs which appears to decline towards low NSC masses.

NSC occurrence is not uniform and varies with host galaxy stellar mass, morphological type, and environment. It is now well established that NSCs are most common in galaxies with stellar masses of $M_\star^{\rm gal} \sim 10^{9.5}\,{\rm M}_\odot$ (Sánchez-Janssen et al., 2019a; Neumayer et al., 2020; Hoyer et al., 2021) and that their rate of occurrence declines towards lower and higher stellar mass. It is speculated that the rivalry between SMBHs and NSCs at the high-mass end can lead to the evaporation of the cluster due to tidal heating (e.g. Côté et al., 2006) and binary black hole mergers (e.g. Antonini et al., 2015). At the low-mass end, it seems that NSCs and GCs are closely linked (e.g. Sánchez-Janssen et al., 2019a; Carlsten et al., 2022) and that the lack of GCs in lower mass galaxies drives the declining NSC frequency.

Numerous new detections were made over the last few years with ground-based surveys, increasing the total number of NSCs beyond 1000 (Muñoz et al., 2015; Venhola et al., 2018; Sánchez-Janssen et al., 2019a; Carlsten et al., 2020; Habas et al., 2020; Poulain et al., 2021; Su et al., 2021). While ground-based surveys have the clear advantage of rapidly increasing number statistics, with the exception of the closest systems, their data cannot be used to determine structural parameters, and very few structural parameter estimates are available for NSCs in low-mass galaxies. To investigate this parameter space, high-resolution imaging data are required, as provided by the *Hubble Space Telescope* (*HST*). In the past, numerous studies have used *HST* data to analyse NSCs (e.g. Carollo et al., 1998; Böker et al., 1999a, 2002; Walcher et al., 2005; Côté et al., 2006; Seth et al., 2006; Baldassare et al., 2014; Georgiev & Böker, 2014; Pechetti et al., 2020), even in galaxies in the ~ 100 Mpc distant Coma galaxy cluster (den Brok et al., 2014; Zanatta et al., 2021).

[1]A few galaxies are known to host both objects; see Table 3 in Neumayer et al. (2020) for a recent compilation.

Recently, we analysed *HST* data for more than 600 galaxies to constrain the frequency of NSCs in the Local Volume (Hoyer et al., 2021). During this analysis, we discovered 21 new NSCs that had not been previously catalogued. In this paper we present structural parameter measurements of these 21 newly discovered NSCs. We investigate possible relations of the NSCs' parameters and their connection to the underlying host galaxy.

Section 3.2 briefly introduces the data and describes the method of identifying nucleated galaxies. Details regarding image processing, PSF generation, and the fitting procedure are presented in Section 3.3. Section 3.4 discusses our results on NSC parameters, their wavelength dependence, and scaling relations. We conclude in Section 3.6. Additional remarks regarding uncertainties are given in Section 3.7.1. All data tables are presented in Section 3.7.2 and are also available online in a machine-readable format.

3.2 Identification of Nuclear Star Clusters

In Hoyer et al. (2021) we determined if galaxies have NSCs through a multi-step process using *HST* ACS, WFPC2, and WFC3 data. In a first step, we visually inspected all available imaging data. During this step, we removed galaxies with obscured centres or if their centres were not visible on the data. Furthermore, we identified bright central and compact objects as potential NSCs.

Next, we created multiple three- and two-dimensional figures, as well as a one-dimensional surface brightness plot. The aim of these plots is to (1) indicate the intensity of the compact source compared to its host galaxy, (2) check the position of the compact source within the galactic body, and (3) visually inspect the extent of the compact source and its host galaxy. As an example, Figure 3.1 shows these plots for the ACS/WFC $F814W$ data of NGC 2337, the most massive galaxy in our sample of newly discovered NSCs. Given that NSCs are dense stellar systems close to the photometric and kinematic centres of their hosts (Neumayer et al., 2011; Poulain et al., 2021), we expect them to (1) have the highest intensity within the galactic body and (2) lie 'close' to the centres of elliptical isophotes which were fit to the galactic body, as visualised in the middle panel of Figure 3.1. In this step, we removed potential NSC candidates if they lay in the outskirts of their host galaxy (with typical distances of ≥ 1 kpc to the galactic centre) or if several other compact sources had similar intensities, indicating that the compact source is either a faint foreground star or one of many GCs.

In a third step we performed a two-dimensional fit to the data to extract the magnitude and extent of the compact source. A point spread function (PSF) was generated at the location of the compact object of the chip using *TinyTim* (Krist, 1993, 1995) and the fit was performed with *Imfit* (Erwin, 2015). The PSF was then convolved with a Sérsic profile (Sérsic, 1968) of the form

$$I(r) = I_{\mathrm{eff}} \exp\left\{ - b_n \left[\left(\frac{r}{r_{\mathrm{eff}}} \right)^{1/n} - 1 \right] \right\}, \tag{3.1}$$

and fit to the data. Here r_{eff} is the effective radius, I_{eff} the intensity at the effective radius, n the Sérsic index, and b_n solves $\Gamma(2n) = 2\gamma(2n, b_n)$ where $\gamma(x, a)$ is the

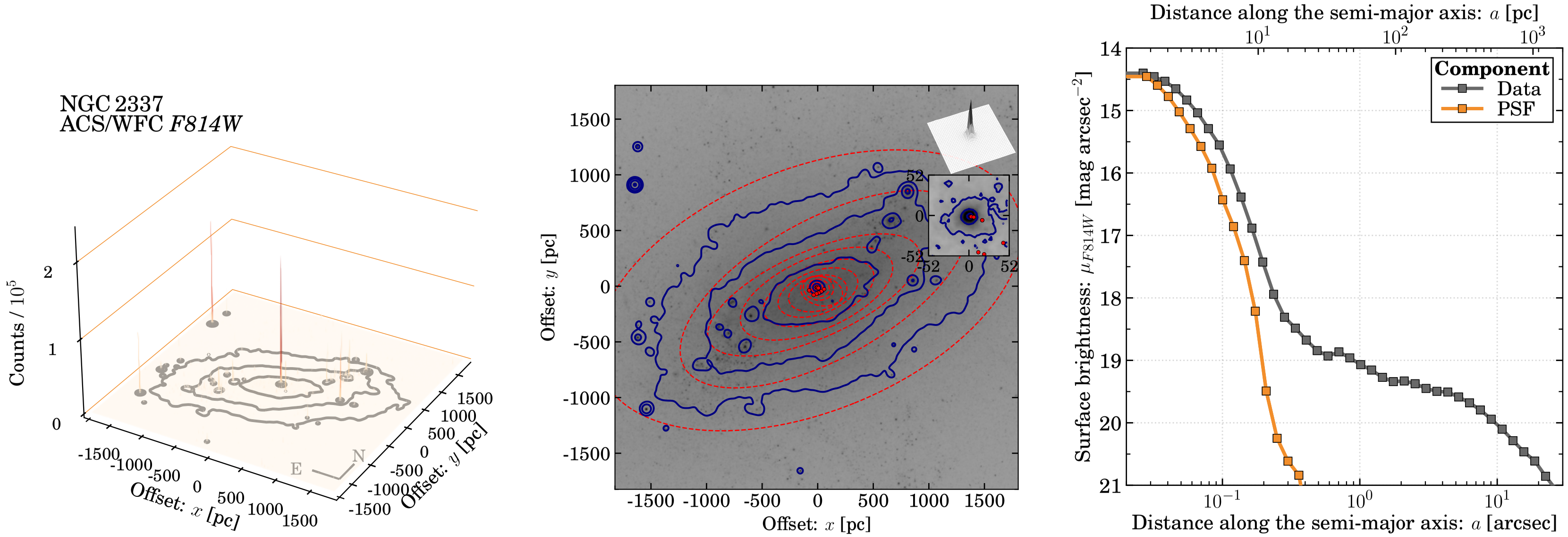

Figure 3.1. Nuclear star cluster (NSC) identification procedure using NGC 2337 as an example, based on the *HST* ACS/WFC *F814W* data product. *Left panel*: Three-dimensional contour plot of NGC 2337 centered on the NSC. North is up and East is left. Contour lines represent the profile of a smoothed version of the data. For smoothing, we use a Gaussian kernel with standard deviation of five pixels. The NSC is the brightest source connected to the galaxy. *Middle panel*: Two-dimensional contour plot of the same data as in the left panel keeping the same orientation and blue contour lines. Red dashed lines give elliptical isophotes which were fit to the smoothed data; red points mark their centres. The two top right panels highlight the direct vicinity of the NSC. *Right panel*: One-dimensional surface brightness (μ_{F814W}) plot of the elliptical isophotes (red colour, middle panel) as a function of semi-major axis (a) in both arcseconds and parsecs. Gray squares indicate the data. Orange squares show the extent of a *TinyTim*-generated PSF for the position of the NSC on the chip.

incomplete and $\Gamma(x)$ the usual Gamma function (see also Graham & Driver, 2005). Such Sérsic profiles have been widely used in fitting nearby NSCs in the recent literature (e.g. Graham & Spitler, 2009; Carson et al., 2015; Pechetti et al., 2020). If the extent of the compact source was larger than 20 % of the width of the PSF (typically ≥1 pc), we classified the compact object as an NSC and considered it for further analysis. In total, 21 compact objects in the central regions of galaxies fulfilled all requirements (including NGC 2337 in Figure 3.1), were classified as NSCs, and are new detections. We show images of these 21 objects in Figure 3.2.

3.3 Analysis

3.3.1 Image Processing

For each galaxy, we combined single exposures using flat-fielded data products obtained from the *Hubble Legacy Archive*[2] (*HLA*). Instead of using the available final data products, we prefer to combine the exposures ourselves to ensure a homogeneous calibration process and to control the pixel scale of the drizzle output.

In a first step, we obtained the raw exposures from the ACS, WFPC2, and WFC3 instruments and updated the world coordinate system of each exposure using the latest reference files. This step was required to obtain a sub-pixel accuracy between individual exposures and to avoid a systematic broadening of the NSC. We fed the aligned exposures to *AstroDrizzle* (Gonzaga et al., 2012) which combined them into a single science product. No sky subtraction was performed. The program allows the user to modify the pixel fraction and pixel scale of the final drizzled image. The pixel fraction varies between zero and one where a value of zero corresponds to pure interlacing and a value of one to shifting and addition of pixel values from individual exposures. The drizzle algorithm (Fruchter & Hook, 1997) combines both techniques and enables a gain in image resolution and reduction in correlated noise. We chose a value of 0.75 for the pixel fraction which is the smallest value for which no artifacts appeared in the weight map of the output image of *AstroDrizzle*. Increasing the value towards one did not change the fit results.

In addition to the pixel fraction, we changed the pixel scale for the ACS data products. The image resolution of the WFPC2 and WFC3 products remain unchanged. The limiting factor in increasing the spatial resolution of our ACS data products is given by the extent of the core of the theoretical PSF. This value is presented for the *F550M* band in the ACS manual[3]. We determine the width of the PSF in a different filter by constructing the ratio of the full-width-half-maximum between *TinyTim*-generated PSFs in that filter and the *F550M* band. The pixel scale of the ACS images was chosen to Nyquist sample the PSF full-width-half-maximum at each wavelength. It ranges between 0.0415 arcsec pixel^{-1} and 0.0472 arcsec pixel^{-1}, depending on the filter. The final resolution of each data product is indicated in Table 3.2 in Section 3.7.2.

Finally, to perform the actual fit, we selected a square region of side length 100 pixels around the position of the NSC. Depending on the image resolution and the distance

[2]URL: http://hla.stsci.edu/

[3]See Ryon et al. (2019) and https://www.stsci.edu/hst/instrumentation/acs.

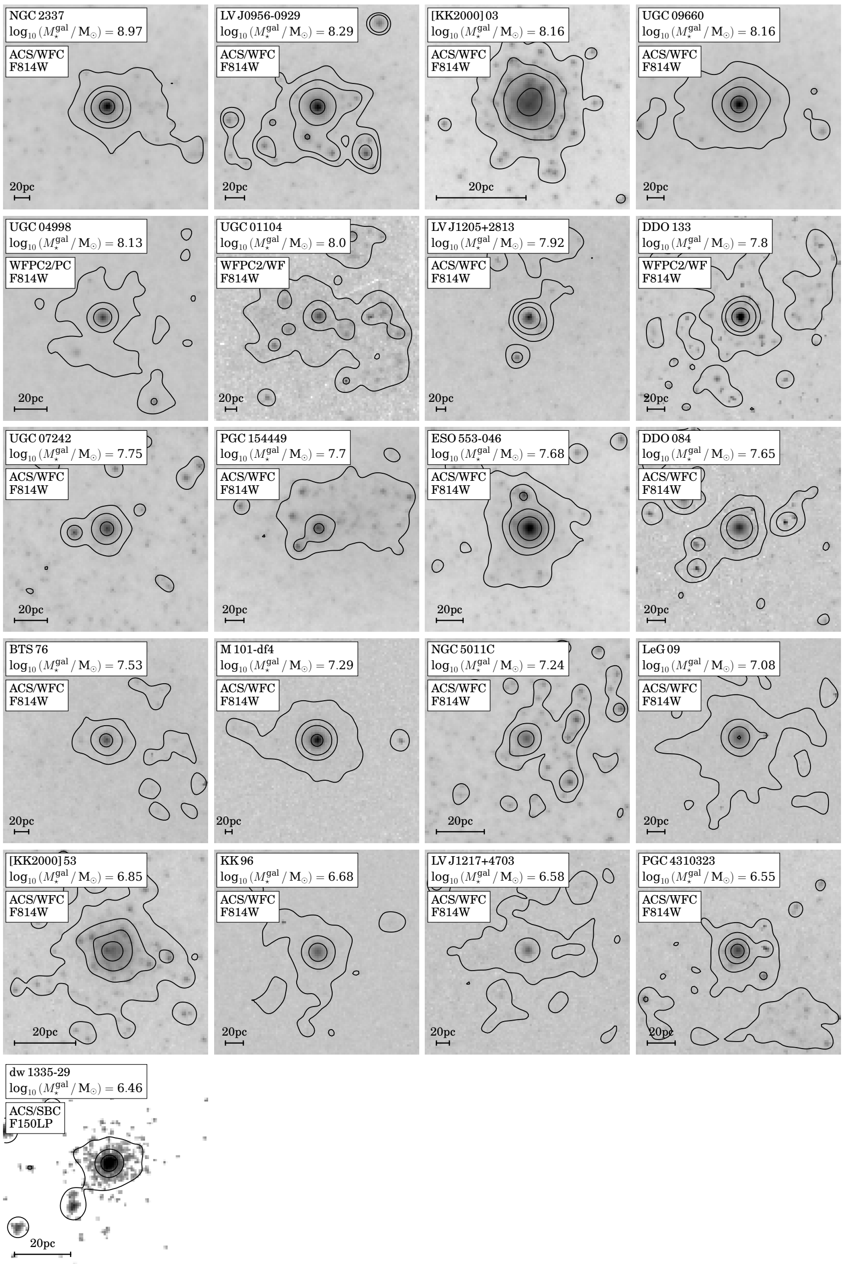

Figure 3.2. Collage of the 21 newly discovered nuclear star clusters, sorted by host galaxy stellar mass from top left to bottom right. Each image shows a square box of side length 100 pixel centered on the nucleus; 20 parsec at the distance to the galaxies are indicated in each panel. North is up and East is left. The contour lines were derived from a smoothed version of the data using a Gaussian kernel with standard deviation of three pixels.

to the galaxy, this square region covers an area between $\sim 50\,\text{parsec} \times \sim 50\,\text{parsec}$ and $\sim 500\,\text{parsec} \times \sim 500\,\text{parsec}$. As NSCs typically have effective radii of a few parsecs (e.g. Neumayer et al., 2020) the selected area ensures that the wings of the NSCs are well captured. Nevertheless, we verified that both doubling the side length of the square and reducing it down to 60 pixels does not affect the final results.

3.3.2 PSF Generation

Detailed knowledge of the PSF at the location of the NSC is required to reliably measure effective radii as they are generally compact and cover only a few pixels on the exposure. The PSF can be recovered from stellar sources in the image or generated synthetically. We decide to generate synthetic PSFs using *TinyTim* for three reasons:

1. It is difficult to find non-saturated stars in the proximity of the NSC. Stars far away from the NSC should not be used as the *HST* PSFs vary significantly across the chip.
2. The extracted PSF from stars may be subject to variations due to the positions of the stars on the chip and their stellar type.
3. Extracting a PSF from stars results in an inhomogeneous treatment of using PSFs across the whole NSC sample.

Synthetic PSFs avoid these issues and allow us to control the input parameters such as position on the chip and the assumed stellar type.

To generate a PSF, we first determined the position of the NSC on each exposure. PSFs were generated using *TinyTim* and the location of the NSC on the chips, while assuming a `G2V` spectral type ($V - I = 0.71$ mag) for the artificial star. After the PSF generation, we created a copy of the science exposures and subtract the image data from the first header file. The PSF was then added to the flattened image data at the previous location of the NSC. We then fed the data to *AstroDrizzle* and executed the program with the same settings as for the science data. This step ensures that the final PSF, which was extracted from the output of the program, is processed in the same way as the NSC on the science data.

Note that the inclusion of the *AstroDrizzle* processing step is crucial as the resulting PSF will change depending on the chosen parameter settings. In our tests the core of the resulting PSFs were slightly larger than the core of any of the *TinyTim*-generated PSFs. Therefore, not performing this step results in systematically larger effective radii compared to their ‘true’ values. We discuss this effect and other potential systematic uncertainties, such as the spectral type of the artificial star or the uncertainty on positioning the PSFs on the chips in Section 3.7.1.

3.3.3 Fitting Procedure

We assume that the NSC light distribution can be accurately modelled with a single Sérsic profile (Sérsic, 1968), as is common practice in the literature (e.g. Turner et al., 2012; Baldassare et al., 2014; Carson et al., 2015; Pechetti et al., 2020). For the background light, which includes the galaxy itself, we used a flat background assuming that local flatness holds in the proximity of the NSC. The only two exceptions are

UGC 01104 and UGC 09660 where the fit required a second Sérsic profile for the underlying galaxy.[4] Using version 1.8.0. of *Imfit*, the Sérsic profile was convolved with the PSF and fit to the data where the goodness of fit is evaluated via standard χ^2 statistics. The data were fit using a differential evolution solver with Latin hypercube sampling (Storn & Price, 1997). The solver is less prone to be stuck in local minima compared to other solvers available in *Imfit* and does not rely on initial parameter estimates as parameter values are randomly sampled given lower and upper boundaries. We list the chosen boundary values in Table 3.1 and note that they are kept the same for all NSCs in all filters.

We additionally tested that other model functions do not significantly change the resulting parameter estimates. For the NSC, the tests included a King profile, multiple Sérsic profiles, point sources, nuclear rings, and various combinations. According to the Bayesian Information Criteria, none of these fits significantly improved over a fit with a single Sérsic profile. In addition, by adding a Sérsic profile to the flat background component to account for the underlying galaxy, we found that the assumption of local flatness is justified. We verified that using Cash statistics instead of the classical χ^2 statistics does not change the results. We defer to Section 3.7.1 for a detailed discussion regarding the choice and justification of these models.

For each NSC, the fits in different filters were performed independently of each other. However, in some cases the Sérsic index diverged towards the upper boundary in one filter, but not in the other. In these cases (BTS 76, DDO 084, ESO 553-046, [KK2000] 53, KK 96, LeG 09, LV J1217+4703, NGC 5011C), we kept all structural parameters of the fit with the diverging Sérsic index fixed such that only the (x, y) position, the intensity at the effective radius, and the flat background component were allowed to vary.

For a number of galaxies the Sérsic index diverged towards high values in all available filters. This behaviour persisted when considering a single point source or a point source in combination with a Sérsic profile, and also occurred independently of the settings chosen for *AstroDrizzle*, *TinyTim*, and *Imfit*. As the NSCs are more extended than the PSFs, no explanation for the diverging Sérsic index could be determined. To quantify the extent of the affected NSCs, we fixed the Sérsic index to a value of $n = 2$. The choice of this value was motivated by the recent work of (Pechetti et al., 2020) who classified their fits into three categories. NSCs which could be fit 'well' (their 'Quality 0' fits) have a mean / median value of $n = 1.9 / 2.9$. Although six out of their 17 NSCs have $n > 3$, we decided to set $n = 2$ and to determine a systematic uncertainty based on fits using $n = 0.5$ and $n = 3$. In the parameter range $n \in [0.5, 3.0]$, the Sérsic index does not correlate with the effective radius, allowing us to put constraints on it. For larger Sérsic indices, the effective radius also increases in a non-linear way. We give more details and discuss this choice further in Section 3.7.1. However, it will become evident in Section 3.4 that the key results of this paper remain unchanged.

[4] If only a single Sérsic profile is used the fit 'prefers' to fit the underlying profile over the NSC.

Table 3.1. Parameters and their boundaries supplemented to *Imfit*. The same values are used for all galaxies and filters.

Parameter	Boundary	Unit	Description
x_0	[45, 55]	[pixel]	NSC position
y_0	[45, 55]	[pixel]	NSC position
PA	[−359.99, 359.99][a]	[deg]	Position angle
ϵ	[0.00, 0.99]	--	Ellipticity
n	[0.00, 15.00]	--	Sérsic index
r_{eff}	[0.00, 50.00]	[pixel]	Effective radius
I_{eff}	[0.00, I_{max}][b]	[counts]	Intensity at r_{eff}

[a] Often the fit was stuck at a boundary of 0°, hence the extension towards negative values. If the best fit position angle was negative, we added 180° (twice) until it became positive.
[b] I_{max} is the peak intensity of the nuclear star cluster.

3.3.4 Stellar Mass

Integrating Equation 3.1 over the radial component while assuming an ellipticity (ϵ) yields the total intensity of the NSC (L) as

$$L = 2\pi(1-\epsilon)r_{\mathrm{eff}}^2 I_{\mathrm{eff}} \times \frac{n\,\mathrm{e}^{b_n}}{(b_n)^{2n}} \times \Gamma(2n) \quad . \tag{3.2}$$

Combining L with the zeropoint magnitudes and exposure times, which are both given in Table 3.2, allows the calculation of apparent magnitudes.

We derived stellar masses using the $V-I$ colour and, therefore, converted from *HST* magnitudes to the $BVRI$ system. Following the approach by Pechetti et al. (2020), magnitudes were converted using different synthetic transformation. For the ACS/WFC data, the magnitudes were transformed using Table 22 and Equation 12 of Sirianni et al. (2005). WFPC2/WF and WFPC2/PC magnitudes were converted using Table 4 and Equation 16 of Dolphin (2009).

Once the magnitudes were transformed, we corrected them for Galactic extinction using a recalibrated version of the Schlegel et al. (1998) dust maps (Schlafly & Finkbeiner, 2011) and assuming the reddening law of Fitzpatrick (1999) with $R_V = 3.1$. The corrected apparent magnitudes were then used to determine absolute magnitudes via the galaxy distance estimates and the absolute magnitude of the Sun.[5] All extinction corrected apparent magnitudes are presented in Table 3.3.

The stellar mass-to-light ratio relies on the I-band luminosity and $(V-I)_0$ colour and is identical to the one used in Pechetti et al. (2020). This relation $(M_\star/L_I)$ is based on the work of Roediger and Courteau (2015) and reads

$$\log_{10}\left(M_\star/L_I\right) = -0.694 + 1.335 \times (V-I)_0 \ , \tag{3.3}$$

where the slope and intercept have been determined by fitting a linear relationship to the underlying data which was provided by Joel Roediger (private communication).

[5] Obtained from http://mips.as.arizona.edu/~cnaw/sun.html.

The uncertainty on the NSC stellar masses are dominated by the uncertainty on the mass-to-light ratio which we assume to be 0.3 dex (Roediger & Courteau, 2015). Other uncertainties, which have been included via Gaussian error propagation, include the statistical and systematic uncertainties of the fit (see Section 3.7.1), the uncertainty on the absolute magnitude of the Sun (assumed to be 0.04 mag), and the uncertainty on the distance estimates. All quoted uncertainties give the 1σ interval. The resulting parameter values and their uncertainties are presented in Table 3.3.

3.4 Results

In total, we derive NSC structural parameters for 19 objects. In the case of dw 1335-29, the signal-to-noise ratio of the ACS/SBC *F150LP* data were to low to allow for an accurate determination of NSC parameters. In the case of PGC 154449, we could not determine parameter estimates from either the ACS WFC *F606W* or *F814W* data as the effective radius was approaching the boundary of 50 pixel in all attempts. We changed the size of the fitting region, the fitting routine, and applied various masks without achieving a stable fit result. For UGC 01104, structural parameters could not be determined in the ACS/WFC *F300W* band.

Furthermore, we derive colours and stellar mass estimates for 17 objects. The blue colour estimate of ESO 553-046 [$(V - I)_0 \sim -3.2$ mag, *c.f.* Table 3.3] leads to an unreliable estimate of the NSC mass. As no structural parameters could be estimated in two filters for dw 1335-29, PGC 154449, and UGC 01104, we do not derive NSC stellar masses. Finally, the stellar mass-to-light ratio of four NSCs is unreasonably high ($M_\star/L_I \gtrsim 4\mathrm{M}_\odot/\mathrm{L}_\odot$). These data points are excluded from the surface brightness and mass density profiles (*c.f.* Section 3.4.4) and the determination of the scaling relation between NSC and host galaxy stellar mass (*c.f.* Section 3.4.5).

3.4.1 Literature Data

We compare our results to other NSCs in the Local Volume, in massive late-type field galaxies, and in dwarf ellipticals in the core of the Virgo cluster. For the Local Volume, we selected all known nucleated galaxies and obtained their NSC parameters, where available, from the most recent literature reference identified by Hoyer et al. (2021, their Table D1). For NSCs in massive late-type field galaxies, we used the data tables of Georgiev and Böker (2014). As the authors do not provide stellar masses, and to avoid systematic differences to our approach, we adopted their *F606W* and *F814W* apparent magnitudes and repeated the steps outlined in Section 3.3.4. Table 5 of Sánchez-Janssen et al. (2019a) provides stellar masses for NSCs in dwarf ellipticals in the core of the Virgo cluster. In addition, we adopt the data from Carlsten et al. (2022) for dwarfs around massive late-type field galaxies. We compare to Galactic globular clusters using the data from Harris (1996) and Baumgardt and Hilker (2018).

We present an overview of the parameters of other NSCs in Local Volume galaxies in Table 3.4. NSC stellar masses for the sample of Georgiev and Böker (2014) are presented in Table 3.5.

Galaxy stellar masses were adopted from Hoyer et al. (2021) for the whole Local

Volume data set and the galaxy sample of Georgiev and Böker (2014). We take galaxy stellar masses for dwarf ellipticals in the core of the Virgo cluster from Table 4 of Sánchez-Janssen et al. (2019a).

3.4.2 Wavelength Dependence

We investigate whether NSC structural parameters are wavelength dependent by comparing differences in parameter estimates between the most commonly available *F660W* and *F814W* bands. Within the uncertainties, we find no significant differences in both ϵ and $r_{\rm eff}$. The position angle changes insignificantly (ΔPA $\lesssim 30°$) for most NSCs.

3.4.3 Structural Properties

Here we investigate the structural properties of the new detections using the *F814W* band. We compare to other data from the Local Volume and Georgiev and Böker (2014) using the same band, if available.[6] In addition, we compare to the globular cluster population of the Milky Way (Harris, 1996; Baumgardt & Hilker, 2018).

Panel A of Figure 3.3 shows the ellipticity versus NSC stellar mass. Most of the new detections have $\epsilon \sim 0.1$ but at most ~ 0.3. With the exception of the most massive NSCs, both the stellar mass and ellipticity compare to Milky Way GCs. The overall increase of ellipticity with increasing mass is in agreement with Figure 24 of Spengler et al. (2017). The new detections reveal that this trend does not continue down to the lowest mass clusters, as suggested by the few existing Local Volume data points from the literature. Similarly, the GC population of the Milky Way does not show a correlation as well.

Panel B shows the effective radius versus NSC mass. The new detections occupy the low-mass and compact-size region in the parameter space. While at higher NSC mass there exists a correlation between the effective radius and NSC mass (e.g. Georgiev & Böker, 2014; Georgiev et al., 2016; Neumayer et al., 2020), this relation appears to break down at $M_\star^{\rm nsc} \sim 10^6\,{\rm M}_\odot$, as revealed by the new detections. The distribution of Galactic GCs overlap with the new detections, corroborating a tight connection between both types of systems in this mass range. Furthermore, the new detections appear to follow the same trend as the GCs by increasing in effective radius with decreasing mass.

There exist six data points with $r_{\rm eff} \geq 10\,{\rm pc}$ and $M_\star^{\rm nsc} \leq 10^6\,{\rm M}_\odot$, which partially overlap with the distribution of Galactic GCs but are otherwise outliers from the NSC distribution. If the NSCs truly reside in this part of the parameter space, one explanation could be that their evolution is similar to that of the NSC of the Pegasus dwarf galaxy: the cluster initially formed in the centre of their host galaxy, was relocated outside of the central region where $r_{\rm eff}$ increased due to the weaker tidal field, and migrated back towards the centre (Leaman et al., 2020). For both UGC 08638 and NGC 4163, this mechanism could still be in process as the projected distance of the NSC to the photometric centre is $\sim 480\,{\rm pc}$ and $\sim 150\,{\rm pc}$, respectively (Georgiev et al., 2009b). The

[6] For the Local Volume data set, we use the reddest band in case the *F814W* is unavailable.

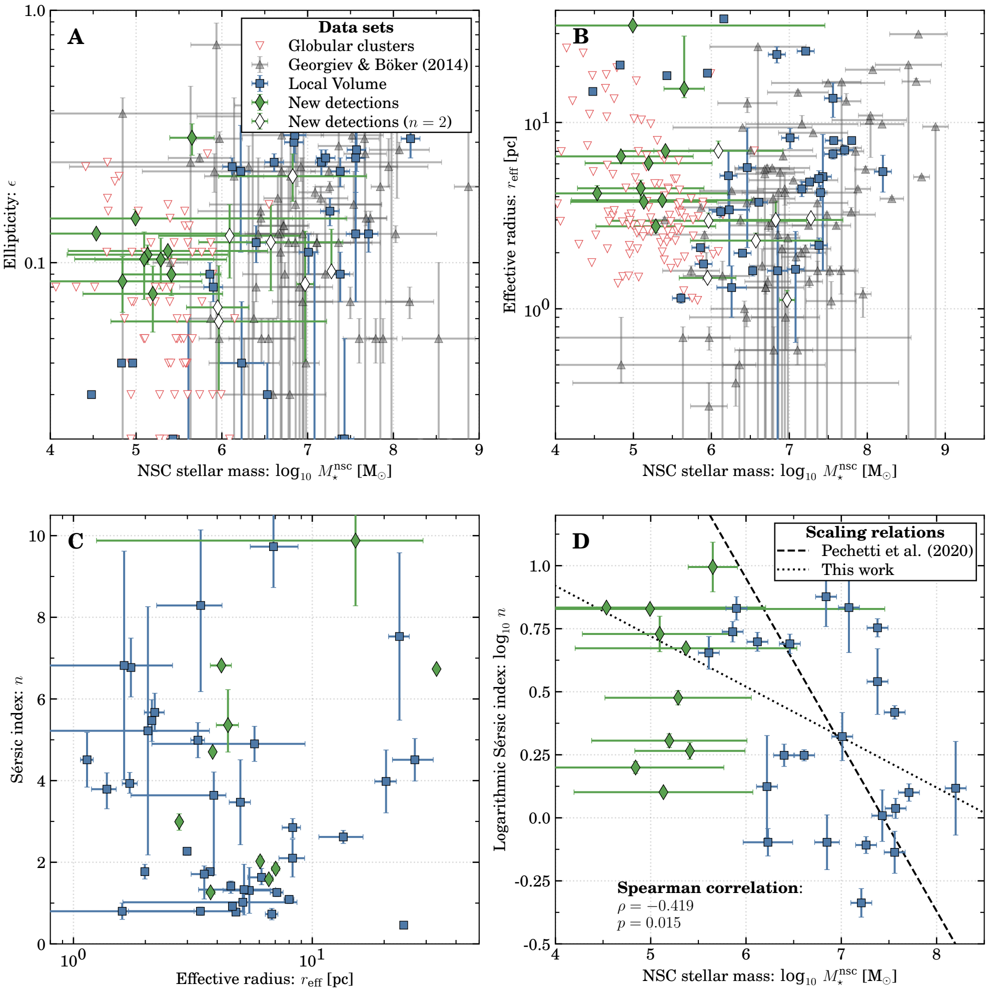

Figure 3.3. *Panel A*: Ellipticity (ϵ) versus nuclear star cluster (NSC) stellar mass ($M_\star^{\rm nsc}$). We compare the new detections (green diamonds) to NSCs in massive late-type spirals (Georgiev & Böker, 2014), a compilation of NSCs in the Local Volume, and Galactic globular clusters (Harris, 1996; Baumgardt & Hilker, 2018). The new detections are split into two categories, depending on whether the Sérsic index (n) needed to be fixed at $n = 2$. *Panel B*: Effective radius ($r_{\rm eff}$) versus NSC stellar mass. The markers and color are the same as in panel A. *Panel C*: Sérsic index versus effective radius. The data from Georgiev and Böker (2014) and Harris (1996) and Baumgardt and Hilker (2018) are not available as the clusters were modelled with King profiles. Most of the Local Volume data come from Pechetti et al. (2020). *Panel D*: Sérsic index versus NSC stellar mass. A dashed black line gives the weak scaling relation identified by Pechetti et al. (2020). The dotted line gives the best-fit linear relation including the new detections. The Spearman correlation index ρ and its associated p-value of thew new fit are given in the lower left corner.

projected distance of the other two galaxies (KK 197 and ESO 269-066) is close to 0 pc (Georgiev et al., 2009b).

Panel C of Figure 3.3 shows the Sérsic index versus effective radius. There appears to be a trend in that the index drops from $n \sim 7$ to ~ 1 when the effective radius increases from $r_{\rm eff} \sim 1$ pc to ~ 10 parsec. However, multiple NSCs occupy the high Sérsic index and high effective radius parameter space, questioning a potential universal correlation. More data and further studies are required to explore this parameter space.

Panel D shows the previously identified weak relationship between the logarithmic Sérsic index and NSC stellar mass by Pechetti et al. (2020). We add the new detections to the figure and fit the combined data sets with a linear function. The best fitting relation reads

$$\log_{10}\, n_{F814W} = \left(0.52^{+0.50}_{-0.38}\right) - \left(0.20^{+0.53}_{-0.29}\right) \times \log_{10}\left(\frac{M_\star^{\rm nsc}}{10^6\,{\rm M_\odot}}\right). \tag{3.4}$$

The parameters differ significantly from the values found by Pechetti et al. (2020) and question the presence of a tight correlation. Therefore, while the Spearman correlation coefficient evaluates the trend as significant ($p = 0.015$), we recommend against using the Sérsic index relation to parameterise NSCs.

3.4.4 Surface Brightness & Surface Mass Density Profiles

Combining the effective radius and stellar mass, we determine a mean surface density for the new detections. We show this parameter space in Figure 3.4, comparing the new detections with literature data from Norris et al. (2014) and Neumayer et al. (2020) for other NSCs, and with Baumgardt and Hilker (2018) for Milky Way GCs. For the newly detected NSCs, we fit the correlation using a linear function to find

$$\log_{10}\left(\Sigma_{\rm eff}/{\rm M_\odot\,pc^{-2}}\right) = \left(-2.72^{+0.61}_{-0.71}\right) + \left(1.13^{+0.13}_{-0.12}\right) \times \log_{10}\left(M_\star^{\rm nsc}/{\rm M_\odot}\right), \tag{3.5}$$

where the parameter values are determined through 10^5 bootstrap iterations. We note that although some of NSCs at $M_\star^{\rm nsc} \sim 10^8\,{\rm M_\odot}$ seem to follow this relation as well, their overall distribution get wider and seems to flatten. At the low-mass end, the newly detected NSCs overlap again with Galactic GCs. Note that about 65 % of these GCs fall above the best-fit relationship.

Next, we explore the surface brightness of the star clusters. Panel A of Figure 3.5 shows the surface brightness as a function of radius where the profiles relate to the Sérsic model fits from the *F814W* band. To highlight uncertainties, we plot the profiles of 100 out of 500 bootstrap iterations, which we used to determine statistical uncertainties (*c.f.* Section 3.7.1). Each set of profiles is colour-coded based on the host galaxy stellar mass.

Similarly, panel B shows the surface mass profile versus radius. We convert the profiles to stellar mass by using the mean colour of the NSCs. Note the assumption that the mass-to-light ratio is radially constant, which is not the case for higher mass NSCs in other Local Volume galaxies (e.g. Carson et al., 2015) and the Milky Way NSC (Feldmeier-Krause et al., 2015, 2017a). However, as a function of wavelength, the size or ellipticity does not differ significantly for the new detections and, therefore, using

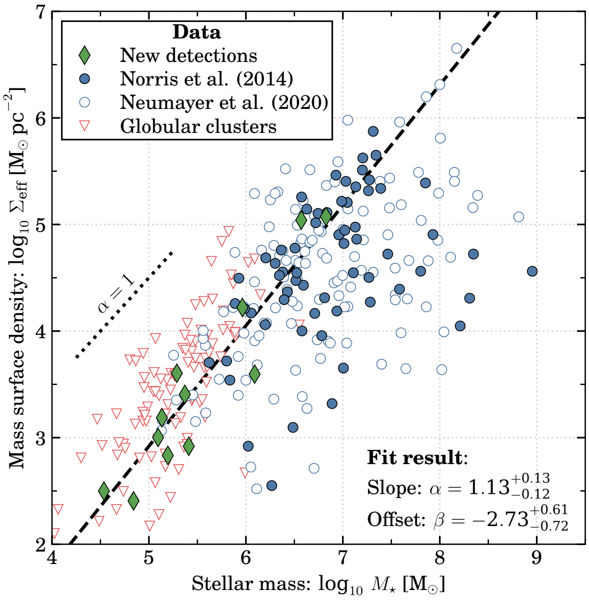

Figure 3.4. Mean stellar mass surface density within the effective radius (Σ_{eff}) versus cluster mass ($M_\star$). We compare the new detections (green diamonds) to other nuclear star clusters from Norris et al. (2014) and Neumayer et al. (2020), and to Milky Way globular clusters (Baumgardt & Hilker, 2018). The best-fit values of a linear relationship fit to the new detections, as determined through 10^5 bootstrap iterations, are indicated in the lower right corner.

the mean colour likely provides a decent estimate of their average stellar populations. The colour-coding of the profiles is the same as in panel A.

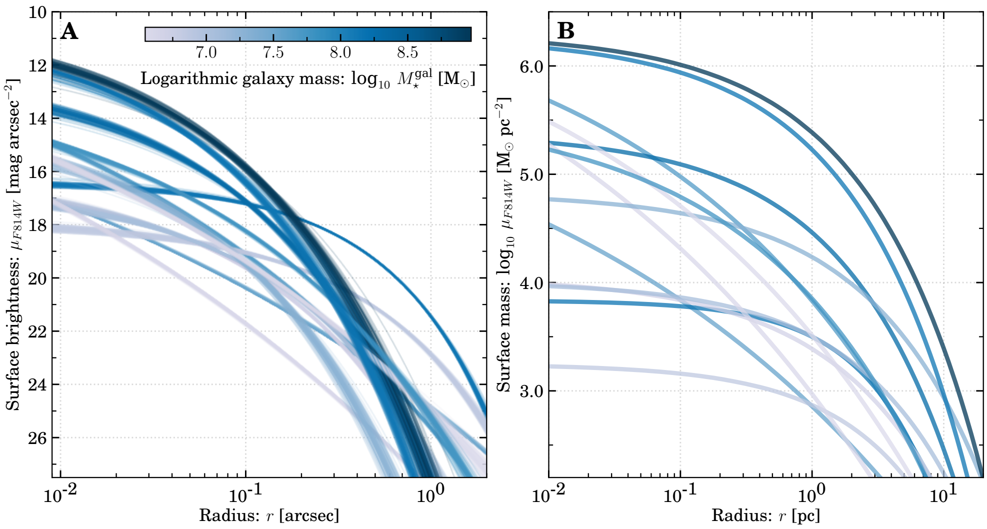

Figure 3.5. *Panel A*: Surface brightness in the *F814W* band (μ_{F814W}) versus radius (r) of the newly detected nuclear star clusters (NSCs). The profiles give the Sérsic models fit to the data. To highlight uncertainties, we show 100 profiles for each NSC, randomly drawn from a total of 500 bootstrap iterations. Each set of profiles is colour-coded by the stellar mass of the host galaxy where a darker colour corresponds to a more massive galaxy. *Panel B*: Surface mass density based on the *F814W* band versus radius. The conversion from the best-fit surface brightness profiles to mass profiles assumes a radially constant mass-to-light ratio. This assumption is invalid in higher-mass NSCs (Carson et al., 2015; Feldmeier-Krause et al., 2015, 2017a), which is why we show only a single profile for each NSC. The colour of the lines is the same as in panel A.

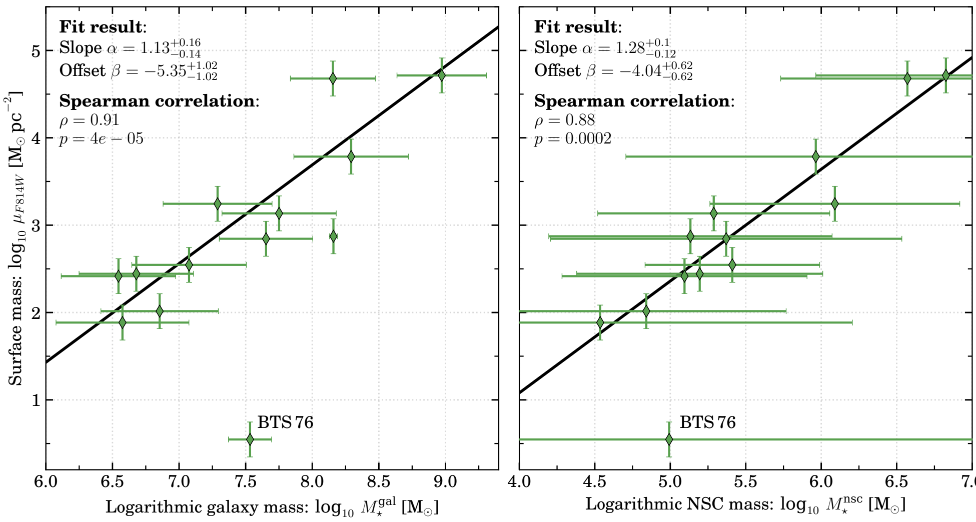

Figure 3.6. Surface mass profile evaluated at the nuclear star clusters effective radius versus host galaxy (*panel A*) and cluster stellar mass (*panel B*). Solid lines give the best-fit linear relation ($\log_{10} \mu = \alpha + \beta \times \log_{10} M_\star$) whose parameters, as determined through 10^5 bootstrap iterations, are indicated in the panels. In addition, we show the Spearman correlation parameter (ρ) and its associated p-value. BTS 76, as indicated, does not fit the overall trend and was excluded from the fits.

From both figures it becomes apparent that the surface brightness of the clusters positively correlates with the host galaxy stellar mass. To quantify this observation further, we show the surface mass profiles evaluated at the clusters' effective radii versus the host galaxy and NSC stellar masses in Figure 3.6. According to the Spearman correlation coefficients, we find a clear correlation between both quantities. A fit using a linear relationship yields

$$\log_{10}\left(\mu/\mathrm{M}_\odot\,\mathrm{pc}^{-2}\right) = \begin{cases} \left(1.13^{+0.16}_{-0.14}\right) - \left(5.3^{+1.0}_{-1.0}\right) \times \log_{10}\left(M/\mathrm{M}_\odot\right), \text{ for } M = M_\star^{\rm gal} \\ \left(1.29^{+0.10}_{-0.12}\right) - \left(4.05^{+0.62}_{-0.62}\right) \times \log_{10}\left(M/\mathrm{M}_\odot\right), \text{ for } M = M_\star^{\rm nsc} \end{cases}, \tag{3.6}$$

where the uncertainties are determined with 10^5 bootstrap iterations. Note that the slope value for the relation using the NSC mass is steeper than one. This is related to both the NSC versus host galaxy stellar mass relation (*c.f.* Section 3.4.5 below) and the observation that the effective radius decreases with increasing NSC mass for the new detections (*c.f.* Figure 3.3, panel B).

From both panels it is apparent that BTS 76 does not follow the relationship and was excluded from both fits. Compared to other NSCs, the effective radius of this nucleus is significantly larger. As discussed in Section 3.4.3, the NSC sub sample with large effective radii and low stellar masses may have evolved differently from the other clusters: if the cluster relaxes in a weaker tidal field (i.e. the outskirts of the host galaxy), its central density may drop while the total mass of the cluster remains roughly the same.

Note that Pechetti et al. (2020) investigated the three-dimensional density of high-mass NSCs in higher-mass galaxies finding a similar trend: the NSC density positively scales with the host galaxy stellar mass. Our data show that such a correlation appears to continue down to lower galaxy and NSC stellar masses, effectively extending the existence of a relation from $\log_{10}\left(M_\star^{\mathrm{gal}}/\mathrm{M}_\odot\right) \sim 11$ to $\log_{10}\left(M_\star^{\mathrm{gal}}/\mathrm{M}_\odot\right) \sim 6.5$.

3.4.5 NSC Stellar Mass versus Galaxy Stellar Mass

In this section we investigate the scaling relation between the NSC stellar mass and its host stellar mass. We combine literature data of the Local Volume, Georgiev and Böker (2014), and Carlsten et al. (2022) with our new detections to gain statistical significance. To this combined data set, we fit the function

$$\log_{10}\left(M_\star^{\mathrm{nsc}}/\mathrm{M}_\odot\right) = \alpha \times \log_{10}\left(M_\star^{\mathrm{gal}}/10^9\,\mathrm{M}_\odot\right) + \beta \quad , \tag{3.7}$$

which has also been used previously (Georgiev et al., 2016; Neumayer et al., 2020). To fit the data, we use the SCIPY implementation of the orthogonal distance regression, which takes into account uncertainties on both axes (see also Boggs & Rogers, 1990). The uncertainty on the stellar masses of literature data are assumed to be 0.3 dex if no value is provided. As the slope α of the relation in Equation 3.7 seems to steepen for galaxies above $M_\star^{\mathrm{gal}} \sim 10^{9.5}\,\mathrm{M}_\odot$ (Georgiev et al., 2016; Neumayer et al., 2020), we restrict the fit to $M_\star^{\mathrm{gal}} < 10^{9.5}\,\mathrm{M}_\odot$. Furthermore, from the fit we removed four NSCs (DDO 133, LV J1205+2813, NGC 5011C, and UGC 04998) as they have high stellar mass-to-light ratios ($M_\star/L_I \gtrsim 4\mathrm{M}_\odot/L_\odot$). The final uncertainties of the fit were determined via 10^5 bootstrap iterations.

Figure 3.7 shows the data set as well as the best-fit relationship for which we find $\alpha = 0.82^{+0.08}_{-0.08}$ and $\beta = 6.68^{+0.13}_{-0.13}$. This slope is steeper than what was found by Neumayer et al. (2020, $\alpha \sim 0.48$) who used data from various publications and a mix of environments. Restricting the fit to the high-mass end yielded a value of $\alpha \sim 0.92$, which agrees with a previously reported value (Georgiev et al., 2016) and our value.

Our results and the observation that the fit by Neumayer et al. (2020) is dominated by dwarfs in a dense cluster environment [Virgo (Sánchez-Janssen et al., 2019a) and Fornax (Ordenes-Briceño et al., 2018)] could suggest that the environment of the dwarf galaxies plays a role in the NSC versus host stellar mass relationship. To test this hypothesis, we add the data set of Sánchez-Janssen et al. (2019a), exploring the relationship for dwarfs in the core of the Virgo galaxy cluster. Only considering their data, we find $\alpha = 0.55^{+0.06}_{-0.05}$ and $\beta = 6.69^{+0.10}_{-0.09}$ using again 10^5 bootstrap iterations. As expected, the slope is comparable to the value found by Neumayer et al. (2020) but significantly smaller than the value for dwarfs in the field.

To check whether the origin for the difference between environments stems from the lowest mass galaxies, we repeat the fit to the Virgo cluster data set forcing $M_\star^{\mathrm{gal}} \geq 10^{6.5}\,\mathrm{M}_\odot$. This results in $\alpha = 0.70^{+0.08}_{-0.07}$ and $\beta = 6.83^{+0.13}_{-0.11}$. As the slope is now comparable to the one found for the field environment we conclude that the low-mass galaxies in the Virgo cluster, which host more massive NSCs than in the field, are responsible for environmental trends.

3.5 Discussion

We presented a comparison between the Milky Way GCs and the newly detected NSCs in the previous sections and argue in Section 3.5.1 that dissipationless GC migration

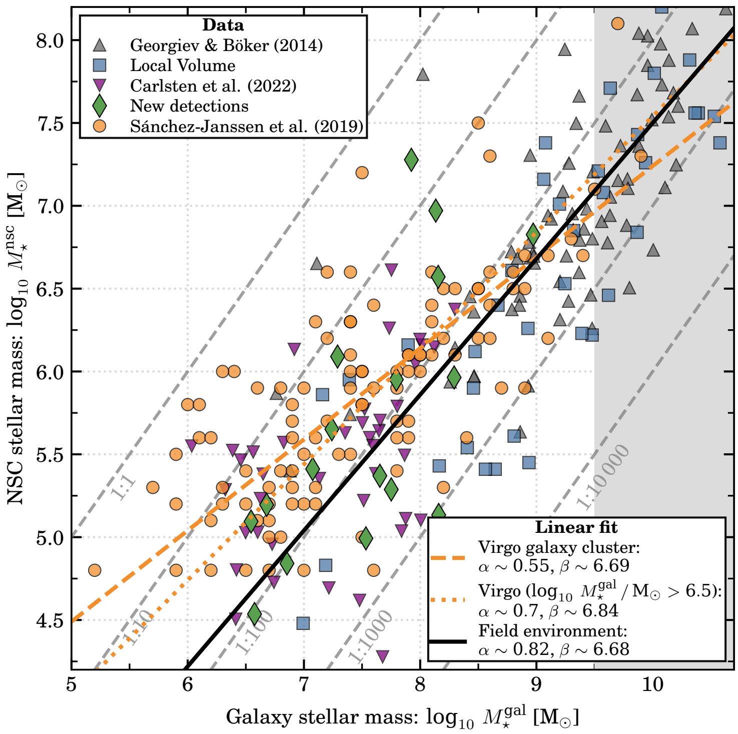

Figure 3.7. Nuclear star cluster (NSC) stellar mass ($M_\star^{\rm nsc}$) versus host galaxy stellar mass ($M_\star^{\rm gal}$) for the new detections (green diamonds), a compilation of Local Volume data (blue squares), massive late-type galaxies in the field (Georgiev & Böker, 2014, gray up-pointing triangles), dwarf galaxies around massive late-types (Carlsten et al., 2022, purple down-pointing triangles), and dwarfs in the core of the Virgo galaxy cluster (Sánchez-Janssen et al., 2019a, orange circles). Uncertainties are omitted for clarity. The combined data of new detections, other Local Volume, and field galaxies are fit with a linear relationship, such that $\log_{10}\left(M_\star^{\rm nsc}/\mathrm{M}_\odot\right) = \alpha \times \log_{10}\left(M_\star^{\rm gal}/10^9\,\mathrm{M}_\odot\right) + \beta$.

is the main formation scenario for NSCs in low-mass dwarf galaxies. Afterwards, in Section 3.5.2, we discuss whether the NSCs are a merger product of multiple GCs or whether they are not.

3.5.1 Formation Scenario

NSCs are believed to form via two mechanisms: at the low-mass end, GC migration appears to dominate the formation of NSCs (e.g. Tremaine et al., 1975; Hartmann et al., 2011; Antonini et al., 2015; Fahrion et al., 2022a) and *in-situ* star formation contributes only a small part to the mass budget, if at all. With increasing galaxy stellar mass *in-situ* star formation gains importance (e.g. Turner et al., 2012; Sánchez-Janssen et al., 2019a; Neumayer et al., 2020) and will eventually dominate over the GC migration scenario (Fahrion et al., 2021, 2022b).

We compared the structural properties of the newly detected NSCs with Milky Way GCs in Figures 3.3 and 3.4 finding a similarity between both systems. More specifically, the ellipticity, effective radius, stellar mass, and surface density of many of the new

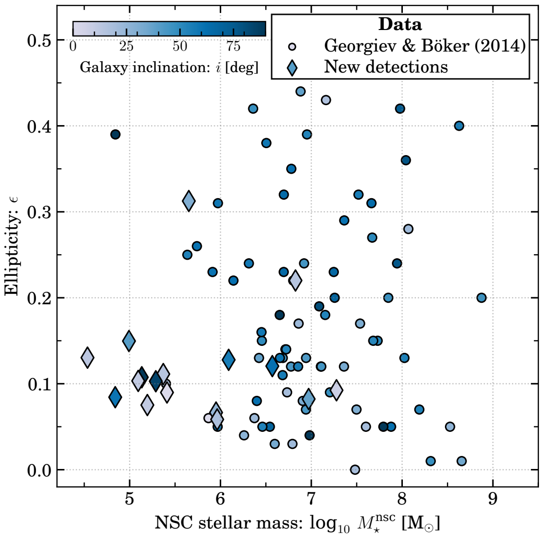

Figure 3.8. Ellipticity (ϵ) versus nuclear star cluster stellar mass ($M_\star^{\rm nsc}$). We show the new detections (diamonds) and compare with NSCs in massive late-type galaxies (Georgiev & Böker, 2014). Each data point is colour-coded by the inclination of the host galaxy.

detections matches the distribution of Milky Way GCs. As speculated in the literature already (e.g. Miller & Lotz, 2007; Sánchez-Janssen et al., 2019a), this is a direct hint that the dissipationless GC migration scenario is the main formation mechanism of these NSC.

We also found that the ellipticity remains roughly constant below $M_\star^{\rm nsc} \sim 10^{6.5}\,\mathrm{M}_\odot$ and starts to increase for higher mass clusters. An increase in ellipticity hints towards *in-situ* star formation as the in-falling gas is expected to form stars in a flattened disk due to its angular momentum. In observations, such a flattening has been observed in combination with young stellar populations in edge-on spiral galaxies (e.g. Seth et al., 2006). In simulations, Hartmann et al. (2011) showed that NSCs, which formed through repeated GC mergers, typically are not very flattened. Crucially, as we show in Figure 3.8, the measured ellipticity of the NSCs does not depend on the inclination of the host galaxy at all stellar masses.

As is shown in Figure 3.7, the NSC versus host galaxy stellar mass correlation appears to be affected by host environment with cluster members typically hosting more massive NSCs than field galaxies. We found that the difference is greatest at the low-mass end $M_\star^{\rm gal} \leq 10^{6.5}\,\mathrm{M}_\odot$ and becomes insignificant towards higher masses. If *in-situ* star formation is unimportant at the lowest galaxy stellar masses, the difference in NSC must arise from differences in the progenitor GCs.

There appear two possibilities to generate more massive NSCs:

1. The NSCs in dwarfs in dense environments experienced more GC merger events than NSCs in a field environment, elevating their masses. We discuss this option further in Section 3.5.2.
2. The difference in mass does not arise from a significant difference in mergers but from a difference in progenitor GC mass.

The argument that the progenitor GC is more massive in a dense environment relies on GC formation scenarios. The cluster formation efficiency (Bastian, 2008) positively correlates with the surface density of star formation (see Stahler, 2018, and references therein) and leads to an elevated mass fraction of stars in clusters. From observations it appears that this effect results in an increased number of GCs in present-day dwarf galaxies in galaxy clusters (e.g. Peng et al., 2008) and not in differences in the GC mass function (Carlsten et al., 2022). The GC luminosity function appears to be roughly equivalent between the environments (Figure 7 in Carlsten et al., 2022) but this may not be the case at high redshift (e.g. Parmentier & Gilmore, 2007; Kruijssen & Cooper, 2012).

If the GC mass function remains unchanged between environments at the time when the NSC formed, the NSC's mass may still be elevated due to the higher number of GCs produced in a dense environment. When drawn from the same distribution, a higher number of GCs correspond to a higher probability that the most massive GC in a galaxy in a dense environment is more massive than its counterpart in a galaxy in a loose environment.

We note that the differences in NSC stellar mass found at the low-mass end could also be related to selection bias. Our data rely on a catalogue of galaxies in the Local Volume (see Karachentsev et al., 2013, and references therein) while the Virgo cluster data of Sánchez-Janssen et al. (2019a) relies on a uniform set of imaging data (Ferrarese et al., 2012). The data of Carlsten et al. (2022) indicate that satellites around massive field galaxies, where a significant mass fraction is contained by the NSC, do exist but in fewer numbers than in the Virgo cluster. Whether this is also a selection effect is unclear. Note that it appears unlikely that higher-mass galaxies were stripped by ~ 1 dex in mass in the galaxy cluster while the NSC mass remains unchanged (e.g. Smith et al., 2016).

Truncated star formation during the galaxy infall may lead to a bias in the NSC versus galaxy mass relationship as well: asynchronous formation timescales of the NSC and its host galaxy leads to a higher cluster mass fraction if most cold gas is removed during infall. This effect could partly be responsible for both the observed environmental dependence of the stellar mass correlation as well as a higher NSC occupation fraction in dense environments (Leaman & van de Ven, 2022). Whether this effect can fully explain the observed environmental dependence remains unclear.

3.5.2 Are Our Newly Detected NSCs Merger Products of GCs?

A second method for forming NSCs is the process of repeated GC mergers. As mentioned in the previous section, at fixed galaxy stellar mass, the number of GCs is higher in a dense environment than in the field. Therefore, a present-day NSC in a galaxy in a dense environment could have experienced more GC mergers than in a loose environment, explaining its increased mass at the low-mass end of galaxies.

One argument in favor of this scenario is shown in Figure 3.4. We found that ~ 65 % of GCs fall above the mass density versus cluster mass relation. Antonini et al. (2012) and Antonini (2013) showed that the merger product of two GCs results in an increase in effective radius of the merger product where $r_{\mathrm{eff}} \propto \sqrt{M_\star}$. If two clusters merge in the density versus mass parameter space, their mass will increase but the overall density will drop, meaning that the data point moves towards the bottom right part in Figure 3.4. Therefore, as the Milky Way GCs are, on average, denser at the same stellar mass than our new detections, NSCs could be a merger product of multiple progenitor

GCs. However, given the uncertainties of the data points it is not possible to prove this scenario for individual objects.

If true in all environments, we would expect that the effective radius of NSCs in the core of the Virgo cluster are more extended than in the field environment, as they experienced more GC merger events. The data of the Next Generation Virgo Cluster Survey (Ferrarese et al., 2012) obtained with MegaCam (Boulade et al., 2003, March) have an effective resolution of ~ 50 pc, prohibiting an analysis of the NSC sizes (Ferrarese et al., 2020).

In a pure dissipationless merger scenario, the steepness of the slope of the cluster may not exceed that of its progenitors (Dehnen, 2005). The slope of the density profiles is determined by evaluating $\mathrm{d}\log_{10} I/\mathrm{d}\log_{10} r$ from Equation 3.1 and converting to $\mathrm{d}\log_{10} M_\star/\mathrm{d}\log_{10} r$ and using the mass-to-light ratio,

$$\frac{\mathrm{d}\log_{10}\, M_\star^{\mathrm{nsc}}}{\mathrm{d}\log_{10} r} = -\frac{\ln 10}{r_{\mathrm{eff}^2}}\frac{b_n}{n}\left(\frac{r}{r_{\mathrm{eff}}}\right)^{1/n} . \tag{3.8}$$

For the new detections, we find an increase in this slope but the trends are not significant. Based on a similar trend and a comparison to typical GC densities, Pechetti et al. (2020) concluded that *in-situ* star formation plays a key role in the formation and evolution of NSCs. For the majority of our clusters, it remains unclear whether *in-situ* star formation contributes to the mass budget at all. Fahrion et al. (2022a) showed that most of the mass fraction of NSCs in similar-mass galaxies comes from old, metal-poor stars but that *in-situ* star formation may still be present.

If low-mass NSC structure argues for GC merging as the primary formation channel, then at the highest NSC masses, we do see some evidence for in-situ formation. The two highest-mass NSCs in our sample are denser than the densest GCs, including Milky Way clusters (e.g. McLaughlin & van der Marel, 2005; Baumgardt & Hilker, 2018), and many ultra-compact dwarfs (e.g. Norris et al., 2014). This hints towards a contribution of *in-situ* star formation, supported by Fahrion et al. (2022b) who found that in-situ star formation gains importance for $\log_{10}\, M_\star^{\mathrm{nsc}}/\mathrm{M}_\odot \gtrsim 6.5$ and may contribute 50 % of the NSCs mass. The stochasticity of the contribution from *in-situ* star formation may also be related to the observed ~ 0.5 dex scatter in the NSC versus host galaxy mass relation at $M_\star^{\mathrm{gal}} \sim 10^8\,\mathrm{M}_\odot$. It is plausible, that the objects in this mass range are primarily a product of repeated GC mergers, but the steepening of the surface brightness profile slopes (Figure 3.5) and the large scatter in NSC masses at this galaxy stellar mass (Figure 3.7) may reflect the increased contribution from central in-situ star formation (see also Turner et al., 2012; Georgiev et al., 2016; Sánchez-Janssen et al., 2019a; Neumayer et al., 2020).

Combining all arguments, it appears to be clear that there is a fundamental connection between GCs and NSCs in these low-mass galaxies. Although likely, it remains unclear whether the lowest-mass NSCs are individual GCs, which experienced no merger events, or whether the NSCs are the product of GCs mergers. At least the two most-massive NSCs in our sample likely experienced *in-situ* star formation, elevating the steepness of their profile slopes and making them denser than any Milky Way GC.

3.6 Conclusions

In this work we presented an analysis of 21 newly discovered nuclear star clusters (NSCs) in Local Volume galaxies using *Hubble Space Telescope* imaging data. We convolved a *TinyTim*-generated point spread function with a Sérsic profile to determine structural parameters. NSC stellar masses were determined based on integrated photometry in different filters.

The new detections are compact with a typical effective radius $r_{\rm eff} \lesssim 12\,\rm pc$ and populate the lower stellar mass end of the whole NSC population at $M_\star^{\rm NSC} \lesssim 10^7\,\rm M_\odot$. We find that the correlation between $M_\star^{\rm nsc}$ and $r_{\rm eff}$ breaks down for the low-mass galaxies, as indicated by Georgiev et al. (2016). In addition to their compact size, the new detections have typically low- to moderate Sérsic indices ($n \lesssim 6$), which compares to other NSCs in the Local Volume. The linear relation between the ellipticity and the mass of the clusters break down below $M_\star^{\rm gal} \sim 10^{6.5}\,\rm M_\odot$ where the NSCs have ellipticities of $\epsilon \sim 0.1$. A comparison to Milky Way globular clusters (Harris, 1996; Baumgardt & Hilker, 2018) reveals that most of the newly detected NSCs have similar ellipticity, effective radius, and stellar mass, corroborating a relation between both types of clusters.

NSCs are the densest stellar systems (e.g. Walcher et al., 2005; Norris et al., 2014; Neumayer et al., 2020) and we find central surface brightness values ranging between ~ 18 and $\sim 12\,\rm mag\,arcsec^{-2}$ in the *F814W* band, corresponding to central surface masses of ~ 3.2 and $6.2\,\rm M_\odot\,parsec^{-2}$, respectively. We find that both the surface brightness and stellar mass profiles correlate with both the NSC and host galaxy stellar mass. Furthermore, the slope of the profiles evaluated at their effective radii weakly correlates with both the NSC and host galaxy stellar mass. A similar trend for three dimensional slope values was observed by Pechetti et al. (2020) for more massive NSCs. Our data reveal that this trend continues down to the lowest-mass nucleated galaxies.

Similar to the surface brightness profiles, the average surface mass density within the effective radius correlates with NSC stellar mass as well. A linear fit reveals that some denser and more massive NSCs follow the same trend, albeit their distribution widens and flattens towards higher masses. Comparing to Milky Way globular clusters, we find that about 65 % fall above the best-fit relation. Again, most of the lowest-mass NSCs coincide with the distribution of Milky Way globular clusters.

We investigated the scaling relation of NSC versus host galaxy mass. A linear fit revealed that the nucleated dwarfs in a field environment have a steeper relationship ($\alpha = 0.82^{+0.08}_{-0.08}$) than dwarfs in the core of the Virgo galaxy cluster ($\alpha = 0.55^{+0.06}_{-0.05}$ Sánchez-Janssen et al., 2019a). However, forcing $M_\star^{\rm gal} \geq 10^{6.5}\,\rm M_\odot$ for the fit results in a relationship with a steepness comparable to the value for dwarfs in the field environment ($\alpha = 0.70^{+0.08}_{-0.07}$). Therefore, the environmental dependence in the $M_\star^{\rm nsc}$-$M_\star^{\rm nsc}$ relation is caused by the lowest-mass nucleated galaxies.

Our results reinforce the connection between globular clusters and nuclear star clusters. They also corroborate other studies in that globular cluster migration is the main formation mechanism in dwarf galaxies and that *in-situ* star formation gains importance with increasing mass (e.g. Neumayer et al., 2020).

We find a clear environmental dependence, such that in low-mass galaxies, the NSCs are fractionally more massive in denser environments. We argue this extra mass is most likely explained by a larger pool of available GCs for mergers, or even just for becoming the NSC. On the flip side, the high stellar density of our two most massive NSCs suggest that in-situ formation, rather than merging, dominated their growth. This interpretation fits well with other recent research, which shows that the *in-situ* fraction of a nuclear star cluster increases with increasing stellar mass (Fahrion et al., 2022b, 2022a). Our data cannot reveal whether there also exists an environmental dependence in the correlation between the NSCs' *in-situ* fraction and stellar mass.

3.7 Appendix

3.7.1 Assessing Uncertainties

In this section we discuss statistical and systematic uncertainties and how we determined them. If applicable, the final 1σ uncertainties in the data tables consist of the sum of the quadratic statistical and systematic uncertainties.

Statistical Uncertainties

For each fit, we determine the statistical uncertainties via bootstrapping. During each iteration of bootstrapping *Imfit* generates a new data array where pixel values are re-sampled from the original data. The new data array is then fit using Levenberg-Marquardt minimisation to speed up the fit. We chose 500 bootstrap iterations which resulted in a "good-enough" sampling of the confidence intervals; increasing the value to 2500 iterations did not change the results.

The quoted uncertainties were determined by the 1σ distribution of the bootstrap results. However, to determine photometric parameter values and to convert the effective radius from pixels to parsecs, the uncertainties needed to be propagated forward. In the case of apparent magnitudes, we used the bootstrap distributions of all required parameter values to determine the total intensity of the NSC (*c.f.* Equation 3.2). The uncertainty on the zeropoint magnitude is small[7] compared to the uncertainty of the instrumental magnitude and was not taken into account. For the determination of colours, we used Gaussian error propagation by assuming that the distributions of apparent magnitudes follow a Gaussian distribution. We used the larger uncertainty of the asymmetric parameter distribution as the symmetric uncertainty of the assumed Gaussian-like distribution. For the apparent magnitudes, this choice seems to be justified, as shown by the symmetry of the uncertainties of the apparent magnitudes in Table 3.3. Afterwards, we determined absolute magnitudes and stellar masses via Gaussian error propagation. The same scheme was applied to transform effective radii from pixels to parsecs.

Systematic Uncertainties

To quantify systematic uncertainties in our work, we conducted various tests involving the choice of model functions and the programs *AstroDrizzle* and *TinyTim*. We will additionally discuss the correlation between the Sérsic index and the effective radius

[7] typically $\mathcal{O}(10^{-3}\,\mathrm{mag})$.

and the induced uncertainty by fixating the index in some of our fits. All fits were performed with *Imfit* and are independent of the chosen solver or fit statistic. Unless otherwise stated, we chose the data of NGC 2337 in the ACS/WFC $F814W$ band.

Model Functions We assumed that the NSCs can be represented well by a single Sérsic function but this choice is rather arbitrary. Complex substructures may be present in extragalactic NSCs but typically are unresolved given their distances and subsequent angular sizes on the *HST* instruments. Nevertheless, in some cases individual stars (e.g. [KK2000] 03) and extended emission around the NSC can be seen which are not well represented by a single Sérsic profile.

We repeated most fits using different model functions for the NSC. We chose a single King profile (King, 1962; King, 1966), a combination of a Sérsic profile and a point source, two Sérsic profiles where the second profile fits the extended emission, and two Sérsic profiles in combination with a point source. The addition of a point source to the fits was tested for all NSCs but did not yield different structural parameters. In most cases the intensity of the point source was insignificant compared to the intensity of the Sérsic profile at the effective radius, thus not adding significant flux to the total apparent magnitude.

Instead of using a Sérsic profile, we used a classical King profile to fit the NSC of LeG 09 in the ACS/WFC $F814W$ band. The boundaries for the core and tidal radii were set to $[0.01, 10]$ and $[0.01, 50]$. Fitting LeG 09 with a Sérsic profiles and using 500 bootstrap iterations resulted in $r_{\text{eff}}^{\text{sérsic}} = 3.19^{+0.12}_{-0.24}$ pixel. Repeating the fit with a King profile and using the transformation from Georgiev et al. (2019), which connects the core and tidal radii of the King profile with the effective radius, results in $r_{\text{eff}}^{\text{king}} = 3.05^{+0.06}_{-0.07}$ pixel. This value lies within the 1σ statistical uncertainty of the previous fit. Additionally, we added a second Sérsic profile to the fit resulting in a similar result: the flux of the fit with two profiles had a higher flux by $\sim 1.6\,\%$ which corresponds to a difference in magnitude of ~ 0.007 mag which is far below the statistical uncertainty. Therefore, based on this test, we conclude that the choice of a single Sérsic profile seems to be justified and that the systematic uncertainties induced by this choice are negligible.

Our fits also assume that a constant offset accounts for the underlying light profile (background and galaxy). The only two exceptions are UGC 01104 and UGC 09660 where a second Sérsic profile needed to be added for the galaxy component. Not including this second profile leads to a fit of the underlying galaxy profile and not the NSC. In all other cases, the assumption of local flatness may not be justified, especially for high surface brightness galaxies with complex central structures. For low surface brightness galaxies, $n \lesssim 1$ (e.g. Carlsten et al., 2022) and $r_{\text{eff}}^{\text{gal}} \gg r_{\text{eff}}^{\text{nsc}}$, and the assumption of local flatness seems justified. Additionally, we only consider the proximity of the NSC where the side length of the fitting area (e.g. 100 pixel) is considerably smaller than $r_{\text{eff}}^{\text{gal}}$. Also, as mentioned in Section 3.3.1, changing the extent of the fitting region does not change the fit results.

To test the systematic uncertainty induced by assuming local flatness, we considered NGC 2337 which features a prominent bar (*c.f.* Figure 3.1) and, thus, should be the most affected galaxy in the sample[8]. As shown in Figure 3.9, we selected a squared region of 1000 pixel centered on the NSC and applied a 2D Gaussian smoothing kernel with a standard deviation of 21 pixel to determine reliable parameter estimates. Point or compact sources do not drastically influence the fit due to the applied smoothing. Approximating the bar component with a Sérsic profile yields $n \sim 1.0$ and $r_{\rm eff}^{\rm bar} \sim 470$ pixel (third panel in Figure 3.9). We repeated the fit of the NSC on the original science product (i.e. without applying the smoothing kernel) while keeping all structural parameters for the Sérsic profile describing the bar component fixed. The fit resulted in $r_{\rm eff} = 1.01^{+0.12}_{-0.03}$ for the NSC, whereas we found $r_{\rm eff} = 1.11^{+0.12}_{-0.08}$ pixel in the fit without accounting for the bar. The difference in magnitude is ~ 0.02 mag and is smaller than the statistical uncertainty. Given these values we conclude that our assumption of local flatness is justified.

Finally, the structure of the underlying light distribution of the galaxy could depend on the filter used for fitting. We evaluated this potential issue by following Pechetti et al. (2020) who fit the NSC in the reddest filter and kept the structural parameters fixed in the bluer filters. For NGC 2337 we first fit the ACS/WFC *F814W* data followed by the *F606W* data. The fit on the *F606W* data with the structural parameters of the *F814W* yielded a difference in magnitude of ~ 0.12 mag which is larger than the statistical uncertainty on the magnitude. However, this magnitude is only used for determining the colour of the NSC and eventually the stellar mass where the uncertainty budget is dominated by the uncertainty on the stellar mass-to-light ratio (0.3 dex). Furthermore, while the galactic background might change, the structural properties of the NSC, such as the Sérsic index or effective radius, may change as well given the complexity of NSCs and potentially radially varying stellar populations (e.g. Georgiev & Böker, 2014, and Section 3.4.2). Finally, as discussed further in Section 3.7.1, the Sérsic index is unknown for this source and may change as a function of wavelength as well. In conclusion, we note that for the apparent magnitude in the *F606W* the found systematic uncertainty appears larger than the statistical uncertainty, but variations in NSC structure could be the origin of these differences. We decide to not follow the approach by Pechetti et al. (2020) and fit all filters independently of each other.

Tests on *AstroDrizzle* & *TinyTim* Using Simulated Data Other systematic uncertainties could be induced by either *AstroDrizzle* or *TinyTim*. To test the chosen settings for both programs, we generated mock NSC data using the `makeimage` function of *Imfit*.

Simulated NSCs were created by convolving a Sérsic profile with a *TinyTim*-generated PSF. We added a flat background component whose values were randomly drawn from a Gaussian distribution. To test the influence of the settings of *TinyTim*, we fed this model and the PSF to *Imfit* and tried to recover the initial Sérsic indices and effective radii. To test the influence of *AstroDrizzle*, we took the science data of NGC 2337 and normalised it. We then superimposed the simulated NSC at the location of the NSCs on each exposure and performed *AstroDrizzle*. Afterwards, the simulated NSC was obtained from the output image of *AstroDrizzle*. The *TinyTim*-generated PSF was processed in the same way. The output data of *AstroDrizzle* were fed to *Imfit* where we

[8]All other galaxies do not show such a bar and could be approximated by a single Sérsic profile.

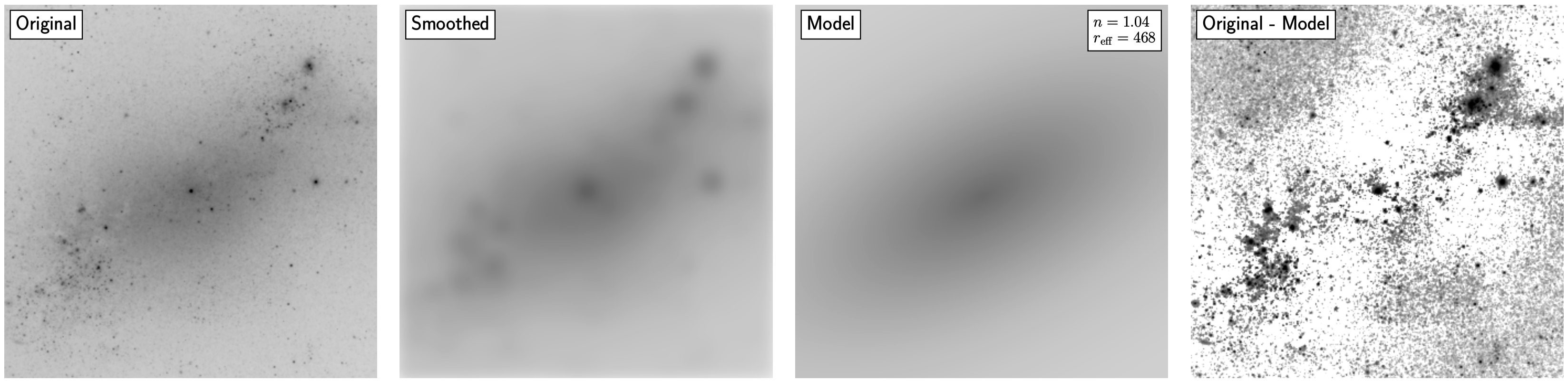

Figure 3.9. *First panel*: NGC 2337 ACS/WFC *F814W* data product centred on the nuclear star cluster. The square region has side length 1000 pixel which corresponds to ~ 2700 parsec. *Second panel*: Smoothed version of the data shown in the first panel. We smooth the data using a two dimensional Gaussian kernel with a standard deviation of σ = 21 pixel. *Third panel*: Fit to the smoothed data product shown in the second panel. We approximate the bar component with a Sérsic profile. The fit was performed with *Imfit* and the resulting Sérsic index n and effective radius $r_{\rm eff}$ are indicated in the top right corner. *Fourth panel*: Residual map showing the difference between the science data (first panel) and the model of the bar (third panel).

tried to recover the initial Sérsic index and the effective radius. We repeated the fits for different Sérsic indices and effective radii starting from $(n = 1, r_{\mathrm{eff}} = 10\,\mathrm{pixel})$ and going to $(n = 3, r_{\mathrm{eff}} = 2\,\mathrm{pixel})$ in steps of $\delta n = 1$ and $\delta r_{\mathrm{eff}} = -1$ pixel (i.e. 27 different settings). Two examples for the PSFs and the simulated NSCs are shown in the two left columns of Figure 3.10. The middle column shows two simulated NSCs convolved with the PSF and the right panels show the residual maps, including the recovered structural parameters and their uncertainties, as determined via 500 bootstrap iterations.

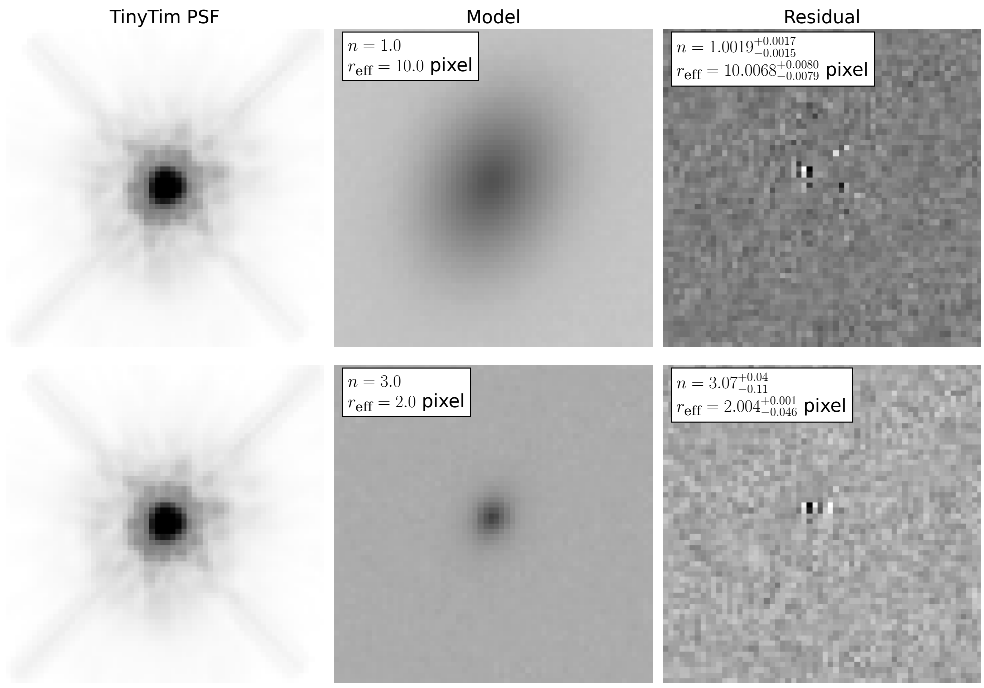

Figure 3.10. *Left panels*: *TinyTim*-generated PSFs using a `G2V` star as stellar template. The PSFs were superimposed on a normalised version of the science data of NGC 2337, processed with *AstroDrizzle* and extracted from the output image. Both PSFs are identical. *Middle panels*: 2D Sérsic profiles which have been convolved with the PSFs shown in the left panels. In addition, a flat background was added where the pixel values were randomly drawn from a Gaussian distribution. The top panel shows an extended profile whereas the bottom one is more compact and has a steeper centre, as indicated by the parameter values. The data processing with *AstroDrizzle* is equal to the approach used for the PSFs shown in the left panels. *Right panels*: Residual maps from fitting the Sérsic models (middle panels) using the PSFs shown in the left panels with *Imfit*. The structural parameters of the fit should equal the values used to generate the Sérsic models and are indicated in the central pictures.

If both the simulated NSC and the *TinyTim*-generated PSFs were not processed by *AstroDrizzle*, we recovered the initial structural parameter values for all combinations of n and r_{eff} to high precision. Once we include *AstroDrizzle* for both the simulated NSC and the PSF, while using the same settings as for the science data, the structural parameters are recovered within the 1σ interval. The agreement with the initial parameter values is best for large effective radii and small Sérsic indices and becomes worse with more compact sources and steep profiles.

The recovered parameters became worse once we did not process the PSF with *AstroDrizzle*. In this case the PSFs were directly taken from *TinyTim* and rotated according to the orientation of the *AstroDrizzle* output. The uncertainty of the fit became larger and, in the case of a compact source with a steep inner slope, we were unable to recover the Sérsic index within the 1σ uncertainty distribution. Therefore, a significant systematic uncertainty is induced if the *TinyTim*-generated PSF is not processed in the same way as the science data.

We also tested settings related to *TinyTim*. We generated different PSFs assuming stellar templates ranging from `F6V` ($V - I$ = 0.55 mag) to `K4V` ($V - I$ = 1.13 mag) which covers the colour-range of typical NSCs (*c.f.* Figure 3.11). Using these different PSFs on various science data yielded no significant differences in the resulting parameter values.

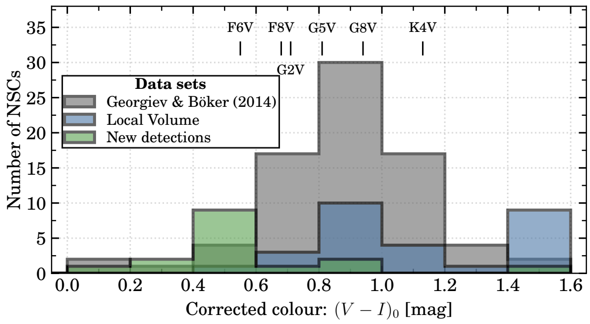

Figure 3.11. Nuclear star cluster $(V - I)_0$ colour. We compare our new detections (green) to other Local Volume data (blue) and the data set of Georgiev and Böker (2014) for nuclear star clusters in massive late-type field galaxies (gray). In addition, we highlight the colour of the different stellar templates tested for the synthetic point spread function. For the analysis in the main part of the paper, the template of a `G2V` star is used.

In addition, we evaluated whether the accuracy of placing PSFs onto normalised science data is an issue. More specifically, taking *TinyTim*-generated PSFs and superimposing them onto the normalised science data results in an accuracy of ±1 pixel. Therefore, we generated subsampled PSF (with subsampling factor ten), superimposed them on normalised single exposures (ACS/WFC data), processed the data with *AstroDrizzle*, resized the PSFs to the resolution of the science data, and applied the charge diffusion kernel. This approach should yield an accuracy of ~ 0.1 pixel. After fitting a few NSCs, we again found no significant differences and conclude that both the settings chosen in *TinyTim* and the uncertainty induced by placing PSFs onto normalised science exposures are insignificant.

Finally, we checked the modified *AstroDrizzle* parameters “pixel fraction” and “resolution”. As briefly discussed in Section 3.3.1, we chose a value of 0.75 for the pixel fraction and increased the final resolution according to the extent of the theoretical PSF for the ACS/WFC products. We conducted tests where we changed both the pixel fraction (between 0.5 and 1.0) and the final resolution [between 0.035 arcsec pixel^{-1} and 0.05 arcsec pixel^{-1} (original resolution)] but found no difference in the resulting parameter values. However, artifacts appeared in the weight maps of the data when choosing a low value for either the pixel fraction and resolution which indicate that *AstroDrizzle* cannot find input pixels from the individual exposures to generate a pixel value on the output grid. We verified that the different *AstroDrizzle* settings do not change the recovered structural parameter values of our mock data.

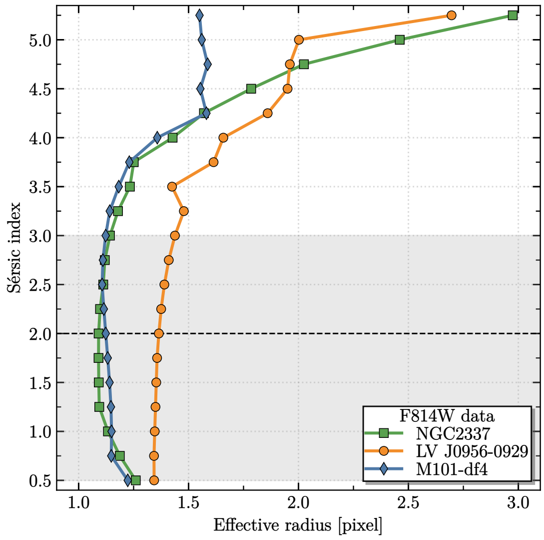

Figure 3.12. Fit results of three different nuclear star clusters (NGC 2337: green, LV J0956-0929: orange, M101-df4: blue) with fixed Sérsic indices. The dashed horizontal line shows the Sérsic value $n = 2$ used to obtain an approximate value for the effective radii of the NSCs. The gray shaded area shows the range of Sérsic values which we consider to be reasonable given the indices of quality zero fits (i.e. 'good' fits) presented by Pechetti et al. (2020).

In conclusion, we cannot find significant systematic uncertainties induced by our approach. Note that systematic uncertainties can become significant once the PSF is not processed in the same way as the science data.

Fixation of Sérsic Indices As discussed in Section 3.3.3, the Sérsic index of a few NSCs diverges. To be able to approximate the effective radius of the NSCs, we fixed the index to a value of $n = 2$. This value roughly equals the median value of the quality zero fits of the data set of Pechetti et al. (2020). We investigated the induced systematic uncertainty of this choice in Figure 3.12 where we show the Sérsic index versus effective radius. The plot shows three NSCs for which we repeated the fit with varying Sérsic indices. You can see that the effective radius is only slightly affected by the choice of Sérsic index between $n = 0.5$ and $n = 3.5$. At higher values of n the effective radius increases and appears to diverge towards higher values. The only exception is M 101-df4 for which r_{eff} appears to remain constant.

The figure shows that there exists a systematic uncertainty induced by fixing the Sérsic index to a value of $n = 2$. Therefore, we determine the largest differences between effective radius between $n = 0.5$ and $n = 3$ and add this value in quadrature to the larger statistical uncertainty obtained from bootstrap iterations. If the 'true' Sérsic index is larger than $n = 3$, our quoted effective radii become systematically too small, but as we show in Section 3.4.3, this issue does not affect our results.

Due to the choice of $n = 2$, the apparent magnitudes of the NSCs are affected as well. In our tests the difference in magnitude is typically $\delta m \sim 0.1$ mag when setting $n = 0.5$ and $n = 3$. Therefore, for the cases where we set $n = 2$ we add in quadrature to the statistical uncertainty the statistical uncertainty 0.1 mag.

Finally, we tested the effect of fixing $n = 2$ for the NSCs where the index did not diverge in the fits. Repeating the fits and using 500 bootstrap iterations we find typical differences of $\delta r_{\mathrm{eff}} \lesssim 5\,\%$ which is comparable to the statistical uncertainty.

3.7.2 Data Tables

Here we present the data tables underlying this article. Table 3.2 gives an overview of the galaxies hosting the newly discovered NSCs and their available *HST* data. Galaxy properties are adapted from Hoyer et al. (2021) and raw images, containing exposure information, are taken from the *HLA*. Table 3.3 presents properties of the newly discovered NSCs. Table 3.4 gives the parameters of other NSCs in the Local Volume and in Table 3.5 we present the NSC stellar mass estimates of the data sample of Georgiev and Böker (2014).

Table 3.2. List of 21 galaxies whose nuclear star clusters are new discoveries, sorted by descending galactic stellar mass. Galactic parameters (columns 2-5) are taken from Hoyer et al. (2021). The Proposal IDs and exposure times $t_{\rm exp.}$ are taken from the data products. For the ACS, we use an online calculator to obtain the zeropoint magnitudes: https://acszeropoints.stsci.edu/ For the WFPC2, we adopt the zeropoint magnitudes from the instrument's manual (McMaster et al., 2008). For the WFC3, we use an online data base: https://www.stsci.edu/hst/instrumentation/wfc3/data-analysis/photometric-calibration/uvis-photometric-calibration.

Name	RA	DE	dm	$\log_{10} M_\star$	Instrument	Filter	Proposal ID	$m_{\rm Inst.}$	$t_{\rm exp.}$	pixel scale
	[deg]	[deg]	[mag]	[M$_\odot$]				[VEGAmag]	[s]	[arcsec pixel^{-1}]
NGC 2337	105.55667	44.45694	30.37 ± 0.49	8.97 ± 0.34	ACS WFC	$F814W$ $F606W$	13442 13442	25.508 26.395	1000 1000	0.0472 0.0415
LV J0956-0929	149.15667	-9.48639	29.86 ± 0.11	8.29 ± 0.43	ACS WFC	$F814W$ $F606W$	12546 12546	25.512 26.398	900 900	0.0472 0.0415
[KK2000] 03	36.17792	-73.51278	26.50 ± 0.09	8.16 ± 0.03	ACS WFC	$F814W$ $F606W$	13442 13442	25.510 26.396	1200 1200	0.0472 0.0415
UGC 09660	235.28875	44.69806	30.16 ± 0.12	8.16 ± 0.32	ACS WFC	$F814W$ $F606W$	13442 13442	25.510 26.396	1000 1000	0.0472 0.0415
UGC 04998	141.30042	68.38306	28.58 ± 0.21	8.13 ± 0.23	WFPC2 PC	$F814W$ $F555W$	8137 8137	21.639 22.545	1500 1600	0.05 0.05
UGC 01104	23.17625	18.31583	29.39	8.00 ± 0.31	WFPC2 WF	$F814W$ $F300W$	9124 9124	21.659 19.433	80 600	0.1 0.1
LV J1205+2813	181.39250	28.23222	31.45	7.92 ± 0.43	ACS WFC	$F814W$ $F606W$	13750 13750	25.510 26.396	1218 1000	0.0472 0.0415
DDO 133	188.22083	31.53917	28.44 ± 0.05	7.80 ± 0.48	WFPC2 WF	$F814W$ $F606W$	10905 10905	21.659 22.896	2200 2200	0.1 0.1
UGC 07242	183.53083	66.09222	28.68 ± 0.03	7.75 ± 0.43	ACS WFC	$F814W$ $F606W$	9771 9771	25.525 26.414	900 1200	0.0472 0.0415
PGC 154449	149.28708	-9.26333	29.93	7.70 ± 0.39	ACS WFC	$F814W$ $F606W$	15922 15922	25.507 26.393	760 760	0.0472 0.0415
ESO 553-046	81.77375	-20.67806	29.13 ± 0.02	7.68 ± 0.63	ACS WFC	$F814W$ $F606W$	12546 12546	25.512 26.395	900 900	0.0472 0.0415

continued

Name	RA	DE	dm	$\log_{10} M_\star$	Instrument	Filter	Proposal ID	$m_{\mathrm{Inst.}}$	$t_{\mathrm{exp.}}$	pixel scale
	[deg]	[deg]	[mag]	[$M_\odot$]				[VEGAmag]	[s]	[arcsec pixel^{-1}]
DDO 084	160.67458	34.44889	29.99	7.65 ± 0.35	ACS WFC	$F814W$ $F606W$	15922 15922	25.507 26.393	760 760	0.0472 0.0415
BTS 76	179.68375	27.58500	30.50	7.53 ± 0.16	ACS WFC	$F814W$ $F606W$	14636 14636	25.509 26.395	1030 1030	0.0472 0.0415
M 101-df4	211.88917	54.71000	32.16	7.29 ± 0.41	ACS WFC	$F814W$ $F606W$	13682 13682	25.510 26.393	1150 1150	0.0472 0.0415
NGC 5011C	198.29958	-43.26556	27.86 ± 0.02	7.24 ± 0.53	ACS WFC	$F814W$ $F606W$	12546 12546	25.512 26.398	900 900	0.0472 0.0415
LeG 09	160.64417	12.15056	30.04 ± 0.07	7.08 ± 0.43	ACS WFC	$F814W$ $F606W$	14644 14644	25.509 26.395	1096 1026	0.0472 0.0415
[KK2000] 53	197.80917	-38.90611	27.33 ± 0.07	6.85 ± 0.44	ACS WFC	$F814W$ $F606W$	13442 13442	25.510 26.397	1000 1000	0.0472 0.0415
KK 96	162.61292	12.36083	30.00 ± 0.04	6.68 ± 0.43	ACS WFC	$F814W$ $F606W$	14644 14644	25.509 26.395	1096 1026	0.0472 0.0415
LV J1217+4703	184.29208	47.06361	30.70 ± 0.22	6.58 ± 0.50	ACS WFC	$F814W$ $F606W$	14644 14644	25.509 26.395	1164 1094	0.0472 0.0415
PGC 4310323	181.37917	31.07611	29.04	6.55 ± 0.43	ACS WFC	$F814W$ $F606W$	15922 15922	25.507 26.393	760 760	0.0472 0.0415
dw 1335-29	203.94167	-29.70667	28.50 ± 0.21	6.46 ± 0.43	ACS SBC	$F150LP$	10608	20.747	5416	0.03

Table 3.3. Structural and photometric parameters of the 21 newly discovered nuclear star clusters in the Local Volume. All values are the median of the parameter distribution after 500 bootstrapping iterations. The uncertainties give the 1σ interval.

Name	Filter	PA	ϵ	n	r_{eff}	m	$M_\star/L_I$	$\log_{10} M_\star$
		[deg]			[pc]	[mag]	[$\mathrm{M}_\odot\,\mathrm{L}_\odot^{-1}$]	[$\mathrm{M}_\odot$]
NGC 2337	$F814W$[b]	$97.2^{+6.3}_{-6.5}$	$0.22^{+0.05}_{-0.04}$	2.0	$3.00^{+0.99}_{-0.99}$	$17.56^{+0.05}_{-0.06}$	0.4 ± 2.0	6.83 ± 0.86
	$F606W$[b]	$90.6^{+6.3}_{-5.2}$	$0.22^{+0.05}_{-0.04}$	2.0	$2.91^{+1.01}_{-1.01}$	$18.40^{+0.03}_{-0.01}$		
LV J0956-0929	$F814W$[b]	53^{+20}_{-20}	$0.058^{+0.033}_{-0.026}$	2.0	$2.97^{+0.41}_{-0.41}$	$18.76^{+0.01}_{-0.01}$	0.69 ± 2.0	6.0 ± 1.3
	$F606W$[b]	80^{+39}_{-39}	$0.037^{+0.023}_{-0.022}$	2.0	$2.80^{+0.33}_{-0.33}$	$19.46^{+0.02}_{-0.01}$		
[KK2000] 03	$F814W$	$181.4^{+2.6}_{-3.1}$	$0.106^{+0.009}_{-0.008}$	$1.265^{+0.036}_{-0.033}$	$3.75^{+0.16}_{-0.16}$	$17.75^{+0.01}_{-0.01}$	0.92 ± 2.0	5.13 ± 0.94
	$F606W$	$179.8^{+2.6}_{-2.7}$	$0.102^{+0.007}_{-0.007}$	$1.213^{+0.029}_{-0.030}$	$3.64^{+0.15}_{-0.15}$	$18.51^{+0.01}_{-0.01}$		
UGC 09660	$F814W$[b]	123^{+13}_{-12}	$0.121^{+0.045}_{-0.038}$	2.0	$2.32^{+0.57}_{-0.57}$	$17.89^{+0.02}_{-0.02}$	1.0 ± 2.0	6.57 ± 0.84
	$F606W$[b]	127^{+11}_{-12}	$0.126^{+0.039}_{-0.031}$	2.0	$2.9^{+1.3}_{-1.3}$	$18.65^{+0.03}_{-0.01}$		
UGC 04998	$F814W$[b],[c]	93^{+25}_{-30}	$0.082^{+0.046}_{-0.037}$	2.0	$1.12^{+0.35}_{-0.35}$	$18.40^{+0.03}_{-0.01}$	19 ± 2	6.97 ± 0.10
	$F555W$[b],[c]	123^{+22}_{-10}	$0.080^{+0.053}_{-0.040}$	2.0	$1.08^{+0.34}_{-0.34}$	$20.31^{+0.06}_{-0.03}$		
⋮								

[a] The structural parameters in this filter were fixed to the values determined via bootstrapping in the other available filter.
[b] The Sérsic index is fixed to $n = 2$ to determine an effective radius. All other parameters are unrestricted (*c.f.* Table 3.1).
[c] The NSC mass estimate is unreliable as the mass-to-light ratio is too large ($M_\star/L_I \gtrsim 4\mathrm{M}_\odot/\mathrm{L}_\odot$).
[d] No fit was possible.

Table 3.4. List of compiled properties of known nuclear star clusters (NSCs) in the Local Volume. Only NSCs with available structural parameters are included.

Name	PA_{F606W}	ϵ_{F606W}	n_{F606W}	$r_{\mathrm{eff},\,F606W}$	PA_{F814W}	...	$(V-I)_0$	$\log_{10} M_\star$	Reference[a]
	[deg]			[pc]	[deg]		[mag]	[$M_\odot$]	
Circinus	--	--	--	--	$160.8^{+5.7}_{-5.7}$	...	1.5	$7.57^{+0.11}_{-0.11}$	13
DDO 042	--	--	--	--	$115.6^{+4.0}_{-9.0}$	...	--	--	7
DDO 082	$154.8^{+3.7}_{-4.0}$	$0.15^{+0.01}_{-0.01}$	--	$0.3^{+0.0}_{-0.0}$	$148.1^{+14.8}_{-13.4}$	...	$0.94^{+0.01}_{-0.01}$	$5.97^{+0.24}_{-0.24}$	7
DDO 088	--	--	--	--	$34.4^{+0.6}_{-0.1}$	...	$1.09^{+0.01}_{-0.01}$	--	7
ESO 059-001	--	--	--	--	--	...	--	6.16	6
⋮									

[a] References: (1) Baldassare et al. (2014); (2) Bellazzini et al. (2020); (3) Calzetti et al. (2015); (4) Carson et al. (2015); (5) Crnojević et al. (2016); (6) Georgiev et al. (2009b); (7) Georgiev and Böker (2014); (8) Graham and Spitler (2009); (9) Kormendy and Bender (1999); (10) Kormendy et al. (2010); (11) Nguyen et al. (2017); (12) Nguyen et al. (2018); (13) Pechetti et al. (2020); (14) Schödel et al. (2014b); (15) Seth et al. (2006)

Table 3.5. List of V- and I-band apparent magnitudes and stellar mass estimates of nuclear star clusters (NSCs) in the galaxy sample of Georgiev et al. (2016). NSC structural parameters are presented in the data tables of Georgiev and Böker (2014).

Name	$m - M$	m_V	m_I	$\log_{10} M_\star$
	[mag]	[mag]	[mag]	[$M_\odot$]
DDO 078	27.71 ± 0.03	19.44 ± 0.01	18.51 ± 0.01	5.87 ± 0.25
ESO 138-010	30.9 ± 1.1	--	--	--
ESO 187-051	31.32 ± 0.89	--	--	--
ESO 202-041	30.58 ± 0.58	--	--	--
ESO 241-006	31.32 ± 0.87	--	--	--
⋮				

3.8 Chapter Summary

- ▹ This work analysed 19 newly discovered NSCs in nearby dwarf galaxies with archival *HST* data.
- ▹ The analysis significantly increases the number of available structural information of NSCs in dwarf galaxies, reaching down to galaxy masses of $\approx 10^{6.5}\,M_\odot$.
- ▹ There exists no apparent difference in structure or photometry between these NSCs and GCs in the Milky Way, supporting the tight link between the formation mechanism of both systems.
- ▹ For the first time the data reveal a dependence of the M_{gal}-M_{NSC} relationship as a function of environment where, in the dwarf galaxy regime, NSCs in a dense galaxy cluster environment are more massive than their counterparts in galaxies located in a field environment.
- ▹ Despite the clear link between NSCs and GCs it remains unknown whether NSCs in dwarf galaxies typically form via GC mergers or *in-situ* as a random realisation of the cluster initial mass function.

Chapter 4

The Heart of M 74

Declaration

The contents of this chapter were previously published in Hoyer et al. (2023b). All co-authors provided commentary that improved the published work and contributed to the comparison between the NSCs of M 74 and the Milky Way. A. K. Leroy assisted with calculations of the upper limit for the gas mass in the centre of M 74.

Abstract

We combine archival *HST* and new *JWST* imaging data, covering the ultraviolet to mid-infrared regime, to morphologically analyze the nuclear star cluster (NSC) of M 74, a grand-design spiral galaxy. The cluster is located in a 200 pc × 400 pc cavity, lacking both dust and gas. We find roughly constant values for the effective radius ($r_{\rm eff}$ ~ 5 pc) and ellipticity (ϵ ~ 0.05), while the Sérsic index (n) and position angle (PA) drop from n ~ 3 to ~ 2 and PA ~ 130 to 90°, respectively. In the mid-infrared, $r_{\rm eff}$ ~ 12 pc, ϵ ~ 0.4, and n ~ 1-1.5, with the same PA ~ 90°. The NSC has a stellar mass of $\log_{10}\left(M_\star^{\rm nsc} / \mathrm{M}_\odot\right) = 7.06 \pm 0.31$, as derived through $B - V$, confirmed when using multi-wavelength data, and in agreement with the literature value. Fitting the spectral energy distribution, excluding the mid-infrared data, yields a main stellar population's age of (8 ± 3) Gyr with a metallicity of $Z = 0.012 \pm 0.006$. There is no indication of any significant star formation over the last few Gyr. Whether gas and dust were dynamically kept out or evacuated from the central cavity remains unclear. The best-fit suggests an excess of flux in the mid-infrared bands, with further indications that the center of the mid-infrared structure is displaced with respect to the optical center of the NSC.

4.1 Introduction

Nuclear star clusters (NSCs) are massive and compact stellar systems in galactic nuclei. The effective radii range from a few to tens of parsecs. Such radii are typical of globular clusters and ultra-compact dwarfs (e.g. Georgiev & Böker, 2014; Norris et al., 2014; Pechetti et al., 2020). Stellar masses may reach up to $10^9\,\mathrm{M}_\odot$ (e.g. Georgiev et al., 2016), which, in combination with the small effective radii, lead to core-densities that can approach $\lesssim 10^8\,\mathrm{M}_\odot\,\mathrm{pc}^{-3}$ (e.g. Stone et al., 2017) effectively making NSCs the densest stellar systems known (see Neumayer et al., 2020, for a review).

The formation and growth of NSCs depends on host galaxy mass (Fahrion et al., 2021), and potentially morphological type (Pinna et al., 2021). Two main scenarios have been proposed in the literature: dissipationless globular cluster (GC) migration dominates in the dwarf galaxy regime ($M_\star^{\mathrm{gal}} < 10^9\,\mathrm{M}_\odot$ Tremaine et al., 1975; Capuzzo-Dolcetta, 1993; Agarwal & Milosavljević, 2011; Hartmann et al., 2011; Arca Sedda & Capuzzo-Dolcetta, 2014; Antonini et al., 2015; Fahrion et al., 2020b, 2022b, 2022a) and *in-situ* star formation in more massive galaxies (Milosavljević, 2004; Bekki et al., 2006; Bekki, 2007; Turner et al., 2012; Sánchez-Janssen et al., 2019a; Neumayer et al., 2020). The latter scenario requires gas inflow, which may be caused by non-axisymmetric potentials (for example bars Shlosman et al., 1990), dynamical friction of star-forming clumps (e.g. Bekki et al., 2006; Bekki, 2007), supernova driven turbulence (e.g. Sormani et al., 2020; Tress et al., 2020), or rotational instabilities of the disk (Milosavljević, 2004). Once the gas settles at the center of the cluster and cools off, star formation begins, leading to the observation of young stellar populations (e.g. Rossa et al., 2006; Walcher et al., 2006; Seth et al., 2008b; Kacharov et al., 2018; Fahrion et al., 2021; Hannah et al., 2021) and structural variations, such as a wavelength-dependent effective radius (Georgiev & Böker, 2014; Carson et al., 2015). Young stellar populations were also directly observed in various nuclei, including the Milky Way's NSC (e.g. Seth et al., 2006, 2008b; Do et al., 2009; Genzel et al., 2010; Carson et al., 2015; Feldmeier-Krause et al., 2015; Kacharov et al., 2018; Nguyen et al., 2019; Hannah et al., 2021; Henshaw et al., 2022). A combination of both GC migration and *in-situ* star formation is also possible if the infalling GC keeps a gas reservoir and continues star formation during inspiral (Guillard et al., 2016). Corroborated by scaling relations between cluster properties and their host galaxies (e.g. Ferrarese et al., 2006; Seth et al., 2008b; Erwin & Gadotti, 2012; Scott & Graham, 2013; Ordenes-Briceño et al., 2018; Sánchez-Janssen et al., 2019b), studying nuclear clusters in detail reveals both their formation history as well as that of their host galaxy. Drawing this connection in M 74 is one of the goals of this work.

NSCs appear frequently, albeit not ubiquitously, at galaxy masses of 10^9-$10^{10}\,\mathrm{M}_\odot$ in various environments (Côté et al., 2006; Turner et al., 2012; Baldassare et al., 2014; den Brok et al., 2014; Neumayer et al., 2020; Hoyer et al., 2021). While this fraction decreases towards higher galaxy masses, there are indications that it drops at a slower rate for late-type galaxies compared to early-types (Neumayer et al., 2020; Hoyer et al., 2021). A majority of NSCs in high-mass galaxies were discovered in spiral galaxies (e.g. Carollo & Stiavelli, 1998; Böker et al., 2002), likely due to high central luminosities of massive elliptical galaxies.

One example for a nucleated, massive ($M_\star^{\mathrm{gal}} \sim 2 \times 10^{10}\,\mathrm{M}_\odot$ Leroy et al., 2021) galaxy is M 74 (NGC 0628), the object of this study. The NSC was analyzed previously by Georgiev and Böker (2014) using *Hubble Space Telescope* (*HST*) WFPC2 imaging data, but no in-depth analysis of all available high-resolution data has been performed yet. With the advent of the *James Webb Space Telescope* (*JWST*) earlier this year, we aim to study the NSC of M 74 across the optical and infrared regimes, analyzing both its structural and photometric properties.

This grand-design spiral galaxy is located at a distance of $d = (9.84 \pm 0.63)\,\mathrm{Mpc}$

(McQuinn et al., 2017; Anand et al., 2021) at the edge of the Local Volume ($\lesssim$ 11 Mpc). Both its relatively isolated position (e.g. Briggs et al., 1980) and nearly face-on orientation ($i \sim 8.9°$; Lang et al., 2020) make the galaxy an optimal test-case for detailed studies of galactic disks, and star- and cluster-formation in massive late-types (see e.g. Elmegreen & Elmegreen, 1984; Condon, 1987; Grasha et al., 2015; Adamo et al., 2017; Mulcahy et al., 2017; Kreckel et al., 2018; Sun et al., 2018; Schinnerer et al., 2019; Vílchez et al., 2019; Zaragoza-Cardiel et al., 2019; Chevance et al., 2020; Yadav et al., 2021).

Figure 4.1 shows an overview of the innermost 20 arcsec × 20 arcsec (approximately 950 pc × 950 pc) of M 74. Corroborated by *AstroSat* UV, *MUSE* Hα (Emsellem et al., 2022), and *ALMA* CO maps (Leroy et al., 2021), the *HST* and *JWST* data reveal a spheroidal component, dust and gas reservoirs along prominent spiral arm structures, and star-forming regions. Instead of continued spiral arms down to the smallest scales, a central cavity of approximately 200 pc × 400 pc lacking both gas and dust is present. The NSC of M 74 appears as a prominent bright source in the center of the galaxy.

Secular evolution plays a key role in the history of M 74, as indicated by the presence of a circum-nuclear region of star formation with radius ~ 25 arcsec (~ 1.2 kpc; Sánchez et al., 2011). While the formation of such a region can be related to the presence of a bar (Piner et al., 1995; Sakamoto et al., 1999; Sheth et al., 2005; Fathi et al., 2007; Sormani et al., 2015; Spinoso et al., 2017; Bittner et al., 2020), as argued to be present in M 74 by Seigar (2002) and Sánchez-Blázquez et al. (2014), more recent work finds that M 74 does not contain an obvious bar (Querejeta et al., 2021), despite an observed metallicity gradient, which is related to mixing of gas induced by a bar-structure in other late-type galaxies (Friedli & Benz, 1995; Martin, 1995; Dutil & Roy, 1999; Scarano & Lépine, 2013). If not by a bar, the presence of a circum-nuclear region of star formation may also be caused by past minor mergers, as speculated for other unbarred late-types by Sil'chenko and Moiseev (2006). Indeed, dwarf galaxies are known to exist around M 74 (Davis et al., 2021). It is also plausible that the galaxy hosted a bar in the past, which was destroyed by minor mergers (Cavanagh et al., 2022).

The large, approximately 200 pc × 400 pc large, central cavity remains challenging to explain. Currently, it is unclear whether inflow of gas and dust is prohibited dynamically, or whether the material has been expelled by star formation, supernovae, or a previously accreting massive black hole. As motivated above, the NSC properties may inform us on the evolution of M 74, if studied in detail. Therefore, one of the goals of this study is to relate the NSC properties to the evolution of its host galaxy.

In this work, we combine archival *HST* and newly obtained *JWST* imaging data to study the NSC of M 74 in great detail. Our data extend from the ultraviolet to the mid-infrared regime (see Figure 4.2 and Table 4.1) and are of high-enough resolution to resolve the cluster at all wavelengths. This study presents the first analysis of an NSC with *JWST* data and highlights the telescope's scientific value for studies of galactic nuclei in the local Universe. Using the available data, we derive photometric and structural parameters for all bands, and model the spectral energy distribution of the NSC.

We introduce the data from both space telescopes in Section 4.2 and briefly discuss the data processing pipelines as well as the generation of synthetic point spread functions. Image analysis is described in Section 4.3 and the main analysis steps are detailed in Section 4.4. The results of the study are discussed in Section 4.5. We conclude in Section 4.6.

4.2 Data

Our analysis is based on archival *HST* ACS & WFC3 taken from the *Hubble Legacy Archive*[1] and recently obtained *JWST* NIRCam & MIRI imaging data (Project ID 02107, PI J. Lee; see Lee et al., 2023). A brief overview of the available data is given in Table 4.1 and Figure 4.2. In the next three subsections we briefly describe the data processing for each instrument, followed by the generation of point spread functions.

4.2.1 *Hubble Space Telescope*

We obtain all available flat-fielded single exposures from the *HLA* to combine them into a single master frame. As a first step, the world coordinate systems of the ACS & WFC3 received updates using the latest reference files. These updated files were fed to *AstroDrizzle* (Fruchter & Hook, 1997; Fruchter et al., 2010; Gonzaga et al., 2012), which combines them into a master science product given user-specified settings. As tested and justified in other work (Hoyer et al., 2023a), we chose a pixel fraction of 0.75 but keep the pixel scale at their original resolutions (see Table 4.1).[2] No additional sky subtraction was performed as we account for background flux from the galaxy with a Sérsic profile (Sérsic, 1968) and a plane offset.

4.2.2 *James Webb Space Telescope*

As part of the "Physics at High Angular resolution in Nearby GalaxieS" (PHANGS) *JWST* Cycle 1 treasury program, M 74 was observed in various NIRCam and MIRI bands on July 17, 2022 [see Table 4.1, and also Lee et al. (2023)]. Data reduction and co-addition were carried out using a custom data reduction pipeline, which among other things, improves the astrometric solutions and zero point offsets compared to the publicly available data products. More specifically, the world coordinate system (WCS) was updated to match the one from the *HST* and *Gaia*, and overall background level were calibrated against e.g. *IRAC4* 8 µm and *WISE3* 12 µm fluxes (Leroy et al., 2023). More detail of the customized version of the data reduction pipeline will be presented in Lee et al. (2023).

4.2.3 Point Spread Functions

For all bands, we used artificially generated point spread functions (PSFs) instead of determining them from non-saturated stars in the images. The main reason for this choice was that no star is unaffected by dust and falls close to the location of the NSC (see Figure 4.1). Especially the latter condition is important for *HST* data as the PSF is known to vary significantly across the whole chip.

[1] URL: https://hla.stsci.edu/

[2] The pixel fraction controls how individual exposures are added: a value of zero corresponds to pure interlacing whereas a value of one results in a "shift-and-add" style of pixel values.

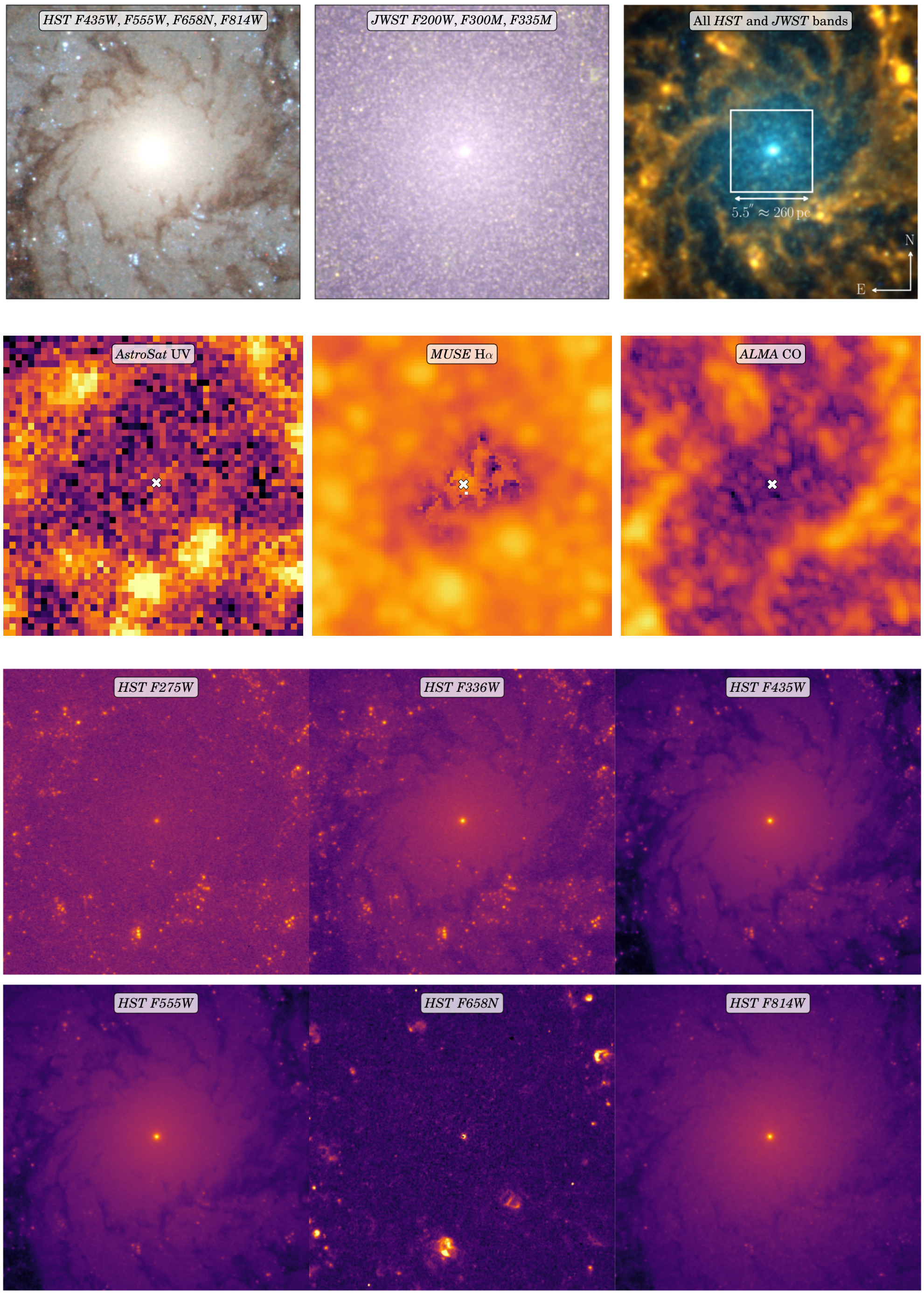

HST F435W, F555W, F658N, F814W
JWST F200W, F300M, F335M
All HST and JWST bands
5.5″ ≈ 260 pc
N
E
AstroSat UV
MUSE Hα
ALMA CO
HST F275W
HST F336W
HST F435W
HST F555W
HST F658N
HST F814W

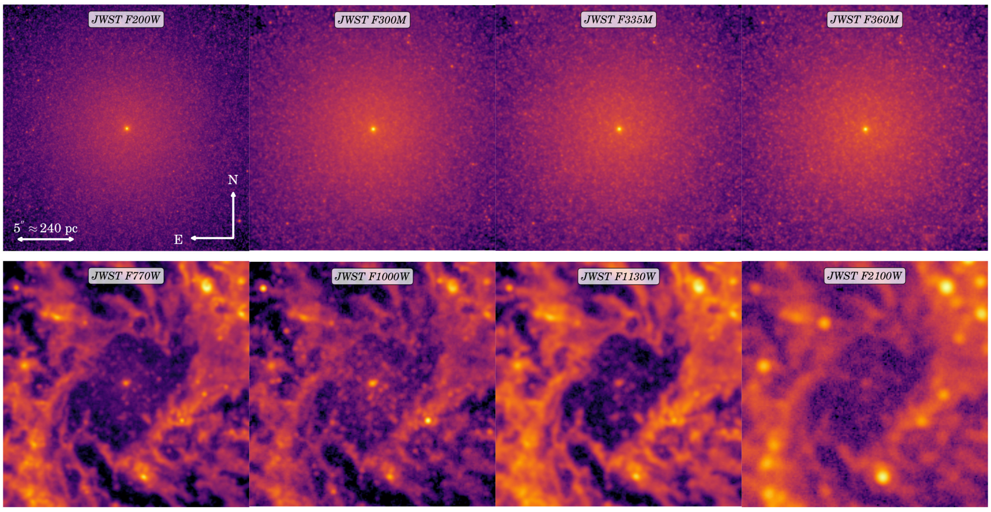

Figure 4.1. Overview of the nuclear region of M 74 in different bands. Each panel gives the central 20 arcsec × 20 arcsec (approximately 950 pc × 950 pc) of the galaxy, centered on the nuclear star cluster. North is up and East is to the left. Color correlates with intensity. The *first row* gives three color-images using *HST* and *JWST* bands, highlighting star-formation by using the continuum-subtracted *HST* ACS *F658N* (Hα) filter. Dust lanes, where star formation occurs, are clearly visible in the first and third panel, while only stellar emission is shown in the second panel. The squared box of side length 5.5 arcsec in the third panel shows the region we considered for the fit of the NSC. The *second row* highlights other available data sets, namely the *AstroSat* ultraviolet emission, *MUSE* Hα, and *ALMA* CO. The first two panels trace again star formation whereas the third panel shows the location of the molecular gas. Note the absence of star formation and gas in the immediate vicinity of the nuclear star cluster, which is marked with a white cross. The *third* and *fourth rows* show the *HST* data, increasing in wavelength. Star forming regions, identified in the *HST* WFC3 *F275W*, become hidden behind dust filaments in other bands. The sixth panel, showing the *HST* ACS *F814W* data, mainly shows stellar emission. We show the newly obtained *JWST* NIRCam (*fifth*) and MIRI (*sixth*) in the last two rows, again in increasing wavelength from the near-infrared to the mid-infrared. The NIRCam data highlights the stellar emission while the MIRI data shows both stellar and dust emission. As for the molecular gas (*ALMA* CO, second row), a central cavity exists and dust is present in the spiral arms of M 74.

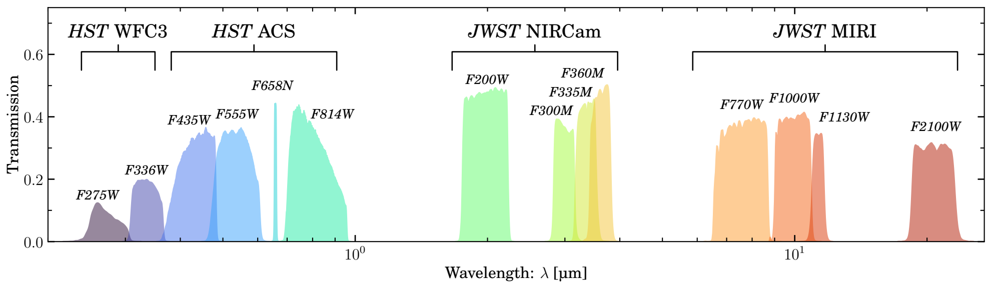

Figure 4.2. Transmission of the *HST* and *JWST* bands.

Table 4.1. *HST* and *JWST* data to analyse M 74.

Instrument	Channel	Filter	PropID	t_{exp} [s]	pixel scale[a] [arcsec pixel^{-1}]
HST	WFC3	*F275W*	13 364	4962.00	0.040
HST	WFC3	*F336W*	13 364	4962.00	0.040
HST	ACS	*F435W*	10 402	2716.00	0.050
HST	ACS	*F555W*	10 402	1716.00	0.050
HST	ACS	*F658N*	10 402	2844.00	0.050
HST	ACS	*F814W*	10 402	1844.00	0.050
JWST	NIRCam	*F200W*	2107	9620.16	0.031
JWST	NIRCam	*F300M*	2107	773.048	0.063
JWST	NIRCam	*F335M*	2107	773.048	0.063
JWST	NIRCam	*F360M*	2107	858.944	0.063
JWST	MIRI	*F770W*	2107	266.40	0.110
JWST	MIRI	*F1000W*	2107	366.30	0.110
JWST	MIRI	*F1130W*	2107	932.412	0.110
JWST	MIRI	*F2100W*	2107	965.712	0.110

[a] Original pixel values, which remained unchanged during data processing.

Following the approach by Hoyer et al. (2023a), PSFs were generated using *TinyTim* (Krist, 1993, 1995) for *HST* bands. To minimize systematic differences in data processing, we did not directly use the resulting PSF from *TinyTim* for deriving the structural properties. Instead, we copied all input science frames and set their first header extension (science data) to zero. We then generated PSFs at the location of the NSC on each individual exposure and placed them into the previously normalized frames, taking into account the orientation of the original science images. Afterwards, we repeated the *AstroDrizzle* processing for the normalized frames in the same way as for the science data. The final PSF was extracted from the output of *AstroDrizzle*. In comparison to a PSF from *TinyTim*, the core of the extracted PSF is slightly more extended due to the drizzling process. Taking this effect into account is important for deriving accurate effective radii, as detailed in Hoyer et al. (2023a).

Generation of PSFs for *JWST* bands was performed with *WebbPSF* (Perrin et al., 2012, 2014). To generate a star at the location of the NSC, we first generated a grid of 36 PSFs for the detector elements where the position of the NSC falls upon. The PSF for the position of the NSC was evaluated based on interpolation of generated PSFs using *WebbPSF*. This step is crucial as the PSF of *JWST* varies in both the spatial and temporal dimension (Nardiello et al., 2022). By default, and in agreement with our choice for the *TinyTim*-based PSFs, we chose a `G2V` star as the stellar template. As explored in Hoyer et al. (2023a), the choice of stellar type plays little to no role on the fit results for *HST* data and we assume the same for *JWST* data.

4.3 Image Fitting

4.3.1 Approach and Model Function

Focusing on the center of M 74, we extracted a square region of side length $5.5''$ (equivalent to ~ 260 pc) centered on the NSC to avoid the more dust- and gas-rich spiral structure, as shown in the first row, right panel of Figure 4.1. Previous investigations used various model functions to describe the light distribution of NSCs, including King profiles [see King (1962) for the original definition; e.g. Matthews et al. (1999), Seth et al. (2006), Georgiev et al. (2009b), and Georgiev and Böker (2014)], Gaussian profiles (e.g. Carollo et al., 1997, 2002; Barth et al., 2009; den Brok et al., 2014), Nuker profiles [see Lauer et al. (2005) for a definition; e.g. Carollo and Stiavelli (1998), Böker et al. (1999b, 2002), and Butler and Martínez-Delgado (2005)], Sérsic profiles (e.g. Côté et al., 2006; Baldassare et al., 2014; Carson et al., 2015; Spengler et al., 2017; Pechetti et al., 2020), or point sources (e.g. Ferrarese et al., 2020; Poulain et al., 2021; Zanatta et al., 2021; Carlsten et al., 2022). Here we use the Sérsic profile of the form

$$I(r) = I_{\text{eff}} \exp\left\{ - b_n \left[\left(\frac{r}{r_{\text{eff}}} \right)^{1/n} - 1 \right] \right\}, \tag{4.1}$$

where r is the radius, r_{eff} the half-light or effective radius, I_{eff} the intensity at r_{eff}, and n the Sérsic index. The parameter b_n solves the equation $\Gamma(2n) = 2\gamma(2n, b_n)$ where $\gamma(a, x)$ is the incomplete and $\Gamma(x)$ the complete Gamma function. For $n \in (0.5, 10)$, $b_n = 1.9992n - 0.3271$ is a good approximation (Capaccioli, 1989; Graham & Driver, 2005).

The background flux from the host galaxy and the sky was modeled with another Sérsic profile and a plane offset. From our fits (see below), we found that in all bands $I_{\text{eff}}^{\text{gal}} \ll I_{\text{eff}}^{\text{nsc}}$, $r_{\text{eff}}^{\text{gal}} \gg r_{\text{eff}}^{\text{nsc}}$, and $n^{\text{gal}} \lesssim 1$, such that the profile of the host galaxy becomes flat in the very center, thus justifying the choice of models. As we describe in Section 4.7.1, two Sérsic profiles describe the NSC worse than a single profile.

To fit the data, we convolved the profiles with the previously generated synthetic PSF at the position of the NSC (see Section 4.2.3). The fit itself was performed with *Imfit* (Erwin, 2015), a specialized program to fit astronomical images. For the minimization technique, we chose the Differential Evolution solver with Latin hypercube sampling. In comparison with other available options, the solver does not rely on initial parameter values but randomly selects parameter values between user-specified boundaries (see Storn & Price, 1997, for details). We list the boundaries for the parameters of the Sérsic profile used for the NSC in Table 4.2. By default, *Imfit* evaluates the goodness of the fit with standard χ^2 statistics.

Unless specified, *Imfit* assumes Poissonian statistics of the input data to generate a noise map. We take this approach for all but the *JWST* MIRI data where noise maps were generated by the previously mentioned custom data calibration pipeline. The noise maps for the MIRI bands were determined from uncertainties of the input data, the read noise and the flat fields, weighted by the fractional contribution to each pixel.

Table 4.2. Sérsic parameters and their boundary values used to fit the data with *Imfit*. The same values are used for all *HST* and *JWST* bands.

Parameter	Boundary	Unit	Description
x_0	[45, 55]	[pixel]	NSC position
y_0	[45, 55]	[pixel]	NSC position
PA	[−359.99, 359.99][a]	[deg]	Position angle
ϵ	[0.00, 0.99]	--	Ellipticity
n	[0.00, 5.00]	--	Sérsic index
$r_{\rm eff}$	[0.00, 10.00]	[pixel]	Effective radius
$I_{\rm eff}$	[0.00, $I_{\rm max}$][b]	[counts]	Intensity at $r_{\rm eff}$

[a] To prevent the fit from running into boundaries at 0°, the lower boundary was changed to negative values. In the case that the best-fit position angle was negative, 180° (or 360°) was added.
[b] $I_{\rm max}$ is the peak of the intensity of the NSC.

As a result, compared to the standard noise map generated by *Imfit*, the MIRI noise maps give lower values for the nucleus itself, but higher values for the faint emission by the background galaxy.

In Figures 4.3 and 4.4 we show the data, best-fit two-component models, and the residuals for the *HST* ACS & WFC3, *JWST* NIRCam, and MIRI data, respectively. For the *JWST* MIRI *F2100W* all attempts failed to find a stable fit. Instead, to get an estimate for the apparent magnitude, we fit a Sérsic profile excluding PSF convolution.

4.3.2 Uncertainties

We determined uncertainties by repeating the fit 500 times using bootstrapping. During each iteration of bootstrapping, *Imfit* generates a new data array where indices of pixels are randomly sampled. During re-sampling, the pixel values of the input data as well as their location are not considered. The quoted best-fit parameters equal the median value of the parameter distribution and the uncertainties give the 1σ interval.

For some physical parameters, such as the determination of NSC mass (see Section 4.4.3) or the transformation of the effective radius to parsec, the bootstrapping uncertainties were propagated forward. Based on the assumption that the underlying probability distributions are Gaussians, we used the Gaussian error propagation.

The uncertainty of the zero point magnitudes for the *HST* bands is of the order $\mathcal{O}(10^{-3})$ and can be neglected. However, recent analyses of early *JWST* data revealed that there exist issues with the flux calibration. As detailed below, these issues persist and remain significant.

For the *JWST* NIRCam data, the uncertainty on the flux calibration can be as high as 0.2 mag (Boyer et al., 2022), depending on the band and detector. Most recent analyses in the community try to solve this issue by introducing multiplicative correction

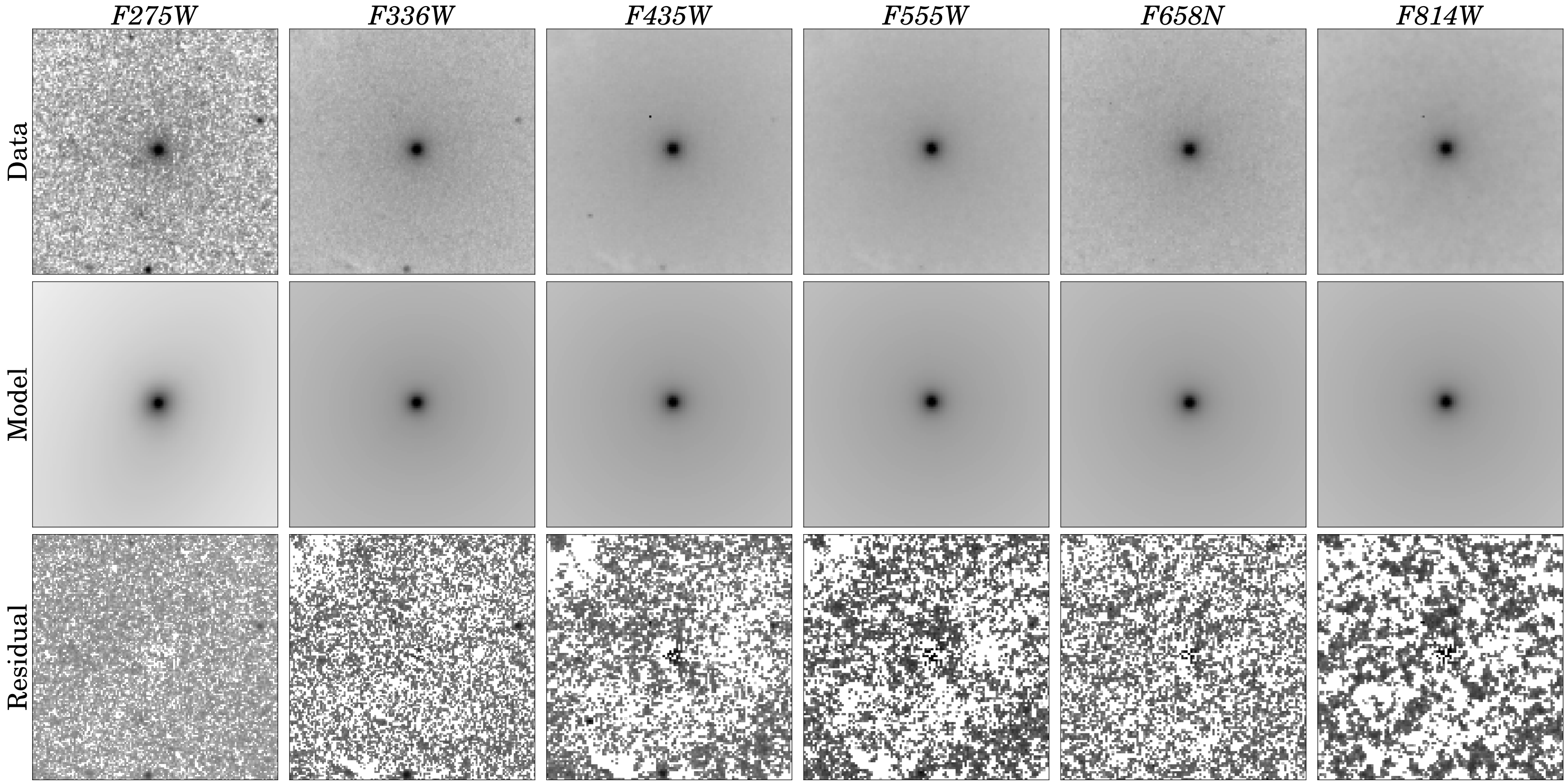

Figure 4.3. Overview of the central 5.5 arcsec × 5.5 arcsec (1 arcsec ≈ 47 pc) of M 74 in six different *Hubble Space Telescope* bands. North is up and East is left. *Top row*: Data products as used for fitting. *Middle row*: Model images of the best fit using one Sérsic profile for the nuclear star cluster, an additional Sérsic profile for the background, and a plane offset. *Bottom row*: Residual map, Data – Model. The gray scale of the maps are logarithmic and vary from 5×10^{-3} to 5×10^{2} times the mean of the residuals.

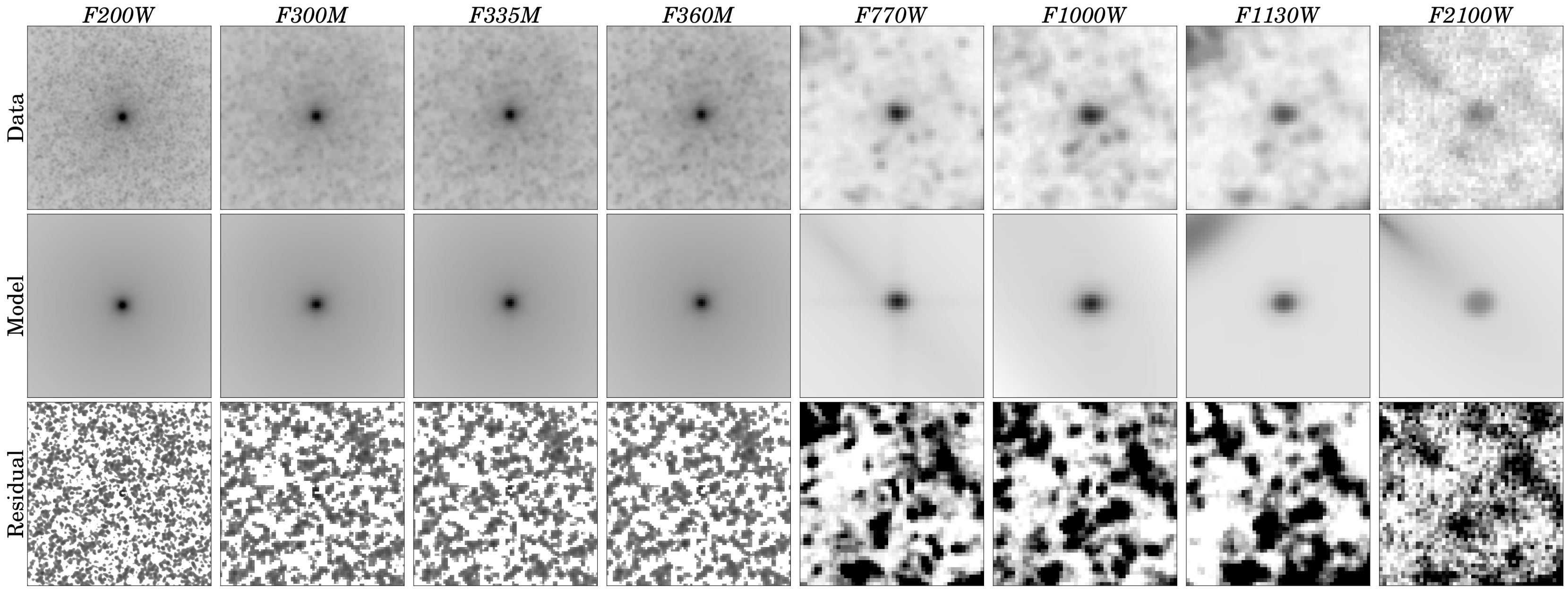

Figure 4.4. Overview of the same central region as in Figure 4.3 but for available *JWST* NIRCam and MIRI data. For the *F2100W*, no fit was possible including PSF convolution. The model shown here is a pure Sérsic profile without PSF convolution to determine the apparent magnitude of the source. For the MIRI data, we adjust the gray scales to 0.99 and 1.01 times the mean.

factors for the data.[3] We corrected the determined fluxes by the mean multiplicative correction factor of G. Brammer and I. Labbe presented in Brammer (2022), 0.7845. The correction factors are presented for the *F090W*, *F115W*, *F150W*, and *F200W*, that is, only the last band overlaps between the filter sets. To remain consistent between all four NIRCam bands, we did not change the value of the apparent magnitude, but determine the uncertainty from the multiplicative correction factor itself. The final uncertainty on the magnitude was then determined through Gaussian error propagation of this systematic uncertainty and the statistical uncertainty obtained from the fit. For the other three NIRCam bands, we assumed that the correction factor equals 0.8, resulting in an uncertainty of ~ 0.24 mag. As for the *F200W*, we combined this value with the statistical uncertainty from bootstrapping for the final uncertainty.

For the *JWST* MIRI data, the background level was, as described in Section 4.2.2, adjusted by comparing the *F770W* flux to the *IRAC4* 8 µm and *WISE3* 12 µm bands. The estimated uncertainty on its value is ±0.1 mag (Leroy et al., 2023).

As pointed out in Section 4.2.3, we did not check the influence the calibration and co-addition of the data have on the synthetic PSF generated by *WebbPSF*. Hoyer et al. (2023a) found for the *HST* data that the co-addition of single exposures results in a slight broadening of the core of the PSF, introducing a systematic overestimation of the NSCs size. To repeat this experiment for the *JWST* data, we focused on the NIRCam *F200W* band and repeated the fit introducing an additional jitter in the form of a Gaussian function convolved with the synthetic PSF. In *WebbPSF*, we increased the jitter by factors of two and five and repeated the fits using the new PSFs. The result was that the structural parameters, as well as magnitude and color, remained well within the 1σ distribution of the original fits. Therefore, we conclude that our results are reliable given the presented uncertainties.

4.4 Analysis

4.4.1 Photometry

Integrating Equation 4.1 with an assumed ellipticity (ϵ) yields the luminosity (L; photon count per energy band and time) as

$$L = 2\pi\,(1-\epsilon)\,I_{\rm eff}\,r_{\rm eff}^2\,\frac{n e^{b_n}}{(b_n)^{2n}}\,\Gamma(2n)\ . \tag{4.2}$$

We use the equation

$$\mathrm{ZP_{AB}} = -2.5 \times \log_{10}\left(\mathrm{PHOTFLAM}\right) - 5 \times \log_{10}\left(\mathrm{PHOTPLAM}\right) - 2.408\ , \tag{4.3}$$

to calculate the zero point magnitudes for *HST* ACS / WFC3 bands. The values of *PHOTFLAM* and *PHOTPLAM* are given in the header extensions of the fits files.[4]

[3] See, for example, https://github.com/gbrammer/grizli/pull/107.

[4] We find the following zero point magnitudes for the *HST* bands: ZP_{F275W} = 24.159 mag, ZP_{F336W} = 24.689 mag, ZP_{F435W} = 25.677 mag, ZP_{F555W} = 25.722 mag, ZP_{F658N} = 22.760 mag, and ZP_{F814W} = 25.950 mag.

Pixel values in *JWST* data products have the unit [MJy sr^{-1}], which we convert to Jy by using Equation 4.2 and the pixel-to-steradian conversion factor *PIXAR_SR* from the header extension. The zero point magnitude is then derived using

$$\mathrm{ZP_{AB}} = -2.5\ \log_{10}(L) + 8.9\ . \tag{4.4}$$

Foreground extinction is taken into account by using the re-calibrated version of the Schlegel et al. (1998) extinction maps (Schlafly & Finkbeiner, 2011) and assuming $R_V = 3.1$ (Fitzpatrick, 1999). Due to the apparent lack of dust in the center of M 74, we do not attempt to correct for intrinsic extinction. For the *HST* bands, we derive $A(\lambda)\,/\,A(V)$ with the model from O'Donnell (1994), which is based on Cardelli et al. (1989).

Figure 4.5 shows spectral flux densities as well as the extinction-corrected apparent magnitudes of the NSC in the AB-magnitude system. The NSC is faintest in the ultraviolet regime and becomes brighter towards the near-infrared. The brightest magnitude is reached at 2 µm after which the nucleus becomes fainter again.

To compare to the values by Georgiev and Böker (2014), we transform our magnitudes from the AB- to the Vega-magnitude system using the approach outlined in Sirianni et al. (2005) and applied in Pechetti et al. (2020) for NSCs. We find $V_0 = (17.85 \pm 0.04)$ mag and $I_0 = (16.69 \pm 0.05)$ mag. Georgiev and Böker (2014) present $V_0 = (17.88 \pm 0.01)$ mag and $I_0 = (16.57 \pm 0.01)$ mag. While the V-band magnitudes agree with each other, we find a significant difference in the I-band. The different magnitude is most likely related to the extracted structural parameters (*c.f.* Section 4.4.4).

4.4.2 SED Modelling

The combined *HST* and *JWST* data cover the ultraviolet to mid-infrared spectrum and enable the study of the spectral energy distribution (SED) in detail. To extract basic parameters describing the stellar population, we set up a model assuming a delayed star formation history, two commonly used different initial mass functions (Salpeter, 1955; Chabrier, 2003), and the Bruzual and Charlot (2003) single stellar population model.

The fits were executed using `CIGALE`, a Python code for modeling the SEDs of galaxies (see Burgarella et al., 2005; Noll et al., 2009; Boquien et al., 2019; Yang et al., 2020, 2022), which has successfully been applied to star clusters (e.g. Fensch et al., 2019; Turner et al., 2021). The program allows to adjust various physical properties such as the age of the stellar populations or their metallicity. We test various parameter values, as detailed in Table 4.3, to find the best possible fit to the data, as evaluated by Bayesian statistics.

The fit was performed twice, excluding the MIRI data in one run. We do this to test their influence to the fit result and disentangle emission from low-mass stars and dust. The addition of a dust emission model yielded worse fits, as evaluated by both the reduced χ^2 and Bayesian statistics, which is why we do not include it in the presented results. We discuss this issue in more detail in Section 4.5.

For the fit including the MIRI data, we find that the mass-weighted age of the main stellar population is (8 ± 2) Gyr with a metallicity of $Z = 0.03 \pm 0.01$, more metal-rich than the Sun (Asplund et al., 2009). The e-folding time of the main stellar population is (500 ± 500) Myr and the mass fraction of the late burst is consistent with zero. The fit preferred a Chabrier (2003)-type initial mass function over a Salpeter (1955) one.

For the fit excluding the MIRI data, we find a mass-weighted age of the main stellar population of (8 ± 3) Gyr with a metallicity of $Z = 0.012 \pm 0.006$. The e-folding time was determined to be (220^{+380}_{-220}) Myr and the mass fraction of the late burst is comparable to zero. The fit again preferred a Chabrier (2003)-type initial mass function.

According to the reduced χ^2 statistics, the fit excluding the MIRI data performed better than the one including them. The results of both fits are consistent with each other, indicating the presence of a 8 Gyr old stellar population with metallicity $Z \sim 0.02$ and no presence of a young stellar population. We discuss the results obtained for the mass of the stellar population in the next section.

Table 4.3. Parameter values for the spectral energy distribution fits. The values remain unchanged between runs including and excluding the MIRI data.

Parameter	Unit	Values	Best-fit	
			Incl. MIRI	Excl. MIRI
		Star formation history		
tau_main[a]	[Myr]	1, 10, 100, 1000, 2000, 3000	500 ± 500	220^{+380}_{-220}
age_main[b]	[Gyr]	3, 4, 5, 6, 7, 8, 9, 10, 11, 12, 13	8 ± 2	8 ± 3
tau_burst[c]	[Myr]	10, 20, 50, 100	57 ± 33	57 ± 33
age_burst[d]	[Myr]	10, 20, 50, 100	27 ± 17	27 ± 17
f_burst[e]	--	0.0, 0.1, 0.2, 0.5	0	0
		Simple stellar population		
imf[f]	--	0, 1	1	1
metallicity[g]	--	0.004, 0.008, 0.02, 0.05	0.027 ± 0.013	0.012 ± 0.006

[a] e-folding time of the main stellar population
[b] Age of the main stellar population
[c] Time of the late star burst
[d] Age of the late star burst
[e] Mass fraction of the late burst
[f] Initial mass function (Salpeter, 1955; Chabrier, 2003)
[g] Metallicity of the stellar population

4.4.3 Stellar Mass

We determine the stellar mass of the NSC in three different ways: (1) we use $B - V$ color and its mass-to-light scaling relations, (2) we combine the apparent magnitude in the *F200W* (roughly K-band) with a constant mass-to-light ratio ranging between 0.5 and 0.6 (in solar units), and (3) we extrapolate a stellar mass from SED fitting. The resulting mass estimates and the literature value from Georgiev et al. (2016) are

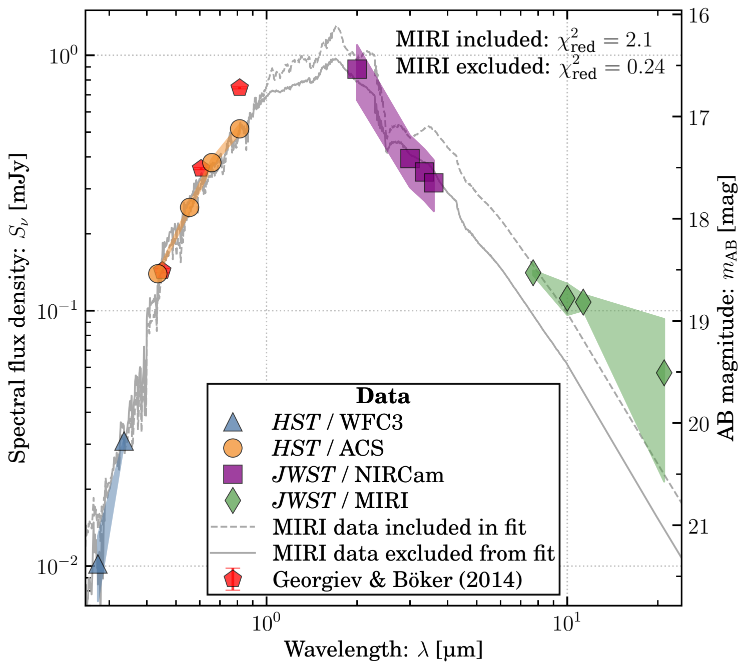

Figure 4.5. Spectral flux density (S_ν, *left axis*) and AB magnitude ($m_{\rm AB}$, *right axis*) versus wavelength (λ). Different instruments are highlighted with marker symbols and colors. Red pentagons give the results by Georgiev and Böker (2014) in the Vega-magnitude system. Uncertainties are indicated with shaded areas. Two gray lines show the spectral energy distribution fits to the data including (dashed line) and excluding (solid line) the *JWST* MIRI data. The goodness of the fits is given by reduced χ^2 values in the panel. For both fits, we use the Bruzual and Charlot (2003) stellar population model and a delayed star formation history. The fit prefers a Chabrier (2003) initial mass function over the prescription by Salpeter (1955). Both fits indicate the presence of a 8 Gyr old stellar population with metallicity $Z \sim 0.02$. No younger stellar population could be detected.

Table 4.4. Determined nuclear star cluster mass as well as the literature value.

Source	Logarithmic stellar mass [$M_\odot$]
$B - V$	7.06 ± 0.31
K-band	7.2 ± 1.1[a]
SED (incl. MIRI)	7.17 ± 0.10
SED (excl. MIRI)	7.11 ± 0.10
Georgiev et al. (2016)	7.05 ± 0.21

[a] The large uncertainty compared to the other values is caused by the high uncertainty on the zero-point values for NIRCam data.

presented in Table 4.4.

Following Hoyer et al. (2021), we use four different $B - V$ color relations and the

V-band luminosity to obtain a stellar mass-to-light ratio. The original relations were published by Bell et al. (2003), Portinari et al. (2004), Zibetti et al. (2009), and Into and Portinari (2013) but we adopt the revised parameters from McGaugh and Schombert (2014), which ensures consistency between the relations. An extended discussion and the assumptions made are detailed in Hoyer et al. (2021).

First, the *HST* ACS *F435W* and *F555W* magnitudes were converted to the Johnson-Cousin system (B- and V-band, respectively) using Equation 12 and Table 22 of Sirianni et al. (2005). Absolute magnitudes were derived using the distance estimate of the galaxy and the absolute magnitude of the Sun (Willmer, 2018).[5]

After transforming the *HST* magnitudes to the Johnson-Cousin system and using magnitudes in the Vega-system, we find $B_0 = (18.59 \pm 0.03)$ mag and $V_0 = (17.86 \pm 0.04)$ mag with a color $(B - V)_0 = (0.73 \pm 0.05)$ mag, which roughly matches the color of a G8V-type star ($B - V \sim 0.75$ mag) and is consistent with the results from the SED fits. From the four scaling relations, we determine individual masses and combine them into one using the weighted average. The resulting mass estimate is $\log_{10}(M_{\star}^{\mathrm{nsc}} / \mathrm{M}_{\odot}) = 7.06 \pm 0.31$. The uncertainty budget is dominated by the uncertainty assumed for the mass-to-light ratio, 0.3 dex (Roediger & Courteau, 2015).

An alternative approach is to use the magnitude in the K-band. McGaugh and Schombert (2014) found that a constant mass-to-light ratio of ~ 0.6 can be used to estimate stellar masses as the near-infrared luminosity is only weakly dependent on color. While we do not directly have a K-band magnitude, we estimate the mass using the *F200W* band from *JWST*, centered on 2 µm. The K-band overlaps with the *F200W* band such that we can use the mass estimate as a benchmark for the other mass estimates.

Using the same four references as for the approach using the $B - V$ color (Bell et al., 2003; Portinari et al., 2004; Zibetti et al., 2009; Into & Portinari, 2013) and their re-calibrated values from McGaugh and Schombert (2014), we find a stellar mass of $\log_{10}(M_{\star}^{\mathrm{nsc}} / \mathrm{M}_{\odot}) = 7.2 \pm 1.1$. The uncertainty is much larger than for the mass determined from the $B - V$ relation due to the uncertainty on the zero point of the NIRCam data.

From the SED fitting in the previous section, the mass of the star cluster was determined as well. In the fit including the MIRI data, we find $\log_{10}(M_{\star,1}^{\mathrm{nsc}} / \mathrm{M}_{\odot}) = 7.17 \pm 0.10$. In the fit excluding the MIRI data, we find $\log_{10}(M_{\star,2}^{\mathrm{nsc}} / \mathrm{M}_{\odot}) = 7.11 \pm 0.10$. As stated above, no young stellar population was found.

The mass of the NSC was previously determined by Georgiev et al. (2016) based on the analysis of Georgiev and Böker (2014). To obtain stellar masses, the authors use stellar population models from Bruzual and Charlot (2003) with solar metallicity and an initial mass function of the type presented in Kroupa (2001). The reported mass for the NSC of M 74 is $\log_{10}(M_{\star}^{\mathrm{nsc}} / \mathrm{M}_{\odot}) = 7.05 \pm 0.23$, which agrees within the uncertainty with our mass estimates.

Overall, we find agreement between all approaches finding that the NSC has a stellar mass of $\sim 10^7\,\mathrm{M}_{\odot}$. In the following, we use the mass value $\log_{10}(M_{\star}^{\mathrm{nsc}} / \mathrm{M}_{\odot}) = 7.06 \pm 0.31$.

[5] See http://mips.as.arizona.edu/~cnaw/sun.html for an overview. The uncertainty on the values is assumed to be 0.04 mag.

4.4.4 Structure

Figure 4.6 shows the effective radius, ellipticity, Sérsic index, and position angle versus wavelength (from Section 4.3). We also add the literature values by Georgiev and Böker (2014).

In panel A, we show the effective radius versus wavelength. It remains roughly constant at ~ 5 pc in the ultraviolet and optical regime, but starts to slightly increase towards ~ 6 pc at 3.6 µm. This trend continues into the mid-infrared where r_{eff} ~ 12 pc.

Georgiev and Böker (2014) find different effective radii ranging from ~ 2 pc to ~ 3.5 pc. They modeled the NSC light distribution by convolving a *TinyTim*-generated PSF with King profiles of different concentration parameters (ratio of the tidal to core radius: 5, 15, 30, and 100). Using `ISHAPE` (Larsen, 1999), they fit the data and used the best-fit model, according to χ^2 residuals to derive the effective radius of the cluster. In their fits, a concentration parameter of 100 gave the best results. The final value for the effective radius was obtained by taking the geometric mean of the full-width-half-maximum along the semi-minor and major axes and using a transformation factor from `ISHAPE`'s manual.

In the ultraviolet and optical regime, the ellipticity is ~ 0.05 (panel B in Figure 4.6). It remains in this range at 2 and 3 µm, but starts to increase to ~ 0.1 at 3.6 µm. At even longer wavelengths, the ellipticity increases to ~ 0.4 and is significantly different from the other wavelength regimes. Our measurements in the optical are consistent with the ones presented by Georgiev and Böker (2014), but are smaller than the typical ellipticity for other NSCs in the same mass range ($\epsilon \gtrsim 0.1$, e.g. Seth et al., 2006; Carson et al., 2015; Spengler et al., 2017; Hoyer et al., 2023a).

The Sérsic index (panel C) appears to vary with wavelength. In the ultraviolet and optical regime, we find n ~ 3, but in the near-infrared the value drops to ~ 2. At the longest wavelengths, the value drops to ~ 1.5, but is also consistent with an exponential profile ($n = 1$). Georgiev and Böker (2014) used a King profile to approximate the light distribution and no comparison can be made.

The position angle of the NSC (panel D) starts at ~ 130° in the ultraviolet regime. Starting in the optical regime, the position angle drops to ~ 100° and shows a mild anti-correlation with wavelength, dropping further to ~ 90° in the mid-infrared. Only the data point from the *HST* WFPC2 PC *F606W* band by Georgiev and Böker (2014) is consistent with our results. The other two data points are significantly elevated to ~ 135° and ~ 160°.

4.4.5 Astrometric Offset

From the previous section it is apparent that the nucleus shows an evolution with wavelength, especially towards the mid-infrared regime. Here we investigate the variability of the central position of the emission in different bands.

In Figure 4.7 we show the emission in the *JWST* MIRI *F2100W* band (gray scale and white contour lines) and overlay the emission from the *HST* WFC3 *F275W* band. The WCS of each band were taken from the bands header files. We find that there exists an offset between the centers of the emission, separated by ~ 0.2 arcsec, which approximates to ~ 9.5 pc at the distance to the galaxy.

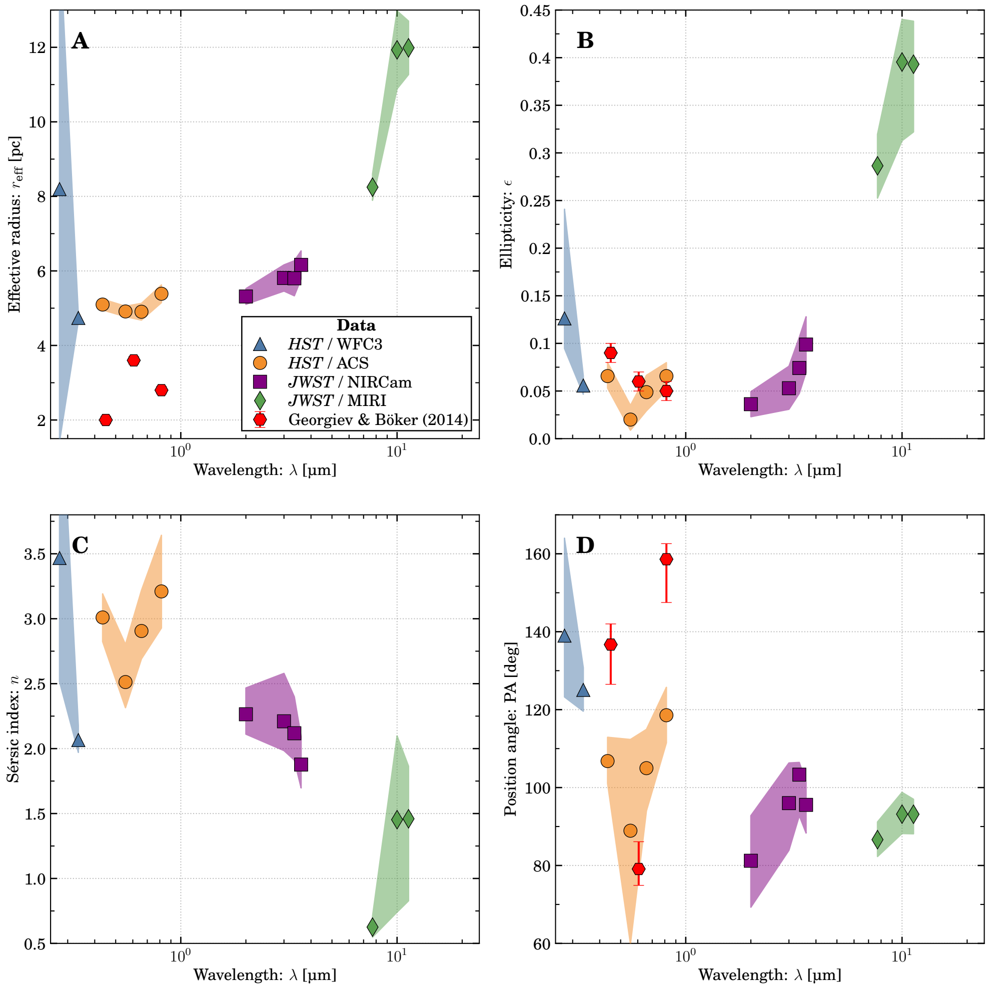

Figure 4.6. Structural properties of the nucleus of M 74: effective radius (panel A), ellipticity (panel B), Sérsic index (panel C), and position angle (panel D) versus wavelength. Marker symbols and colors highlight different instruments. Uncertainties are shown with shaded areas. Red pentagons show literature values from Georgiev and Böker (2014).

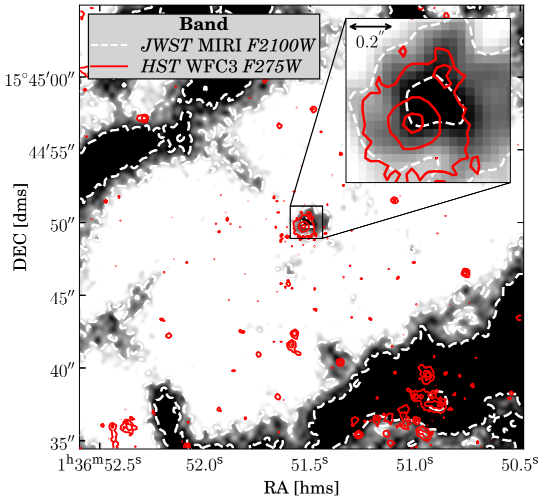

Figure 4.7. *Main panel*: Central 5.5″ × 5.5″ of M 74 in the *JWST* MIRI *F2100W*. A darker shade and white contours show high flux in the *F2100W*. Red contours highlight the *HST* WFC3 *F275W* emission. Both maps are matched based on the most up-to-date world coordinate solutions. *Inset panel*: Zoom into the nucleus of M 74. The white and red contours highlight again the emission in the *F2100W* and *F275W*, respectively. The offset between the centers of the contours measures approximately 0.2″.

To test whether the offset persists in other bands, we perform the following experiment: we determine the angular coordinates for other bands based on the central position of the Sérsic profile fit to the light distribution. Figure 4.8 presents the resulting angular separation using the *HST* WFC3 *F275W* band as reference. We find that the angular separation is of the order of $\lesssim 0.1''$ ($\lesssim 5$ pc) in the optical, which is comparable to the effective radius of the cluster. In the infrared the separation drops to $\lesssim 0.06''$ but increases up to $0.21''$ in the mid-infrared regime.

Depending on the band used as reference, the angular separation can become insignificant. For example, while using the *F200W* as reference, the offsets in the MIRI bands are still significant, whereas they become insignificant, except for the *F1000W*, when using the *F335M* as reference. This behavior could point towards issues with the calibration of the WCS': while we calibrated all *HST* data with the most recent WCS solutions from MAST, no reliable solutions exist so far for the *JWST* data. The PHANGS-internal versions of the data were calibrated in the following way: The NIRCam data was calibrated using *HST* and *Gaia* astrometric solutions using asymptotic giant branch stars. Furthermore, the direction of the separation is the same in the MIRI bands, towards the North-West (as seen in Figure 4.7).

Compared to the *HST* data, the NIRCam calibration should yield "accurate" astrometric values (see below). The MIRI data are astrometrically aligned to the *F335M* image by cross-correlating the images and solving for relative offsets. However, due to variations in the polycyclic aromatic hydrocarbons emission structure between different bands and the lack of point-like emission in the MIRI bands, the astrometric calibration is less certain.

To further quantify the offsets and benchmark the values, we compute the angular separation of (a) a star outside the central cavity, (b) multiple stars less than 1 arcsec South of the NSC within the cavity, and (c) a GC about 10 arcsec South-West from the NSC. The star outside the cavity has *Gaia* EDR3 designation 2 589 386 446 469 602 688, is non-saturated in all but the *HST* ACS *F435W*, *F555W*, and *F814W* bands and lies about 60″ South-East of the NSC. For the star outside the cavity and the GC, we fit the light distribution with a two-dimensional Gaussian function, which yields the position

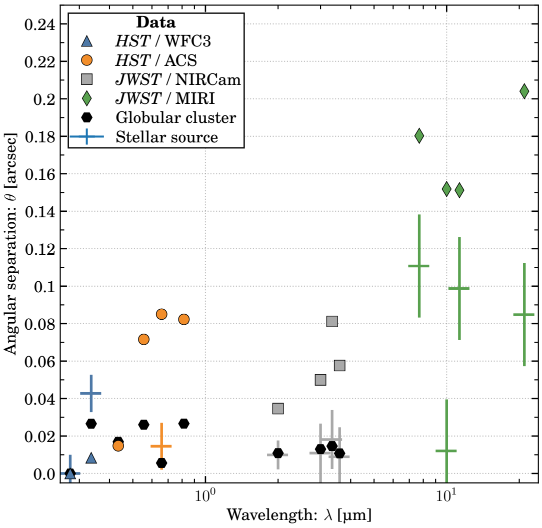

Figure 4.8. Angular separation (θ) versus wavelength (λ) of the nuclear star cluster position with respect to the *HST* WFC3 *F275W*. Different instruments are highlighted with different marker symbols and colors. Crosses show the angular separation of a star with *Gaia* EDR3 designation `2589386446469602688`. The vertical lengths of the crosses give 0.5 pixel, which we assume as an upper limit on extracting the position of the star. Data points above the crosses indicate that either the world coordinate system is offset, or the center of the nucleus is offset compared to the *HST* WFC3 *F275W*. In some bands (for example the *HST* ACS *F814W*), the star is saturated and no central position could be determined. The separations for a globular cluster, located ~ 10 arcsec South-West of the nucleus is shown with black hexagons. The offsets agree with the offsets of the star in the NIRCam data.

of the center of the sources, which we deem accurate within 0.5 pixel. For the other stars close to the NSC, we extract the position manually.

In Figure 4.8 we show the offset of the star outside the cavity and the GC in addition to the offsets for the NSC. If we use the *HST* WFC3 *F275W* data as reference, the offsets are significant in both the NIRCam and MIRI data. The same result is found if we use the *F200W* as reference. However, the offsets become insignificant in all except two bands (*F200W* & *F1000W*) if we use the *F335M* data as reference. With the currently available WCS calibrations, while there are hints of an astrometric offset, we cannot conclude whether they are significant.

4.5 Discussion

One of the most striking features of the *JWST* observations of the center of M 74 is that the prominent NSC sits in a nuclear stellar component that is devoid of gas and dust. It appears that both gas and dust have been evacuated from the central cavity. The mechanism that created this cavity is not obvious. There are no young stars that could have blown out the gas recently. Alternatively, the central cavity could have been created by consumption of the gas in the last star formation event, and the re-supply of gas is hindered by a potential bar resonance, in case a bar is (or previously was) present.[6]

[6]As mentioned in the introduction, Querejeta et al. (2021) find that M 74 hosts no bar.

4.5.1 Nuclear Star Cluster Properties

We show the mass ratio (NSC mass divided by host galaxy mass) in the left panel of Figure 4.9 where the NSC of M 74 is highlighted with a blue cross. Data from the Local Volume (a field environment with distance $\lesssim 11$ Mpc; Seth et al., 2006; Georgiev et al., 2009a; Graham & Spitler, 2009; Baldassare et al., 2014; Schödel et al., 2014b; Calzetti et al., 2015; Carson et al., 2015; Crnojević et al., 2016; Nguyen et al., 2017; Baumgardt & Hilker, 2018; Nguyen et al., 2018; Bellazzini et al., 2020; Pechetti et al., 2020) are added for comparison. Dwarfs around massive field galaxies and Virgo cluster members are taken from Carlsten et al. (2022) and Sánchez-Janssen et al. (2019a), respectively.[7] Data for other massive late-type galaxies in the field are taken from Georgiev and Böker (2014). The NSC of M 74 follows the overall trend in that the NSC mass becomes insignificant compared to the host galaxy. However, other late-types of the same host galaxy mass typically host more massive NSCs.

The effective radius of the NSC in M 74 also compares well to those of other NSCs in late-type galaxies (in the *F814W* band; middle panel in Figure 4.9). Finally, the ellipticity in the *F814W* band is smaller than the typical value in other late-types (right panel). This figure shows there exists no apparent correlation with the inclination of the host. Since the mass of the NSC is smaller than most other masses of such a cluster at $M_\star^{\rm gal} \sim 10^{10}\,{\rm M}_\odot$ and assuming that stars formed *in-situ* should dominate the mass budget, we speculate that the NSC had a quiet evolution and that, compared to other NSCs, only little mass formed *in-situ* over the last few Gyr. This speculation is corroborated by our results in Sections 4.4.1, 4.4.2 and 4.4.4: the effective radius shows no wavelength dependence from the ultraviolet to the near-infrared regime, staying roughly constant at 5 pc. The color of the NSC was determined to be $B - V = (0.73 \pm 0.05)$ mag, which compares to a star of `G8V`-class. Finally, the resulting best-fit SED model indicate that all stellar mass is assembled in an "old" stellar population, with the mass of the "young" stellar population being consistent with zero. As indicated by the fit, "old" refers to an age of 8 Gyr. If true, this could also mean that the cavity has existed for a few Gyr and that any massive black hole in the center of M 74 did not grow significantly via gas accretion over the same time period. So far, no reliable black hole mass measurement is available (see also Section 4.5.3 below).

The SED fit indicates that the metallicity of the NSC is $Z \sim 0.02$, which is comparable to NSCs in similar mass galaxies (Koleva et al., 2009; Paudel et al., 2011; Spengler et al., 2017; Kacharov et al., 2018; Neumayer et al., 2020), and also the Milky Way NSC (Do et al., 2015; Feldmeier-Krause et al., 2017a). In combination with the age estimate of the stellar population, this reveals that the NSC formed in a dense environment where rapid enrichment took place. Such conditions could take place either during the formation of the galaxy itself or during a past merger event.

As mentioned above, while *in-situ* star formation is expected to contribute a significant mass fraction to the NSC, as measured in other galaxies, our results indicate that no *in-situ* star formation occurred over the last few Gyr. This means that, since the formation of the NSC, either no or very little amount of gas fell towards the center or

[7] Although not considered here, data for nucleated dwarf galaxies in the Fornax galaxy cluster is presented by Muñoz et al. (2015), Eigenthaler et al. (2018), Ordenes-Briceño et al. (2018), Venhola et al. (2018), and Su et al. (2021).

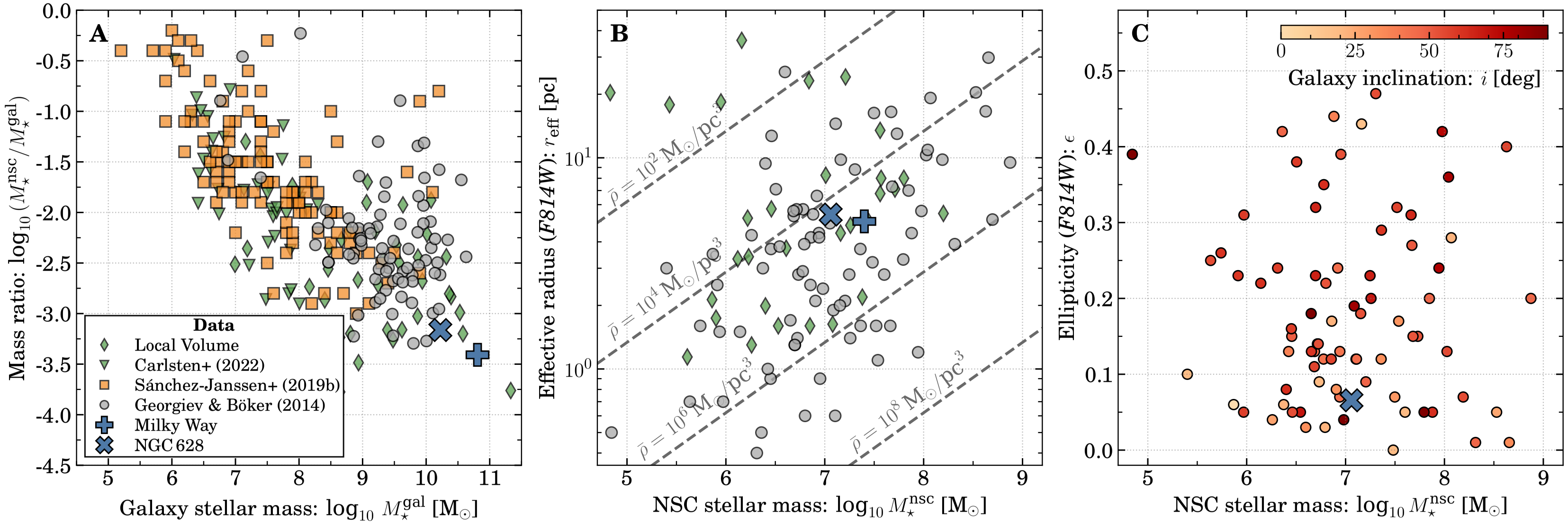

Figure 4.9. *Left panel*: Mass ratio of nuclear star cluster (NSC) and host galaxy stellar mass ($M_\star^{\rm nsc}/M_\star^{\rm gal}$) versus galaxy stellar mass. The NSC of M 74 is highlighted with a blue cross. Other data sets from the Local Volume (a field environment with a distance $\lesssim 11$ Mpc; green diamonds; Seth et al., 2006; Georgiev et al., 2009a; Graham & Spitler, 2009; Baldassare et al., 2014; Schödel et al., 2014b; Calzetti et al., 2015; Carson et al., 2015; Crnojević et al., 2016; Nguyen et al., 2017; Baumgardt & Hilker, 2018; Nguyen et al., 2018; Bellazzini et al., 2020; Pechetti et al., 2020), the Virgo galaxy cluster (orange squares; Sánchez-Janssen et al., 2019a), dwarfs around massive field galaxies (green triangles; Carlsten et al., 2022), and massive field galaxies (gray circles; Georgiev & Böker, 2014) show the general distribution of NSCs. The Milky Way NSC is highlighted with a blue plus-sign. In comparison to other massive field late-type galaxies, the NSC of M 74 appears under-massive. *Middle panel*: Effective radius ($r_{\rm eff}$) in the *F814W* versus NSC stellar mass. The markers and colors of the data points are the same as in the left panel. Dashed lines give the mean density of clusters. *Right panel*: Ellipticity (ϵ) versus NSC stellar mass. We show the data by Georgiev and Böker (2014) and color-code them by the host galaxy inclination. There exists no apparent correlation between ellipticity, mass, or inclination. For M 74, the inclination has a value of $i \sim 8.9°$ (Lang et al., 2020).

that star formation was inefficient. One possibility is that the shape of the gravitational potential limits the amount of inflow. Indeed, it is well known that in a viscous accretion disk, the amount of inward mass transport depends on the amount of shear (e.g. Shakura & Sunyaev, 1973; Lynden-Bell & Pringle, 1974). One way to limit the inflow of gas is to have a low shear, meaning that the rotation curve is close to solid body rotation (e.g. Lesch et al., 1990; Krumholz & Kruijssen, 2015). Note, however, that it is still unclear what mechanism drives the ISM turbulence responsible for creating the required viscosity (e.g. Klessen & Glover, 2016; Sormani & Li, 2020). Alternatively, it could be that the in-flow is irregular and triggered by mergers or interactions with satellite galaxies (e.g. Storchi-Bergmann & Schnorr-Müller, 2019). Multiple dwarfs are known to reside around M 74 (Davis et al., 2021) and numerous accretion events occurred in the galaxy's history (Kamphuis & Briggs, 1992).

4.5.2 Comparison with the Milky Way

The obtained NSC size using near-infrared data seems to be very similar to the Milky Way's (MWNSC) with an effective radius of ~ 5 pc (e.g. Fritz et al., 2016; Gallego-Cano et al., 2020). However, the MWNSC also presents a similar size when analyzed with Spitzer/IRAC mid-infrared data (Schödel et al., 2014a; Gallego-Cano et al., 2020), which is in contrast to the significantly larger effective radius we obtained for the NSC of M 74 from MIRI mid-infrared data. In addition, the mass estimates compare, with the MWNSC having a mass of ~ 2×10^7 $M_\odot$ (Launhardt et al., 2002; Schödel et al., 2014b; Feldmeier-Krause et al., 2017b).

The predominantly old (~ 8 Gyr) and metal-rich (Z ~ 0.02) population detected in M 74's NSC is also in agreement with the results obtained for the MWNSC (e.g. Feldmeier-Krause et al., 2017a; Schödel et al., 2020; Nogueras-Lara, 2022), though recent work suggested a younger age for the MWNSC of ~ 5 Gyr (Chen et al., 2022). However, the MWNSC also shows recent star formation activity, about 6 Myr ago (Paumard et al., 2006), which is not present in M 74's NSC, according to the best-fit SED model.

Overall, we find that little to no star formation occurred in the last few Gyr in M 74's center. This results in an under-massive NSC, compared to other similar-mass late-type galaxies, a likely under-massive central black hole, if present, and that the central cavity spanning approximately 200 pc × 400 pc existed for a similar period.

4.5.3 Nature of the Mid-Infrared Emission

While an old (8 Gyr) population with metallicity Z ~ 0.02 accounts for the emission in the ultraviolet to near-infrared regime, we found an excess of emission in the mid-infrared bands (*c.f.* Figure 4.5), which cannot be explained by that same population. In addition, the effective radius and ellipticity do not change with wavelength until the mid-infrared regime, the Sérsic index shows a weak wavelength dependence, and the position angle does not change significantly between the near- and mid-infrared (*c.f.* Figure 4.6). We speculate about the nature of the emission in the following sections.

Active Galactic Nucleus Contribution

One possibility is that the emission in the mid-infrared bands is caused by an active galactic nucleus (AGN) once X-ray photons are absorbed by dust, which re-emits the radiation at longer wavelengths.

The presence of a massive black hole in M 74 is still disputed: Dong and De Robertis (2006) use the black hole mass versus bulge K_S-magnitude relation to find $\log_{10}(M_{\mathrm{BH}} / \mathrm{M}_\odot) \sim 6.7$ but such a relation assumes that the bulge did not significantly grow through secular processes, which is believed to be the case for M 74. She et al. (2017) found an X-ray excess in the galaxy's center, which they attribute to the presence of an AGN with a black hole mass of $\log_{10}(M_{\mathrm{BH}} / \mathrm{M}_\odot) \sim 6.0$. The X-ray luminosity was determined to be $\log_{10}(L_{2\text{-}10\,\mathrm{keV}} / \mathrm{W}) = 31.15^{+0.32}_{-0.19}$, as determined through the hardness ratios of soft-, medium-, and hard X-ray bands.

We determine the spectral flux density of the emission in the mid-infrared by using this luminosity and the scaling relation by Asmus et al. (2015), which connects the X-ray luminosity of an AGN to the mid-infrared luminosity at 12 µm. The result is $S_\nu^{\mathrm{BH}} \sim 1.9 \times 10^{-4}$ mJy. We compare this value to the difference between the observed emission and the model flux excluding the MIRI data in the 11.3 µm band. The difference equals $\Delta S_\nu^{11.3\,\mu\mathrm{m}} \sim 0.06$ mJy, far exceeding the expected flux density of an AGN. Therefore, while the X-ray excess measured by She et al. (2017) originating from a possible AGN could contribute to the mid-infrared emission, it cannot fully explain it by itself. Furthermore, little to no dust is present in the NSC, making this scenario unlikely.

Infalling Star Cluster

A possible scenario, which could perhaps explain the offset in Figure 4.7, if real, is that we see the NSC and an in-falling star cluster, where the latter could be in a late stage of tidal disruption by the more massive NSC. Such a scenario for the build-up of NSCs has been proposed for a few decades (Tremaine et al., 1975) and is sometimes referred to as the "dry-merger" scenario (e.g. Arca Sedda & Gualandris, 2018) with ample observational and theoretical evidence in both the Galactic but also extragalactic NSCs (e.g. Antonini, 2013, 2014; Arca-Sedda & Capuzzo-Dolcetta, 2017; Fahrion et al., 2020b; Feldmeier-Krause et al., 2020).

The proposed scenario could occur as follows: the star cluster would form outside the nuclear region and spiral inwards. During this time, the star cluster can be considered self-gravitating, which implies that it evolved predominantly due to its internal collisional dynamics. During the infall of the cluster, it will experience gravothermal-gravogyro contraction and core-collapse (e.g. Kamlah et al., 2022), mass segregate, and form a subsystem of black holes in its center, or even an intermediate-mass black hole, if the star cluster is massive enough. The most-massive stars accumulate in the star cluster's center and lower-mass stars occupy the halo of the star cluster. Some of these low-mass stars will be stripped by the tidal field of the surrounding field or may be ejected through dynamical interactions, while the star cluster approaches the NSC. Some of the stripped or ejected stars might be visible as asymptotic giant branch (AGB) stars (see also Section 4.5.3) with their strong, dust-driven stellar winds (see

Decin, 2021, and sources therein) in the near- to mid-infrared bands as single sources scattered around the NSC (see Figure 4.4).

From N-body simulations by Arca Sedda and Gualandris (2018), modeling the MWNSC and an infalling star cluster, we know what the infall, merger, and merger product phases look like in spatial coordinates [Figure 2 in Arca Sedda and Gualandris (2018) and Figure 1 in Arca Sedda et al. (2020)]. If the infalling star cluster has already crossed the effective radius of the NSC, after which the star cluster becomes entirely tidally disrupted and cannot be considered a self-gravitating system anymore (Arca Sedda et al., 2020), the simulation snapshots could explain the potential astrometric offset. The star cluster's core would eventually fall into the core of the NSC and the remaining halo stars would tidally disperse. Among these would be AGB stars that may partly be responsible for the astrometric offset shown in Figure 4.7 and contribute to the elliptical increase in panel B of Figure 4.6 (see also Section 4.5.3 below).

One counter-argument is that it is unlikely to witness such an event: Arca Sedda (2020) simulated the infall of a star cluster on an NSC whose properties mimic the ones of the Milky Way NSC. They find that the star clusters enters a region 10 pc around the center of the NSC after 60 Myr and that the cluster is not a self-gravitating system anymore after another 1 Myr. Note that the bulge component in their simulation is likely more massive than the bulge-component of M 74 and that the time scale for in-spiral will be longer. Nevertheless, the time scale will be short compared to the age of the cluster, ~ 8 Gyr.

Dust from AGB Stars

While on the AGB, the outer layers of a star expand drastically leading to a circum-stellar envelope, which leads to an enrichment of the interstellar medium, contributing to the mass budget for future star formation (e.g. Loup et al., 1997; van Loon et al., 1998). Material from the stellar winds can produce dust, which cools off and becomes visible in the mid-infrared regime. Note that the dust would reside "close" to the star (at a few hundred stellar radii for a temperature of (~ 100 K; Decin, 2021), thus not obscuring the emission of other stars in the NSC, which is why we observe no dust obscuration in the ultraviolet and optical regime. Here we explore whether AGB stars can account for the emission in the MIRI bands (*c.f.* Figure 4.5).

We first determine the residual flux, which is not accounted for by the SED model excluding the data. The residual values are $\Delta S_\nu = 0.096$, 0.062, 0.049, and 0.014 mJy in the *F770W*, *F1000W*, *F1130W*, *F2100W*, respectively. Next, we generate absolute magnitudes of AGB stars using `PARSEC` tracks (Bressan et al., 2012), with 60 % Silicate and 40 % AlOx for M-type stars, and 85 % AMC and 15 % SiC for C-type stars (Groenewegen, 2006), long-period variabilities from Trabucchi et al. (2021), a log-normal Chabrier (2003) initial mass function, and a metallicity of $Z = 0.012$.[8] The last two settings equal the results found from SED fitting. We then convert the absolute magnitudes to spectral flux densities using the distance estimate to M 74 and Vega- to AB-magnitude conversion factors for the Sun (Willmer, 2018).

[8]The models were calculated by using http://stev.oapd.inaf.it/cgi-bin/cmd_3.6 (Bressan et al., 2012; Chen et al., 2014; Tang et al., 2014; Chen et al., 2015; Marigo et al., 2017; Pastorelli et al., 2019, 2020).

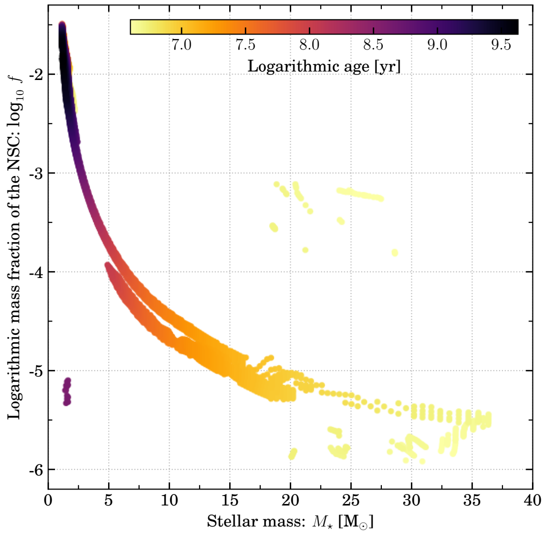

Figure 4.10. Logarithmic fraction of the number of AGB stars multiplied by their mass and divided by the total nuclear star cluster mass ($\log_{10} f$) versus AGB star mass. Each data point is color-coded according to the age of the star. Note that all AGB stars are younger than the main stellar population of the NSC, as identified by fitting the spectral energy distribution.

First, we limit the AGB model stars to reside within the 1σ interval of the measured colors.[9] Afterwards, we determine how many AGB stars are required to account for the residual emission in the MIRI bands and multiply that number by the mass of the stars. Figure 4.10 shows the logarithmic mass fraction of AGB stars compared to the total NSC mass versus the mass of the individual AGB stars. The data are color-coded by the age of the AGB stars. We find that both a few young and many old AGB stars could be responsible for the emission in the mid-infrared. However, all model AGB stars that satisfy the color-cuts are younger than 5 Gyr, which gives the lower uncertainty on the age of the main stellar population of the NSC. Therefore, if AGB stars are responsible for the emission in the MIRI data, there must have been star formation *in-situ* after the initial formation of the NSC.

In case the AGB stars are old, meaning that many AGB stars are required to account for the emission in the mid-infrared, it remains unclear why both the effective radius and ellipticity change significantly, as the cluster with the AGB star should have relaxed between their formation and today. In contrast, only few massive and young AGB stars are required to account for the mid-infrared emission, which could explain the increased effective radius and ellipticity, if they formed outside the center of the NSC. However, this would require in-flow of gas in the past few Myr but we cannot detect the presence of a young stellar population in the NSC. Therefore, it remains challenging to explain both the structural and photometric parameters using only AGB stars.

A Circum-Nuclear Gaseous Disk

Another possibility is that the infrared emission originates from a circum-nuclear gaseous disk or ring with a radius of a few pc, similar to the one present in the MW. Indeed, the MW hosts a clumpy, asymmetric, inhomogeneous, and kinematically disturbed concentration of molecular/ionized gas at $R \lesssim 5$ pc known as the circum-

[9] We use the six colors *F770W – F1000W*, *F770W – F1130W*, *F770W – F2100W*, *F1000W – F1130W*, *F1000W – F2100W*, and *F1130W – F2100W*.

nuclear disk (e.g. Lau et al., 2013; Hsieh et al., 2021). The MW circum-nuclear disk occupies similar radii to its NSC, has a total mass of $M_{\rm gas}^{\rm disk} \simeq 10^4$-$10^5\,\mathrm{M}_\odot$ and it is probably a transient structure (on a timescale of few Myr) originating from a series of randomly oriented in-flow events (Requena-Torres et al., 2012). By analogy, we could hypothezise that M 74 hosts a similar gaseous structure and that this is producing the observed mid-infrared emission. While the emission from the gas disk could explain the observed photometry, it is unclear why we do not detect a "young" (formed in the last few Gyr) stellar population in the NSC. While the *ALMA* CO band does not show significant emission in M 74's center (see Figure 4.1), this may be related to the sensitivity of the ALMA measurements and could not exclude a low-mass disk: in the PHANGS–ALMA v4p0 "broad" CO (2-1) map, the intensity measurement at the position of the NSC is $I_{\rm (CO)2-1} = (-0.3 \pm 1.3)\,\mathrm{K\,km\,s^{-1}}$. Given the beam size ($\theta = 1.12\,\mathrm{arcsec}$) and distance to the target, translating this value to a 3σ upper limit to the CO (2-1) luminosity yields $\log_{10}\, L_{\rm (CO)2-1}\,/\,\mathrm{K\,km\,s^{-1}\,pc^2} < 4.1$. For a standard Milky Way CO to H_2 conversion factor and CO (2-1) to CO (1-0) line ratio appropriate for M 74 (Bolatto et al., 2013; den Brok et al., 2021), this luminosity limit corresponds to an upper mass limit of $\log_{10}\, M_{\rm H_2}\,/\,\mathrm{M}_\odot < 4.9$. In comparison, the circum-nuclear disk of the Milky Way has a mass of $M_{\rm gas} \sim 1.2 \times 10^4\,\mathrm{M}_\odot$ (Requena-Torres et al., 2012).

Background Galaxy

It is also plausible that the emission in the MIRI data originates from a background galaxy, which happens to be aligned with the NSC along the line of sight. Although an alignment of the order $0.1''$ is unlikely, we investigate this scenario further based on the photometry found in the MIRI data.

Hassani et al. (2023) investigate the properties of compact sources at 21 µm for all four PHANGS–JWST targets for which data are available. Using a dendogram-based algorithm, they find 1271 compact sources of which 115 are classified as "potential background sources" (or HZ). This classification was performed using flux density ratios between MIRI bands (their Equations 1 and 2). The MIRI structure coinciding with the NSC of M 74 was also classified as a potential background object.

A search in the *NASA Extragalactic Database*[10] revealed that the 114 sources were previously detected by the *WISE / ALLWISE* mission (Wright et al., 2010; Cutri et al., 2013) and all objects were classified as "infrared sources". While these sources show a galaxy-like morphology at 2 µm, their detailed properties remain unclear at this point.

To compare to the other potential background objects, we select the measured spectral flux densities for the MIRI bands and subtract the extrapolated emission from the NSC using the SED fit excluding the MIRI data (solid line in Figure 4.5). While the flux density values compare to other potential background sources, their evolution with wavelength does not: none of the 114 identified potential background objects follow a similar trend in that the flux densities decrease with increasing wavelength.

Therefore, if the other 114 sources are background galaxies, the differences in the evolution of flux densities with wavelength suggest that the MIRI emission coinciding with the NSC of M 74 is not related to a background galaxy. Such a scenario becomes

[10]URL: https://ned.ipac.caltech.edu/

more unlikely if we combine it with the probability of alignment with the NSC along the line of sight.

4.6 Conclusions

In this work we analysed the nuclear star cluster (NSC) of M 74, a nearby late-type spiral galaxy, with archival *Hubble Space Telescope* (*HST*) ACS & WFC3 and newly obtained *James Webb Space Telescope* (*JWST*) NIRCam & MIRI data. The combined data cover the ultraviolet to mid-infrared wavelength, enabling an unprecedented analysis of an extragalactic NSC. Our findings can be summarized as follows:

1. Combining the $B - V$ color with various mass-to-light relations results in an NSC stellar mass of $\log_{10}(M_\star^{\mathrm{nsc}} / \mathrm{M}_\odot) = 7.06 \pm 0.31$. We compare this number to an estimate derived using the K-band magnitude (resulting in 7.2 ± 1.1) and the results from fitting the spectral energy distribution (SED; resulting in ~ 7.1). These values are consistent with the literature value of 7.05 ± 0.21 (Georgiev et al., 2016).
2. The effective radius and ellipticity of the NSC are ~ 5 pc and ~ 0.05, respectively, across the ultraviolet, optical, and near-infrared regime. The Sérsic index drops from ~ 3 to ~ 2 and the position angle drops from $\sim 130°$ to ~ 90-$100°$. These values supersede literature values, which varied significantly across neighboring bands (Georgiev & Böker, 2014).
3. In the mid-infrared bands, the effective radius and ellipticity increase to ~ 12 pc and ~ 0.4, respectively. The Sérsic index drops further to ~ 1.5 while being consistent with an exponential profile, and the position angle remains unchanged compared to the near-infrared.
4. We fit the SED from the ultraviolet to the near-infrared with a total of ten data points to find an old stellar population of (8 ± 3) Gyr with a metallicity of $Z = 0.012 \pm 0.006$. The fit indicates that no younger stellar population is present.
5. Fitting the SED with the inclusion of the MIRI data yields an overall worse fit, as evaluated by χ^2 statistics. Nevertheless, the age and metallicity of the main stellar population remain unchanged within the uncertainties. The differences in both fits to the SED indicate that the MIRI data do not trace the stellar population found in the lower wavelength regimes.
6. We find different angular separations between the center of the NSC in different bands, being most significant in the mid-infrared data. However, depending on the band from which the world coordinate system is taken as reference, the separations become less significant. This could hint at persistent calibration issues with the world coordinate systems of individual bands.

The color, age, and metallicity of the main stellar population of M 74 NSC indicate that no star formation has taken place in the previous few Gyr in its center. This is caused either by a dynamical mechanism preventing gas and dust inflow, or by central feedback. The lack of a young stellar population hints that the central cavity, which lacks both gas and dust and has a size of approximately 200 pc × 400 pc around the NSC, has existed for the last few Gyr as well. The reason for the lack of recent *in-situ* star formation and origin of the central cavity remains unknown.

The nature of the emission in the mid-infrared bands remains a mystery as well. From our SED fits it is clear that the old stellar population of the NSC cannot completely explain the emission in *JWST*'s MIRI bands. We discussed five different mechanisms, which may cause the emission: (1) contribution from a central active galactic nucleus, (2) an infalling star cluster, (3) dust from asymptotic giant branch (AGB) stars, (4) the presence of a circum-nuclear disk, and (5) alignment with a background galaxy.

The AGB scenario could explain the observed photometry. However, we find that the AGB stars whose colors fit the measurements are younger than the main stellar population. From a comparison to model AGB stars, we find that either a large number of old or a small number of young stars are required. While the first scenario cannot explain the wavelength dependence of the structural parameters, the latter scenario requires recent (a few Myr ago) in-falling gas, however, no stellar population younger than 5 Gyr was detected from SED fitting. In conclusion, none of the four discussed scenarios can fully explain both the structural and photometric measurements.

Our analysis highlights the potential *JWST* data has for exploring galactic nuclei in the nearby Universe. An ongoing analysis of the stellar population using PHANGS–MUSE data can improve the situation, albeit it cannot resolve the NSC. To solve the riddle of the nucleus of M 74 at long wavelengths, we will propose high-resolution spectroscopic observations, ideally Integral Field Unit spectroscopic data with *JWST*, to determine the kinematic properties of the NSC and its direct surroundings. In addition to the nature of the structure in the mid-infrared bands, these data will constrain further the presence of a young stellar population, the kinematic signature compared to the cluster, and help to constrain the presence of a black hole in M 74 as there is currently no available robust mass measurement or upper limit.

4.7 Appendix

4.7.1 Number of Sérsic Profiles

The description of the projected light distribution of NSCs is often approximated by a single simple analytic function such as a Sérsic profile, with few exceptions (Nguyen et al., 2018; Pechetti et al., 2022). With increasing spatial resolution at all wavelength ranges, accurate descriptions of the light distribution of NSCs may warrant multiple profiles. The NSC of M 74 was analyzed previously by Georgiev and Böker (2014) and modeled with a single King profile, but the goodness of the fit was not indicated.

Here we explore whether adding a second Sérsic profile improves the fit compared to a single Sérsic profile. The goodness of the two fits may not be compared via the standard χ^2 statistics, as different number of free parameters are at play. To compensate for the increased number of free parameters k, a penalty is introduced by adding a term linear in k to the standard χ^2 evaluation. We use the Bayesian Information Criteria (BIC, Schwarz, 1978), defined as

$$\mathrm{BIC} = -2 \ln \mathcal{L} + k \ln N \,, \tag{4.5}$$

where $\mathcal{L}$ is the likelihood value and N the total number of data points. Model (A) is generally preferred over model (B) if $\Delta\mathrm{BIC} = \mathrm{BIC}_B - \mathrm{BIC}_A > 0$, but note that the BIC is a heuristic approach and includes approximations.

Table 4.5. Differences in the Bayesian Information Criteria (ΔBIC) between two (A) and a single Sérsic profile (B) for the NSC of M 74.

Band	$\mathrm{BIC}_{(A)}$	$\mathrm{BIC}_{(B)}$	ΔBIC	$\frac{\mathrm{BIC}_{(A)}}{\mathrm{BIC}_{(B)}}$
F275W	269	203	66	1.33
F336W	225	156	69	1.44
F435W	234	155	79	1.51
F555W	227	162	65	1.40
F658N	216	150	66	1.44
F814W	284	222	62	1.28
F200W	14 191	14 121	70	1.00
F300M	940	870	70	1.08
F335M	1167	1047	120	1.11
F360M	1133	1105	27	1.03
F770W	421	343	78	1.23
F1000W	DNF[(a)]	382	--	--
F1130W	DNF[(a)]	482	--	--
F2100W	DNF[(a)]	DNF[(a)]	--	--

[(a)] The fit failed to terminate or parameter values ran into boundary conditions in all attempts.

We highlight the results for the single (labeled "A") and double Sérsic profile (labeled "B") fits for the NSC in Table 4.5. The *F2100W* is excluded from the list as the fit with two profiles for the NSC did not converge under any circumstance.

The conclusion from this experiment is that a single Sérsic profile is preferred over fitting two Sérsic profiles for the NSC.

4.7.2 Data Table

In Table 4.6 we present the best-fit parameters using a single Sérsic profile.

Table 4.6. Best-fit parameter estimates for the nuclear star cluster of M 74 using a single Sérsic profile. The parameter values and their uncertainties were determined via 500 bootstrap iterations, where the best-fit value gives the median and the uncertainties the 1σ interval.

Band	RA [hms]	DEC [dms]	PA [deg]	ϵ	n	r_{eff} [arcsec]	r_{eff} [pc][(b)]	m_0[(a)] [mag]
F275W	01:36:41.742	15:47:01.167	139^{+16}_{-25}	$0.13^{+0.03}_{-0.12}$	$3.5^{+1.0}_{-1.5}$	$0.17^{+0.03}_{-0.14}$	$8.2^{+6.7}_{-6.7}$	$21.38^{+0.31}_{-0.16}$
F336W	01:36:41.742	15:47:01.173	$125.1^{+5.5}_{-5.7}$	$0.056^{+0.009}_{-0.010}$	$2.07^{+0.10}_{-0.11}$	$0.099^{+0.002}_{-0.002}$	$4.74^{+0.09}_{-0.09}$	$20.18^{+0.02}_{-0.02}$
F435W	01:36:41.743	15:47:01.174	$106.8^{+5.7}_{-6.1}$	$0.066^{+0.013}_{-0.014}$	$3.01^{+0.19}_{-0.18}$	$0.107^{+0.003}_{-0.003}$	$5.10^{+0.14}_{-0.14}$	$18.54^{+0.02}_{-0.02}$
F555W	01:36:41.738	15:47:01.216	89^{+29}_{-23}	$0.020^{+0.011}_{-0.015}$	$2.51^{+0.20}_{-0.29}$	$0.103^{+0.003}_{-0.003}$	$4.91^{+0.14}_{-0.14}$	$17.89^{+0.04}_{-0.02}$
F658N	01:36:41.736	15:47:01.186	105^{+11}_{-10}	$0.049^{+0.020}_{-0.018}$	$2.91^{+0.21}_{-0.31}$	$0.103^{+0.003}_{-0.005}$	$4.91^{+0.22}_{-0.22}$	$17.45^{+0.04}_{-0.02}$
F814W	01:36:41.738	15:47:01.227	$118.6^{+7.1}_{-7.2}$	$0.066^{+0.015}_{-0.014}$	$3.21^{+0.28}_{-0.43}$	$0.113^{+0.004}_{-0.005}$	$5.39^{+0.24}_{-0.24}$	$17.12^{+0.04}_{-0.03}$
F200W	01:36:41.741	15:47:01.133	81^{+12}_{-12}	$0.036^{+0.013}_{-0.013}$	$2.26^{+0.15}_{-0.02}$	$0.111^{+0.004}_{-0.004}$	$5.31^{+0.21}_{-0.21}$	$16.54^{+0.27}_{-0.27}$
F300M	01:36:41.738	15:47:01.177	96^{+12}_{-10}	$0.053^{+0.022}_{-0.023}$	$2.21^{+0.23}_{-0.37}$	$0.122^{+0.006}_{-0.007}$	$5.81^{+0.35}_{-0.35}$	$17.41^{+0.25}_{-0.25}$
F335M	01:36:41.737	15:47:01.219	103^{+11}_{-3}	$0.074^{+0.027}_{-0.032}$	$2.12^{+0.21}_{-0.28}$	$0.122^{+0.008}_{-0.010}$	$5.80^{+0.47}_{-0.47}$	$17.54^{+0.25}_{-0.25}$
F360M	01:36:41.741	15:47:01.223	$95.6^{+7.2}_{-5.8}$	$0.099^{+0.029}_{-0.033}$	$1.88^{+0.18}_{-0.21}$	$0.129^{+0.007}_{-0.008}$	$6.16^{+0.38}_{-0.38}$	$17.65^{+0.25}_{-0.25}$
F770W	01:36:41.733	15:47:01.294	$86.6^{+4.3}_{-4.5}$	$0.296^{+0.034}_{-0.033}$	$0.63^{+0.08}_{-0.08}$	$0.173^{+0.007}_{-0.007}$	$8.25^{+0.36}_{-0.36}$	$18.53^{+0.02}_{-0.02}$
F1000W	01:36:41.733	15:47:01.245	$93.2^{+5.0}_{-5.6}$	$0.395^{+0.083}_{-0.045}$	$1.45^{+0.71}_{-0.64}$	$0.250^{+0.015}_{-0.022}$	$11.9^{+1.0}_{-1.0}$	$18.78^{+0.15}_{-0.15}$
F1300W	01:36:41.733	15:47:01.247	$93.1^{+5.0}_{-3.9}$	$0.393^{+0.071}_{-0.045}$	$1,46^{+0.63}_{-0.40}$	$0.251^{+0.009}_{-0.015}$	$11.99^{+0.72}_{-0.72}$	$18.82^{+0.08}_{-0.08}$
F2100W[(c)]	01:36:41.728	15:47:01.231	--	--	--	--	--	$19.51^{+0.68}_{-0.68}$

(a) Apparent magnitude in the AB-magnitude system. The values are corrected for extinction.
(b) Uncertainties were determined based on the assumption that the parameter distribution is Gaussian.
(c) No fit to the data succeeded if PSF convolution was enabled. To determine the central position of the NSC and the magnitude, the data were fit without PSF convolution.

4.8 Chapter Summary

- This work presents the first-ever analysis of an NSC using newly obtained *JWST* and archival *HST* data, ranging from the far ultraviolet to the mid-infrared regime.
- The analysis provides structural information as well as a fit to the NSC's spectral energy distribution, resulting in estimates of the dominant stellar population's age and metallicity.
- The NSC is relatively old (≈ 8 Gyr) and has roughly solar metallicity, which agrees with stars in the "pseudo-bulge".
- Consequentially, the accretion history of the MBH within the NSC, if present, was quiet over the last few Gyr given that no younger stellar population appears to be present.
- The data reveal a secondary extended and offset component that is prominent in the mid-infrared. The data are inconclusive about the origin of this component, requiring additional data in the mid-infrared.

Chapter 5

Low-Luminosity Active Galactic Nuclei in Nuclear Star Clusters

Declaration

The contents of this chapter were previously published in Hoyer et al. (2024). All co-authors provided commentary that improved the published work.

Abstract

Massive black holes (MBHs) are hosted in the centres of massive galaxies but they seem to become rarer in lower mass galaxies where instead nuclear star clusters (NSCs) frequently appear. The transition region, where both an MBH and NSC co-exist, is poorly studied and only a few dozens of galaxies are known to host them. One avenue to detect new galaxies with both an MBH and NSC is to look for accretion signatures of MBHs. Here we use new *SRG*/eROSITA all-sky survey *eRASS:4* data to search for X-ray signatures of accreting MBHs in NSCs, investigating also their combined occupation fraction. We collect more than 200 galaxies containing an NSC, spanning multiple orders in galaxy stellar mass and morphological type, within the footprint of the German eROSITA Consortium survey. We determine the expected X-ray contamination from binary stellar systems using the galaxy stellar mass and star formation rate as estimated from far-ultraviolet and mid-infrared emission. We find significant detections for 18 galaxies (~ 8.3 %), including one ultra-luminous X-ray source, however, only three galaxies (NGC 2903, 4212, and 4639) have X-ray luminosities higher than the expected value from X-ray binaries, indicative of the presence of an MBH. In addition, the X-ray luminosity of six galaxies (NGC 2903, 3384, 4321, 4365, and 4701) differs from previous studies and could indicate the presence of a variable AGN. For NGC 4701 specifically, we find a variation of X-ray flux within the *eRASS:4* data set. Stacking X-ray non-detected galaxies in the dwarf regime ($M_\star^{\rm gal} \leq 10^9\,\mathrm{M}_\odot$) results in luminosity upper limits of a few times $10^{38}\,\mathrm{erg\,s^{-1}}$. The combined occupation fractions of accreting MBHs and NSCs become non-zero for galaxy masses above ~ $10^{7.5}\,\mathrm{M}_\odot$ and are slightly elevated compared to the literature. Our data extent for the first time towards the dwarf elliptical galaxy regime and identify promising MBH candidates for higher-resolution follow-up observations. At most galaxy masses and with the exception of three cases, the X-ray constraints are consistent with the expected emission from binary systems or an Eddington fraction of at most

0.01 % assuming a black holes mass of $10^{6.5}\,\mathrm{M}_\odot$. This work confirms the known complexities in similar-type of studies but provides an appealing alternative of using X-ray survey data to in-depth observations of individual targets with higher-resolution instruments.

5.1 Introduction

Since the first detections of massive compact objects in nearby galaxy centers almost forty years ago (Tonry, 1984), it became evident that massive black holes (MBHs) occupy many nearby galaxy centers (e.g. Kormendy & Richstone, 1995; Maggorian et al., 1998; Tremaine et al., 2002; Kormendy & Ho, 2013). This insight was made possible by significant advancements in the performance and capabilities of many ground-based facilities [with examples including *NIRC* on Keck (Ghez et al., 1998; Filippenko & Ho, 2003; Walsh et al., 2012), *SHARP* on NTT (Genzel et al., 2000; Gillessen et al., 2009), *GRAVITY* (Abuter et al., 2017, 2021), *SAURON* (Bacon et al., 2001a; van den Bosch & de Zeeuw, 2010), *CFHT* (Bender et al., 1996; Kormendy et al., 1997), *SINFONI* (Nowak et al., 2008; Rusli et al., 2011; Saglia et al., 2016), *VLBI* (Kuo et al., 2011), *GEMINI*/NIFS (Nguyen et al., 2018; Merrell et al., 2023), *VLT* (Marconi et al., 2001)] and with the *Hubble Space Telescope* (*HST*; e.g. Devereux et al., 2003; Gebhardt et al., 2003; Atkinson et al., 2005; Gültekin et al., 2009; Walsh et al., 2010; Nguyen et al., 2019), as well as improvements in dynamical models of galaxy centers (e.g. Cappellari & Emsellem, 2004; Thater et al., 2019; Cappellari, 2020; Thater et al., 2022b, 2022a). These measurements were only performed on massive galaxies as secure detections of MBHs towards the lowest galaxy masses become rare both because of weaker observational signatures and an apparent decline in the MBH occupation fraction, as suggested by observational (e.g. Miller et al., 2015a; Trump et al., 2015; Nguyen et al., 2018) and theoretical (e.g. Volonteri et al., 2003; Bellovary et al., 2011; Habouzit et al., 2017; Haidar et al., 2022) studies.[1] Despite numerous investigations (see e.g. Sharma et al., 2022; Beckmann et al., 2023; Spinoso et al., 2023, for recent studies), the functional shape and value of the galaxy stellar (or halo) mass of the decline of the occupation fraction from unity remains only loosely constrained.

Galaxy centres can also host dense stellar systems, known as nuclear star clusters (NSCs), which are more commonly found in the dwarf galaxy regime, occupying about 80 % of $M_\star^{\mathrm{gal}} \sim 10^9\,\mathrm{M}_\odot$ galaxies in the local universe (Sánchez-Janssen et al., 2019a; Neumayer et al., 2020; Hoyer et al., 2021; Ashok et al., 2023). Contrary to MBHs, their occupation fraction rapidly declines in the most massive galaxies, where MBHs are most common, potentially due to interactions between the two objects (e.g. Antonini et al., 2015; Arca-Sedda & Capuzzo-Dolcetta, 2017) or tidal evaporation of progenitor clusters (Leaman & van de Ven, 2022). Nevertheless, a transition region where both types of nuclei are present exists and includes, for example, the Milky Way (e.g. Genzel et al., 2010). As the functional shape of the MBH occupation fraction with respect to the host galaxy stellar mass is currently unclear, the extent of this transition region is

[1] See Bustamente-Rosell et al. (2021) and Regan et al. (2023) for a discussion on a $10^6\,\mathrm{M}_\odot$ MBH in the nearby Leo I ($M_\star^{\mathrm{gal}} \sim 10^7\,\mathrm{M}_\odot$) dwarf galaxy.

unclear as well.

Due to observational constraints all firm MBH detections within NSCs are confined to relatively nearby galaxies [see e.g. Figure 2 in Greene et al. (2020) and the compilation of Neumayer et al. (2020)] and are located in the NSC's centre with the exception of M 31 (e.g. Lauer et al., 1993; Bacon et al., 1994, 2001b; Bender et al., 2005). Consequently, the total number of these systems is limited to a few dozens (e.g. Neumayer et al., 2020; Nguyen et al., 2022; Thater et al., 2023), including ultra-compact dwarfs as previous NSCs of accreted galaxies (e.g. Seth et al., 2014; Pfeffer et al., 2016; Ahn et al., 2017; Pechetti et al., 2022). As we are now aware of more than 1000 nucleated galaxies (Muñoz et al., 2015; Venhola et al., 2018; Sánchez-Janssen et al., 2019a; Carlsten et al., 2020; Habas et al., 2020; Poulain et al., 2021; Su et al., 2021; Hoyer et al., 2023a) and given the significant overlap between the NSC and MBH occupation fractions, we should expect a significantly higher number of galaxies with both an MBH and NSC. While dynamical measurements are important to obtain reliable mass measurements for MBHs within NSCs, focusing on accretion signatures can help to identify larger samples out to higher distances, including dwarf galaxies where NSCs are most common (e.g. Kauffmann et al., 2003; Baldassare et al., 2018; Birchall et al., 2020; Mezcua & Domínguez Sánchez, 2020; Mezcua et al., 2023; Cann et al., 2024).

Accretion events onto MBHs from gas or stars via tidal disruption events (Rees, 1988) leads to bright X-ray emission (e.g. Komossa & Bade, 1999; Esquej et al., 2008; Maksym et al., 2010) which can be used to study the mass of the black hole (e.g. Mockler et al., 2019) and potentially that of black hole binaries (Mockler et al., 2023). Additionally, data from large-scale surveys was previously used to trace MBHs (e.g. Miller et al., 2015b) and to constrain their occupation fraction (Miller et al., 2015a). One avenue to detect more MBHs in NSCs is to combine optical and X-ray data to detect and characterise the NSC and MBH, respectively, requiring an AGN that does not outshine the NSC in the optical regime.

Previous work already took advantage of combining various wavelength regimes (Seth et al., 2008a; Baldassare et al., 2022), using, among other instruments, *Chandra* for X-rays. Another approach compared to using high-resolution archival and newly obtained *Chandra* data is to perform a shallower wide-area survey, allowing us to study a greater number of NSCs in galaxies of various masses and morphologies. The "extended ROentgen Survey with an Imaging Telescope Array" (or eROSITA in short; Predehl et al., 2021) aboard the *Spectrum-Roentgen-Gamma* (*SRG*; Sunyaev et al., 2021) takes this approach and is the ideal laboratory for such a study. The poorer resolution of eROSITA operating in its survey mode (half-energy width of $26''$; Predehl et al., 2021) does not allow us to distinguish clearly between nuclear and off-nuclear emission as securely as *Chandra* but can still be used to detect MBH candidates for follow-up studies and to potentially probe MBH signatures in a large number of NSCs directly.

In this paper, we explore these possibilities using the cumulative data from eROSITA's already completed four all-sky surveys (dubbed *eRASS:4*; Predehl et al., 2021) to locate X-ray emission in a large sample of NSCs. We introduce the eROSITA, galaxy, and literature data sets in Section 5.2 and analyse their properties in Section 5.3. Section 5.4 contains a discussion of the results and Section 5.5 concludes the paper.

5.2 Data

5.2.1 Sample of Nucleated Galaxies

To generate an all-sky catalogue of nucleated galaxies, we first consider all galaxies up to a distance of 100 Mpc, which are part of the HyperLEDA[2] data base (Makarov et al., 2014), containing approximately 63 000 objects. Based on this catalogue, we search the *Hubble Legacy Archive*[3] for available high-resolution imaging data (*Advanced Camera for Surveys*, *Wide Field and Planetary Camera 2*, and *Wide Field Camera 3*). Based on these data, we assign a nuclear classification to all galaxies, not taking into account previous classifications in the literature. The HyperLEDA data base becomes incomplete towards the dwarf galaxy regime, which is why we add to the classified galaxy sample the data of den Brok et al. (2014), Muñoz et al. (2015), Sánchez-Janssen et al. (2019a), Zanatta et al. (2021), and Su et al. (2022) for members of the Fornax, Virgo, and Coma galaxy clusters. The combined catalogue contains 888 nucleated galaxies across the whole sky, which we use to cross-match with the German footprint of eROSITA.

5.2.2 eROSITA Observations: *eRASS:4*

We systematically extracted X-ray photometry at the input coordinates of the nucleated galaxies in the cumulative *eRASS:4* images within the footprint of the German eROSITA Consortium (i.e. Galactic longitudes between 179.944 and 359.944). This led to a starting sample of 239/888 galaxies, with mean exposure of ~ 418 s and standard deviation of ~ 58 s (see Figure 5.1 for three examples). A detailed description of the methodology is presented in Arcodia et al. (2024b) and we only outline here the basic steps.

X-ray counts were extracted between 0.2-2.0 keV within a circular aperture of 30″, corresponding to ~ 75 % of the encircled energy fraction of eROSITA's point spread function in the adopted energy band. The background contribution was estimated from an annulus with inner and outer radii of 120″ and 360″, respectively. Contaminating X-ray sources were masked following the prescription from Comparat et al. (2023, Appendix A). For a small number of cases (21/239), >70 % of the source aperture was masked out and the NSC is, therefore, excluded from the analysis. Consequentially, the sample size of nucleated galaxies with extracted X-ray properties from the automated pipeline reduced down to 239 − 21 = 218. We follow the method from Arcodia et al. (2024b) and adopt as threshold for a significant detection $P_{\mathrm{binom}} = 3 \times 10^{-4}$, which corresponds to a spurious fraction of ~ 1 %.

eRASS:4 X-ray spectra were extracted from the same aperture using the `srctool` task in the eROSITA Science Analysis Software System (`eSASS`; Brunner et al., 2022), with products version `020`. The spectral analysis was performed with the Bayesian X-ray Analysis software (`BXA`) version `4.0.5.` (Buchner et al., 2014), which connects the nested sampling algorithm `UltraNest` (Buchner, 2019, 2021) with the fitting environment `XSPEC` version `12.12.0.` (Arnaud et al., 1996), in its Python version

[2]URL: https://leda.univ-lyon1.fr/
[3]URL: https://hla.stsci.edu/

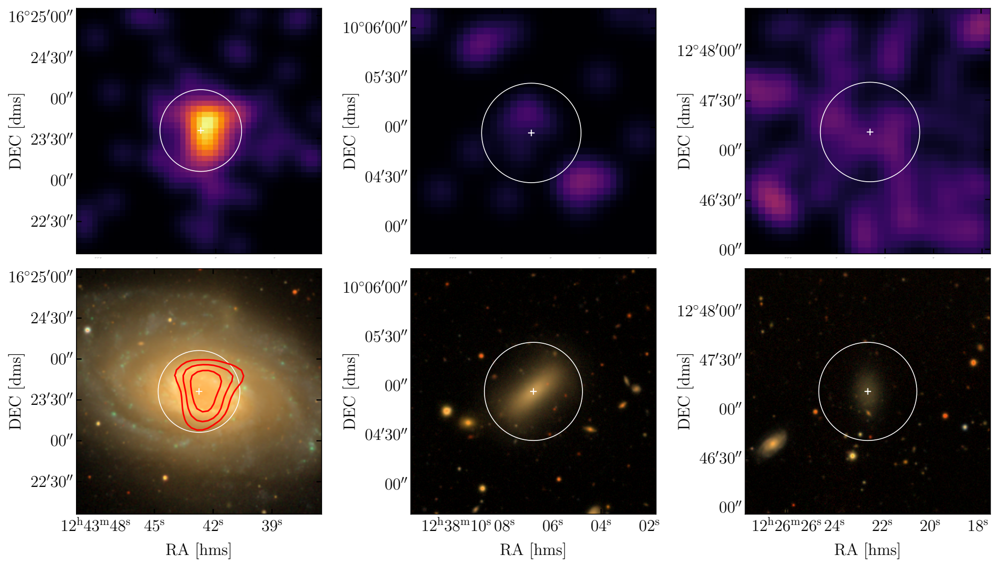

Figure 5.1. Cutouts of eROSITA *eRASS:4* images (*top panels*) and of the *DESI* Legacy Imaging Surveys (*bottom panels*) Data Release 10 [Legacy Surveys / D. Lang (Perimeter Institute)] of three galaxies in our sample: NGC 4651, IC 3602 and LEDA 40679. Both images are centered at the input optical coordinates of the NSC (white cross), with the 30″ aperture circle used for X-ray photometry highlighted in white. In case of an X-ray detection (*left column*) X-ray contours are also overlayed to the optical image (red).

`PyXspec`.[4] We adopted a simple power-law model (`zpowerlw`) with absorption fixed at the Galactic column density from HI4PI (HI4PI Collaboration et al., 2016) and redshifted to rest-frame. We quote median and 1$^{\text{st}}$ and 99$^{\text{th}}$ percentiles from fit posteriors for fluxes and luminosity, unless otherwise stated. For non-detections ($P_{\text{binom}} > 0.0003$), we quote upper limits using the 99$^{\text{th}}$ percentiles of the fit posteriors, unless otherwise stated.

Potential individual sources of contamination from within the source aperture were treated a posteriori after visual inspection and were considered on a case by case basis. For instance, we cross-matched our sample with the catalog from Walton et al. (2022), which compiled ultraluminous X-ray sources (ULXs) candidates from *XMM–Newton*, *Swift-XRT*, and *Chandra* data. We manually masked out a handful of apertures with known ULX candidates and other obvious off-nuclear X-ray sources, whose centroid lied within the source aperture. In some cases, this resulted in the NSC being non-detected after the masking: the galaxy NGC 4559 contains a known ULX (Walton et al., 2022) and after its masking the whole source aperture is masked-out and no products from the NSC can be analysed. Therefore, after visual inspection, the number of galaxies with extracted X-ray properties from the automated pipeline was 217/218. We provide in Tables 5.1 and 5.2 the properties of all 217 galaxies, derived as explained in the next subsections, with their measured *eRASS:4* X-ray luminosities.

From this sample we obtain that 18/217 targets are significantly detected. Computing

[4]The documentation for `PyXspec` can be found here: https://heasarc.gsfc.nasa.gov/docs/xanadu/xspec/python/html/index.html

1σ binomial uncertainties on this fraction from Cameron (2011), this results in a detection fraction of $8.3^{+2.3}_{-1.5}$ %.

Finally, we performed stacking analysis of non-detections following the methodology outlined in Comparat et al. (2022) and Arcodia et al. (2024b). Around each galaxy, we retrieved a photon cube with the angular position, the physical distance to the associated galaxy, the exposure time, the observed, and emitted energy (shifted to the rest-frame of the galaxy) and the effective area for each photon. Detected sources in the field were masked. The cubes were merged for the desired sub-sample of non-detected galaxies. We took a weighted mean of all events within 10 kpc using the weight described in Equ. 3 of Comparat et al. (2022) to obtain the surface brightness. We estimated the background surface brightness by repeating the procedure with events located at a distance between 15 and 50 kpc. Finally, we subtracted the background from the mean surface brightness (within a 10 kpc radius) and converted it to a luminosity.

5.2.3 NSC and Galaxy Parameters

The imaging data from *HST* used to classify galaxies are inhomogeneous with different spatial resolutions and available filters. Instead of deriving new NSC parameter estimates from these data, we looked for available values in the literature. As a consequence, not all nucleated galaxies of our sample have available NSC properties (which can be seen in Figures 5.4 and 5.5 below). More specifically, we searched for available NSC parameters for nucleated galaxies within the Local Volume ($d \lesssim 11$ Mpc; Seth et al., 2006; Georgiev et al., 2009a; Graham & Spitler, 2009; Baldassare et al., 2014; Schödel et al., 2014b; Calzetti et al., 2015; Carson et al., 2015; Crnojević et al., 2016; Nguyen et al., 2017; Baumgardt & Hilker, 2018; Nguyen et al., 2018; Bellazzini et al., 2020; Pechetti et al., 2020; Hoyer et al., 2023a), the field environment outside the Local Volume (Georgiev & Böker, 2014; Georgiev et al., 2016), and the Virgo galaxy cluster (Sánchez-Janssen et al., 2019a). Nucleated galaxies in the Coma and Fornax galaxy clusters are not part of our data set.

Galaxy stellar masses were determined as presented in the next subsection. Morphological type values are adopted from HyperLEDA and for the data sample of Sánchez-Janssen et al. (2019a) we assumed a value of −5, corresponding to elliptical galaxies.

Galaxy Stellar Masses

To compute galaxy stellar masses, we used three different tracers: (1) the $B - V$ colour, (2) the $g - r$ colour, and (3) the K-band luminosity. First, we obtained the photometric parameters and distance estimates from both the HyperLEDA and NED data bases. We then computed the aforementioned colours and B-, g-, and K-band luminosities using the absolute magnitude of the Sun[5] (Willmer, 2018), accounting for Galactic extinction via the re-calibrated version of the Schlegel et al. (1998) extinction maps (Schlafly & Finkbeiner, 2011) assuming $R_V = 3.1$ (Fitzpatrick, 1999). Internal extinction was not taken into account. The mass-to-light ratios for the different colours and K-band luminosity were taken from McGaugh and Schombert (2014) and Du et al. (2020),

[5] URL: http://mips.as.arizona.edu/~cnaw/sun.html

which give re-calibrated versions of the original relations by Bell et al. (2003), Portinari et al. (2004), Zibetti et al. (2009), Into and Portinari (2013), and Roediger and Courteau (2015). The uncertainties on the final stellar mass estimates were based on the ones of the photometric parameters, the distance estimate, the absolute magnitude of the Sun (assumed to be 0.04 mag) and the stellar mass-to-light relation (assumed to be 0.3 dex). Usually, the latter one dominates over all other uncertainties.

For the dwarf galaxies in the Virgo cluster, we directly took the mass estimates from Sánchez-Janssen et al. (2019a), which are based on fits to the spectral energy distributions and overall match to the other three approaches outlined above (Hoyer et al., 2021). Their stellar mass estimates lack an uncertainty which is why we assumed a value of 0.3 dex.

5.2.4 Literature X-Ray Data

As pointed out in the Introduction, previous work investigated the X-ray emissivity of NSCs in search for MBHs. Based on optical spectroscopy as well as Radio and X-ray data (via *Chandra*, *ROSAT*, and *XMM-Newton*), Seth et al. (2008a) found X-ray emission indicative of the presence of MBHs consistent with the position of NSCs in a sample of 176 early- and late-type galaxies. Most recently, Baldassare et al. (2022) used data from the *Chandra* X-ray observatory to search for such signatures in 108 nearby ($d \lesssim 40$ Mpc) nuclei from the galaxy sample of Georgiev and Böker (2014) which is composed of massive late-type galaxies. They classified 29 targets as having significant X-ray emission and, thus, harbouring AGN.

Some other studies investigated the X-ray luminosity of the central region of galaxies without taking into account their nuclear classification. Here we took into account data from She et al. (2017) and Ohlson et al. (2023), which used archival *Chandra* data.

We extracted fluxes and luminosities in the 0.5-7 keV to compare with Ohlson et al. (2023) and in the 2-10 keV to compare with Baldassare et al. (2022). We note that, compared to *Chandra*, eROSITA is most sensitive in the 0.2-2.3 keV energy band (Predehl et al., 2021). From Ohlson et al. (2023) we used their luminosity values for a circular aperture with a radius of $3''$ to better match the PSF of eROSITA. Baldassare et al. (2022) gives luminosities in both bands and we confirmed that the results drawn in Section 5.3.3 remain unchanged when changing to the 0.5-7 keV band.

5.3 Analysis

5.3.1 X-Ray Contamination from Binaries

Both low- and high-mass X-ray binaries, i.e. binary stellar systems composed of a donor and either a neutron star or stellar mass black hole, can significantly contribute to a galaxy's total X-ray luminosity (e.g. Iwasawa et al., 2009), sometimes rivalling active galactic nuclei (e.g. Lehmer et al., 2010). This contribution is especially important for our analysis given the size of eROSITA's PSF (half-energy width of approximately 30 arcsec; Predehl et al., 2021). The formation of low-mass X-ray binaries (LMXBs) typically takes 1-10 Gyr (Verbunt & van den Heuvel, 1995) as one requires stellar evolution to first produce a neutron star which then has to dynamically enter into a binary system with a donor. The collective X-ray luminosity of these systems in older disks and bulges is related to the stellar mass of the galaxy (Gilfanov, 2004) via $L_X^{\mathrm{LMXB}} = \alpha \times M_\star^{\mathrm{gal}}$ (e.g. Colbert et al., 2004; Lehmer et al., 2010) where $\log_{10} \alpha = 29.15^{+0.07}_{-0.06}\,\mathrm{erg\,s^{-1}\,M_\odot}^{-1}$ (Lehmer et al., 2019).

In contrast, high-mass X-ray binaries (HMXBs) require a stellar mass black hole and their X-ray emission is related to the stellar evolution timescale of the massive donor star, resulting in a luminous phase about 100 Myr after formation of the binary (Verbunt & van den Heuvel, 1995). Due to the high-mass of the donor and its short life time, the X-ray luminosity is related to the star formation rate (SFR) of the host galaxy via $L_X^{\mathrm{HMXB}} = \beta \times \mathrm{SFR}$ (e.g. Grimm et al., 2003) where $\log_{10} \beta = 39.73^{+0.15}_{-0.10}\,\mathrm{erg\,s^{-1}}\,(\mathrm{M_\odot\,yr^{-1}})^{-1}$ (Lehmer et al., 2019).

To estimate the current star formation rate of our sample, which we assume to be constant over the last 100 Myr (i.e. no star bursts or quenching effects from tidal interactions or bright active galactic nuclei), we used a correlation by Hao et al. (2011) and Kennicutt and Evans (2012) relating the emission in the far-ultraviolet (L_{FUV}) with the mid-infrared (L_{MIR}) and star formation rate via

$$\log_{10} \mathrm{SFR} = \log_{10} \left(L_{\mathrm{FUV}} + 3.89 \times L_{\mathrm{MIR}} \right) - 43.35\,. \tag{5.1}$$

We took this approach, opposite to e.g. an estimation via X-rays (Colbert et al., 2004; Symeonidis et al., 2011; Riccio et al., 2023), due to the availability and homogeneity of the available luminosities: to estimate the far-ultraviolet luminosity, we used the publicly available data from *Galex* (Morrissey et al., 2007). For the mid-infrared luminosity, we use *AllWISE W4* (Wright et al., 2010; Cutri et al., 2013) or *Spitzer MIPS* (Rieke et al., 2004) magnitudes. For dwarf elliptical galaxies in the Virgo cluster we assumed that no star formation occured over the last few hundred Myr and that the expected X-ray binary contamination is solely produced by LMXBs.

After computing the galaxy stellar mass and star formation rates, we determined the luminosities of both classes of binary systems. The expected contamination by X-ray binary systems is the sum of the two components, $L_X^{\mathrm{bin}} = L_X^{\mathrm{LMXB}} + L_X^{\mathrm{HMXB}}$. Objects, which were detected above this expected X-ray binary emission could indicate the presence of an MBH (but see Section 5.4.2 for caveats).

5.3.2 Properties of X-Ray Detected Sources

We compare the expected X-ray luminosity from the binary populations in the 2-10 keV range with the *eRASS:4* data in Figure 5.2, distinguishing between X-ray detected sources ($P_{\mathrm{binom}} \leq 3 \times 10^{-4}$) and undetected sources ($P_{\mathrm{binom}} > 3 \times 10^{-4}$, shown as upper limits). We also distinguish between objects only detected with eROSITA and the ones also detected with other instruments taken from Seth et al. (2008a), She et al. (2017), and Baldassare et al. (2022) or Ohlson et al. (2023). All significant detections in the *eRASS:4* data have measured X-ray luminosities of $L_{X,\,\mathrm{obs}}^{2-10\,\mathrm{keV}} > 10^{38}\,\mathrm{erg\,s^{-1}}$ and similarly high expected luminosities from the galaxies LMXBs and HMXBs. Only three galaxies in our sample (NGC 2903, NGC 4212, and NGC 4639) have measured luminosities greater than the expected values from binaries at 3σ confidence. Some of the X-ray detected sources are also measured below the expected value which may be related to uncertainties in the estimates of the galaxy-only predictions. We will discuss this observation further in Section 5.4.2. Below $L_{X,\,\mathrm{obs}}^{2\text{–}10\,\mathrm{keV}} \sim 5 \times 10^{38}\,\mathrm{erg\,s^{-1}}$ we find no significant emission and can only determine upper limits.

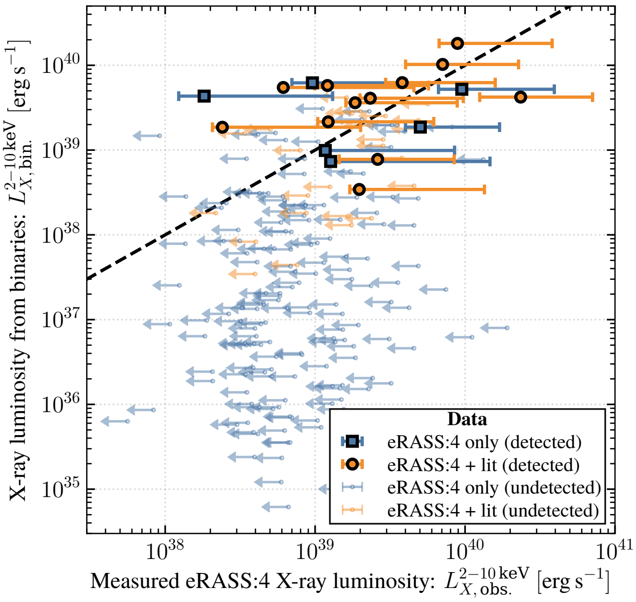

Figure 5.2. Expected X-ray luminosity from the combined high- and low-mass binary population in the 2-10 keV range $\left(L_{X,\,\mathrm{bin}}^{2\text{–}10\,\mathrm{keV}}\right)$ versus the measurements $\left(L_{X,\,\mathrm{obs}}^{2\text{–}10\,\mathrm{keV}}\right)$. We show the significantly detected galaxies ($P_{\mathrm{binom}} \le 0.0003$) in the *eRASS:4* footprint with blue squares. For non-detections, we plot upper limits using the 99$^{\mathrm{th}}$ percentile of the X-ray luminosity (blue arrows). Additionally, we highlight the *eRASS:4* luminosities of galaxies with available literature X-ray data (see Section 5.2.4; orange circles). These include data from Seth et al. (2008a), She et al. (2017), Baldassare et al. (2022), and Ohlson et al. (2023). Some of the galaxies are not significantly detected in the *eRASS:4* data but have secure measurements from other instruments available in the literature (orange arrows). A more detailed comparison between the *eRASS:4* and literature data is presented in Section 5.3.3.

Some of the NSCs with X-ray upper limits in Figure 5.2 reside in dwarf elliptical galaxies in the core of the Virgo cluster (29/117 galaxies at $M_\star^{\mathrm{gal}} \le 10^9\,\mathrm{M}_\odot$). A lack of photometric data in the literature makes it challenging to determine star formation rates and we assumed that no star formation takes place for these objects. While this assumption may be justified for the dwarf galaxy sample, the presented X-ray luminosity from binaries remains only a lower limit.

Figure 5.3 shows the distribution of measured X-ray luminosity versus galaxy stellar mass. To further constrain the emission in the dwarf galaxies, we stack non-detected galaxies within bins of stellar mass of 1 dex starting at $M_\star^{\mathrm{gal}} = 10^{5.5}\,\mathrm{M}_\odot$ until $10^{10.5}\,\mathrm{M}_\odot$ (see Section 5.2.2). None of the stacked X-ray images contains signals above background level, with upper limits of the order of $2 \times 10^{38}\,\mathrm{erg\,s^{-1}}$ found in each stellar mass bin. Estimating the expected X-ray luminosity from LMXBs with these galaxy stellar masses reveals that these upper limits are either matching or higher than the expected values, thus, being consistent with the X-ray emission of "normal" (i.e. non AGN X-ray dominated) galaxies.

From the low-mass towards the high-mass end in Figure 5.3 the X-ray luminosity of

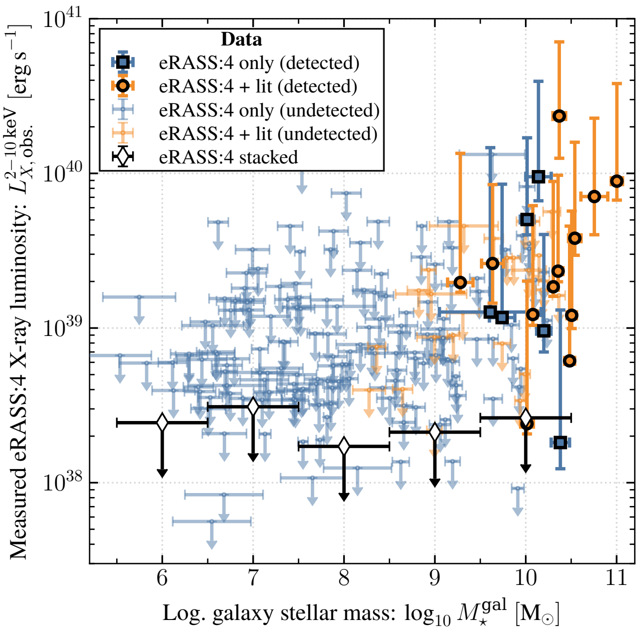

Figure 5.3. Measured X-ray luminosity in the 2-10 keV range ($L_{X,\,\mathrm{obs}}^{2-10\,\mathrm{keV}}$) versus galaxy stellar mass ($\log_{10} M_\star^{\mathrm{gal}}$). The markers, colour-coding and literature references are all the same as in Figure 5.2. We stack non-detections (upper limits, blue and orange arrows) in mass bins of 1 dex width starting at a galaxy mass of $10^{5.5}\,\mathrm{M}_\odot$ to set tighter constraints on the X-ray emission in dwarf galaxies. Only galaxies above galaxy masses of approximately $10^{9.3}\,\mathrm{M}_\odot$ are significantly detected in the *eRASS:4* data.

the significant detections appears to increase, starting around $M_\star^{\mathrm{gal}} \sim 10^{10}\,\mathrm{M}_\odot$. While this increase could be related to the increasing contribution from the nuclear emission, as seen for a few sources in Figure 5.2, most of the significantly detected sources feature the expected luminosities from X-ray binary systems. Therefore, it appears plausible that this increase is mostly related to the increasing strength of LMXBs and not due to the presence of AGN.

NSC Properties

Regarding NSC properties, we show the NSC versus host galaxy stellar mass relation (e.g. Georgiev et al., 2016; Neumayer et al., 2020; Ashok et al., 2023) in Figure 5.4. We complement our data with the sample of Baldassare et al. (2022), which is based on the data of Georgiev and Böker (2014). Similar to the previous observation for galaxy masses in Figure 5.3, only the most massive NSCs are significantly detected, above $M_\star^{\mathrm{nsc}} \sim 10^7\,\mathrm{M}_\odot$. Other lower-mass NSCs are not significantly detected, including objects, which were detected previously with *Chandra* down to $M_\star^{\mathrm{nsc}} \gtrsim 10^5\,\mathrm{M}_\odot$.

Figure 5.5 shows the NSC effective radius versus stellar mass plane. The *eRASS:4* detected NSCs have both high stellar mass and large radii, as is expected from scaling relations (Georgiev et al., 2016; Neumayer et al., 2020; Ashok et al., 2023). The average half-mass density of these objects, $\overline{\rho}$, is consistent with other significantly detected but lower-mass NSCs in the literature, falling between $10^4\,\mathrm{M}_\odot\,\mathrm{pc}^{-3} \lesssim \bar{\rho} \lesssim 10^6\,\mathrm{M}_\odot\,\mathrm{pc}^{-3}$.

Baldassare et al. (2022) also investigated the properties of their NSC sample distinguishing between X-ray luminosities likely originating from a massive black hole and X-ray binaries. Due to our limited sample of new detections, we refer to their study for further discussion with NSC properties.

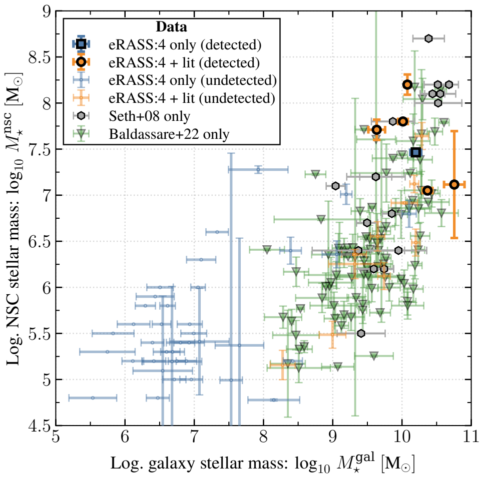

Figure 5.4. Nuclear star cluster ($\log_{10} M_\star^{\mathrm{nsc}}$) versus host galaxy stellar mass ($\log_{10} M_\star^{\mathrm{gal}}$). We show X-ray detected NSCs with full colour, distinguishing between sources only detected with eROSITA (blue) and sources also detected with other instruments (orange). A fainter shade is used for non-detection in the *eRASS:4* data. In addition, we show NSCs analysed by Seth et al. (2008a, grey hexagons) and Baldassare et al. (2022, green triangles) for NSCs with X-ray emission outside the *eRASS:4* footprint (or with significant contamination). A lack of literature data for NSC properties limits the included data set.

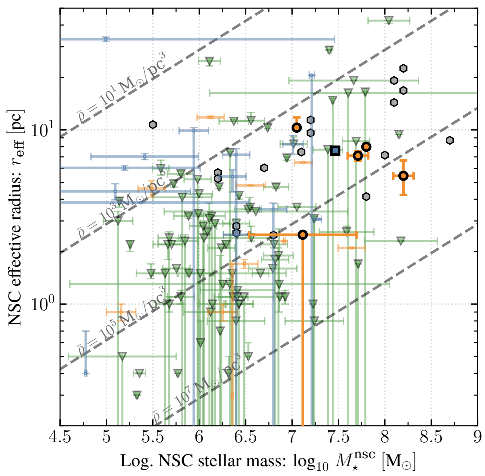

Figure 5.5. Nuclear star cluster effective radius (r_{eff}) versus stellar mass ($\log_{10} M_\star^{\mathrm{nsc}}$). The colour-coding and symbols are the same as in Figure 5.4. Note that compared to Figure 5.4 fewer NSCs are shown because of a lack of measured effective radii for the dwarf galaxy sample in the core of the Virgo cluster (Sánchez-Janssen et al., 2019a; Ferrarese et al., 2020). Uncertainties are omitted for clarity.

5.3.3 X-Ray Variable Sources

We compare in Figure 5.6 the X-ray luminosity of nucleated galaxies in the German footprint of the *eRASS:4* data with matches in *Chandra*, *ROSAT*, or *XMM-Newton* data from Seth et al. (2008a), She et al. (2017), Baldassare et al. (2022), and Ohlson et al. (2023), as introduced in Section 5.2.4. Given their upper limits, most of the *eRASS:4* values are in agreement with the literature. However, six other galaxies (NGC 2903, 3384, 4321, 4365, 4639, and 4701) have values not in agreement with the literature.

For one galaxy, NGC 2903, there exist literature data from both Baldassare et al. (2022) and Ohlson et al. (2023). Although the same data were analysed, they quote fluxes differing by a factor ~ 100, which is likely due to the difference between catalogue fluxes (Evans et al., 2010; Ohlson et al., 2023) and those estimated through aperture photometry (Baldassare et al., 2022). We computed the X-ray fluxes through spectral

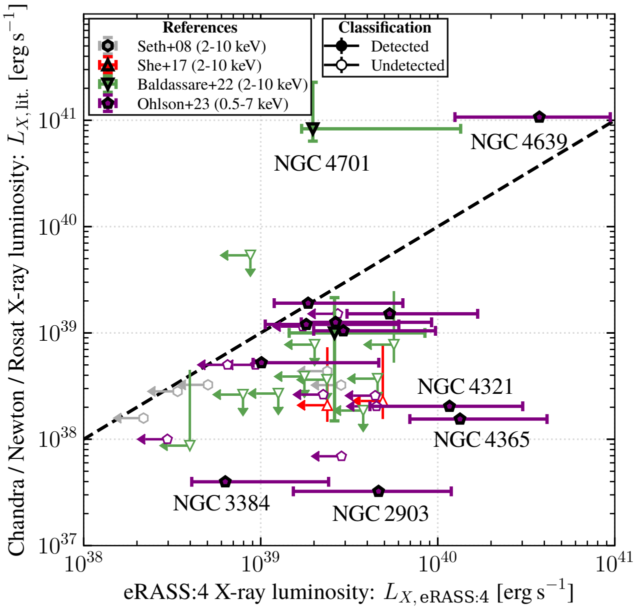

Figure 5.6. Comparison of literature *Chandra*, *XMM-Newton*, or *ROSAT* X-ray luminosity versus *eRASS:4* values. Full colour-coded symbols show X-ray detections in *eRASS:4*. The dashed line gives the one-to-one values. We compare to Seth et al. (2008a), She et al. (2017) and Baldassare et al. (2022) using the 2 to 10 keV band. Ohlson et al. (2023) give *Chandra* X-ray data in the 0.5 to 7 keV band. Galaxies, which likely show some X-ray variability, are specifically named.

analysis and obtained that the *eRASS:4* spectrum is sufficiently well described by a simple power-law with photon index 2.08 ± 0.20, although a more complex spectral model would be most likely required with higher count statistics in the 2-10 keV band. Based on this, we are not able to infer whether the difference between eROSITA and *Chandra* values is due to intrinsic variability or differences in the flux estimate methods.

We investigate this object further by looking at the X-ray luminosity in each eROSITA survey to find that it was significantly detected in *eRASS2* (with $L_{X,\mathrm{obs}}^{0.2-2.0\,\mathrm{keV}} \sim 1.1 \times 10^{40}\,\mathrm{erg\,s^{-1}}$) but not in any other individual image. This indicates that NGC 2903 likely hosts an AGN, which is variable on time scales of at least six months (i.e. the time between all-sky scans by eROSITA).

For the other five galaxies, we find no significant signs of X-ray variability within the *eRASS:4* data. This could indicate that the inconsistency detected here, if not caused by any differences in analysis strategy between our approach and the one of Ohlson et al. (2023), occurs on time scales longer than six months but shorter than the time difference between the *Chandra* and eROSITA observations of a few years.

5.4 Discussion

5.4.1 Presence of Massive Black Holes?

Most of the significantly detected NSCs in *eRASS:4* are in agreement with the expected luminosity from binary systems, therefore, we are not able to unambiguously associate it with AGN. Three NSCs (NGC 2903, NGC 4212, and NGC 4639) have emission above the expected value and this supports the presence of an AGN.

For NGC 4212 the NSC properties are not known and no secure black hole measurement exists. For the other two galaxies, She et al. (2017) estimates the black hole mass using the $M_{\rm bh}$-σ relation from Kormendy and Ho (2013) to find $\log_{10} M_{\rm bh}^{2903} / \mathrm{M}_\odot = 6.48^{+0.10}_{-0.10}$ and $\log_{10} M_{\rm bh}^{4639} / \mathrm{M}_\odot = 6.65^{+0.09}_{-0.09}$, resulting in $\lambda_{\rm Edd}^{2903} \sim 7 \times 10^{-5}$ and $\lambda_{\rm Edd}^{4639} \sim 4 \times 10^{-4}$, respectively, after taking into account a bolometric correction from Duras et al. (2020). The NSC masses are $\log_{10} M_\star^{\rm nsc,\,2903} / \mathrm{M}_\odot \sim 7.71$ (Pechetti et al., 2020) and $\log_{10} M_\star^{\rm nsc,\,4639} / \mathrm{M}_\odot \sim 7.05$ (Georgiev et al., 2016), resulting in mass fractions of $\log_{10}(M_{\rm bh} / M_\star^{\rm nsc}) \sim -1.23$ and -0.4, respectively. These values compare well to other literature values, as we show in Figure 5.7.

In comparison to previous studies, our investigation also takes into account a large sample of 111 early-type galaxies of various stellar masses. We show in Figure 5.8 the galaxy stellar mass versus Hubble morphological type plane, with additions of Seth et al. (2008a) and Baldassare et al. (2022) for NSCs without observational data in *eRASS:4*.

As previously explored, only the most massive galaxies ($M_\star^{\rm gal} \gtrsim 10^{10}\,\mathrm{M}_\odot$) have significant X-ray emission, irrespective of the host galaxy's morphology. The focus of Baldassare et al. (2022) on the late-type sample of Georgiev and Böker (2014) results in detections down to galaxy masses of $\sim 10^8\,\mathrm{M}_\odot$, as explored previously. In contrast, with the exception of one NSC (NGC 4467) from Seth et al. (2008a), no early-type galaxy in the same mass range is significantly detected. This could imply several points:

1. The accreting MBHs fall below the sensitivity of the cumulative data of eROSITA.
2. The black hole occupation fraction is different for galaxies of different Hubble type resulting in fewer X-ray detections at the same host galaxy stellar mass.
3. Assuming that the massive black hole occupation fraction does not depend on environment, this could indicate smaller black hole masses in these elliptical galaxies assuming the same Eddington fraction.
4. Assuming the same massive black hole occupation fraction and typical black hole masses, our results could indicate that the Eddington fraction is different between different morphologies, likely caused by a lack of gas available for accretion in the centres of early-type galaxies.

Regarding the first and last items, we can estimate an upper limit to the Eddington fraction of these objects. Assuming that we can ignore the contributions of HMXBs, the expected X-ray luminosity from binaries for a galaxy with stellar mass $M_\star^{\rm gal} \sim 10^{8.5}\,\mathrm{M}_\odot$ is $L_{X,\,\rm bin.} \sim 10^{37}\,\mathrm{erg\,s^{-1}}$, which is about a factor ten below the upper limits of *eRASS:4* (see Figure 5.3). Using a bolometric correction factor of about ten (Duras et al., 2020), the upper limit on the luminosity of a massive black hole would be

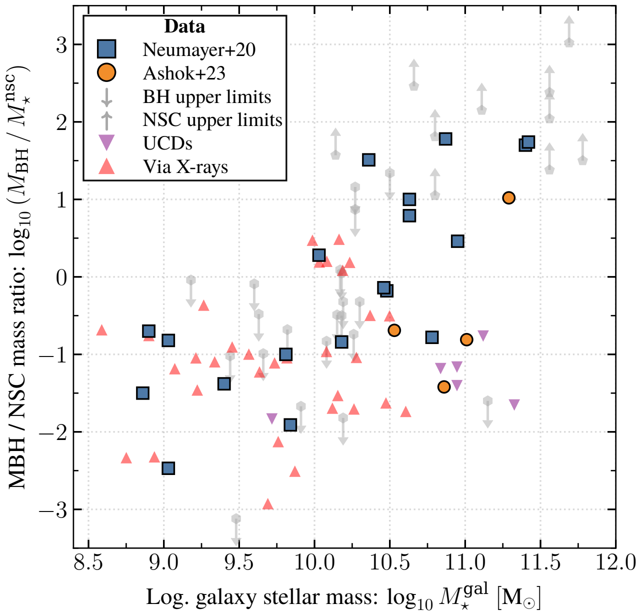

Figure 5.7. Mass ratio of the SMBH and NSC stellar mass ($\log_{10}\ M_{\rm bh}/M_\star^{\rm nsc}$) versus the host galaxy stellar mass. We show the compiled data of Neumayer et al. (2020) and add to that data for NGC 1336 (Saulder et al., 2016; Fahrion et al., 2019; Thater et al., 2023), NGC 3593 (Bertola et al., 1996; Nguyen et al., 2022), all shown with blue squares. Several galaxies from Ashok et al. (2023) are added as orange circles. The sample of ultra-compact dwarf galaxies (UCDs, purple triangles) include the compilation of Neumayer et al. (2020) and the additional B023-G078, M 31's most massive globular cluster, from Pechetti et al. (2022). We estimate the most likely previous UCD's host galaxy mass using the $M_\star^{\rm nsc}$-$M_\star^{\rm gal}$ relation of Neumayer et al. (2020) for massive galaxies (their Equation 2). Additionally, we add nucleated galaxies with significant X-ray excess, hinting at the existence of a massive black hole, by using a black hole mass estimate from She et al. (2017) and NSC mass estimates from Georgiev et al. (2016), shown with red triangles. We add to this last group the data points of NGC 2903 and NGC 4639, which could host massive black holes based on their X-ray variability (see Figure 5.6).

$L_{\rm bol,\,max} \sim 10^{39}\,{\rm erg\,s^{-1}}$. In galaxies of this mass, we would expect to find MBHs with $M_{\rm BH} \sim 10^5\,M_\odot$ from observational data in early-type galaxies (Erwin & Gadotti, 2012; Reines & Volonteri, 2015; Capuzzo-Dolcetta & Tosta e Melo, 2017; Greene et al., 2020) and $M_{\rm BH} \sim 10^{6.5} M_\odot$ from simulations (e.g. Spinoso et al., 2023). For these MBH masses ($10^5\,M_\odot$, $10^{6.5}\,M_\odot$), a Bolometric luminosity as quoted above ($L_{\rm bol,\,max} \sim 10^{39}\,{\rm erg\,s^{-1}}$) would imply an Eddington fraction of at most 0.01 %. This value roughly matches the values determined for NGC 2903 and NGC 4639 above, yielding an explanation for why we most likely do not detect these low-luminosity AGN in X-rays, if present. This also sets an upper limit to the hot gas accretion of such systems.

Regarding the other items, current observational data indicate that MBHs in early-type galaxies are more massive than their counterparts in late-types (see the compilation of Greene et al., 2020) but the scaling relations are solely based on measurements in massive galaxies and were extrapolated to the dwarf galaxy regime. The occupation fraction of MBHs appears to be similar, according to recent X-ray and dynamical

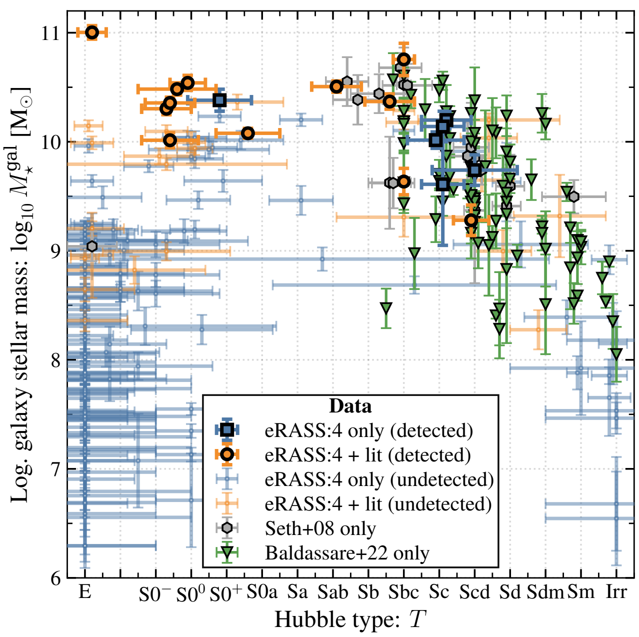

Figure 5.8. Galaxy stellar mass ($\log_{10} M_\star^{\rm gal}$) versus Hubble morphological type (T) of the significantly detected (solid blue) and non-detected (fainter blue points) *eRASS:4* data. Galaxies, which are part of *eRASS:4* but were also detected by previous work (Seth et al., 2008a; She et al., 2017; Baldassare et al., 2022; Ohlson et al., 2023) are shown in orange colour. In addition, we show the data by Seth et al. (2008a) and Baldassare et al. (2022) with grey hexagons and green triangles, respectively, for galaxies, which are not part of the *eRASS:4* sample. The single significantly detected early-type galaxies at a galaxy stellar mass of approximately 10^9 M$_\odot$ is NGC 4467, whose X-ray properties were analysed by Seth et al. (2008a) and Graham and Soria (2019).

results (see, again, the compilation of Greene et al., 2020), making the first and last items of the above list most likely.

MBH Occupation Fraction from X-Rays

Assuming that all significantly X-ray detected NSCs host an AGN, we can infer the combined occupation fraction of NSCs and AGN. To gain statistical significance, we add to the *eRASS:4* data the sample of Baldassare et al. (2022). For their sample we assume that all galaxies classified as having "diffuse" emission are non-detections.

We show the fraction of detected over the total sample as a function of galaxy and NSC stellar mass in Figure 5.9. For comparison, we also add the sample occupation fraction of Seth et al. (2008a) for NSCs and the AGN occupation fractions (without information of whether an NSC is present) from Miller et al. (2015a) and Ohlson et al. (2023) from observations and Tremmel et al. (2024) from a simulation. We find that above $M_\star^{\rm gal} \sim 10^7$ M$_\odot$ the combined AGN & NSC fraction increases and reaches 100 % around 10^{10} M$_\odot$. Our data are slightly elevated compared to the data of Seth et al. (2008a) and Ohlson et al. (2023) which could be related different selection effects (Seth et al., 2008a, use Optical spectroscopy, Radio, and X-ray data to find evidences

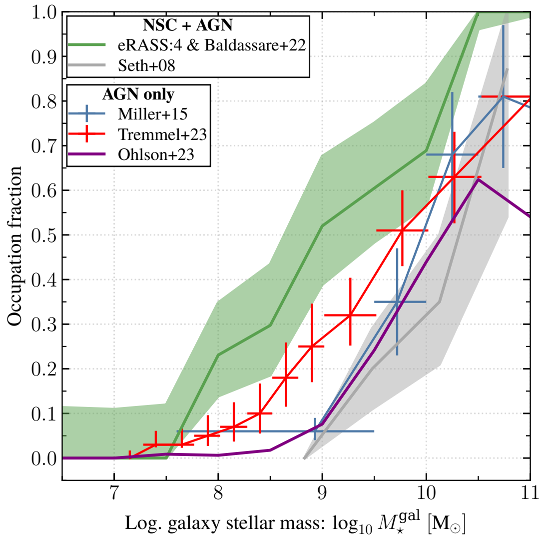

Figure 5.9. Occupation fraction of nuclear star clusters and active galactic nuclei versus host galaxy stellar mass ($\log_{10} M_\star^{\rm gal}$). We combine the *eRASS:4* data with the data from Baldassare et al. (2022) to gain statistical significance (green line). Literature data for NSCs and AGN come from Seth et al. (2008a, gray line). In addition, we show the occupation fractions of AGN from the observational studies of Miller et al. (2015a) and Ohlson et al. (2023, blue and purple lines, respectively), and the computational results of Tremmel et al. (2024, red line).

of the presence of an AGN) of the samples or instrument-related response functions. Additionally, because of the big half-energy width of eROSITA's PSF (half-energy width of about 30 arcsec; Predehl et al., 2021), off-nuclear star forming region can contaminate the measurements and result in a too-high estimate of the NSC and AGN fraction. Given the uncertainties of the data it remains unclear whether the presence of an NSC can enhance the occupation fraction of active galactic nuclei, not taking into account an enhanced rate of tidal disruption events (Pfister et al., 2020).

5.4.2 Caveats

There exist several caveats in the analysis both related to the measured and expected X-ray luminosities. The spatial resolution of eROSITA results in an uncertainty on both the central position of the emission (roughly 4″) and allows for contamination by off-nuclear sources, thus, not guaranteeing that the emission stems from the NSC. Instead, HMXBs or ULXs may mimic the emission of an accreting massive black hole in NSCs. Such contaminating sources may still be present in our sample, despite matching it with the ULX sample of Walton et al. (2022) (Section 5.2.2), thus requiring follow-up observations with higher spatial resolution facilities like Chandra.

In low-mass galaxies, the above argument is not problematic because the circular aperture typically contains the galaxy's stellar body out to at least one effective radius (*cf.* middle and right columns in Figure 5.1). However, there are several other challenges in this mass range. As noted by Lehmer et al. (2019), the scaling relations to track the contribution by HMXBs and LMXBs contain uncertainty in the low-mass regime because of a poorly sampled X-ray luminosity function. This makes it unclear how to interpret measured X-ray emission in dwarf galaxies in future eROSITA data releases in case dwarf galaxies (or stacks of dwarf galaxies) become significantly detected. Additionally, the scaling relations of Lehmer et al. (2019) apply for the expected X-ray luminosity of the whole galaxy. However, in most cases, the aperture used to extract the X-ray photometry only covers part of the galaxy (see Section 5.2.2), thus, overestimating the contamination from binaries.

Additionally, the influence of globular clusters to the X-ray binary contamination remains unclear. It is well-known that globular clusters efficiently produce LMXBs (e.g. Clark, 1975; Sivakoff et al., 2007; Cheng et al., 2018) and that they can heavily influence the X-ray properties of elliptical galaxies (e.g. Irwin, 2005; Lehmer et al., 2014, 2020) and, to some degree, late-types as well (Pfahl et al., 2003; Peacock et al., 2009; Hunt & Reffert, 2023). This effect is especially important in the dwarf galaxy regime where the importance of globular clusters towards the total mass budget of the galaxy increases, as probed by the specific globular cluster frequency (e.g. Miller & Lotz, 2007; Liu et al., 2019; Carlsten et al., 2022).[6] There also exists some scatter in the specific frequency of dwarf galaxies (see e.g. the environmental dependence discussed in Carlsten et al., 2022) requiring a detailed investigation of the X-ray luminosity from globular clusters in dwarf galaxies.

Furthermore, what is not taken into account here is the X-ray contributions from binaries within the NSC itself. This contribution may be similar to globular clusters, especially in dwarf galaxies where the properties of both systems become similar (e.g. Fahrion et al., 2022a; Hoyer et al., 2023a) but it remains somewhat unclear in higher-mass NSCs. Several works found that denser globular clusters have a higher probability of hosting X-ray binaries (e.g. Kundu et al., 2002; Jordán et al., 2007b; Sivakoff et al., 2007; Riccio et al., 2022; Hunt & Reffert, 2023) and this probability should increase further for NSCs, which are the densest stellar systems known (Neumayer et al., 2020), especially in massive galaxies (Pechetti et al., 2020). The expected LMXB contribution to the X-ray budget of NSCs is currently unknown and distinguishing them from low-luminosity AGN requires future work.

In summary, there exist several caveats related to both the measured X-ray luminosity and the expected value from X-ray binaries. Further studies disentangling the contributions from binaries are required for the targets with significant detections, which are currently high-mass galaxies. The sample size may increase and extend towards the dwarf galaxy regime if future eROSITA or Athena (Nandra et al., 2013) data are added.

5.5 Conclusions

We combined a compilation of galaxies containing a nuclear star cluster (NSC) with eROSITA *eRASS:4* data to probe X-ray signatures of an accreting massive black hole (MBH) within them. Using a sample of more than 200 nucleated galaxies with overlapping *eRASS:4* data within the footprint of the German eROSITA Consortium, we find 18 significant detections of which one is related to the presence of an off-nuclear ultra-luminous X-ray source. However, compared to the expected X-ray contamination from both low- and high-mass X-ray binaries, only three galaxies (NGC 2903, 4212, and 4639) have measured luminosities indicative of the presence of an MBH. Another six galaxies (NGC 2903, 3384, 4321, 4365, 4639, and 4701) have significantly different X-ray luminosities compared to previous archival measurements, which we interpret as indicative of a variable X-ray AGN. For NGC 4701, we find variability within

[6] The specific globular cluster frequency is often calculated as the total number of globular clusters divided by the galaxy's stellar mass, $S_N = N_{\mathrm{gc}} \,/\, M_\star^{\mathrm{gal}}$.

the *eRASS:4* data set, which could be related to an intrinsic variability or changes in obscuration. To confirm the nature of these objects, follow-up observations are necessary.

The MBH to NSC stellar mass fraction versus host galaxy stellar mass compares well to other known systems. By adding X-ray-based black hole mass estimates, we can significantly expand this parameter space towards lower galaxy stellar masses, apparently confirming a drop in the mass ratio around galaxy stellar masses of 10^{10} $M_\odot$.

Assuming that all significantly detected NSCs above the expected luminosity from X-ray binaries host AGN, we construct an NSC + AGN occupation fraction by adding data from Baldassare et al. (2022) to gain statistical significance. The resulting curve has higher occupation fraction than the one of Seth et al. (2008a) and the AGN only fractions of Miller et al. (2015a) and Tremmel et al. (2024) and Ohlson et al. (2023). The differences may be related to instrument-related response functions and the different half-energy widths of the instruments used.

Large-scale surveys, as carried out by eROSITA or Athena in the future, offer a unique view on X-ray emission in dwarf galaxies, covering also low-mass early-type galaxies, whose X-ray properties were not investigated previously with respect to their NSCs.

5.6 Appendix

We present in Tables 5.1 and 5.2 the data used in this work.

Table 5.1. Galaxy properties for the considered sample based on literature information. The combined data table with Table 5.2 is available for download online.

Galaxy	RA	DEC	$m - M$	T	$\log_{10} M_\star^{\rm gal}$	$\log_{10}$ SFR [(a)]
	[deg]	[deg]	[mag]		[$M_\odot$]	[$M_\odot$ yr^{-1}]
(1)	(2)	(3)	(4)	(5)	(6)	(7)
BTS 76	179.68375	27.58500	30.50	10.0 ± 2.0	7.53 ± 0.16	-3.47
DDO 084	160.67458	34.44889	29.99	9.8 ± 0.6	7.65 ± 0.35	-3.84
DDO 088	161.84292	14.07028	29.44	8.9 ± 0.3	7.88 ± 0.15	N/A
dw 1048+13	162.14917	13.06000	30.13 ± 0.12	-2.0 ± 1.0	6.71 ± 0.43	N/A
dw 1049+12b	162.35833	12.55250	30.17 ± 0.06	-2.0 ± 1.0	7.55 ± 0.06	N/A
...	...	...	...	...	...	...

Columns: (1) galaxy name; (2) Right ascension; (3) Declination; (4) Distance modulus; (5) Hubble type; (6) Galaxy stellar mass; (7) Star formation rate

[(a)] The star formation rate is set to zero for dwarf elliptical galaxies in the core of the Virgo cluster.

Table 5.2. X-ray properties of the selected galaxy sample from SRG/eROSITA.

Galaxy	$L_{X,\,\mathrm{median}}^{2-10\,\mathrm{keV}}$	$L_{X,\,1^{\mathrm{st}}}^{2-10\,\mathrm{keV}}$	$L_{X,\,99^{\mathrm{th}}}^{2-10\,\mathrm{keV}}$	$L_X^{\mathrm{cont}\ (a)}$	t_{exp}	P_{binom}
	[erg s^{-1}]	[erg s^{-1}]	[erg s^{-1}]	[erg s^{-1}]	[s]	
(1)	(2)	(3)	(4)	(5)	(6)	(7)
BTS 76	--	--	3.97×10^{38}	$(6.2 \pm 2.3) \times 10^{36}$	326	0.06078
DDO 084	--	--	1.07×10^{38}	$(8.1 \pm 6.5) \times 10^{36}$	325	0.39909
DDO 088	--	--	6.54×10^{38}	$(1.37 \pm 0.48) \times 10^{37}$	282	0.04318
dw 1048+13	--	--	4.25×10^{38}	$(9.3 \pm 9.2) \times 10^{35}$	297	0.40543
dw 1049+12b	--	--	1.84×10^{38}	$(6.37 \pm 0.81) \times 10^{36}$	275	0.76436
...	...	...	...	...	...	...

Columns: (1) galaxy name; (2) Median X-ray luminosity in the 2-10 keV band; (3) & (4) 1^{st} and 99^{th} percentiles of the X-ray luminosity; (5) Expected X-ray luminosity due to binary systems; (6) Exposure time; (7) Binomial probability that the detection is a background fluctuation.
$^{(a)}$ If no star formation rate could be determined, the estimated X-ray luminosity due to binaries is a lower limit.

5.7 Chapter Summary

- This work combines information of NSCs (location, photometry, structure) with accumulated *SRG*/eROSITA all-sky data in the X-ray regime to search for low-luminosity AGN.
- The analysis reveals several AGN candidates within NSCs based on X-ray variability and a measured luminosity that exceeds expected values from binary systems.
- Stacked X-ray data constrain the luminosity of MBH in dwarves to $L_{\mathrm{X}}^{2-10\,\mathrm{keV}} \approx 2 \times 10^{38}\,\mathrm{erg\,s^{-1}}$, which translates to an MBH mass of the order of $10^6\,\mathrm{M_\odot}$ when assuming an Eddington factor of 0.01 % (or vice versa).
- Combining X-ray detected AGN from the literature, the black hole to bulge mass relationship, and adding our new results further constrain the MBH to NSC mass ratio versus host galaxy mass plane. Below galaxy masses of $\approx 10^{10}\,\mathrm{M_\odot}$, $M_{\mathrm{SMBH}}/M_{\mathrm{NSC}} \lesssim 0$ whereas the fraction increases up to a couple of dex for the most massive systems.

Chapter 6

Massive Star Clusters in Simulated Galaxies

Declaration

The contents of this chapter were submitted to Astronomy & Astrophysics and are published in Hoyer et al. (2025). All co-authors provided commentary that improved the work.

Abstract

It is established that there exists a direct link between the formation history of star cluster populations and their host galaxies, however, our lacking understanding of star cluster assembly prohibits us to make full use of their ability to trace galaxy evolution. In this work we introduce a new variation of the 2020 version of the semi-analytical galaxy formation model "*L-Galaxies*" that includes the formation of star clusters above 10^4 $M_\odot$ and probes different physical assumptions that affect their evolution over cosmic time. We use properties of different galaxy components and localised star formation to determine the bound fraction of star formation in disks. After randomly sampling masses from an environmentally-dependent star cluster initial mass function, we assign to each object a half-mass radius, metallicity, and distance from the galaxy centre. We consider up to 2000 individual star clusters per galaxy and evolve their properties over time taking into account stellar evolution, two-body relaxation, tidal shocks, dynamical friction, and a re-positioning during galaxy mergers. Our simulation successfully reproduces several observational quantities, such as the empirical relationship between the absolute V-band magnitude of the brightest young star clusters and the host galaxy star formation rate, the mass function of young star clusters, or mean metallicities of the star cluster distributions versus galaxy masses. The simulation reveals great complexity in the $z = 0$ star cluster population resulting from differential destruction channels and origins, including *in-situ* populations in the disk, a major merger-induced heated component in the halo, and accreted star clusters. Model variations point out the importance of e.g. the shape of the star cluster initial mass function or the relationship between the sound speed of cold gas and the star formation rate. Our new model provides new avenues to trace individual star clusters and test cluster-related physics within a cosmological set-up in a computationally efficient manner.

6.1 Introduction

A natural consequence of star formation in cold gas-dense and rotationally unstable regions is the formation of bound stellar structures, ranging from few-body systems to massive star clusters that rival in mass the baryonic components of entire (dwarf) galaxies. The properties and survival times of these star clusters heavily depend on their changing environment, which makes them excellent tracers of galaxy assembly. To date, a large body of work has used the present-day star cluster population, such as globular clusters, to constrain the evolutionary history of their current host galaxy, including the Milky Way, M 31, and other nearby systems (e.g. Huchra et al., 1991; Barmby et al., 2000; Perrett et al., 2002; West et al., 2004; Brodie & Strader, 2006; Forbes & Bridges, 2010; Leaman et al., 2013; Huxor et al., 2014; Cantiello et al., 2015; Veljanoski et al., 2015; Myeong et al., 2018; Callingham et al., 2022; Hammer et al., 2023, 2024; Ines Ennis et al., 2024; Usher et al., 2024). However, despite the clear link between galaxy and star cluster formation that is expressed via, for example, the scaling relation between the number of star clusters and host galaxy mass (e.g. West et al., 1995; Blakeslee, 1999; Peng et al., 2008; Spitler & Forbes, 2009; Hudson et al., 2014; El-Badry et al., 2019; Bastian et al., 2020; Burkert & Forbes, 2020; Zaritsky, 2022; Le & Cooper, 2024), precise details about the formation environments and initial properties of $z = 0$ star clusters remain elusive (e.g. Forbes et al., 2018).

Constraints on the ages of globular clusters in galaxies, including the Milky Way, suggest that they form at redshifts $z \gtrsim 1$ (e.g. Carretta et al., 2000; Krauss & Chaboyer, 2003; Lee, 2003; Kaviraj et al., 2005; Strader et al., 2005; Correnti et al., 2016). Studying the natal environment of clusters at these distances is challenging; however, observations with the *Very Large Telescope*, the *Hubble Space Telescope*, and *James Webb Space Telescope*, combined with strong gravitational lensing, make such observations possible (e.g. Vanzella et al., 2017, 2019; Kikuchihara et al., 2020; Mowla et al., 2022; Claeyssens et al., 2023; Forbes & Romanowsky, 2023; Vanzella et al., 2023; Mowla et al., 2024). Most recently, Adamo et al. (2024) discussed the properties of young and massive star clusters in the "Cosmic Gems Arc" at redshift $z \approx 10$ (Salmon et al., 2018; Bradley et al., 2024). Such clusters are compact (half-light radius ≤ 2 pc), massive (stellar mass $\gtrsim 10^6\,\mathrm{M}_\odot$), and could potentially contribute to the $z = 0$ star cluster population. Irrespective of whether they survive until $z = 0$, they constitute a significant baryonic component of high-z galaxies ($\gtrsim 30\,\%$ for the Cosmic Gems Arc; Adamo et al., 2024) and most likely influence the host galaxy's evolution.

Simulations are required to understand the properties of the full star cluster distribution as observations can only trace the brightest / most massive and most unobscured star clusters. Detailed simulations of star cluster formation and evolution have now become feasible in high-resolution hydrodynamical simulations of galaxy formation, ranging from dwarf galaxies to Milky Way-analogues. These simulations either include star clusters in full cosmological simulations, sometimes including adaptive mesh-refinement or zoom-in techniques (e.g. Li et al., 2017, 2018; Li & Gnedin, 2019; Brown & Gnedin, 2022; Reina-Campos et al., 2022a; Garcia et al., 2023; Calura et al., 2024) or use high spatial- and temporal resolutions but evolve for less than one Gyr (e.g. Lahén et al., 2020; Hislop et al., 2022; Lahén et al., 2023; Elmegreen & Lahén, 2024; Lahén et al., 2024a, 2024b; Reina-Campos et al., 2024). Another approach is to add star cluster-related physics to existing simulations. This approach was realised by e.g. the *E-MOSAICS* project (Pfeffer et al., 2018; Kruijssen et al., 2019a) that adds prescriptions for star cluster formation in post-processing to the *EAGLE* simulation (Crain et al., 2015; Schaye et al., 2015). Focussing on *E-MOSAICS*, their simulation can reproduce a number of observables related to the globular clusters mass and metallicity distributions as well as relations with properties of their host galaxy and dark matter halo (see details in Horta et al., 2011; Hughes et al., 2019; Kruijssen et al., 2019a, 2019b; Pfeffer et al., 2019a, 2019b; Reina-Campos et al., 2019; Bastian et al., 2020; Hughes et al., 2020; Keller et al., 2020; Kruijssen et al., 2020a; Reina-Campos et al., 2020; Trujillo-Gomez et al., 2021; Dolfi et al., 2022; Hughes et al., 2022; Reina-Campos et al., 2022b, 2023b; Newton et al., 2024; Pfeffer et al., 2024a, 2024b).

All of the above mentioned simulations follow in detail the evolution of stars within individual star clusters or of individual baryonic particles, which contain star clusters, but are expensive to run. In contrast, semi-analytical models sacrifice resolution to lower the computational expense and gain the ability to explore a wide parameter space of various astrophysical mechanisms (e.g. White & Rees, 1978; White & Frenk, 1991; Baugh, 2006; Somerville et al., 2008; Somerville & Davé, 2015). This approach has proven to be successful in reproducing observational quantities related to, for example, the co-evolution of galaxies and massive black holes (e.g. Kauffmann & Haehnelt, 2000; Croton, 2006; Croton et al., 2006; De Lucia & Blaizot, 2007; Monaco et al., 2007; Bonoli et al., 2009, 2014; Izquierdo-Villalba et al., 2020; Gabrielpillai et al., 2022; del P. Lagos et al., 2024), which allows to constrain values of free parameters of the assumed physical models.

For star clusters in a semi-analytical galaxy formation framework specifically, most recently De Lucia et al. (2024) added prescriptions for their formation to the *GAEA* model (De Lucia et al., 2014; Hirschmann et al., 2016). The authors were able to reproduce the empirical relationship between the total mass in globular clusters and the parent halo mass (see also e.g. Kravtsov & Gnedin, 2005; Prieto & Gnedin, 2008; Muratov & Gnedin, 2010; Li et al., 2017) but utilised simple prescriptions related to mass loss and dynamical friction and relied on global star cluster population statistics.

In this first paper, we introduce an implementation of the formation and evolution of star clusters into a public version of the semi-analytical galaxy formation model "*L-Galaxies*" (Henriques et al., 2020; Yates et al., 2021). Our work differs from the above mentioned work by De Lucia et al. (2024) in that we track the evolution of individual clusters and use different sets of astrophysical prescriptions that make use of the radially-resolved gas and stellar discs in the 2020 version of the code. This effort enables us to study individual star clusters across different galaxy types, masses, environments, and redshifts, and offers new avenues to study the formation of nuclear star clusters and the co-evolution of black holes with star clusters in future work.

We start in Section 6.2 by detailing the governing equations of the model, starting with galaxy components to evaluate the formation efficiency of star clusters, the initial properties of the star clusters, and eventually the evolution of star clusters within the evolution of their host galaxies. We then evaluate results of our model in Section 6.3 focussing on young massive star clusters in disk-dominated galaxies, and metallicity distributions of *in-situ* and accreted star clusters for different galaxy morphologies, and discuss caveats of our approach. We conclude in Section 6.4 and present an outlook for

Formation

Evaluated for each annulus:

- ▹ Star formation in galaxy disks (§ 6.2.1)
- ▹ Star cluster formation (§ 6.2.3)
  → Bound fraction of star formation
  - – Cold gas surface density (§ 6.2.1)
  - – Epicyclic frequency (§ 6.2.3)
  - – Toomre stability parameter (§ 6.2.3)
- ▹ Star cluster initial mass function (§ 6.2.4)
  Power-law with upper truncation

- ▹ Other initial properties:
  - – Location within annuli (§ 6.2.4)
  - – Half-mass radius (§ 6.2.4)
  - – Tidal radius (§ 6.2.4)
  - – Metallicity (§ 6.2.4)

Evolution

- ▹ Mass loss (§ 6.2.5)
  - – Stellar evolution
  - – Two-body relaxation
  - – Tidal shocks
- ▹ Radial expansion (§ 6.2.5)
  - – Two-body relaxation
  - – Tidal shocks
- ▹ Dynamical friction (§ 6.2.5)
- ▹ Re-distribution during galaxy mergers (§ 6.2.5)
  - – Minor mergers: accreted clusters move to halo
  - – Major mergers: all clusters move to halo

Figure 6.1. Relevant prescriptions for the assembly of star clusters implemented into a modified version (Yates et al., 2021) of *L-Galaxies* 2020 (Henriques et al., 2020).

future papers in this series. Section 6.5 presents variations of key model parameters.

6.2 Model Description

Below we outline the basic principles behind our model that we summarise in Figure 6.1. Going forward, when mentioning the term *L-Galaxies* we specifically refer to a modified version of the 2020 model introduced by Yates et al. (2021). This version of the code improves over the default model (Henriques et al., 2020) by modifying the prescriptions for metal injection from stellar winds and supernovae into the circum-galactic medium.

6.2.1 The *L-Galaxies* Semi-Analytical Galaxy Formation Model

The *L-Galaxies* model combines merger trees from dark matter-only N-body simulations with a set of partial differential equations for the evolution of baryonic components. It has been developed to primarily run on the Millennium (Springel et al., 2005) and Millennium-II (Boylan-Kolchin et al., 2009) simulations with box sizes / dark matter particle masses of $480.3\,h^{-1}\,\mathrm{Mpc}$ / $9.61 \times 10^{8}\,h^{-1}\,\mathrm{M}_{\odot}$ and $96.1\,h^{-1}\,\mathrm{Mpc}$ / $7.69 \times 10^{6}\,h^{-1}\,\mathrm{M}_{\odot}$, respectively. Dark matter (sub-)halos are identified using a “Friends-of-Friends” (Davis et al., 1985) and the “subfind” algorithm (Springel et al., 2001; Dolag et al., 2009) and are used as input to *L-Galaxies*. As discussed in the works related to the last few major releases (Guo et al., 2011; Henriques et al., 2015, 2020), the model can reproduce many observables of baryonic components, such as the redshift-dependent galaxy mass function, passive galaxy fraction, and the cosmic density of the star formation rate (SFR).

Many extensions to *L-Galaxies* have been developed, including those that focus on the gas (Vijayan et al., 2019; Ayromlou et al., 2021; Yates et al., 2021; Parente et al., 2023; Zhong et al., 2023b, 2023a; Parente et al., 2024; Yates et al., 2024), stars (Bluck et al., 2016; Wang et al., 2018; Irodotou et al., 2019; Izquierdo-Villalba et al., 2019; Murphy et al., 2022; Wang & Peng, 2024), massive black holes (Bonoli et al., 2009, 2014; Izquierdo-Villalba et al., 2020, 2022; Spinoso et al., 2023; Polkas et al., 2024), and other components (Barrera et al., 2023; Vani et al., 2025). This shows that *L-Galaxies* is a versatile utility to explore the assembly of galaxies and has the potential to investigate the formation of star clusters as well.

One of the key features of the 2020 version of *L-Galaxies* that was adapted from Fu et al. (2013) is the introduction of concentric annuli. By default, the model features twelve such annuli that are logarithmically-spaced and act as the resolution limit for the cold gas and stars within a galaxy's disk and stars within a galaxy's bulge. The annuli's outer radii have values of

$$w_j \,/\, [h^{-1}\,\mathrm{kpc}] = 0.01 \times 2^j \quad \text{with } j \in [1,\, 12]\,, \tag{6.1}$$

resulting in $w_1 \approx 29.7\,\mathrm{pc}$ and $w_{12} \approx 60.8\,\mathrm{kpc}$.

One of the affected properties of the separation into annuli is the star formation prescription. *L-Galaxies* assumes that the molecular gas in each annuli collapses on a dynamical time-scale τ_{dyn} and is transformed to stars with an efficiency $\epsilon_{\mathrm{H_2}}$ (e.g. Fu et al., 2012). Thus, in terms of surface mass density, the SFR for ring j is

$$\Sigma_{\mathrm{SFR},\,j} = \epsilon_{\mathrm{H_2}}\, \tau_{\mathrm{dyn}}^{-1}\, \Sigma_{\mathrm{H_2},\,j}\ . \tag{6.2}$$

The model assumes for the dynamical time

$$\tau_{\mathrm{dyn}} = R_{\mathrm{g}} \,/\, v_{\mathrm{max}}\ , \tag{6.3}$$

where we introduced the disk scale-length of the cold gas and the maximum value of the rotation velocity of the dark matter halo. The amount of molecular gas itself is derived from the available cold gas in each ring and, in turn, is related to the gas' metallicity and clumping of gas clouds. Extensive discussions and recipes for computing the molecular mass (per annuli) are presented in (Krumholz et al., 2009; Fu et al., 2010; McKee & Krumholz, 2010; Fu et al., 2013; Henriques et al., 2020).

In this work we adopt the 2014 cosmology of *Planck* (Planck Collaboration, 2014) with $\Omega_{\Lambda,0} = 0.685$, $\Omega_{\mathrm{m},0} = 0.315$ (with $\Omega_{\mathrm{b},0} = 0.0487$), $\sigma_8 = 0.826$, $n_{\mathrm{s}} = 0.96$, and $h = 0.673$ throughout the paper. *L-Galaxies* itself utilises dark matter-only simulations that are re-scaled (Angulo & White, 2010; Angulo & Hilbert, 2015) to these cosmological parameters.

6.2.2 Gravitational Potential

The computation of the fraction of star formation that is bound in star clusters (Section 6.2.3) requires knowledge of the underlying gravitational potential. We consider the contributions of all available galaxy components that *L-Galaxies* considers during the simulation, namely a central massive black hole, dark matter, a bulge, gaseous and stellar disks, and gaseous and stellar halos.

Massive Black Hole In case a massive black hole occupies a galaxy centre, we introduce a gravitational potential of a point mass, i.e.

$$\Phi_{\mathrm{BH}}(w) = -\frac{\mathrm{G}\, M_{\mathrm{BH}}}{w}\ , \tag{6.4}$$

where G is the gravitational constant, M_{BH} the black hole mass, and w the galactocentric distance. We assume here that the galaxy centre remains in the dark matter halo's centre at all times and that the massive black hole does not 'wander' within the galaxy (see Izquierdo-Villalba et al., 2020; Untzaga et al., 2024, for a discussion on wandering black holes in *L-Galaxies*).

Dark Matter Halo We select a classical NFW profile (Navarro et al., 1996) to describe the distribution of dark matter. The gravitational potential is given by

$$\Phi_{\mathrm{DM}}(w) = -\frac{\mathrm{G}\,M_{\mathrm{vir}}}{w}\,\frac{\ln(1 + c_{\mathrm{vir}}\,w/R_{\mathrm{vir}})}{\ln(1 + c_{\mathrm{vir}}) - c_{\mathrm{vir}}/(1 + c_{\mathrm{vir}})}\,, \tag{6.5}$$

where we introduced the virial mass M_{vir} and radius R_{vir}, respectively. For the concentration parameter, c_{vir}, which relates the profile's scale-radius to R_{vir}, we assume a relation from Dutton and Macció (2014) that connects it to M_{vir} via

$$\log_{10}\, c_{\mathrm{vir}} = \alpha(z) + \beta(z) \times \log_{10}(M_{\mathrm{vir}}\,/\,[10^{12}\,h^{-1}\,\mathrm{M}_{\odot}])\;. \tag{6.6}$$

The redshift-dependent coefficients $\alpha(z)$ and $\beta(z)$ take values according to Table 3 of Dutton and Macció (2014) with $\alpha(0) = 1.025$ and $\beta(0) = -0.097$.

Galactic Bulge We model a galaxy's bulge with a Jaffe (1983) profile of the form

$$\Phi_{\mathrm{B}}(w) = -\frac{\mathrm{G}\,M_{\mathrm{B}}}{w_{\mathrm{B}}}\ln(1 + w_{\mathrm{B}}/w)\;, \tag{6.7}$$

with a scale-length w_{B} that encloses half of the bulge's mass M_{B}.

Gaseous and Stellar Disks We follow the default assumption in *L-Galaxies* that both the gaseous and stellar disks are well described by two-dimensional exponential density profiles. The mid-plane gravitational potential of the two disks is expressed with modified Bessel functions of the first and second kind, I_ν and K_ν, respectively (e.g. Watson, 1944; Kuijken & Gilmore, 1989). The gravitational potential for disk i reads

$$\Phi_{\mathrm{D},\,i}(w) = -\pi\mathrm{G}\,\Sigma_{\mathrm{D},\,i}\,w\left[I_0(y_i)K_1(y_i) - I_1(y_i)K_0(y_i)\right], \tag{6.8}$$

where $y_i = w/(2 \times w_{\mathrm{D},\,i})$, $w_{\mathrm{D},\,i}$ a characteristic scale-length, and $\Sigma_{\mathrm{D},\,i}$ as the central surface mass density (Freeman, 1970; Binney & Tremaine, 2008).

Hot Gas and Stellar Haloes We assume that a galaxy's halo contains both hot gas that is unable to form stars and a stellar medium that originates entirely from stripped satellite galaxies. For simplicity, we assume that an isothermal profile can describe well both the gaseous and stellar halo, i.e.

$$\Phi_{\mathrm{H},\,i}(w) \propto -\frac{\mathrm{G}\,M_{\mathrm{H},\,i}}{R_{\mathrm{H},\,i}}\ln(w)\;. \tag{6.9}$$

Furthermore, we assume that all mass is enclosed within the virial radius such that $R_{\mathrm{H},\,i} = R_{\mathrm{vir}}$.[1]

[1] Yates et al. (2017, 2024) discuss and utilise more physically motivated profiles within *L-Galaxies*.

6.2.3 Star Cluster Formation

The total mass of newly formed stars that are bound in star clusters equals the SFR multiplied by the simulation time step and the cluster formation efficiency (Bastian, 2008). In principle, the latter must be computed considering local conditions of the gas phase, mergers from substructures, and accretion of gas during cluster formation (e.g. Karam & Sills, 2022, 2023) but this is not feasible with our approach.

Here, we follow the prescription outlined by Kruijssen (2012) to estimate the cluster formation efficiency. The model relies on three quantities: (1) the cold gas surface mass density Σ_{g}, which we compute as an annuli's molecular mass divided by it's area, (2) the epicyclic frequency κ, and (3) the Toomre disk stability parameter Q. We compute these values for the logarithmic mean galactocentric distance of each annuli j, unless stated otherwise, and assume that it is applicable to a wide range of environments and redshifts.[2] Furthermore, we assume that all star clusters form in galaxy disks, thus, neglecting cluster formation during galaxy mergers or outside of dark matter halos at high-z (Lake et al., 2021, 2023).

Epicyclic Frequency

Based on the combined gravitational potential of all previously introduced galaxy components, $\Phi_{\mathrm{tot}}(w) = \sum_c \Phi_c(w)$, we can easily determine the epicyclic frequency for circular orbits. For annulus j and log-mean distance $\langle w_j \rangle$,

$$\kappa_j = \sqrt{\frac{3}{\langle w_j \rangle} \frac{\partial \Phi_{\mathrm{tot}}}{\partial w}\bigg|_{\langle w_j \rangle} + \frac{\partial^2 \Phi_{\mathrm{tot}}}{\partial w^2}\bigg|_{\langle w_j \rangle}} \,. \tag{6.10}$$

Note that, when evaluating this property for galaxy disks, we assume co-rotation of the gaseous and stellar disks resulting in only a single value of these quantities per annuli.

Toomre Stability Parameter

The Toomre stability criterion (Safronov, 1960; Toomre, 1964) evaluates whether a disk is stable against collapse considering gravity, pressure, and shear. For the gaseous and stellar disks we determine

$$Q_{\mathrm{g},\,j} = \frac{\kappa_j \sigma_{\mathrm{D,\,g},\,j}}{\pi \mathrm{G}\, \Sigma_{\mathrm{g},\,j}} \,, \tag{6.11a}$$

$$Q_{\mathrm{D},\,j} = \frac{\kappa_j \sigma_{\mathrm{D,\,s},\,j}}{3.36 \mathrm{G}\, \Sigma_{\mathrm{s},\,j}} \,, \tag{6.11b}$$

where $Q > 1$ for a stable disk. Here we introduced for the gaseous and stellar disks, respectively, the surface densities ($\Sigma_{\mathrm{g}} \,/\, \Sigma_{\mathrm{s}}$) and the velocity dispersions ($\sigma_{\mathrm{D,\,g}} \,/\, \sigma_{\mathrm{D,\,s}}$).

[2] Using the same cluster formation efficiency calculations from Kruijssen (2012), Pfeffer et al. (2024a) recently showed that the *E-MOSAICS* simulation can well reproduce observed properties of star clusters at high-z.

We follow Bottema (1993) and van der Kruit and Freeman (2011) to calculate the velocity dispersion of the stars[3] as

$$\sigma_{\mathrm{D,\,s,}\,j} = \frac{v_{c,\,j}}{2} \exp\left(- \frac{\langle w_j \rangle}{2 w_{\mathrm{D}}} \right), \tag{6.12}$$

with circular velocity

$$v_{c,\,j} = \sqrt{\langle w_j \rangle \frac{\partial \Phi_{\mathrm{tot}}}{\partial w}\bigg|_{\langle w_j \rangle}} \; . \tag{6.13}$$

We assume that the velocity dispersion of the cold gas equals the speed of sound of the interstellar medium, which correlates with the star formation surface density, i.e.

$$c_{\mathrm{s,\,cold,}\,j} = \alpha_{\mathrm{cold}} + \beta_{\mathrm{cold}} \times \left(\frac{\Sigma_{\mathrm{SFR,}\,j}}{[\mathrm{M}_\odot\,\mathrm{kpc}^{-2}\,\mathrm{yr}^{-1}]} \right)^{\gamma_{\mathrm{cold}}} , \tag{6.14}$$

with free parameters α_{cold}, β_{cold}, and γ_{cold}. This relationship shows significant scatter in observations across various redshifts (see e.g. Lehnert et al., 2009; Genzel et al., 2011; Green et al., 2014; Krumholz & Burkhart, 2016; Zhou et al., 2017; Krumholz et al., 2018; Mai et al., 2024, and references therein). In our fiducial model we assume the parameter values $\alpha_{\mathrm{cold}} = 5\,\mathrm{km\,s^{-1}}$, $\beta_{\mathrm{cold}} = 20\,\mathrm{km\,s^{-1}}$, and $\gamma_{\mathrm{cold}} = 1/3$, i.e. a turbulence-dominated energy dissipation prescription for the cold gas (Zhou et al., 2017). We explore the impact of different values in Section 6.5.1.

It is well known that the gaseous and stellar disks interact dynamically (e.g. Lin & Shu, 1966; Bertin & Romeo, 1988) and that, for example, the stability of a stellar disk may be impacted by even small amounts of gas. To retain the same guidelines for the Toomre stability parameter in the prescription provided by Kruijssen (2012) we follow the approach by Romeo and Wiegert (2011) and compute an "effective" Toomre parameter as

$$Q_{\mathrm{eff,}\,j}^{-1} = \begin{cases} \psi_{Q,\,j} Q_{\mathrm{s,}\,j}^{-1} + Q_{\mathrm{g,}\,j}^{-1} & \text{if } Q_{\mathrm{s,}\,j} \geq Q_{\mathrm{g,}\,j} \; , \\ Q_{\mathrm{s,}\,j}^{-1} + \psi_{Q,\,j} Q_{\mathrm{g,}\,j}^{-1} & \text{otherwise} \; , \end{cases} \tag{6.15}$$

with the weighting factor

$$\psi_{Q,\,j} = 2 \frac{\sigma_{\mathrm{D,\,s,}\,j} \times \sigma_{\mathrm{D,\,g,}\,j}}{\sigma_{\mathrm{D,\,s,}\,j}^2 + \sigma_{\mathrm{D,\,g,}\,j}^2} \; . \tag{6.16}$$

We show in Figure 6.2 an overview of the cold gas surface mass density, the epicyclic frequency, and the Toomre stability parameter for disk- and bulge-dominated galaxies from running our model on tree-files of the Millennium simulation. For comparison, we add the position of the solar neighbourhood.

The epicyclic frequency and cold gas surface density decrease at larger galactocentric distances. The Toomre parameter shows a more complex behaviour, typically ranging between one and ten, except for the largest distances, where it sharply increases for most galaxies and the centre of ellipticals, where it increases as well. The latter effect is

[3] Here we completely neglect the increase in velocity dispersion as a function of stellar age caused by interactions with giant molecular clouds or spiral waves, potentially resulting in a more stable disk.

caused by the importance of the bulge component, which is weaker in spirals. At large radii the disks of low-mass galaxies are barely populated with gas and stars, which drive $Q_{\rm eff}$ to large values. For the same reason the Toomre parameter drops for more massive galaxies, which is reflected by an increase in the disk's scale-length. Overall we find good agreement between our simulated galaxies and the solar neighbourhood.

Bound Fraction of Star Formation

The bound fraction of newly formed stars in star clusters is closely related to the cluster formation efficiency (Bastian, 2008; Goddard et al., 2010; Adamo et al., 2011; Silva-Villa & Larsen, 2011), which takes into account its survival rate during the first few Myr. Although important in many aspects, it is unclear how the bound fraction and cluster formation efficiency are related to the interstellar medium and star formation (see Andersson et al., 2024, for a recent discussion on how feedback influences the cluster formation efficiency).

As mentioned above, we follow the model outlined by Kruijssen (2012) to estimate the bound fraction based on its epicyclic frequency, cold gas surface density, and Toomre stability parameter, all equated at the log-mean galactocentric distance. We briefly highlight key aspects of the model and refer the interested reader to the original work for a more detailed description.

Note that we do not directly determine the bound fraction during the execution of the simulation. Instead, to reduce the computational cost, we create lookup tables for a set of $\{\Sigma_{\rm g}, Q_{\rm eff}, \kappa\}$. In total, we utilise 18 lookup tables with varying values of $Q_{\rm eff}$ (between 0.01 and 4.0) and 500 values of $\Sigma_{\rm g}$ and κ each, resulting in 4.5×10^6 data points. The simulation then determines the closest match in all three parameters and extract the bound fraction from the table.

Following an extensive literature (e.g. Padoan et al., 1997; Vázquez-Semadeni et al., 1998; Ostriker et al., 2001; Kritsuk et al., 2007; Padoan & Nordlund, 2011; Kritsuk et al., 2017; Burkhart, 2018) we assume that the density contrast of the interstellar medium follows a log-normal distribution of the form

$$\mathrm{d}p_j = \frac{1}{\sqrt{2\pi}\varsigma_{\rho,j}} \exp\left[-\left(\frac{\ln\delta_j - \overline{\ln\delta_j}}{\sqrt{2}\varsigma_{\rho,j}}\right)^2\right] \mathrm{d}(\ln\delta_j) \,, \tag{6.17}$$

with relative density $\delta_j = \rho/\rho_{\rm ISM,\,j}$, $\overline{\ln\delta_j} = -0.5\,\varsigma^2_{\rho,\,j}$ (e.g. Vazquez-Semadeni, 1994), and standard deviation

$$\varsigma_{\rho,\,j} = \sqrt{\ln(1 + 3\gamma_\rho^2 \mathcal{M}^2_{\rm cold,\,j})} \,, \tag{6.18}$$

where $\gamma_\rho \approx 0.5$ (Nordlund & Padoan, 1999; Padoan & Nordlund, 2002). We determine the density of the interstellar medium as

$$\rho_{\rm ISM,\,j} = \frac{\phi_{\rm P}}{2\pi \rm G}\left(\frac{\kappa_j}{Q_{\rm eff,\,j}}\right)^2 \,, \tag{6.19}$$

with $\phi_{\rm P} = 3$ (see Appendix A of Krumholz & McKee, 2005). The Mach number of the cold gas is related to the cold gas surface density, the epicyclic frequency, and the

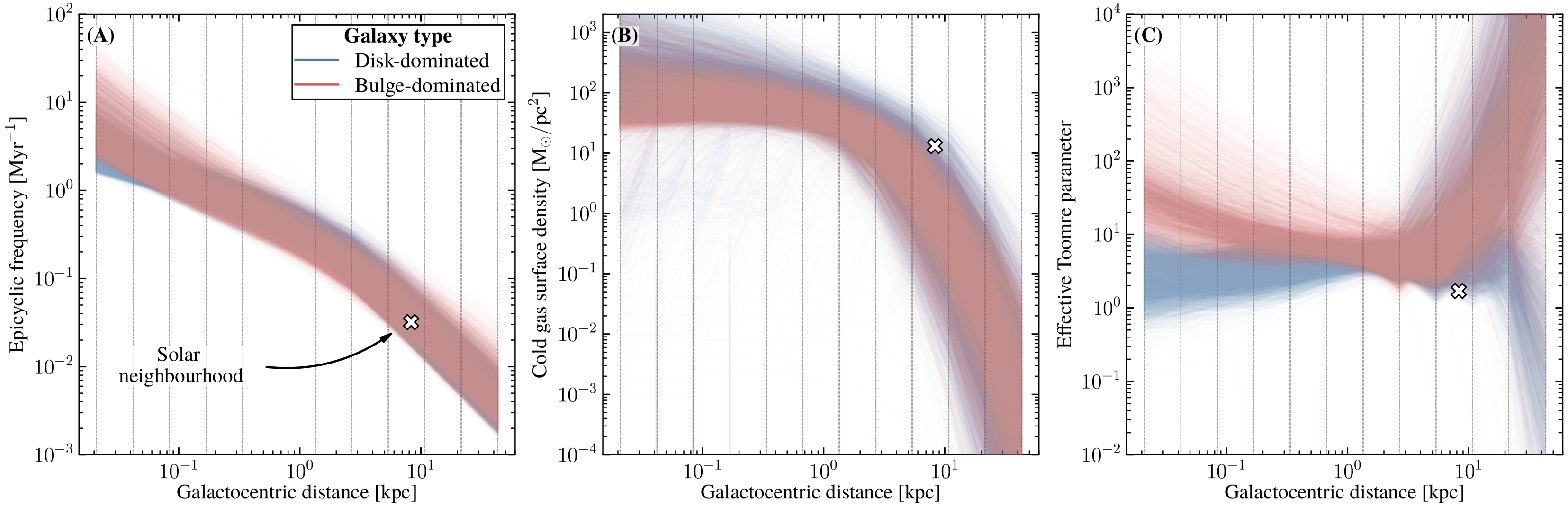

Figure 6.2. Epicyclic frequency, cold gas surface mass density, and the Toomre stability parameter as a function of galactocentric distance for disk- (blue) and bulge-dominated (red) galaxies, defined as having a bulge-to-total stellar mass ratio of $B/T < 0.2$ and $B/T \geq 0.9$, respectively. We add for comparison the value of the solar neighbourhood: we calculate $\kappa_{\mathrm{D},\odot} \approx 0.046\,\mathrm{Myr}^{-1}$, as derived from the Oort constants $A = 15.6\,\mathrm{km\,s^{-1}\,kpc^{-1}}$ and $B = -15.8\,\mathrm{km\,s^{-1}\,kpc^{-1}}$ taken from Guo and Qi (2023); $\Sigma_{\mathrm{g},\odot} \approx 13\,\mathrm{M_\odot\,pc^{-2}}$ from Flynn et al. (2006); and $Q_{\mathrm{eff},\odot} \approx 1.7$ (Binney & Tremaine, 2008, with $Q_{\mathrm{s},\odot} \approx 2.7$ and $Q_{\mathrm{g},\odot} \approx 1.5$), a typical value for disks (e.g. Rafikov, 2001; Leroy et al., 2008; Feng et al., 2014; Westfall et al., 2014).

Toomre stability parameter via

$$\mathcal{M}_{\mathrm{cold},\,j} = \sqrt{2}\phi_{\overline{\mathrm{P}},\,j}^{1/8}\,\frac{Q_{\mathrm{eff},\,j}\Sigma_{\mathrm{g},\,j}}{\kappa_j}\,, \tag{6.20}$$

where $\phi_{\overline{\mathrm{P}},\,j}$ is the ratio of the mean pressure of a gaseous cloud related to the pressure at its surface (Krumholz & McKee, 2005) with typical values close to two in dense regions (Heyer et al., 2004; Rosolowsky & Blitz, 2005; Schuster et al., 2007; Colombo et al., 2014). Notice that the parameter $\phi_{\overline{\mathrm{P}},\,j}$ is directly related to the fraction of cold gas contained in giant molecular clouds (GMCs) as $\phi_{\overline{\mathrm{P}},\,j} \approx 10 - 8 \times f_{\mathrm{GMC},\,j}$. We assume that this fraction only depends on the cold gas surface density (Krumholz & McKee, 2005), i.e.

$$f_{\mathrm{GMC},\,j} = \left[1 + 250/(\Sigma_{\mathrm{g},\,j}/[\mathrm{M}_\odot\,\mathrm{pc}^{-2}])^2\right]^{-1}\,. \tag{6.21}$$

Next, we need to evaluate the minimum-value star formation efficiency. If star formation occurs on the free-fall time scale, this efficiency can be expressed as a combination of the specific SFR, $\mathrm{sSFR}_{\mathrm{ff}}$, and the ratio of the feedback time scale, t_{fb}, to the free-fall time scale, t_{ff}, i.e.

$$\epsilon_{\mathrm{ff},\,j} = \mathrm{sSFR}_{\mathrm{ff},\,j} \times t_{\mathrm{fb},\,j}\,/\,t_{\mathrm{ff},\,j}\,. \tag{6.22}$$

For a spherical symmetric and homogeneous mass distribution,

$$t_{\mathrm{ff},\,j} = \sqrt{\frac{3\pi}{32\mathrm{G}\,\rho_{\mathrm{ISM},\,j}}}\,. \tag{6.23}$$

For the feedback time scale (Kruijssen, 2012),

$$t_{\mathrm{fb},\,j} = \frac{t_{\mathrm{SN}}}{2}\left[1 + \sqrt{1 + \frac{4\pi^2\mathrm{G}^2\,t_{\mathrm{ff},\,j}}{\phi_{\mathrm{fb}}\,\mathrm{sSFR}_{\mathrm{ff},\,j}\,t_{\mathrm{SN}}^2} \times \left(\frac{Q_{\mathrm{eff},\,j}\,\Sigma_{\mathrm{g},\,j}}{\kappa_j}\right)^2}\,\right], \tag{6.24}$$

where t_{SN} is the time scale for the first supernovae, which we assume to be 3 Myr, $\phi_{\mathrm{fb}} = 5.28 \times 10^2\,\mathrm{pc}^2\,\mathrm{Myr}^{-3}$ (Kruijssen, 2012), and

$$\frac{\mathrm{sSFR}_{\mathrm{ff},\,j}}{0.13} = 1 + \mathrm{erf}\left[\frac{\varsigma_{\rho,\,j}^2 - \ln\left(0.68\,\alpha_{\mathrm{vir}}^2\,\mathcal{M}_{\mathrm{cold},\,j}^4\right)}{2^{3/2}\varsigma_{\rho,\,j}}\right], \tag{6.25}$$

with the virial parameter of GMCs α_{vir} (Larson, 1981). It relates the mass, size, and velocity dispersion of a GMC and takes values between 10^{-1} and 10^1 (e.g. Myers & Goodman, 1988; Bertoldi & McKee, 1992; Heyer et al., 2009; Dobbs et al., 2011; Hopkins et al., 2012). We set $\alpha_{\mathrm{vir}} = 1.3$ as proposed by McKee and Tan (2003).

In case star formation is less efficient than is assumed in Equation 6.22 we take $\epsilon_{\mathrm{inc},\,j} = \epsilon_{\mathrm{ff},\,j} \times t_{\mathrm{ff},\,j}/10\,\mathrm{Myr}$. If star formation is more efficient we set an upper bound of $\epsilon_{\mathrm{inc},\,j} = \epsilon_{\mathrm{max}} = 0.5$ (Matzner & McKee, 2000). The resulting effective star formation efficiency is the minimum of the above values,

$$\epsilon_j = \min\left(\epsilon_{\mathrm{ff},\,j}\,,\,\epsilon_{\mathrm{inc},\,j}\,,\,\epsilon_{\mathrm{max}}\right). \tag{6.26}$$

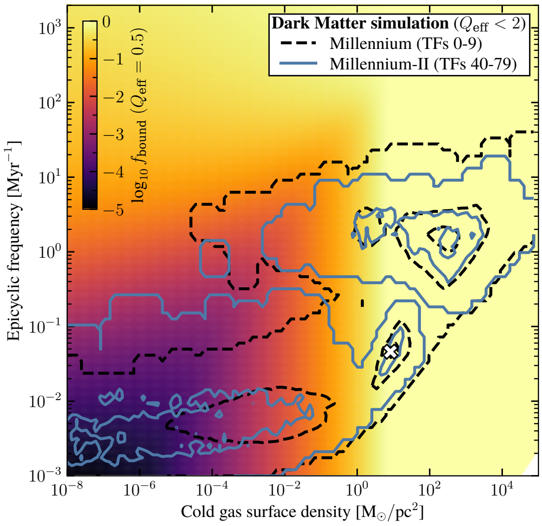

Figure 6.3. Bound fraction of star formation, evaluated for $Q_{\rm eff} = 0.5$, as a function of epicyclic frequency and cold gas surface density. Blue solid and dashed black contours give the smoothed distribution (with standard deviation of 1 dex) of all annuli of all galaxies with $Q_{\rm eff} < 2$ after running *L-Galaxies* tree-files 0-9 and 40-79 on the Millennium and Millennium-II simulations, respectively. Contour lines are smoothed with a Gaussian kernel with standard deviation of 0.5 dex. The location of the solar neighbourhood (see Figure 6.2 for details) is marked with a white cross.

Finally, the bound fraction of star formation can be computed by the normalised integral of the probability density function of contrast of the interstellar medium combined with the minimum star formation efficiency,

$$f_{{\rm bound},\,j} = \epsilon_{\rm max}^{-1} \frac{\int_{-\infty}^{\infty} {\rm d}\delta_j\, \epsilon_j^2(\delta_j)\, \delta_j ({\rm d}p_j/{\rm d}\delta_j)}{\int_{-\infty}^{\infty} {\rm d}\delta_j\, \epsilon_j(\delta_j)\, \delta_j ({\rm d}p_j/{\rm d}\delta_j)} \,. \tag{6.27}$$

Figure 6.3 shows the bound fraction for different environments with $Q_{\rm eff} = 0.5$ for the background. The $z = 0$ distributions of annuli from running *L-Galaxies* on halos identified in the Millennium and Millennium-II simulations that satisfy $Q_{\rm eff} < 2$ are added on top and reveals a large range bound star formation that depends on the location within the galaxy: the innermost regions feature high surface densities and epicyclic frequencies (*c.f.* Figure 6.2) and have high bound fractions approaching one. In contrast, the outermost regions of galaxies have low surface densities and epicyclic frequencies, prohibiting the formation of bound structures. As a consequence, this result already predicts that massive star clusters at distances a few times the disk's scale-length likely originate from accreted satellite galaxies, assuming that heating processes within their host galaxy are insignificant.

While not shown in Figure 6.3, we find a decrease in bound fraction for an increasing Toomre stability parameter value when keeping the epicyclic frequency and cold gas surface density constant. This is related to the specific SFR, sSFR$_{\rm ff}$, which decreases for an increasing Toomre parameter as per Equations 6.20 and 6.25, and because the gas disk becomes more stable with an increase in $Q_{\rm eff}$. As a result the mid-plane density of the interstellar medium decreases, which, in turn, decreases the star formation efficiency and, thus, the bound fraction.

6.2.4 Initial Star Cluster Properties

Here we detail the initial properties of star clusters that form in galaxy disks. Note that we deliberately exclude star clusters that form in the innermost ring with a radius of approximately 30 pc. These star clusters will either be disrupted quickly or merge to form a nuclear star cluster, which will be the subject of future work.

Another computational limit is the number of star clusters whose properties will be tracked over time. In this work, we focus on the most massive star clusters that survive until $z = 0$ and decide to completely ignore star clusters below $10^3\,\mathrm{M}_\odot$ (see below). In the simulation we track the properties of the 1000 most massive star clusters in the disk and halo, respectively, resulting in up to 2000 objects per galaxy. Although somewhat arbitrary, these numbers compare to the total number of star clusters of M 31 (potentially more than 1000; e.g. Barmby & Huchra, 2001; Huxor et al., 2014) and is much larger than the number of known globular clusters for the Milky Way (about 200; see e.g. Minniti et al., 2017; Garro et al., 2024, and references therein). In case a galaxy forms less than 1000 massive star clusters above throughout its life time, all other masses are ignored and not considered in the below analysis.

Stellar Mass

The mass of each star cluster is a random realisation of the underlying cluster initial mass function (CIMF), which we assume to follow a classical power-law function that is truncated at the upper mass end with an environmentally-dependent mass-scale, i.e.

$$\xi_j(m_\mathrm{c}) \propto m_\mathrm{c}^{\alpha_\mathrm{CIMF}} \times \exp(-m_\mathrm{c} \,/\, m_{\mathrm{cl,\,max},\,j}) \,. \tag{6.28}$$

We assume here that $\alpha_\mathrm{CIMF} = -2$, motivated by observational studies of young star clusters in nearby galaxies (e.g. Zhang & Fall, 1999; Bik et al., 2003; Hunter et al., 2003; McCrady & Graham, 2007; Portegies Zwart et al., 2010; Emig et al., 2020; Levy et al., 2024). The truncation mass-scale is a product of the star formation efficiency (ϵ_cloud), the bound fraction of star formation (f_bound), the Toomre mass (m_T), and the fraction of molecular gas that is critical to undergo gravitational collapse (f_coll; Kruijssen, 2014; Reina-Campos & Kruijssen, 2017; Reina-Campos et al., 2022a), i.e.

$$m_{\mathrm{cl,\,max},\,j} = \epsilon_\mathrm{cloud} \times f_{\mathrm{bound},\,j} \times m_{\mathrm{T},\,j} \times f_{\mathrm{coll},\,j} \,, \tag{6.29}$$

resulting in a typical value of the order of $10^5\,\mathrm{M}_\odot$ at lower redshifts and up to $10^9\,\mathrm{M}_\odot$ in extreme cases. We assume

$$m_{\mathrm{T},\,j} = 4\pi^5 \mathrm{G}^2 \times \Sigma^3_{\mathrm{D,\,g},\,j} \times Q^4_{\mathrm{eff},\,j} / \kappa^4_j \,, \tag{6.30}$$

and

$$f_{\mathrm{coll},\,j} = \min(1,\, t_{\mathrm{fb},\,j} \,/\, t_{\mathrm{ff,\,2D},\,j})^4 \,, \tag{6.31}$$

for the Toomre mass and collapse fraction, respectively. The two-dimensional free-fall time scale is $t_{\mathrm{ff,\,2D},\,j} = \sqrt{2\pi}/\kappa_j$.

In the above equations we assume a constant value of $\epsilon_\mathrm{cloud} = 0.1$ for star formation within a GMC, motivated by numerical results (e.g. Oklopčić et al., 2017; Chevance et al., 2020). Notice that this value is potentially smaller than the assumed star formation efficiency in the determination of the bound fraction in Equation 6.26. A higher efficiency would results in a higher upper truncation mass-scale of the CIMF and could result in the formation of more massive star clusters. However, as we show in

Section 6.5.3 the main results of our work do not significantly change when assuming no upper truncation mass-scale but a pure power-law function instead.

For computational efficiency of the code, we consider only star clusters with initial masses in the range of 10^4 to $10^8\,\mathrm{M}_\odot$. At the same time, we assume that the minimum star cluster mass that could, in principle, form is $10^2\,\mathrm{M}_\odot$, meaning that we do not fully sample the CIMF. Therefore, we only sample a total star cluster mass of $f_{\mathrm{sample}} \times f_{\mathrm{bound}} \times \mathrm{SFR} \times \delta t$ where

$$f_{\mathrm{sample}} = \frac{\int_{10^4\,\mathrm{M}_\odot}^{10^8\,\mathrm{M}_\odot} m_{\mathrm{c}}\,\xi(m_{\mathrm{c}})\,\mathrm{d}m_{\mathrm{c}}}{\int_{10^2\,\mathrm{M}_\odot}^{10^8\,\mathrm{M}_\odot} m_{\mathrm{c}}\,\xi(m_{\mathrm{c}})\,\mathrm{d}m_{\mathrm{c}}}\,. \tag{6.32}$$

In the case of a power-law CIMF with index -2 this ratio is two-thirds, i.e. one-third of the total mass in star clusters is contained in objects below $10^4\,\mathrm{M}_\odot$. For the more complex case of Equation 6.28, we pre-compute the integral numerically for seven equally-spaced values between 10^3 and $10^9\,\mathrm{M}_\odot$, resulting in, for example, $f_{\mathrm{sample}} \approx 2.3 \times 10^{-6}$ for $m_{\mathrm{cl,\,max}} = 10^3\,\mathrm{M}_\odot$. Afterwards, we randomly sample the CIMF with $m_{\mathrm{cl,\,max}}$ that agrees best with the computed value of Equation 6.29.

Finally, to reduce computational cost we utilise lookup tables for initial star cluster masses. For simplicity, we generated seven lookup tables for different values of $m_{\mathrm{cl,\,max}}$, equally spaced between 10^3 and $10^9\,\mathrm{M}_\odot$, with 10^5 data points each. Randomly sampling data points from the lookup tables turned out to be computationally more efficient than direct random sampling from the cluster initial mass functions as many of the drawn star cluster masses are too low to be stored in arrays.

Initial Galactocentric Distances

For each annulus we assume that the galactocentric distribution of initial values is uniform and independent of other star cluster parameters.

Half-Mass Radius

The physical processes that govern the distribution of the initial half-mass radius of star clusters is still unknown, and many theoretically motivated and observational-based prescriptions seem to fail to reproduce the distribution at $z = 0$ in nearby galaxies (e.g. Reina-Campos et al., 2023a). For that reason we adopt a simplified prescription by using a constant initial value of $r_{\mathrm{c,\,h}} = 1.0\,\mathrm{pc}$ for all clusters, independent of mass and redshift of formation. We explore more complex prescriptions in Section 6.5.2.

Tidal Radius

The half-mass sizes of star clusters increase over time (*c.f.* Section 6.2.5) and are limited to the tidal radius where the gravitational acceleration of the cluster equals the tidal acceleration. The tidal field is directly related to the local gravitational potential and the tidal radius is related to the first eigenvector of the diagonalised tidal tensor. Assuming circular orbits and a mass concentration in the galaxy centre we apply the definition of King (1962), Renaud et al. (2011), and Renaud (2018) and calculate

$$r_{\mathrm{c},t} = \left[\frac{\mathrm{G}\, m_\mathrm{c}}{(\Omega^2 - \partial^2\Phi_\mathrm{tot}/\partial w^2)_{w_\mathrm{c}}} \right]^{1/3}, \tag{6.33}$$

where Ω equals the angular frequency equated at the galactocentric distance of the star cluster. More generally, for each ring j,

$$\Omega_j = \sqrt{\frac{1}{\langle w_j \rangle} \frac{\partial \Phi_\mathrm{tot}}{\partial w}\bigg|_{\langle w_j \rangle}}. \tag{6.34}$$

Note that this prescription ignores the tidal effect of nearby baryonic over-densities, such as star forming regions or clouds, which may be dominant over the global galactic field. Other works that use hydrodynamical approaches (such as Reina-Campos et al., 2022a) determine a local tidal tensor from neighbouring cells, which is not possible in our model. We discuss this issue in Section 6.3.5.

Metallicity

For the metallicity (and individual elemental abundances of H, He, C, N, O, Ne, Mg, Si, S, Ca, Fe) of a star cluster we assume that it equals the metallicity of the cold gas in the ring it forms in, $Z_\mathrm{c} = Z_\mathrm{g}$, and that this value remains constant over the star cluster's lifetime. The first assumption neglects any azimuthal variations of metallicity profiles which are known to exist in some galaxies due to asymmetric structures such as bars or spiral patters in the Milky Way (e.g. Poggio et al., 2022; Spina et al., 2022; Filion et al., 2023; Hawkins, 2023; Hackshaw et al., 2024) and other spiral galaxies (e.g. Sánchez-Menguiano et al., 2016; Ho et al., 2017; Sánchez-Menguiano et al., 2018; Ho et al., 2019; Hwang et al., 2019; Metha et al., 2021, 2024) but see Kreckel et al. (2019) for counterexamples. Nevertheless, despite lacking such an implementation we argue in Section 6.3.4 that the metallicity distributions of our cluster populations are reasonable.

6.2.5 Star Cluster Evolution

We detail in the next subsections the main processes that affect the evolution of star clusters: mass loss rates, expansion of the half-mass radius, and re-location.

Mass-Loss

We consider three mechanisms for cluster mass-loss: stellar evolution, tidal stripping due to an expanding cluster, and tidal shocks from interactions with GMCs, i.e.

$$\frac{\mathrm{d}m_\mathrm{c}}{\mathrm{d}t} = \frac{\mathrm{d}m_\mathrm{c}}{\mathrm{d}t}\bigg|_\mathrm{ev} + \frac{\mathrm{d}m_\mathrm{c}}{\mathrm{d}t}\bigg|_\mathrm{rlx} + \frac{\mathrm{d}m_\mathrm{c}}{\mathrm{d}t}\bigg|_\mathrm{sh}. \tag{6.35}$$

Stellar Evolution To take into account cluster mass-loss from stellar evolution we assume that cluster members represent a random realisation of a single stellar population assuming a Chabrier IMF (Chabrier, 2003), resulting in varying expected lifetimes. Then, for an individual $10^5\,\mathrm{M}_\odot$ star cluster we utilise the "Stochastically Lighting Up Galaxies" library (da Silva et al., 2012, 2014; Krumholz et al., 2015) with non-rotating "Geneva" 2013 stellar tracks (Schaller et al., 1992; Meynet et al., 1994; Ekström et al., 2012; Georgy et al., 2013) and fit a linear relationship to the retained mass as a function of time. The resulting mass-loss rate at time t in [yr] is

$$\left.\frac{\mathrm{d}m_\mathrm{c}}{\mathrm{d}t}\right|_\mathrm{ev} = -\frac{0.13}{\ln(10)}\frac{m_\mathrm{c}^\mathrm{init}}{t}, \quad \text{for } t \geq t_\mathrm{SN} \,. \tag{6.36}$$

We find that this relation holds, to first order, irrespective of cluster metallicity. Note that the above determination does not take into account other mass-loss channels that we introduce below, which is why we update the "initial" star cluster mass, denoted here with $m_\mathrm{c}^\mathrm{init}$, at each time-step.

Relaxation Multi-body encounters between stars within a cluster result in energy transfer between the individual bodies and can cause stars to either orbit the star cluster's centre at larger radii or leave the cluster completely in case its velocity exceeds the escape velocity. For bound stars, if the new orbit crosses the tidal radius, the star can be stripped from the cluster, resulting in an effective mass loss.

We consider this effect by following an extensive literature (e.g. Spitzer, 1940; Hénon, 1961; Spitzer, 1987; Lamers et al., 2005) and set

$$\left.\frac{\mathrm{d}m_\mathrm{c}}{\mathrm{d}t}\right|_\mathrm{rlx} = -\xi_\mathrm{rlx}\frac{m_\mathrm{c}}{\tau_\mathrm{rlx}} \,, \tag{6.37}$$

with a relaxation time scale

$$\tau_\mathrm{rlx} = 0.138\frac{\sqrt{N}}{\ln(\gamma_\mathrm{rlx}N)}\sqrt{\frac{r_{\mathrm{c},h}^3}{\mathrm{G}\,\langle m_\star\rangle}} \,. \tag{6.38}$$

Here $\langle m_\star\rangle$ is the average stellar mass of the star cluster, $N = m_\mathrm{c}\,/\,\langle m_\star\rangle$, and $0.07 \lesssim \gamma_\mathrm{rlx} \lesssim 0.14$ (Giersz & Heggie, 1994). We assume a Chabrier (2003) initial stellar mass function, such that $\langle m_\star\rangle = 0.42\,\mathrm{M}_\odot$ and $\gamma_\mathrm{rlx} = 0.11$. Finally, we choose $\xi_\mathrm{rlx} = 0.08$ as suggested in the literature (e.g. Hénon, 1961; Gieles et al., 2011; Gieles & Renaud, 2016) for equal-mass cluster members, avoiding a proper treatment of the star cluster's direct tidal environment (Alexander & Gieles, 2012).

Tidal Shocks When a star cluster is located within the thin disk, i.e. has not been accreted during a galaxy merger event, it frequently interacts with GMCs if the fraction of cold gas bound within clouds is high. Depending on the impact parameter between the interaction the GMC can inject a significant amount of energy into the star cluster resulting in an increase in velocity dispersion and causing a fraction of the stars to escape the cluster as their velocity exceeds the cluster's escape velocity.

To model this effect we approximate a cluster's internal energy by assuming that it follows a Plummer-like density profile (Plummer, 1911). Following the equations outlined in Kruijssen (2012) we set

$$\left.\frac{\mathrm{d}m_\mathrm{c}}{\mathrm{d}t}\right|_\mathrm{sh} = -\frac{m_\mathrm{c}}{\tau_\mathrm{sh}} , \tag{6.39}$$

with

$$\tau_\mathrm{sh} = \frac{3\sqrt{\pi}}{2\sqrt{2^{2/3}-1}} \frac{\mathrm{G}}{g\phi_\mathrm{sh}\phi_\mathrm{ad}\phi_\mathrm{P} f_\mathrm{sh}} \times \left[\frac{Q_{\mathrm{eff},\,j}}{\kappa_j f_\mathrm{GMC}^{1/3}}\right]^3_{w_\mathrm{c}} \frac{m_\mathrm{c}}{r^3_{\mathrm{c},\,h}} , \tag{6.40}$$

with $g = 1.5$, $\phi_\mathrm{sh} = 2.8$, $f_\mathrm{sh} = 3$ and $\phi_\mathrm{ad} = \exp(-0.062)$. We use Equation 6.21 to equate f_GMC for the annuli corresponding to the star cluster's current galactocentric distance.

Note that, as mentioned above, only star clusters in galaxy disks are affected by tidal shocks due to encounters with GMCs, i.e. we set $\mathrm{d}m_\mathrm{c}/\mathrm{d}t|_\mathrm{sh} = 0$ for star clusters in a galaxy's halo. Our implementation also does not couple the time scale of tidal shocks to the strength of the local tidal field tensor (see e.g. Alexander et al., 2014; Reina-Campos et al., 2022a, for details) because we do not attempt to model GMCs. However, because *L-Galaxies* already separates the atomic from the molecular gas in each annulus (see Henriques et al., 2020; Yates et al., 2021, 2024) future efforts may implement clouds and improve on the current prescription.

Radial Expansion

Star clusters expand adiabatically due to contributions from mass-loss from two-body interactions and tidal shocks (e.g. Reina-Campos et al., 2022a). This results in a radial expansion of the form

$$\frac{\mathrm{d}r_{\mathrm{c},\,h}}{\mathrm{d}t} = \left[\left(2 - f_\mathrm{sh}^{-1}\right)\left.\frac{\mathrm{d}m_\mathrm{c}}{\mathrm{d}t}\right|_\mathrm{sh} + \left(2 + \zeta\xi_\mathrm{rlx}^{-1}\right)\left.\frac{\mathrm{d}m_\mathrm{c}}{\mathrm{d}t}\right|_\mathrm{rlx}\right]\frac{r_{\mathrm{c},\,h}}{m_\mathrm{c}} , \tag{6.41}$$

Following Gieles and Renaud (2016) we assume that $f_\mathrm{sh} = 3$ and following Gieles et al. (2011),

$$\zeta\xi_\mathrm{rlx}^{-1} = \frac{5}{3}\left[\left(\frac{r_{\mathrm{c},\,h}}{r_{\mathrm{c},\,j}}\right)_1 \frac{r_{\mathrm{c},\,j}}{r_{\mathrm{c},\,h}}\right]^{3/2} \approx 0.092\left(\frac{r_{\mathrm{c},\,t}}{r_{\mathrm{c},\,h}}\right)^{3/2} , \tag{6.42}$$

where we assumed in the approximation that the Jacobi radius equals the tidal radius and that $\left(r_{\mathrm{c},\,h}/r_{\mathrm{c},\,j}\right)_1 \approx 0.145$ (Hénon, 1961).

Note that we neglect here any impact of stellar-mass black holes on the evolution of the cluster, which contributes and may even dominate the dissolution of some star clusters, depending on, among others, mass and metallicity (e.g. Giersz et al., 2019; Gieles et al., 2021; Rostami-Shirazi et al., 2024). We discuss this issue again in Section 6.3.5.

Galactocentric Migration

Without any external perturbations star clusters in a galaxy's disk and halo migrate towards the inner regions through dynamical friction caused by interactions with constituents of three components: (1) field stars belonging to the stellar halo and bulge, (2) the gaseous halo, and (3) the dark matter halo. For the stellar and dark matter components, we follow the well-known Chandrasekhar (1943) prescription and assume an isotropic velocity distribution function of the components as well as circular orbits of the star clusters. As a consequence, a star cluster experiences a radial acceleration of

$$\frac{\mathrm{d}v_\mathrm{c}}{\mathrm{d}t} = -4\pi \mathrm{G}^2 \frac{m_\mathrm{c}\rho_\mathrm{f}}{v_\mathrm{c}^2} \ln\Lambda \left[\mathrm{erf}(X) - \frac{2X}{\sqrt{\pi}} \exp\left(-X^2\right) \right] , \tag{6.43}$$

where $X = v_\mathrm{c} \,/\, (2\sigma_\mathrm{f})$ and ρ_f is the density of dark matter and stars in the halo evaluated at the position of the star cluster. The circular velocity of each object is computed via Equation 6.13. For the Coulomb logarithm, we follow Binney and Tremaine (2008) and assume

$$\ln\Lambda = \ln\left[\frac{w_\mathrm{c}}{\max(r_{\mathrm{c},\,h}\,, \mathrm{G}\,m_\mathrm{c} \,/\, v_\mathrm{typ}^2)} \right] , \tag{6.44}$$

where we replaced the maximum impact parameter with the galactocentric distance of the star clusters and assume for the typical velocity of the stellar disk $v_\mathrm{typ} = \sqrt{\mathrm{G}\,M_\mathrm{D,\,s}/R_\mathrm{D,\,s}}$. For the velocity dispersion of halo stars we assume that their orbits are dominated by the underlying dark matter profile. Based on the Jeans equation for an isotropic system Zentner and Bullock (2003) give the following approximation for the velocity dispersion,

$$\sigma_\mathrm{H,\,s} = v_\mathrm{max} \times \frac{1.4393\,x_\mathrm{c}^{0.354}}{1 + 1.1756\,x_\mathrm{c}^{0.725}} , \tag{6.45}$$

with maximum circular velocity within the dark matter halo that we introduced in Equation 6.3 and $x_\mathrm{c} = w_\mathrm{c}/R_\mathrm{vir}$.

The radial acceleration caused by the hot gaseous component is slightly different compared to Equation 6.43. Following Ostriker (1999) and Escala et al. (2004) we take

$$\frac{\mathrm{d}v_\mathrm{c}}{\mathrm{d}t} = -\frac{4\pi \mathrm{G}^2\, m_\mathrm{c}\rho_\mathrm{H}}{v_\mathrm{c}^2} g(\mathcal{M}_\mathrm{hot}) , \tag{6.46}$$

where ρ_H is the density of the gaseous halo evaluated at the star clusters position and

$$g(\mathcal{M}_\mathrm{hot}) = \begin{cases} \ln\Omega \times k(\mathcal{M}_\mathrm{hot}) & \text{if } \mathcal{M}_\mathrm{hot} < 0.8 \,, \\ 3\ln\Omega \times k(\mathcal{M}_\mathrm{hot}) & \text{if } 0.8 \le \mathcal{M}_\mathrm{hot} \le 1.5 \,, \\ \ln(1 - \mathcal{M}_\mathrm{hot}^{-2}) + 2\ln\Lambda & \text{otherwise} \,. \end{cases} \tag{6.47}$$

Here Ω is the angular frequency, as introduced in Equation 6.34, evaluated at the position of the star cluster and $\ln\Lambda$ the Coulomb logarithm from Equation 6.44. Finally,

$$k(\mathcal{M}_\mathrm{hot}) = \mathrm{erf}\left(\frac{\mathcal{M}_\mathrm{hot}}{2}\right) - \sqrt{\frac{2}{\pi}}\mathcal{M}_\mathrm{hot} \exp\left(-\frac{\mathcal{M}_\mathrm{hot}^2}{2}\right) . \tag{6.48}$$

We calculate the Mach number of a cluster within the hot gas halo as $\mathcal{M}_{\rm hot} = v_{\rm c} \, / \, c_{\rm s,\,hot}$ where (Tanaka & Haiman, 2009; Choksi et al., 2017)

$$\frac{c_{\rm s,\,hot}}{[{\rm km\,s^{-1}}]} = 1.8\sqrt{1+z}\left(\frac{M_{\rm vir}}{10^7\,{\rm M_\odot}}\right)^{1/3}\left(\frac{\Omega_{\rm M,\,0}\,h^2}{0.14}\right)^{1/6} . \tag{6.49}$$

Re-Distribution During Galaxy Mergers

Explanations for the observed presence of star clusters in galaxy halos generally favour (a) interactions with massive perturbers (such as other star clusters or GMCs) that heat the object from its birth-place in a disk, (b) star cluster formation in galaxy outskirts during tidal interactions, or (c) a direct re-distribution during galaxy mergers. The lower tidal field and absence of tidal shocks may be an important ingredient in cluster survival as indicated by Baumgardt and Hilker (2018) who find that the Milky Way's halo hosts all Galactic star clusters older than approximately five Gyr. Therefore, re-positioning of star clusters is an essential physical ingredient in simulating star cluster properties.

We consider two different scenarios based on the ratio of the baryonic masses of the two galaxies. Here we follow the prescription by *L-Galaxies* and assume that a major merger occurs if the mass ratio exceeds 0.1. In this case, we assume that the disks of both galaxies are destroyed and that all star clusters from both galaxies are contained within the halo of the successor galaxy. For minor galaxy mergers where the mass ratio is smaller than 0.1 we assume that the star cluster population of the more massive galaxy remains unaffected and that all accreted star clusters migrate into the halo of their new host.

Note that we assume here that all star clusters survive the tidal shock experienced during galaxy mergers, i.e. resulting in a "survival fraction" of unity (see Kruijssen & Cooper, 2012; De Lucia et al., 2024, for a different approach). Furthermore, we do not add another mass-loss term for this scenario.

Generally speaking, the resulting baryonic distribution after galaxy mergers is sensitive to the initial conditions such as the galaxy mass ratio and their respective positions, orientations, and velocity vectors and magnitudes to each other. Therefore, when re-distributing star clusters from their old galactocentric distance, $w_{\rm c}^{\rm old}$, to the new galactocentric distance, $w_{\rm c}^{\rm new}$, we assume the following simple relationship,

$$w_{\rm c}^{\rm new} = D_{1\leftrightarrow 2} \times \left(\frac{w_{\rm c}^{\rm old}}{D_{\rm max}}\right)^{\alpha_w} \times \exp\left(-\frac{w_{\rm c}^{\rm old}}{D_{\rm max}}\right) . \tag{6.50}$$

Here we introduced two distance measures and a free parameter α_w that we set to four. The first distance measure, $D_{1\leftrightarrow 2}$, equals the three-dimensional separation between the two galaxy centres once the lower mass galaxy loses its dark matter halo. The other distance measure, $D_{\rm max}$, equals either the largest galactocentric distance of the star cluster population or three times the stellar disk's scale length, i.e.

$$D_{\rm max} = \begin{cases} \max\limits_{i\in N_{\rm c}}(w_{{\rm c},\,i}^{\rm old}) & \text{if } \max\limits_{i\in N_{\rm c}}(w_{{\rm c},\,i}^{\rm old}) \geq 3R_{\rm D,\,s} , \\ 3R_{\rm D,\,s} & \text{otherwise} . \end{cases} \tag{6.51}$$

6.3 Results

In this work we focus on basic properties of the star cluster populations at $z = 0$. In the following sections, we refer to a star cluster as young (old) if its age is $\tau_c < 0.3$ Gyr ($\tau_c \geq 8$ Gyr). Disk-dominated ("spiral"[4]) galaxies are assumed to be the ones with a bulge-to-total stellar mass ratio of $B/T < 0.2$ whereas bulge-dominated ("elliptical") systems have $B/T \geq 0.9$.

We focus our analysis on the output of running the model on Millennium (Springel et al., 2005) tree-files 0-9 (out of 512 total) that contain 118 558 galaxies at $z = 0$ and provide us with a representative sub-sample. The model performs similarly when running on Millennium-II (Boylan-Kolchin et al., 2009) tree-files 40-79 (a representative sub-sample; out of 512), going down to lower galaxy stellar masses, and we will detail a brief comparison in each subsection in case of differences.

6.3.1 M_V-SFR Relationship

A first test for our model is to reproduce the empirical relationship between the absolute V-band magnitude of the brightest young star cluster (local quantity within a galaxy) versus the host galaxy's SFR (global quantity) within disk-dominated galaxies (e.g. Larsen, 2002; Bastian, 2008; Larsen, 2010). Since this relation is not used as input for the simulation it serves as both a check of the models capabilities and a test to explore secondary correlations with other third quantities.

For the simulated data, as we store star cluster masses, we need to convert to the Johnson-Cousins V-band. We perform the conversion by using the Python version (Johnson et al., 2023) of the "Flexible Stellar Population Synthesis" code (Conroy et al., 2009; Conroy & Gunn, 2010, October a, 2010b; Conroy et al., 2010) that uses as input the metallicity and age of a stellar population and yields an absolute magnitude in selected filterbands. Furthermore, for the computation, we assume that all star clusters are composed of a single stellar population that follows a Chabrier (2003) stellar initial mass function. To compare to observations we compile the data from Johnson et al. (2000), Larsen (2002), Rafelski and Zaritsky (2005), Bastian (2008), Annibali et al. (2009), Goddard et al. (2010), Adamo et al. (2011), Annibali et al. (2011), Pasquali et al. (2011), Silva-Villa and Larsen (2011), Cook et al. (2012), Ryon et al. (2014), Whitmore et al. (2014), Adamo et al. (2015), Lim and Lee (2015), and Cook et al. (2023). Additionally, we use data from Maschmann et al. (2024) and Thilker et al. (2025, accepted), representing the results for PHANGS galaxies (see Lee et al., 2022, 2023, for details). For that data set specifically, we use stellar mass estimates from Emsellem et al. (2022) and SFR estimates from Sun et al. (2022). Otherwise, galaxy stellar masses are taken from the 50 Mpc catalogue provided by Ohlson et al. (2023).

We show the resulting parameter space for young massive star clusters in disk-dominated galaxies in Figure 6.4. Our results show an increasing star cluster mass with increasing SFR, in qualitative agreement with the observations, although with a slightly steeper slope. To quantify the level of (dis-)agreement we perform a linear fit to the data

[4] *L-Galaxies* does not model any spiral-wave patterns in galaxies, which is why we prefer the term "disk-dominated" over "spiral"

sample and obtain uncertainties through a 10 000 Monte Carlo iterations. The resulting slope values are $\alpha_{\rm sim} = -2.607^{+0.009}_{-0.009}$ for the simulated data and $\alpha_{\rm obs} = -2.02^{+0.09}_{-0.09}$ for the observations. This difference becomes smaller when constraining star clusters to younger ages (e.g. $\alpha_{\rm sim} \approx -2.457$ for $\tau_{\rm c} \leq 50\,{\rm Myr}$). Nevertheless, most of our star clusters are located in galaxies with SFRs of the order of $10^{-1}\,{\rm M_\odot\,yr^{-1}}$ and have absolute V-band magnitudes of $M_V \approx -11$, which is in excellent agreement with observations.

When running the model on Millennium-II data we find a better agreement for the lowest-mass (but still the most massive and young) star clusters towards lower galaxy SFRs, which is because of the higher mass resolution offered by the simulation. We observe that the slope values of the relationship changes: applying the same galaxy mass cut of $10^{9.5}\,{\rm M_\odot}$ results in a slope of $\alpha_{\rm sim,\,mrii} = -2.02^{+0.09}_{-0.09}$, which is basically identical to the results of the observational data.

We identify a secondary dependence on galaxy stellar mass in panel (B) where the slope of the relationship is steeper for massive galaxies: when constraining the galaxy sample to stellar masses above $10^{10}\,{\rm M_\odot}$ the slope value decreases to $\alpha_{\rm sim} \approx -3.64$.[5] This trend is mainly related to the the upper truncation mass-scale for the CIMF, which decreases due to a decreasing Toomre mass and bound fraction. Galaxies with stellar masses below $10^{9.5}\,{\rm M_\odot}$ have comparable $Q_{\rm D,\,g}$ values to more massive galaxies but their $Q_{\rm D,\,s}$ values are larger because of their disk mass is dominated by gas and not stars and $Q_{{\rm D},\,i} \propto \Sigma_{{\rm D},\,i}^{-1}$. As a consequence, the slope value of these low-mass galaxies is $\alpha_{\rm sim} \approx -2.63$.

For the cluster formation efficiency, which equals the bound fraction introduced in Equation 6.27 and the survival rate of star clusters during the initial few Myr (see Kruijssen, 2012; Kruijssen & Cooper, 2012, for details on this "cruel cradle effect"), we find an increase with SFR (panel C). This is expected given the direct relationship between the SFR surface density and cold gas surface density (*c.f.* Equation 6.2) and because $f_{\rm bound}$ positively correlates with $\Sigma_{\rm g}$ (*c.f.* Figure 6.3). Our results are in excellent agreement with literature data.

We conclude that this relationship is sensitive to the resolution of the simulation and that taking into account biases in the mass range of the selected galaxy samples is important.

6.3.2 Half-Mass Radius and Stellar Mass

We show in Figure 6.5 the one-dimensional histograms of star cluster masses and half-mass radii. Here we do not distinguish between galaxy morphologies because of the similar prescriptions of star cluster formation. *L-Galaxies* assumes that star formation only occurs in galaxy disks and ellipticals will exhibit similar disk properties to disk-dominated galaxies in case cold gas is accreted (see Henriques et al., 2015, 2020, for details). Therefore, given the similar disk properties the upper truncation

[5] Note that the secondary dependence on galaxy mass is also present in the *E-MOSAICS* model (Figure 10 in Pfeffer et al., 2019b), however, they only include 153 galaxies and have an additionaly y-axis offset of 0.5 to 1 dex.

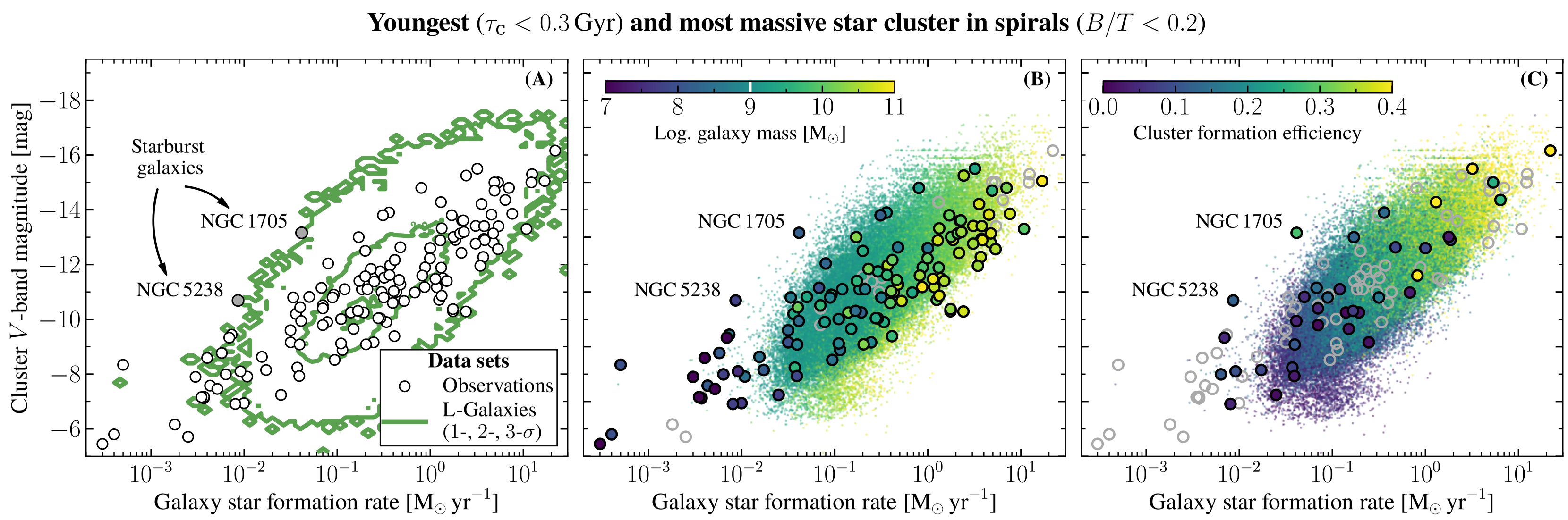

Figure 6.4. Absolute V-band magnitude of the youngest and most massive star cluster (excluding all star clusters in the central annulus) versus the galaxy-averaged star formation rate. The galaxy sample is limited to disk-dominated galaxies that have a bulge-to-total stellar mass ratio of $B/T < 0.2$. We compare our results to various observations of nearby disk-dominated galaxies (see main text for details). For both the simulated data and the observations, we set an age cut of $\tau_c \leq 0.3$ Gyr on the star clusters. *Panel A:* Full observational and simulated data samples. For the simulated data, we show the 1-, 2-, and 3-σ intervals. *Panel B:* Same as in the first panel but colour-coding all data point by the host galaxy's stellar mass. If no stellar mass estimate is available for observational data points, we show them with gray symbols. *Panel C:* Same as the central panel but colour-coding the data points by the cluster formation efficiency, which is a combination of the bound fraction of star formation and the "cruel cradle effect" (Kruijssen, 2012; Kruijssen & Cooper, 2012) that takes the interaction of a proto-star cluster with its natal environment and nearby giant molecular clouds into account. Note that the two outliers, NGC 1705 and NGC 5238, are starburst galaxies and that their massive star clusters were previously classified as nuclear star clusters (Pechetti et al., 2020; Hoyer et al., 2021). Nuclear star clusters often exhibit complex formation histories (e.g. Spengler et al., 2017; Kacharov et al., 2018; Fahrion et al., 2021) and cannot easily be compared to our simulated star clusters.

mass of the CIMF and most star cluster properties remain comparable.[6]

For young star clusters we find an approximate power-law distribution of star cluster masses down to about $10^4\,\mathrm{M}_\odot$ that equals the lowest possible mass value randomly sampled from the CIMF (see Section 6.2.4 for details). The distribution of simulated star clusters agree well to observational results of Brown and Gnedin (2021) who analysed the structural properties of young star clusters in a set of nearby galaxies from the *LEGUS* programme (Calzetti et al., 2015).[7] The only apparent difference exists at the high-mass end where there is a lack of massive star clusters in nearby disk-dominated galaxies, which may be both a result of simple number statistics, as massive and young star clusters above $10^6\,\mathrm{M}_\odot$ are rare in our simulated data as well ($\approx 0.5\,\%$), and because our data includes galaxies with high SFRs ($\gtrsim 10\,\mathrm{M}_\odot\,\mathrm{yr}^{-1}$ in some of the most massive disk-dominated systems), resulting in higher probability to form massive star clusters.

For old star clusters we find a broad distribution of masses. The shape of the distribution is partly related to the origin of the objects: clusters that were never displaced from a galaxy's disk lost a significant amount of mass and populate the low-mass end. In contrast, accreted clusters in a galaxy halo lose mass at lower rates and, thus, retain a larger fraction of their birth mass over time resulting in the broad distribution and "peak"-like structures at mass values of 10^5 to $10^6\,\mathrm{M}_\odot$. We presume that clusters with masses lower than $10^3\,\mathrm{M}_\odot$ quickly dissolve and do not track their evolution, hence the sharp truncation at this mass value.

We find some slight differences based on the host galaxies morphology. The peak of the distribution at masses of approximately $10^5\,\mathrm{M}_\odot$ differs by a factor of a few between disk-dominated galaxies (peak at higher-masses) and ellipticals. This difference is related to a more diverse accretion history of ellipticals resulting in a superposition of various cluster populations. Disk-dominated galaxies feature a higher fraction of massive star clusters ($m_\mathrm{c} \gtrsim 10^6\,\mathrm{M}_\odot$), which is due to their elevated star formation.

The distribution of half-mass radii for young star clusters is confined to small radii ranging between 1 and 5 pc. The lower bound is due to the constant half-mass radius chosen in our model, thus, the range of half-mass radii displays the environmental effect on the star clusters within the first few hundred Myr.

Our simulation fails to account for the most extended young star clusters in the sample of Brown and Gnedin (2021) that extend to $\approx 25\,\mathrm{pc}$. At the same time, their data include a large fraction of star clusters ranging from ≈ 0.1 to a peak value of $\approx 2\,\mathrm{pc}$, where the distribution of the simulated clusters peaks as well. If the data by Brown and Gnedin (2021) present a representative distribution of half-mass radii shortly after cluster birth then they indicate that the radii are potentially constrained by the clusters environment and may evolve quickly (see e.g. Banerjee & Kroupa, 2017, for *N*-body simulations). Evidence for the latter comes from hydrodynamical simulations of Lahén et al. (2024b) that show a rapid half-mass radius evolution from $\approx 0.1\,\mathrm{pc}$ to $\approx 1\,\mathrm{pc}$ over 100 Myr. We explore different prescriptions for initial half-mass

[6] There still remains some difference in the metallicities of newly formed star clusters between galaxies of different morphology, as we show in Section 6.3.4.

[7] For the comparison we applied the same age cut to the observational sample. Star cluster ages come from fitting the spectral energy distribution; see details in Adamo et al. (2017) and Ryon et al. (2017).

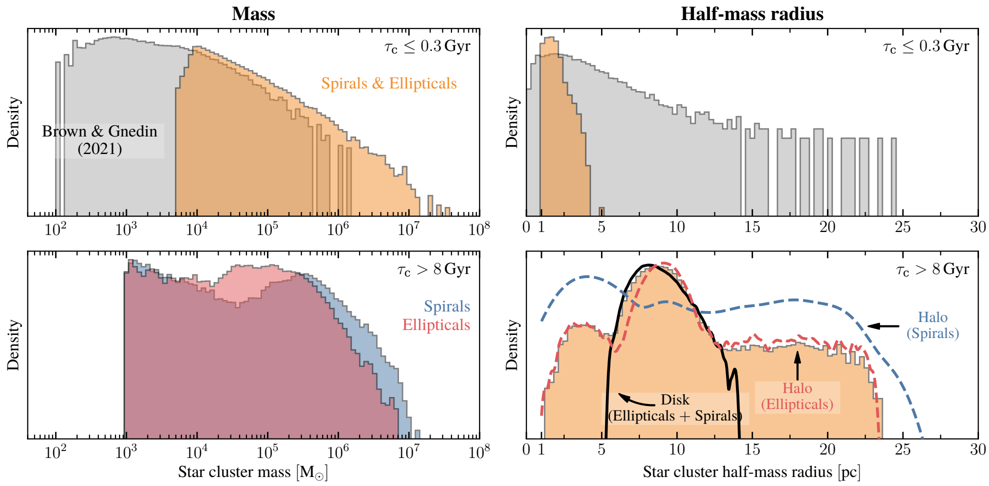

Figure 6.5. *Left column:* Mass distribution of star clusters in all galaxies (orange), disk- ("spirals"; blue) and bulge-dominated ("ellipticals"; red) galaxies. The gray histogram gives the data sample of Brown and Gnedin (2021) applying an age cut of 0.3 Gyr. Star clusters are separated into young / old systems in the top / bottom row, respectively. *Right column:* Distribution of half-mass radii. The colour-coding is identical to the left panel. In the bottom panel we show the kernel density estimates for a Gaussian distribution when separating the star cluster population into the disk (solid line) and halo (dashed lines) components.

radii in Section 6.5.2 but note that Reina-Campos et al. (2023a) found that none of their prescriptions, including one that depends on the local environment, can recover the $z = 0$ distribution of the Milky Way.

The distribution of half-mass radii for old star clusters is complex and ranges from about 1 to $\approx 25\,$pc. For both galaxy morphologies the peak-structure between 5 and 10 pc is related to *in-situ* star clusters that still reside in a galaxy's disk or were heated to the halo during galaxy mergers. The peak of the distribution has similar values for disk-dominated systems and ellipticals, which is, again, related to the properties of the galaxy's disk. The peak is less prominent for disk-dominated systems because of a lack of major mergers.

In contrast, the broad distribution of half-mass radii is dominated by star clusters in the halo. We find that the most compact star clusters are relatively old and low-mass, approaching 13 Gyr and $2 \times 10^3\,$M$_\odot$, and that the most extended clusters are younger and more massive, around 8 Gyr and $2 \times 10^4\,$M$_\odot$. This difference is partly caused by different accretion histories: the more compact clusters were accreted at earlier times and experienced fewer tidal shocks, which would increase the clusters half-mass size. Observations may point towards a similar picture in that star clusters with different metallicity, and potentially of different origin, show differences in half-mass radii as well (e.g. Webb et al., 2012; Puzia et al., 2014).

Overall, we find that the properties of young star clusters are similar between galaxy morphologies. The picture becomes more complex for the old star cluster population due to their different evolutionary histories.

6.3.3 Galactocentric Distances

We show the distribution of galactocentric distances of star clusters in Figure 6.6. We split the galaxies again into disk-dominated systems and ellipticals and into massive ($M_\star \geq 10^{10}\,\mathrm{M}_\odot$) and dwarf ($M_\star < 10^{10}\,\mathrm{M}_\odot$) systems. As before, star clusters are separated into young and old populations. Furthermore, we distinguish between the location of the star clusters into "halo" and "disk" components. Star clusters in disks always form *in-situ* whereas objects in the halo are either accreted from another galaxy (minor and major merger scenarios) or are heated from the disk to the halo (in case of a major merger event). All star cluster galactocentric distances are normalised by either the stellar disk scale-length for disk-dominated galaxies or the half-mass radius for ellipticals.

Our model predicts that the most distant star clusters in galaxies are all accreted and are typically old, irrespective of galaxy type and mass. On the other hand, towards galaxy centres the model predicts that the cluster population is dominated by *in-situ* and young clusters. We find that, when normalising the galactocentric distance by a mass-weighted-scale, there is no significant difference in the overall shape of the cluster distribution between different galaxy morphologies. However, when taking into account the respective scale-lengths, star clusters in more massive systems are more extended. Furthermore, in massive disk-dominated galaxies the star cluster distribution is more extended than in massive ellipticals. This trend reverses in the dwarf galaxy regime.

The old star cluster population exhibits a double-peak structure whereas the young star clusters do not. For both galaxy types this observation is explained by different star cluster origins: the inner peak is caused by old *in-situ* star clusters and the outer peak is related to accreted clusters. For disk-dominated galaxies the double-peak structure is not as prominent because they experience fewer major mergers, if any, than bulge-dominated systems.

Finally, we find that disk and halo clusters contribute equally to the total populations at relative distances of around ten. For massive disk- and bulge-dominated systems, the absolute numbers are, therefore, ≈ 17 and ≈ 15 kpc, respectively. These values are a few kpc larger than what is presented in Keller et al. (2020) for the *E-MOSAICS* simulation, however, these authors only focus on Milky Way-analogues, which may exhibit different scale-lengths than the typical disk-dominated galaxies in *L-Galaxies*. We plan to investigate the properties of the star cluster population of Milky Way-analogues in a future work.

6.3.4 Metallicity Distributions

Mean Cluster Metallicity

We show in Figure 6.7 the mean metallicity of a galaxy's star cluster population, as traced by their iron-abundances, versus galaxy stellar mass. The iron abundance values are calculated by the galactic chemical evolution model introduced into *L-Galaxies* by Yates et al. (2013) that takes into account contributions from stellar winds and (type-Ia and -II) supernovae with different delay-time-distributions. We split the galaxies by

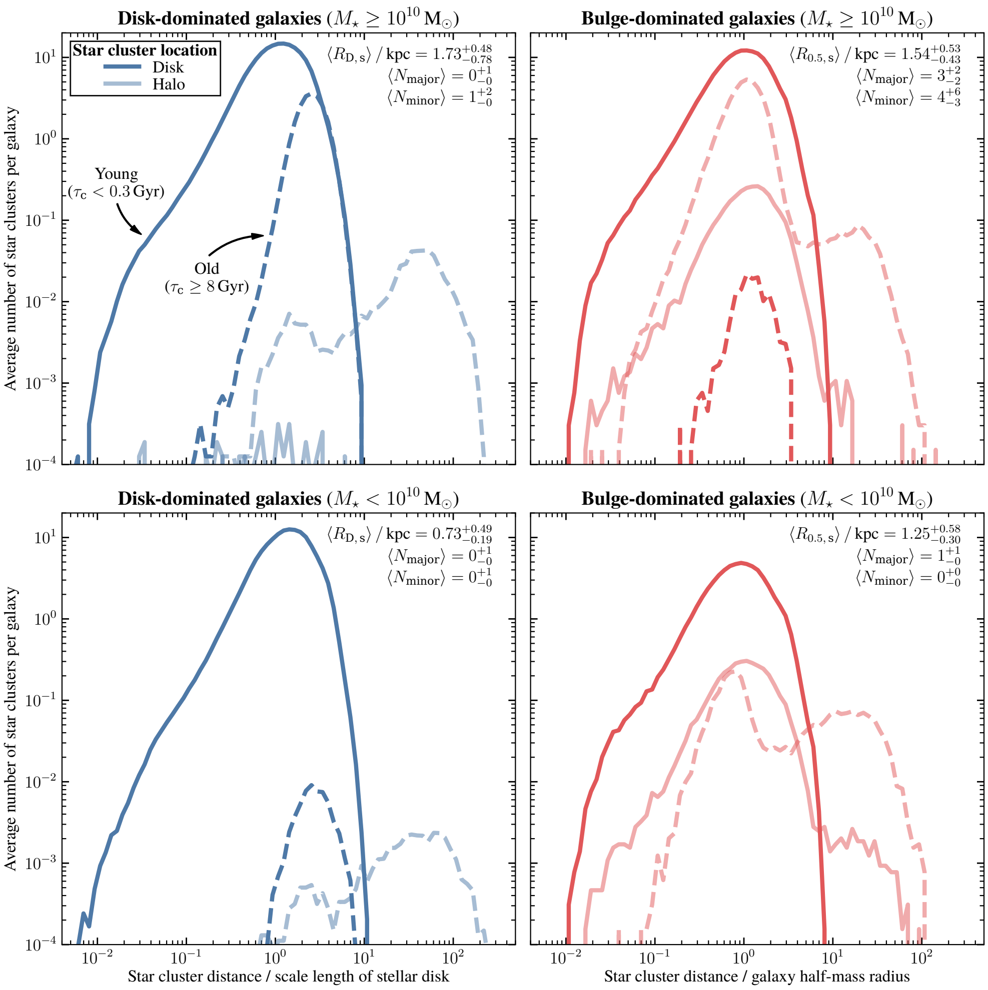

Figure 6.6. Normalised galactocentric distribution of star clusters in disk-dominated (*left column*) and elliptical (*right column*) galaxies separated into massive (*top row*) and dwarf (*bottom row*) systems. Star clusters are further distinguished into young and old systems as well as their location: star clusters located in the disk are formed *in-situ* whereas objects in the halo are either accreted or re-positioned their during a major galaxy merger. The normalisation factors for disk-dominated and elliptical galaxies are the scale-length of the stellar disk and the galaxy's half-mass radius, respectively. Each panel gives the median and 1-σ interval for the normalisation factors and the number of major and minor mergers.

their morphological type (disk-dominated versus elliptical; see above) and separate the star cluster population by their age (young versus old; see above).

Irrespective of the star clusters age and galaxy morphology we find that the mean metallicity increases as a function of galaxy mass, similar to the mass-metallicity relationship for galaxies (as traced via oxygen-abundances; e.g. Tremonti et al., 2004; Kewley & Ellison, 2008; Torrey et al., 2019; Sanders et al., 2021). Despite some overlap younger star clusters have higher metallicity than their older counterparts at fixed stellar mass for both galaxy types. This difference appears to be more significant for disk- than for bulge-dominated galaxies, which is related to the origin of the cold gas that forms stars: in disk-dominated systems stars are predominantly formed from gas that has been continuously enriched by the above-mentioned stellar winds and supernovae channels resulting in metal-rich young star clusters. In bulge-dominated galaxies that form stars (and star clusters) a significant fraction of the cold gas comes from accreted lower-mass systems that contain relatively metal-poor gas.

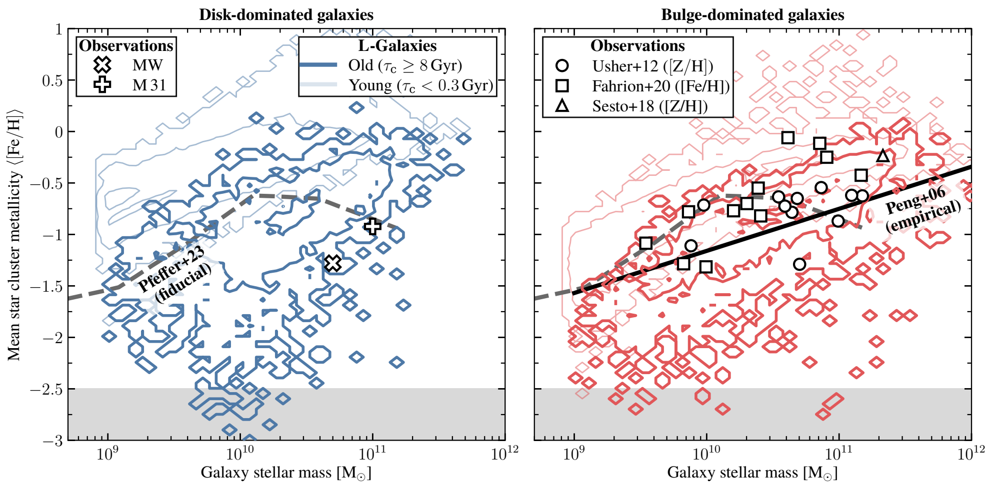

Figure 6.7. Mean star cluster metallicity per galaxy versus host galaxy stellar mass, separated into disk- (*left panel*) and bulge-dominated (*right panel*) galaxies. Strong / faint contours give the 1-, 2-, and 3-σ distribution for old / young star clusters. The gray dashed line gives the fiducial model of Pfeffer et al. (2023), which assumes, similar to our model, an environmentally-dependent prescription for the upper truncation mass of the cluster initial mass function and the cluster formation efficiency. The black solid line gives the empirical relationship for ellipticals in the nearby Virgo galaxy cluster (Peng et al., 2006). Data for the Milky Way and M 31 stem from a self-compiled data table that will be presented in future work. Other data points come from Usher et al. (2012), Sesto et al. (2018), and Fahrion et al. (2020a). The gray-shaded area marks the "lower-limit floor" at $\langle[\mathrm{Fe/H}]\rangle = -2.5$ of observed star cluster metallicities in other galaxies (Beasley et al., 2019).

We compare to the *E-MOSAICS* simulations by showing the results of the fiducial model of Pfeffer et al. (2023). Their model considers environmentally-dependent prescriptions for the cluster formation efficiency and the upper truncation mass of the cluster initial mass function, similar to what we consider for our fiducial model. The results between both simulations are in decent agreement although our data suggest higher mean metallicities at larger galaxy masses that are in better agreement with the literature. This may be a result of their poorer number statistics or different assumptions on stellar yields, resulting in other normalisation values.

We also compare our results to observational data. For disk-dominated galaxies, we consider the Milky Way and M 31 as they have the most robust and quantitative measurements of globular cluster metallicities. To obtain the mean metallicity values, we collected the cluster information from a diverse set of literature that we present in a future paper (another table is presented in Pace, 2024). Here we find that our simulated disk-dominated galaxies have, on average, about 0.5 dex higher median metallicity than the observed values in the Milky Way and M 31, which might be related to a lack of accreted dwarf galaxies that would contribute mainly low-metallicity star clusters.

For bulge-dominated galaxies we collect data from Usher et al. (2012), Sesto et al. (2018), and Fahrion et al. (2020a) and take the empirical scaling relation from Peng et al. (2006) that was fit to elliptical Virgo galaxy cluster members more massive than $M_\star = 10^9\,\mathrm{M}_\odot$. Our simulated star cluster populations show excellent agreement with the observations across the whole mass scale, especially for ellipticals. A couple of literature data points lie outside the 3-σ contours, which could be related to either poor number statistics of the or a bias in the ages of the star clusters in the observations with respect to our simulated galaxies.

Finally, we find that a small fraction of disk- ($\approx 0.3\,\%$) and bulge-dominated ($\approx 1.5\,\%$) galaxies host at least one star cluster that has $\langle[\mathrm{Fe/H}]\rangle < -2.5$. This threshold is often used to indicate a "metallicity floor" due to an apparent lack of globular clusters in nearby galaxies below this value (Beasley et al., 2019). However, the detection of a low-metallicity stellar stream of a former massive star cluster in the Milky Way halo (Martin et al., 2022) and the detection of a massive star cluster with $[\mathrm{Fe/H}] \approx -2.9$ in M 31 (Larsen et al., 2020) challenge this notion. For M 31 specifically, our results agree with the observations, assuming that the galaxy hosts a few hundred globular clusters (Galleti et al., 2004, 2007; Huxor et al., 2008, 2014; Caldwell & Romanowsky, 2016).

Bimodality

An extensive set of literature work argues that the star cluster population of many, perhaps all, galaxies shows a bi- or multi-modal colour or metallicity distribution (e.g. Cohen et al., 1998; Kundu & Whitmore, 2001; Beasley et al., 2008; Blom et al., 2012; Brodie et al., 2012; Usher et al., 2012, 2013; Escudero et al., 2015; Caldwell & Romanowsky, 2016; Bassino & Caso, 2017; Villaume et al., 2019; Fahrion et al., 2020a; Hixenbaugh et al., 2022; Lomelí-Núñez et al., 2024). An often referred to explanation is that the bi-modality is a result of different origins of clusters with the bluer (more metal-poor) population having an *ex-situ* origin (e.g. Strader et al., 2005; Brodie & Strader, 2006; Katz & Ricotti, 2013; Tonini, 2013). Numerical work has argued that the bi- or multi-modality could be a result of either different epochs of star cluster formation, different cluster origins, as suggested by the above literature, or details related to cluster formation and destruction, or some combination thereof (see e.g. Kruijssen, 2015; Choksi & Gnedin, 2019). However, as pointed out by the observational work of Pastorello et al. (2015) and the numerical findings by Pfeffer et al. (2023) the bimodality may only be present in a minority ($\lesssim 50\,\%$) of systems.

To determine the bimodality in our simulation we use an Bayesian Gaussian Mixture

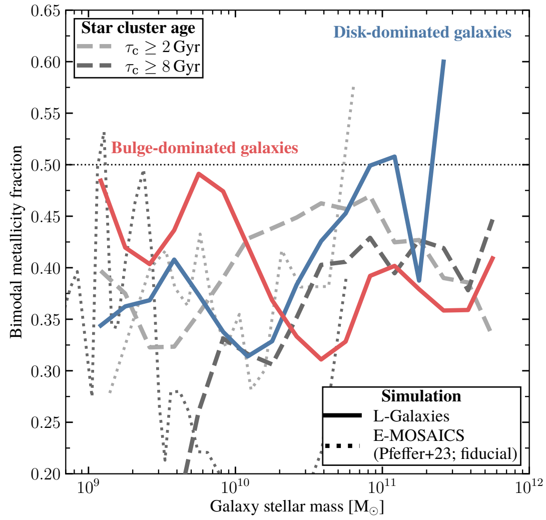

Figure 6.8. Fraction of galaxies exhibiting a bimodality in the metallicity distribution of their star cluster population versus stellar mass for disk- (blue) and bulge-dominated (red) galaxies. We show the bimodality when restricting the cluster population to ages $\tau_c \geq 2$ Gyr (light gray) and $\tau_c \geq 8$ Gyr (dark gray) in order to compare the results to the ones for the *E-MOSAICS* simulation from Pfeffer et al. (2023, dotted lines).

Model approach with Dirichlet initial conditions for all galaxies than contain more than 30 clusters. Following Muratov and Gnedin (2010) and Pfeffer et al. (2023) we first determine

$$-2\ln\lambda = -2\ln\left[\frac{\max(\mathcal{L}_1)}{\max(\mathcal{L}_2)}\right], \tag{6.52}$$

where $\max(\mathcal{L}_j)$ is the maximum value of the likelihood function evaluated over the metallicity distribution when considering j number of Gaussians (either one or two). Afterwards, we perform 100 bootstrap iterations to evaluate the probability that the solution is bi-modal with a probability threshold of 90 %, as chosen in Pfeffer et al. (2023).[8] Finally, we calculate the weighted distance between the two Gaussians,

$$D_{\mathrm{G}} = \frac{|\mu_1 - \mu_2|}{\sqrt{\sigma_1^2 + \sigma_2^2}} \overset{!}{\geq} \sqrt{2}\,, \tag{6.53}$$

where μ_j and σ_j are the mean and standard deviations of Gaussian j, respectively. If $D_{\mathrm{G}} < \sqrt{2}$, we classify the distribution as uni-modal, as adopted in Muratov and Gnedin (2010) and Pfeffer et al. (2023).[9]

We show the bimodality of the star cluster distribution as a function of galaxy stellar mass in Figure 6.8 where we split all galaxies into disk- and bulge-dominated. Irrespective of galaxy morphology we find that the bimodal fraction (i.e. the fraction of galaxies that exhibits a bimodal metallicity distribution) is constrained to values ranging between ≈ 30 and ≈ 50 %.

There exist some fluctuations within the data that can, in part, be attributed to galaxy merger events (e.g. the peak in ellipticals at approximately $5 \times 10^9\,\mathrm{M}_\odot$) and we find some slight overall trends with metallicity: as an increasing function of galaxy stellar

[8] We confirmed that the random sampling of initial values during bootstrapping affects the bi-modal fractions at most by 0.05.

[9] Note that we do not utilise a cut on the kurtosis of the Gaussians as we find in some cases that, if there is one dominant and another sub-dominant star cluster population in a galaxy, the kurtosis is greater than zero, indicating a "peaked" distribution, thus, rejecting the hypothesis of a bimodal distribution.

mass the bimodality of disk-dominated galaxies appears to slightly increase from ≈ 35 to $\approx 45\,\%$ whereas the fraction decreases for ellipticals from ≈ 45 to $\approx 40\,\%$. These trends are, in part, related to the accretion history of the galaxies. The accumulated star cluster population from minor merger events typically has lower metallicity and results in a bimodal fraction. The merger history is much richer for ellipticals where we start to see that the accreted star cluster populations exhibit a wide range of metallicity values. As a result the overall metallicity distribution at $z = 0$ extends over a large range and individual sub-structures or features become diffused. This effect can be seen in observations as well, such as massive galaxies like M 87 (see Fig. 20 in Cohen et al., 1998) or massive galaxy clusters (e.g. Harris et al., 2017).

We compare our results to the *E-MOSAICS* simulation where Pfeffer et al. (2023) performed part of the metallicity analysis. When looking at the bimodal fractions with respect to an age cut in the cluster populations, we find good agreement between the two models. The most striking difference occurs for old clusters ($\tau_c \geq 8\,\mathrm{Gyr}$) in low-mass galaxies ($M_\star \lesssim 5 \times 10^9\,\mathrm{M}_\odot$) where our data indicate a low bimodal fraction. These galaxies contain only relatively few (old) star clusters and most of them formed from gas of similar metallicity. Star cluster accretion plays a sub-dominant role because $\approx 90\,\%$ of dwarf galaxies below $M_\star \sim 5 \times 10^9\,\mathrm{M}_\odot$ are disk-dominated galaxies that have a quiet merger history.

The bimodality weakly depends on the location within a galaxy. Compared to the average bimodal fraction of all star clusters we find similarity for the inner-most galaxy regions, an increase at intermediate distances, and statistical fluctuations for the outer regions, all normalised to the disk's scale-length and half-mass radius for disk- and bulge-dominated, respectively. This trend is a consequence of the location of accreted star clusters as the central regions are dominated by *in-situ* star clusters and the outer regions by *ex-situ* ones. The overall trend of the bimodal fraction with galaxy stellar mass remains roughly unchanged.

Our results indicate a lower bimodality when compared to observations and the general notion that a bimodal distribution appears frequently in galaxies. To test the origin of this notion and the difference we compile a list of galaxies that were classified as uni- or bimodal from the above-mentioned literature and bin the data by galaxy mass. Overall we find bimodal fractions ranging between 50 and 100 %, however, galaxy number statistics are low. It appears likely that the discrepancy between these results and our simulations are due to differing methodologies and inhomogeneities when analysing data. For example, several studies consider a bimodality in the colour-distribution whereas others use iron abundances. Furthermore, taking the metallicity values of globular cluster candidates from Beasley et al. (2008) for NGC 5128 and applying our methodology results in a classification of uni-modal (because the weighted distance D_G is smaller than $\sqrt{2}$) whereas the authors classify the distribution as multi-modal. Unfortunately, the metallicities of many star clusters in galaxies are not publicly available and do not allow us to test the effect of different methodologies further.

6.3.5 Caveats

Our semi-analytical approach to model star cluster populations comes with several caveats. Here we summarise a few of the most important issues.

Axisymmetric Structures of Galaxies

Several effects of non-axisymmetric features can impact star clusters, some of which are discussed below. A thorough review is presented in Renaud (2018).

Some basic assumptions of *L-Galaxies* potentially break down as the gas fraction of galaxies increases, resulting in a "clumpier" structure (e.g. Conselice et al., 2004; Förster Schreiber et al., 2011; Shibuya et al., 2016). This raises some doubt about whether our model captures the properties of star clusters at redshifts of about one to two where clumpy galaxies start to make up a dominant fraction of the whole galaxy population (e.g. Sattari et al., 2023; Huertas-Company et al., 2024) and whether the $z = 0$ star cluster population evolved in a similar fashion compared to observed star clusters. However, as argued by Ono et al. (2025) the basic principle of a disk-dominated formation scenario for galaxies may be a reasonable assumption for redshifts of $z \gtrsim 9$.

A related issue is that *L-Galaxies* does not consider non-axisymmetric components like bars. Molecular gas can gather at tips of the bars due to orbital crowding (Kenney & Lord, 1991) leading to collisions of GMCs, triggering the formation of stars and star clusters (e.g. Davies et al., 2012; Fukui et al., 2014; Ramírez-Alegría et al., 2014). A bar can influence the dynamical evolution of star clusters as well. For instance, both Bajkova et al. (2023) and Dillamore et al. (2024) argue that the Galactic bar directly influences the orbit of a number of Milky Way globular clusters, possibly supporting accelerating their radial migration to the Galactic Center. While halo star clusters are most likely not significantly affected by the lacking implementation of bars, objects in the galactic disk will likely be influenced, thus potentially changing the expected galactocentric distribution discussed in Section 6.3.3.

Finally, *L-Galaxies* does not consider the existence of spiral arms. As argued by Saha et al. (2010), (transient) spirals and bars can introduce additional energy sources for tidal heating that would increase the orthogonal velocity dispersion of star clusters compared to the orientation of the galactic disk. This effect could thus contribute star clusters to the halo of a galaxy without invoking galaxy-galaxy interactions, as indicated by the presence of metal-rich open clusters in the Milky Way's halo (see Paunzen & Netopil, 2006; Meibom et al., 2009; Brogaard et al., 2012; Heiter et al., 2014; Önehag et al., 2014; Straižys et al., 2014; Gustafsson et al., 2016; Hunt & Reffert, 2023, for examples).

Impact of Stellar-Mass Black Holes

Over time, stellar mass black holes segregate towards the cluster's centre and build up a dense core, injecting energy into the stellar system of the star cluster (e.g. Merritt et al., 2004; Mackey et al., 2008). This can result in some star clusters having relatively large half-mass radii, such as Palomar 5 (Gieles et al., 2021), rivalling the most extended objects we find in our simulation. However, note that we only consider star-star interactions in the formalism of Equation 6.38, thus neglecting the effect of dynamical heating due to black holes. One consequence of adding feedback from black holes is a metallicity-dependent expansion rate that was already explored in the literature (e.g. Downing, 2012; Mapelli & Bressan, 2013; Banerjee, 2017; Chattopadhyay et al., 2022; Rostami-Shirazi et al., 2024). This may result in a change in half-mass radii of young star clusters between different galaxy morphologies that we do not detect in Figure 6.5. We aim to implement this feedback channel in future versions.

Galaxy-Galaxy Interactions

Interactions between galaxies result in collisions between gas clouds and can cause efficient star formation outside of galaxy disks, often including the formation of star clusters (e.g. Fellhauer & Kroupa, 2005; Annibali et al., 2011; Maji et al., 2017; Randriamanakoto et al., 2019; Rodruck et al., 2023). Such star clusters, especially during the first passage of the accreted galaxy, can survive for significant time and could contribute to the $z = 0$ globular cluster population in the halo (e.g. Li et al., 2022). Keller et al. (2020) find that around 20 % of globular clusters form during galaxy-galaxy merger events. If true, this would indicate that our model approach does not explain the origin of a significant fraction of globular clusters at $z = 0$. Nevertheless, as argued by the authors, repositioning of globular clusters from the dense inner-galactic regions into a galaxy's halo is important for cluster survival, which matches our results.

6.4 Conclusions

We introduced a modified version of the semi-analytical galaxy formation model "*L-Galaxies*" (Henriques et al., 2020; Yates et al., 2021) that accounts for the formation of massive ($m_c \geq 10^4\,\mathrm{M}_\odot$) star clusters. This implementation relies on galaxy constituents to derive the bound fraction of star formation and the total star cluster mass via *L-Galaxies*' prescription of star formation within galaxy disks. Star cluster masses are random realisations of an environmentally-dependent cluster initial mass function, that is assumed to be a truncated power-law function, and are assigned initial half-mass radii, metallicities, and galactocentric distances. We evolve the properties of up to 2000 individual star clusters per galaxy taking into account the effects of stellar evolution, two-body relaxation, tidal shocks, dynamical friction, and a redistribution during galaxy mergers.

Running the simulation on output merger trees from the Millennium (Springel et al., 2005) and Millennium-II (Boylan-Kolchin et al., 2009) simulations yields the following results.

1. The most massive and young ($\tau_c < 0.3\,\mathrm{Gyr}$) star clusters in disk-dominated galaxies follow the observed empirical relationship between their absolute V-band magnitude of the total host galaxies star formation rate. There exist secondary dependencies on the host galaxy's stellar mass and cluster formation efficiency; the convolved bound fraction of star formation and initial star cluster survival rate.
2. The star cluster mass function for young clusters exhibits a profile similar to the observational results of nearby disk-dominated galaxies (Brown & Gnedin, 2021). At the same time, the half-mass radii evolve away from the assumed constant initial value of $r_{c,h} = 1\,\mathrm{pc}$ up to a few parsecs but do not reproduce well the observed distribution that exhibits a tail up to $\approx 25\,\mathrm{pc}$. Reproducing these observations remains challenging with simulations.

3. The mass, half-mass radius, and galactocentric distance functions of old ($\tau_c \geq 8\,\mathrm{Gyr}$) star clusters display complex shapes, which results from different star cluster origins (*in-situ*, accreted, heated during galaxy mergers), and environmentally-dependent prescriptions that impact star cluster evolution. Galaxy-galaxy interactions and mergers play a vital role in shaping the properties of the $z = 0$ star cluster population.
4. Our model is in excellent agreement with observations of the correlation between a bulge-dominated galaxy's mean star cluster metallicity, as traced by iron abundance, and its host galaxy stellar mass over four dex. This result corroborates the importance of taking into account metal enrichment of the circum-galactic medium from supernovae, as introduced in Yates et al. (2021).
5. Our results predict that the presence of a bimodality in the metallicity distribution of star clusters ranges between ≈ 30 and ≈ 50 % of the $z = 0$ galaxy population and does not approach 100 % on any galaxy mass scale. Both different methodological approaches and the inaccessibility of a statistically significant data set of star cluster populations do not allow for a clean comparison with observations.
6. The assumption of the relationship between the sound speed of cold gas in the interstellar medium and the surface star formation rate directly influences the properties of young star clusters. For example, assuming that the turbulence in the interstellar medium is mainly related to gravity results in a slope value of the relationship between the V-band magnitude and the star formation rate being too shallow.
7. We find that the distribution of half-mass radii of old star clusters is insensitive on the prescription for the initial half-mass radii.

Our simulation offers a computationally efficient and flexible approach to probe different physical effects that influence the assembly history of star clusters across diverse galaxy populations in mass, type, and evolution over cosmic time. In future work we plan to look at additional aspects of the model, such as the star cluster properties of Milky Way analogues or their evolution with redshift, and to consider the formation of nuclear clusters as well as their interactions with (massive) black holes.

6.5 Appendix: Model Variations

We present here additional variations of model parameters that influence the assembly history of $z = 0$ star cluster populations.

6.5.1 Velocity Dispersion of the Cold Gas

One of the most crucial parameters for modelling the Toomre parameter is the velocity dispersion of the cold gas. As discussed in e.g. Lehnert et al. (2009) and Zhou et al. (2017) there exists substantial scatter in the relationship between the velocity dispersion of the cold gas and the star formation rate surface density (*c.f.* Equation 6.14). In our fiducial model we adopted $\alpha_{\mathrm{cold}}^{\mathrm{fid}} = 5\,\mathrm{km\,s^{-1}}$, $\beta_{\mathrm{cold}}^{\mathrm{fid}} = 20\,\mathrm{km\,s^{-1}}$, and $\gamma_{\mathrm{cold}}^{\mathrm{fid}} = 1/3$ for the offset, slope, and exponent, respectively.

Here we explore a wider parameter range by testing a first version where we increase the slope value to $\beta^{\mathrm{var}}_{\mathrm{cold}} = 100\,\mathrm{km\,s^{-1}}$ and a second version where we set the exponent to $\gamma^{\mathrm{var}}_{\mathrm{cold}} = 1/2$. Additionally, we test a separate prescription based on the Jeans mass (see e.g. Elmegreen et al., 2007) where

$$\sigma_{\mathrm{g},\,j} \sim M_{\mathrm{J}}^{1/4} \mathrm{G}^{1/2} \Sigma_{\mathrm{g},\,j}^{1/4} = 4.4\,\mathrm{pc\,Myr^{-1}} \times \Sigma^{0.18}_{\mathrm{SFR},\,j}\,, \tag{6.54}$$

with M_{J} as the Jeans mass, which we assume to be $10^9\,\mathrm{M_\odot}$ for the equality, and converted from the cold gas surface density to the star formation rate density using Equation 7 from Kennicutt (1998) with $\Sigma_{\mathrm{D,\,g}}$ in units of $10^6\,\mathrm{M_\odot\,pc^{-2}\,Myr^{-1}}$. In addition, we add a velocity floor of $5\,\mathrm{km\,s^{-1}}$, the same value that we used in Equation 6.14.

To probe the effect of this relationship on the properties of newly formed star clusters, we fit linear relationships to the resulting M_V-SFR parameter space, as presented in Section 6.3.1, and present the slope values in Table 6.1.

We find that an increase of β_{cold} results in a steeper slope value of the M_V-SFR relationship for both dwarf and massive galaxies. This change is a direct consequence of modifications to the Toomre parameter. Since $Q_{\mathrm{D,\,g}} \propto c_{\mathrm{s,\,cold}}$, the Toomre parameter of the gas increases/decreases, which then also results in an increase/decrease of Q_{eff}, albeit not as strong as $Q_{\mathrm{D,\,g}}$ due to taking a weighted average with $Q_{\mathrm{D,\,s}}$. This increase/decrease has a direct consequence on the star cluster masses because the upper truncation mass in Equations 6.28 and 6.29 scales as $m_{\mathrm{cl,\,max}} \propto Q^4_{\mathrm{eff}}$, resulting in an increased/decreased probability to randomly sample massive clusters.

When modifying the power-law index to $\gamma_{\mathrm{cold}} = 1/2$ when find a significant increase in the slope value for massive galaxies whereas it is less strong for dwarfs. While the above argument is valid for this case as well, the secondary dependence comes from the galaxy-mass to star formation rate dependency. It can be seen in panel (B) of Figure 6.4 that more massive galaxies have, on average, higher star formation rates and are, thus, more significantly affected from the change in γ_{cold}.

Finally, when assuming a prescription based on the Jeans mass we find significantly shallower slopes for the same reasons outlined above. These slopes are also too shallow compared to the observational constraints

Our simulations indicate that the slope of the relationship is steeper for more massive galaxies irrespective of the assumed cold gas velocity dispersion versus surface star formation rate relationship.

6.5.2 Initial Half-Mass Radius

The distribution of initial half-mass radii remains an unsolved problem. Measurements of the half-light size of young star clusters give typical values in the range of a few parsecs to about 0.5 pc (e.g. Bastian et al., 2012; Ryon et al., 2015; Brown & Gnedin, 2021) but the scatter at similar cluster ages is large, going up to ≈ 20 pc for W 3 in NGC 7252 (Maraston et al., 2004; Fellhauer & Kroupa, 2005). This could indicate that the initial half-mass radius of clusters is similar and diverges due to a different initial evolutionary phase given the local environment, or that other parameter influence the initial half-mass radius, such as cluster mass or the local physical conditions. Reina-Campos et al. (2023a) tested different prescriptions of initial half-mass radii,

Table 6.1. Slope values of the M_V-SFR relationship when adjusting parameters for the $c_{\rm s,\,cold}$-$\Sigma_{\rm SFR}$ relationship.

Model	Slope values	
	high-mass	low-mass
Fiducial	$-3.64^{+0.02}_{-0.02}$	$-2.63^{+0.02}_{-0.01}$
$\beta^{\rm var}_{\rm cold} = 100\,{\rm km\,s^{-1}}$	$-3.98^{+0.02}_{-0.02}$	$-3.27^{+0.02}_{-0.02}$
$\gamma^{\rm var}_{\rm cold} = 1/2$	$-3.73^{+0.02}_{-0.02}$	$-2.70^{+0.02}_{-0.02}$
$c_{\rm s,\,cold} \propto (M_{\rm J}\Sigma_{\rm g})^{1/4}$	$-2.32^{+0.01}_{-0.01}$	$-1.31^{+0.02}_{-0.02}$

considering constant values, constant densities, a linear relationships from the data provided by Brown and Gnedin (2021), and a theoretical model from Choksi and Kruijssen (2021) that reads

$$r_{{\rm c},\,h} = \left(\frac{3}{10\pi^2} \frac{\alpha_{\rm vir}}{\phi_P \phi_{\overline{P},\,j}} \frac{m_{\rm c}^2}{\Sigma_{\rm g}^2} \right)^{1/4} \frac{\epsilon_{\rm c}^{1/2}}{2\epsilon_c - 1} \frac{f_{\rm acc}}{Q_{\rm eff}^2}\,, \tag{6.55}$$

with $f_{\rm acc} = 0.6$, $\epsilon_c = 1.0$, and environmentally-dependent parameters evaluated for each ring.[10] Reina-Campos et al. (2023a) conclude that none of the prescriptions reproduce the size-mass relationship after evolving the cluster population for a few Gyr within the *EMP-Pathfinder* simulation suite (Reina-Campos et al., 2022a).

Similar to Reina-Campos et al. (2023a) we implement different prescriptions for the initial half-mass radius, that we outline in Table 6.2, to test their influence on the stellar mass versus size distribution at $z = 0$, as discussed in Section 6.3.2. We find that the precise details of the initial half-mass radius clearly change the resulting distribution of young star clusters, however, the distribution of radii of old star clusters remain largely unchanged. The greatest differences compared to the fiducial model are for a constant $r_{{\rm c},\,h} = 0.1\,{\rm pc}$ and the empirical relationship where $r_{{\rm c},\,h} \propto m_{\rm c}^{0.18}$. The compact initial size of star clusters results in the most massive star clusters to rapidly expand up to 30 pc, values that are not reached with other prescriptions. The increased half-mass radius of the empirical relationship causes an apparent impact on the size of old star clusters within the galactic disk as well: on average, the star clusters in a disk become larger by two to three parsecs.

Overall, we find that the precise prescription of the initial half-mass radius does not significantly impact the results at $z = 0$.

6.5.3 Cluster Initial Mass Function

To test the effect of the upper truncation mass on the resulting star cluster populations we re-run the model considering a pure power-law cluster initial mass function, i.e.

[10] The parameter ϵ_c refers to the efficiency of star formation within a giant molecular cloud and not the average efficiency of star formation within the interstellar medium that was introduced in Section 6.2.3.

Table 6.2. Variations in the initial half-mass radii of star clusters.

Model	Prescription
Fiducial	$r_{c,h} = 1\,\mathrm{pc}$
Compact	$r_{c,h} = 0.1\,\mathrm{pc}$
Density	$r_{c,h} = 1\,\mathrm{pc} \times (m_c/10^4\,\mathrm{M}_\odot)^{0.3}$
Empirical[(a)]	$r_{c,h} = 2.37\,\mathrm{pc} \times (m_c/10^4\,\mathrm{M}_\odot)^{0.18}$
Theoretical[(b)]	$r_{c,h} \propto \sqrt{m_c/\Sigma_g}$

[(a)] Fitting results provided by Reina-Campos et al. (2023a) for the data of Brown and Gnedin (2021) when limiting the star cluster population to ages $1\,\mathrm{Myr} \leq \tau_c \leq 10\,\mathrm{Myr}$.
[(b)] Adopted from Choksi and Kruijssen (2021). To avoid extremely compact or extended clusters we introduce a lower and upper boundary to a star cluster's half-mass radius of 0.1 and 100 pc, respectively.

$\xi(m_c) \propto m_c^\alpha$. Similar to the fiducial model we pre-compute a list of 10^6 random realisations of this mass function between 10^2 and $10^8\,\mathrm{M}_\odot$ and randomly sample it to reduce computational cost.

The overall shape and distribution of the half-mass radii remain unchanged. A significant difference occurs at the high-mass end of the mass distribution, which is much more densely populated. This change impacts the data points on the M_V-SFR relationship by shifting them to lower absolute magnitudes, resulting in a steeper relationship when compared to both the fiducial model and observations. The model then also fails to account for the faintest young star clusters in galaxies above star formation rates above $\approx 1\,\mathrm{M}_\odot\,\mathrm{yr}^{-1}$.

In the *E-MOSAICS* simulation Pfeffer et al. (2023) find that the median metallicity values of star clusters in dwarf galaxies is elevated by 0.2 to 0.4 dex, depending on galaxy mass (their Figure 7). In our simulation we find a difference of about 0.2 dex below galaxy stellar masses of $M_\star \approx 8 \times 10^9\,\mathrm{M}_\odot$, which is in excellent agreement with the results by Pfeffer et al. (2023). At higher galaxy masses we see no change in the distribution between the two models likely reflecting that the upper truncation mass was high enough at typical star cluster formation redshifts (see e.g. Figure 8 in Pfeffer et al., 2018). We will investigate the redshift-dependence of our model parameters in future efforts.

6.6 Chapter Summary

- ▹ I introduced a new semi-analytical galaxy formation model that includes the formation and evolution of massive ($m_c \geq 10^4\,\mathrm{M}_\odot$) star clusters.
- ▹ The simulation successfully reproduces a number of observables, such as the mass function of young star clusters or the mean metallicity of the star cluster distribution as a function of galaxy mass.
- ▹ The simulation is computationally efficient and allows to probe different model

assumptions. For example, the scaling relationship between the sound speed of the cold molecular gas and the surface star formation rate directly impacts the parameter values of $z = 0$ star clusters.

- ▹ Extensions of the model towards galaxy centres will enable me to probe the formation of nuclear star clusters.

Chapter 7

Conclusions

7.1 Summary

This dissertation revolved around the assembly of nuclear star clusters (NSCs), which are located in galaxy centres and form in diverse and complex ways. For my analyses I relied on observational data sets and constructed a new semi-analytical galaxy formation model that focusses on massive star clusters, which may contribute to the build-up of NSCs by migrating to galaxy centres.

In Chapter 3, I used archival *Hubble Space Telescope* imaging data to analyse 19 newly discovered NSCs in nearby dwarf galaxies (Hoyer et al., 2023a). This data set significantly increased the known structural properties of NSCs at the lowest-mass end and the results make an important contribution to calculations of, for example, the tidal disruption event rates (Hannah et al., 2024).

In this work, I found that the NSCs share similar properties to globular clusters (GCs) in the Milky Way that were likely accreted from dwarf galaxies (e.g. Kruijssen et al., 2020b). This similarity suggests that dwarf nuclei are simply a realisation of the high-mass tail of the GC mass function. The data were inconclusive as to whether the merger of multiple GCs are necessary to form an NSC. In addition, I identified a secondary dependence of the NSC to host galaxy stellar mass relationship on environment where, at the same galaxy mass, NSCs are more massive in denser galaxy environments. It is unclear if this observation simply reflects an increased number of migrating star clusters, which could be related to the environmentally-dependent number statistics of GCs in low-mass dwarf galaxies.

In Chapter 4, I presented an analysis of the NSC in Messier 74, a nearby grand-design spiral galaxy using archival *Hubble* and newly obtained *James Webb Space Telescope* data, ranging from the far-ultraviolet to the mid-infrared regime (Hoyer et al., 2023b). This marked the first study of an NSC across such a large wavelength range and enabled the analysis of stellar populations from broad-band filters.

The analysis revealed a half-light radius of $r_{\rm eff} \approx 5\,{\rm pc}$, a typical value for NSCs. The mass of $M_{\rm NSC} \approx 10^7\,{\rm M}_{\odot}$ is slightly lower compared to NSCs in other spiral galaxies of similar stellar mass alluding to a quieter assembly history. A fit to the spectral energy distribution constrained the dominant stellar populations to an age of $\tau \approx 8\,{\rm Gyr}$ and a metallicity that is roughly solar, which compares to neighbouring stars in the bulge of Messier 74, suggesting a common formation scenario. The results indicate a lack of star formation within the last few Gyr, which constrains (1) the accretion history of the massive black hole (MBH) within the NSC, if present, (2) the time scale of the central gas- and dust-lacking cavity that the NSC is embedded in, and (3) the merger history of Messier 74 because minor or major mergers would have likely resulted in in-spiral of cold gas and subsequent star formation. The mid-infrared data showed a more extended component (about three-times the half-light radius of the NSC) that is off-centre by about 5 pc, i.e. located at approximately the half-light radius of the NSC. This component dominates the emission of the galaxy centre in the mid-infrared and I tested five different scenarios for its origin, however, without success: the source of the mid-infrared emission remains elusive.

In Chapter 5, I analysed soft X-ray (2 - 10 keV) imaging data from the *SRG*/eROSITA space-based telescope that was collected over a two-year time span in search of accretion signatures of MBHs in nearby NSCs (Hoyer et al., 2024). This work presented the first constraints on the accretion signatures of low luminosity AGN in the dwarf galaxy regime, taking into account NSCs. Detecting such signatures requires a comparison between the observed X-ray flux and the expected emission from low- and high-mass binaries, as traced by the galaxy's stellar mass and star formation rate, respectively.

In total, 18 galaxies showed significant X-ray emission but only three targets (NGC 2903, 4212, and 4639) have measured flux that is higher than the expected background. For six galaxies (NGC 2903, 3384, 4321, 4365, and 4701) I detected variable emissions values either on the baseline of the *SRG*/eROSITA survey (six months) or on longer baselines when compared to literature values (predominantly from *Chandra*; years). Whether this variability is due to changes in gas funnelling to the central MBH or due to obscuration along the line-of-sight is unclear. Stacking the non-detected galaxies in the dwarf galaxy regime resulted in an upper luminosity of $L_{2-10\,\mathrm{keV}} \approx 2 \times 10^{38}\,\mathrm{erg\,s^{-1}}$, roughly constant for galaxy masses below $M_\star \approx 10^{10}\,\mathrm{M_\odot}$.

Finally, in Chapter 6, I introduced a new semi-analytical galaxy formation model that considers the formation and evolution of massive star clusters (Hoyer et al., 2025). Due to the computationally efficient structure of the code the simulation allowed for various tests of star cluster-related physics at high significance for a high number of galaxies with a diverse set of properties. The star cluster model was built on top of the existing *L-Galaxies* galaxy formation model in its 2021 version (Henriques et al., 2020; Yates et al., 2021). My model considered the formation of star clusters in twelve concentric rings based on the Toomre stability parameter, cold gas surface density, and epicyclic frequency—local quantities that affect the expected bound fraction of star formation (Bastian, 2008). Afterwards, the model evolved the 2000 most massive star clusters per galaxy, taking into consideration (1) mass loss from stellar evolution, two-body relaxation, and tidal shocks, (2) expansion due to two-body relaxation and tidal shocks, (3) dynamical friction due to interactions with stars, dark matter, and gas, and (4) a re-distribution during galaxy mergers.

In a comparison to observational constraints, I found that my simulation can reproduce well (1) the star cluster mass function for young ($\tau \lesssim 300\,\mathrm{Myr}$) objects, and (2) the empirical relationship between the absolute V-band magnitude of the brightest (i.e. most massive) and young star cluster (local quantity) and the host galaxy's star formation rate (global quantity). In addition, the simulation reproduced well the average metallicity of the star cluster populations for galaxy masses over three orders of magnitude, matching the results of observational studies and agreeing with predictions of other more computationally expensive hydrodynamical simulations. Regarding the metallicities, my simulation reinforced the notion that the bimodality of the metallicity distribution of GCs in galaxies is not ubiquitous but is constrained to $\lesssim 50\,\%$ at all galaxy masses and morphologies.

In summary, I provided new analyses of NSCs in dwarf galaxies that constrained their relationship to GCs and MBHs. The analysis of the NSC of Messier 74 explicitly showed that NSCs are useful tools to directly constrain the assembly history of their host galaxy. Finally, my new semi-analytical galaxy formation model builds the foundation for future investigations for probing the relative strength of the different formation channels of NSCs.

7.2 Future Directions

I present here potential future directions towards improving our knowledge of NSC assembly. These projects are separated into an observational and a numerical branch and can be considered follow-up studies of the work presented in this dissertation.

7.2.1 Observational Efforts

I presented in this dissertation that the structural properties of NSCs in nearby dwarf galaxies are similar to the Milky Way's GCs. A follow-up project to the one presented in Chapter 3 would be to analyse the GC population in the dwarf galaxies themselves and compare their properties to the ones of the NSCs. The nearby Fornax and Virgo galaxy clusters are ideal targets for such an analysis because they feature galaxies of similar properties (e.g. stellar and halo masses, shape, and star formation rate). Most of the dwarf galaxies will be ellipticals and lack star formation, which makes the identification of GC candidates easier compared to their dwarf irregular counterparts.

Using the data one could compare the structure and mass of the different star cluster types to determine whether NSCs are a merger product of GCs or simply the high-mass realisation of the GC initial mass function. As mentioned in Chapter 2, one expects the size of a cluster to increase with repeated mergers such that the NSC should have, on average, a larger half-mass radius than the average GC. Stacking the data sets from different galaxies of comparable stellar (and, thus, halo mass) will yield statistically significant results.

Another extension of this analysis is to determine the galactocentric distance of the most massive star clusters that often reside outside the galaxy centre (e.g. Poulain et al., 2021). Dwarf elliptical galaxies are ideal targets for this analysis because they lack star formation that could make the determination of the photometric (and, thus, likely the kinematic) galaxy centre uncertain. As discussed in Modak et al. (2023), the migration of massive star clusters into the galaxy's centre can stall if the dark matter slope is too shallow (see also Read et al., 2006; Inoue, 2009). Therefore, by analysing (stacked) data of galaxy light distributions, GC luminosity functions, and the distribution of the galactocentric distances of the most massive GCs (or NSCs), it is possible to constrain the slope of the inner dark matter profile in dwarf galaxies. One potential challenge of this analysis is to distinguish between massive GCs that form *ex-situ* and stall in their migration towards the centre and a massive *in-situ* star cluster that wanders around the galaxy centre. The latter scenario was proposed for the extended and massive star cluster in the Pegasus dwarf galaxy (Leaman et al., 2020).

A third possible project could focus at nuclear multiplicities. The presence of multiple central star clusters was reported for both dwarf and massive galaxies in Georgiev and Böker (2014), Poulain et al. (2021), and Voggel et al. (2022) and we may be able to detect more such examples with already existing and future imaging data to obtain a frequency relative to the NSC frequency presented in Section 2.1.1. Focussing on dwarf ellipticals, it would be possible to follow-up these observations with numerical work: after characterising the three-dimensional shape of the galaxy and the orbits of the star clusters with observational data, the numerical study may help to constrain the time scale for the merger as well as the properties of the emerging massive star cluster. In addition, given the large number of known NSCs at different galaxy masses, it is feasible to estimate the volumetric merger rate of such systems, which would be interesting for the gravitational wave community in case the star clusters contain MBHs.

For the above three projects one requires high-spatial resolution data, which the *HST* (either via archival or new data sets) provides. Another data set is provided by *Euclid* (Euclid Collaboration, 2024d, 2025b), whose imaging resolution compares to that of the *HST* (0.1 arcsec pixel^{-1} for *Euclid* compared to 0.05 arcsec pixel^{-1} for *HST* in the I-band; Euclid Collaboration, 2024e) but offers a much larger field-of-view. Several works showed that *Euclid* can be used for star cluster-related science cases (Euclid Collaboration, 2024b, 2024c, 2024f, 2025a), including NSCs (Euclid Collaboration, 2024a, 2025c). The new data sets from *Euclid* (1) increase the significance of the previous *HST* data by simply providing more galaxies, and (2) offer the possibility to probe different galaxy environments. The latter option may help to constrain further the formation scenarios for NSCs in dwarf galaxies and possibly explain the different NSC frequencies in different galaxy environments at the same galaxy stellar mass, as mentioned in Section 2.1.1 and directly shown in Figure 2.1.

Finally, for more massive galaxies that contain an NSC, it is feasible to analyse *HST* and *JWST* data in similar fashion as presented in Chapter 4 for Messier 74. The *PHANGS* team has now collected data for 74 galaxies with *HST*, *JWST*, and *ALMA*, with additional (spectral) data from e.g. *MUSE* for a smaller subset. This multi-wavelength data set will allow for analyses of NSCs and the central star cluster population in the nucleated sub-sample. With these powerful data sets will allow a comparison between the stellar populations of NSCs with other centrally located star clusters, and the results may possibly allude to past galaxy-wide events such as disk instabilities that may funnel large amounts of cold gas to a galaxy's centre resulting in star formation events that leave an imprint in the star cluster properties.

The great variety of the properties of the different galaxies would make constraints on the importance of other galaxy components as well. For example, it is still unclear how the presence (and the properties of) a bar influence the assembly of NSCs. The presence and properties of bars appear to affect central MBHs at least in the *IllustrisTNG* simulations (Kataria & Vivek, 2024) but probing NSCs in that simulation suite is impossible due to the selected mass- and spatial scales. Likewise, we still do not know how nuclear rings and disks co-evolve (or not) with NSCs.

Overall, both archival and new data sets have the potential to evolve our current understanding of NSC formation and how they relate to other constituents like the dark matter profile of the host galaxy, MBHs, and other central objects like young star clusters, (nuclear) bars, disks, and rings.

7.2.2 Numerical Efforts

New numerical studies may focus on extending my new semi-analytical galaxy formation model that I introduced in Chapter 6. It is interesting to extend the analysis to higher-redshift galaxies in light of recent *JWST*-based observations that reveal the half-mass radii of star clusters at $z \lesssim 10$ in gravitationally-lensed galaxies (Claeyssens et al., 2023; Vanzella et al., 2023; Adamo et al., 2024; Mowla et al., 2024). Such a comparison was already performed with the *E-MOSAICS* simulation (Pfeffer et al., 2024a) and the authors find good agreement with the observed data: they find that the formation mechanisms of star clusters at different redshifts may be similar to each other despite a clear difference in host galaxy properties (extended and regular in the local Universe, and compact and "clumpy" at high-redshift; e.g. Shibuya et al., 2016). It would be interesting to test these interpretations with a much larger and more diverse galaxy population that *L-Galaxies* (and my own simulation) provides.

As a first preliminary test I show in Figure 7.1 the half-mass radii and masses of star clusters in galaxies for $1 \lesssim z \lesssim 6$. The star cluster model that I used for this simulation differs from the fiducial model presented in Chapter 6 by allowing for an environmentally-dependent initial half-mass radius, which could be lower than the assumed value of 1 pc in the fiducial model. Other assumptions of the model, such as the environmentally-dependent upper truncation mass of the cluster initial mass function, remain unchanged.

The preliminary results show that, for decreasing redshift, (1) the half-mass radius distribution becomes broader, (2) the mode increases, and (3) the distribution of masses becomes wider. The compact half-mass radii distributions of star clusters at high redshift is related to the properties of their hosts: galaxies are more compact at higher redshifts (for *L-Galaxies* specifically, see Figure 12 in Vani et al., 2025), directly resulting in higher gas densities and more compact initial half-mass radii of star clusters, as per Equation 6.55 ($r_{\mathrm{c},h} \propto \Sigma_{\mathrm{g}}^{-1/2}$). Extended star clusters quickly dissolve due to strong tidal shears, causing a sharp decrease in star cluster numbers beyond 2 pc. Likewise, due to the harsh galaxy environments, low-mass star clusters that would be compact (as $r_{\mathrm{c},h} \propto m_{\mathrm{c}}^{1/2}$ via Equation 6.55) dissolve more quickly than their massive counterparts.

Galaxy mergers that re-distribute star clusters into a galaxy's halo, where cluster survival times increase, become more dominant at lower redshifts. This is evident when comparing the distribution of accreted and *in-situ* star clusters: at $z = 5.92$ the half-mass distributions between the two star cluster populations is roughly the same, indicating that (1) they recently moved into a galaxy's halo, and (2) have lower number statistics that is evident from the scatter in the stacked histogram of all galaxies.

Another possible study would be to use my semi-analytical model to study Milky Way analogues.[1] The Milky Way and Messier 31 as our most massive neighouring

[1] A "Milky Way analogue" is a simulated galaxy that has similar properties as our own Galaxy, such as

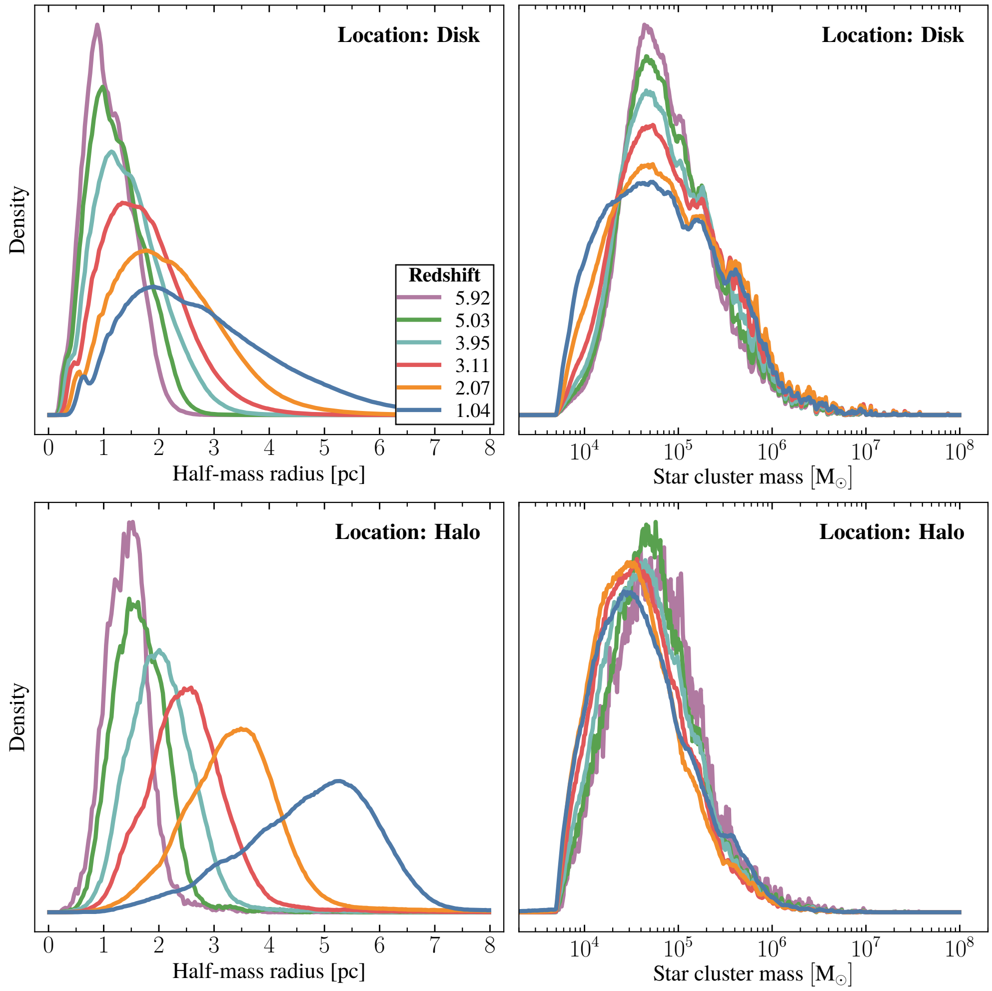

Figure 7.1. One-dimensional histograms of half-mass radii (*left*) and stellar masses (*right panels*) of star clusters in galaxies between $1.04 < z < 5.92$. Star clusters are separated by their current location in the disk (*upper*) or in a galaxy's halo (*lower panels*).

galaxy make good targets to compare my numerical results to because of the exquisite knowledge about the properties of their GCs. To show a first result of the simulation, I present in Figure 7.2 the half-mass radius and stellar mass distributions of star clusters located in the disk and halo of Milky Way analogues. Note that all star clusters in the disk exclusively form *in-situ* whereas both *in-situ* clusters that were heated during major mergers and accreted systems during minor galaxy mergers contribute to the halo population. I restrict all star clusters to $\tau_c \geq 8\,$Gyr to compare to observational data of the Milky Way and M 31 that I obtained from various literature, as presented in Hoyer et al. (2025, in preparation).

For star clusters in the galaxies disks I find that the simulated star clusters are a factor of a few more massive and about twice as extended compared to the Milky

the virial and stellar masses, scale-length of the galactic disk, or merger history. I present a definition of Milky Way analogues within the scope of *L-Galaxies* in Figure 7.2.

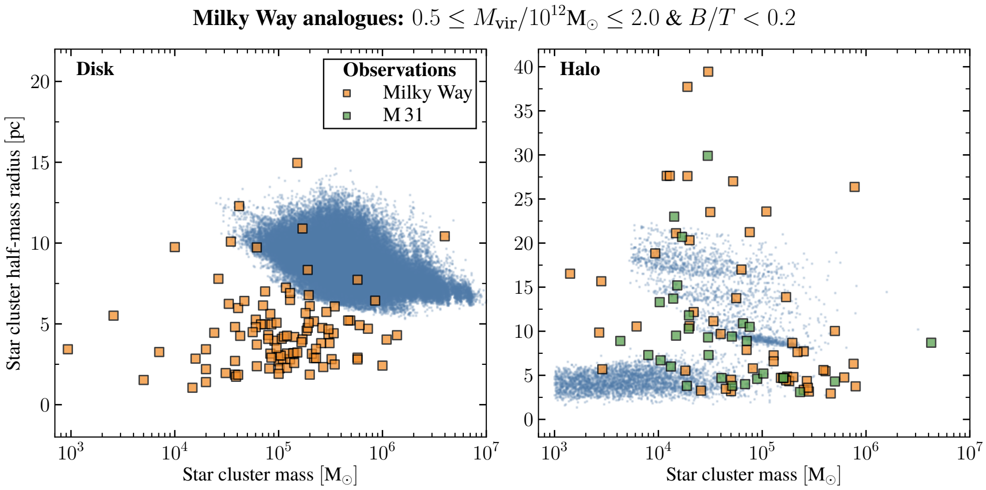

Figure 7.2. Half-mass radii versus stellar masses of old ($\tau_c \geq 8$ Gyr) star clusters in galaxy disks (*left*) and halos (*right panel*) in Milky Way analogues, which I define as fulfilling $5 \times 10^{11}\,\mathrm{M}_\odot \leq M_{\rm vir} \leq 2 \times 10^{12}\,\mathrm{M}_\odot$, $B/T < 0.2$, and a quiet merger history (i.e. only minor mergers with mass ratio up to 0.1). I compare the simulated star clusters (blue) to observations from the Milky Way (orange) and M 31 (green) using a self-compiled literature data set, which will be presented in Hoyer et al. (2025, in preparation).

Way sample. This indicates that the simulation does not yet capture well the exact evolutionary histories of star clusters in Milky Way-like galaxies. However, this issue persists across all simulations of star cluster populations. For example, the overall successful *E-MOSAICS* simulation suite assumes no radial expansions of star clusters at all, keeping their value fixed at 4 pc (Pfeffer et al., 2018).

In the case of star clusters in the halo, I find a diverse picture of star cluster properties. The simulated star clusters are roughly separated into two groups that are accreted from dwarf galaxies, as discussed in Section 6.3.2: the more compact star clusters are older than their more extended counterparts and were exposed to fewer tidal interactions that would have significantly increased their half-mass radii. Overall, when compared to the observational data, I find that the simulated star clusters can roughly reproduce the observed trends in that at least part of the halo population is much more extended than their counterparts in galaxy disks.

A third research project related to my simulation is to consider the formation of NSCs. In the current version of the simulation, all star clusters in the central ring (with radius of approximately 30 pc) are excluded as the model does not yet consider mergers of star clusters. Additional complications arise from the uncertain contribution of *in-situ* star formation: as I showed in Figure 2.5 the *in-situ* fraction already shows large scatter as a function of galaxy mass for the relatively simple model of Leaman and van de Ven (2022). Furthermore, the presence of (stellar mass or massive) black holes influence the evolution of star clusters: stellar mass black holes increase a star clusters half-mass radius (e.g. Gieles & Gnedin, 2023) while more massive black holes could prevent the migration of GCs to a galaxy's centre (e.g. Antonini, 2013) and provide additional feedback channels to evacuate gas from an NSC during star formation episodes.

Finally, I add here other potential research lines related to NSCs.

- ▹ *Follow-up work of Partmann et al. (2024).* Their work considers an idealised scenario where the NSC and MBH already exist in a dwarf galaxy and co-evolve over time. However, the simulation does not yet consider the merger with migrating GCs, feedback from accretion on the MBH, or the impact of galaxy mergers. Partmann et al. (2025, in preparation) indicate that various accretion mechanisms for the MBH always result in an evacuation of cold gas from the galaxy, halting star formation for approximately a Hubble time (see also Petersson et al., 2025, for the importance of stellar feedback). This indicates that our general understanding of accretion on MBHs is still lacking. Future efforts are clearly needed to additionally consider black hole seeding and their growth to the intermediate-mass scale.
- ▹ *Active Galactic Nuclei (AGN) in dwarf galaxies.* Some recent work suggest that feedback mechanisms in dwarf galaxies may not only include re-ionisation and supernovae events but also AGN (e.g. Silk, 2017; Dashyan et al., 2018; Arjona-Gálvez et al., 2024). Additionally, these AGN must not be located in the galaxy's centre but could wander around the galaxy (e.g. Mezcua & Domínguez Sánchez, 2020). NSCs come into play because they may host these (intermediate-mass) black holes and often wander in their host galaxy (e.g. Poulain et al., 2021). Numerical work could investigate how NSCs seed these black holes, how they wander within the potential of their host, and how accretion onto the black hole shuts (or sometimes supports) star formation. Furthermore, these simulations could probe the frequency of dwarf-dwarf mergers and the importance of NSCs and the MBHs within them for the future evolution of the merger remnant.
- ▹ *Redshift dependence of the MBH to host galaxy mass correlation.* It remains unclear how the mass correlation between MBHs and their host galaxy evolves with redshift with some work suggestion an evolution (e.g. Zhang et al., 2023) while other works disagree (e.g. Sun et al., 2025). NSCs may be important for the evolution of this relationship as they can support gas funnelling to the MBH as well as solve the "final-parsec" problem, significantly reducing the merger time between two MBHs. Simulations should, therefore, start to include dense stellar cusps around MBHs and evaluate their importance for the above mentioned correlation: are some MBHs over-massive compared to the local relationship because of the presence of an NSC?

In total I believe that considering nuclear star clusters for future research of galaxy evolution is essential to interpret data from new large-scale surveys. Computational simulations of massive black holes should consider nuclear star clusters as well given their ability to seed them and enhance their growth. Generally speaking, nuclear star clusters provide us with an unique opportunity to gain knowledge of the universe we live in and how galaxies, including our own Milky Way, assemble.

Bibliography

Abazajian, K. N., Canac, N., Horiuchi, S., & Kaplinghat, M. (2014). Astrophysical and dark matter interpretations of extended gamma-ray emission from the Galactic Center. *Physical Review D*, *90*(2), 023526. https://doi.org/10.1103/PhysRevD.90.023526

Abbate, F., Mastrobuono-Battisti, A., Colpi, M., Possenti, A., Sippel, A. C., & Dotti, M. (2018). Probing the formation history of the nuclear star cluster at the Galactic Centre with millisecond pulsars. *Monthly Notices of the Royal Astronomical Society*, *473*(1), 927–936. https://doi.org/10.1093/\mnras/stx2364

Abuter, R., Accardo, M., Amorim, A., Anugu, N., Ávila, G., Azouaoui, N., Benisty, M., Berger, J. P., Blind, N., Bonnet, H., Bourget, P., Brandner, W., Brast, R., Buron, A., Burtscher, L., Cassaing, F., Chapron, F., Choquet, É., Clénet, Y., . . . Zins, G. (2017). First Light for GRAVITY: Phase referencing optical interferometry for the Very Large Telescope Interferometer. *Astronomy & Astrophysics*, *602*, A94. https://doi.org/10.1051/0004-6361/201730838

Abuter, R., Amorim, A., Bauböck, M., Berger, J. P., Binnet, H., Brandner, W., Clénet, Y., Davies, R., de Zeeuw, P. T., Dexter, J., Dallilar, Y., Drescher, A., Eckart, A., Eisenhauer, F., Förster Schreiber, N. M., Garcia, P., Gao, F., Gendron, E., Genzel, R., . . . an G. Zins, A. Y. (2021). Improved GRAVITY astrometric accuracy from modeling optical aberrations. *Astronomy & Astrophysics*, *647*, A59. https://doi.org/10.1051/0004-6361/202040208

Ackermann, M., Ajello, M., Albert, A., Baldini, L., Ballet, J., Barbiellini, G., Bastieri, D., Bellazzini, R., Bissaldi, E., Bloom, E. D., Bonino, R., Bottacini, E., Brandt, T. J., Bregeon, J., Bruel, P., Buehler, R., Cameron, R. A., Caputo, R., Caragiulo, M., . . . Zhou, M. (2017). Observations of M 31 and M 33 with the Fermi Large Area Telescope: A Galactic Center Excess in Andromeda? *The Astrophysical Journal*, *836*(2), 208. https://doi.org/10.3847/1538-4357/aa5c3d

Adamo, A., Bradley, L. D., Vanzella, E., Claeyssens, A., Welch, B., Diego, J. M., Mahler, G., Oguri, M., Sharon, K., Abdurro'uf, Hsiao, T. Y.-Y., Xu, X., Messa, M., Lassen, A. E., Zackrisson, E., Brammer, G., Coe, D., Kokorev, V., Ricotti, M., . . . Tamura, Y. (2024). Bound star clusters observed in a lensed galaxy 460 Myr after the Big Bang. *Nature*, *632*(8025), 513–516. https://doi.org/10.1038/s41586-024-07703-7

Adamo, A., Kruijssen, J. M. D., Bastian, N., Silva-Villa, E., & Ryon, J. (2015). Probing the role of the galactic environment in the formation of stellar clusters, using M 83 as a test bench. *Monthly Notices of the Royal Astronomical Society*, *452*(1), 246–260. https://doi.org/10.1093/\mnras/stv1203

Adamo, A., Östlin, G., & Zackrisson, E. (2011). Probing cluster formation under extreme conditions: massive star clusters in blue compact galaxies. *Monthly Notices of the Royal Astronomical Society*, *417*(3), 1904–1912. https://doi.org/10.1111/j.1365-2966.2011.19377.x

Adamo, A., Ryon, J. E., Messa, M., Kim, H., Grasha, K., Cook, D. O., Calzetti, D., Lee, J. C., Whitmore, B. C., Elmegreen, B. G., Ubeda, L., Smith, L. J., Bright, S. N., Runnholm, A., Andrews, J. E., Fumagalli, M., Gouliermis, D. A., Kahre, L., Nair, P., . . . Zackrisson, E. (2017). Legacy ExtraGalactic UV Survey with The Hubble Space Telescope: Stellar Cluster Catalogs and First Insights Into Cluster Formation and Evolution in NGC 628. *The Astrophysical Journal*, *841*(2), 131–156. https://doi.org/10.3847/1538-4357/aa7132

Agarwal, M., & Milosavljević, M. (2011). Nuclear Star Clusters from Clustered Star Formation. *The Astrophysical Journal*, *729*(1), 35. https://doi.org/10.1088/0004-637X/729/1/35

Aharon, D., & Perets, H. B. (2015). Formation and Evolution of Nuclear Star Clusters With In Situ Star Formation: Nuclear Core and Age Segregations. *The Astrophysical Journal*, *799*(2), 185. https://doi.org/10.1088/0004-637X/799/2/185

Ahn, C. P., Seth, A. C., Cappellari, M., Krajnović, D., Strader, J., Voggel, K. T., Walsh, J. L., Bahramian, A., Baumgardt, H., Brodie, J., Chilingarian, I., Chomiuk, L., den Brok, M., Frank, M., Hilker, M., McDermid, R. M., Mieske, S., Neumayer, N., Nguyen, D. D., . . . Spitler, L. (2018). The Black Hole in the Most Massive Ultracompact Dwarf Galaxy M59-UCD3. *The Astrophysical Journal*, *858*(2), 102. https://doi.org/10.3847/1538-4357/aabc57

Ahn, C. P., Seth, A. C., den Brok, M., Strader, J., Baumgardt, H., van den Bosch, R., Chilingarian, I., Frank, M., Hilker, M., McDermid, R., Mieske, S., ROmanowsky, A. J., Spitler, L., Brodie, J., Neumayer, N., & Walsh, J. L. (2017). Detection of Supermassive Blakc Holes in Two Virgo Ultracompact Dwarf Galaxies. *The Astrophysical Journal*, *839*(2), 72. https://doi.org/10.3847/1538-4357/aa6972

Alexander, P. E. R., & Gieles, M. (2012). A prescription and fast code for the long-term evolution of star clusters. *Monthly Notices of the Royal Astronomical Society*, *422*(4), 3415–3432. https://doi.org/10.1111/j.1365-2966.2012.20867.x

Alexander, P. E. R., Gieles, M., Lamers, H. J. G. L. M., & Baumgardt, H. (2014). A prescription and fast code for the long-term evolution of star clusters - III. Unequal masses and stellar evolution. *Monthly Notices of the Royal Astronomical Society*, *442*(2), 1265–1285. https://doi.org/10.1093/mnras/stu899

Alfaro-Cuello, M., Kacharov, N., Neumayer, N., Bianchini, P., Mastrobuono-Battisti, A., Lützgendorf, N., Seth, A. C., Böker, T., Kamann, S., Leaman, R., Watkins, L. L., & van de Ven, G. (2020). A Deep View into the Nucleus of the Sagittarius Dwarf Spheroidal Galaxy with MUSE. II. Kinematic Charaterization of the Stellar Populations. *The Astrophysical Journal*, *892*(1), 20. https://doi.org/10.3847/1538-4357/ab77bb

Alfaro-Cuello, M., Kacharov, N., Neumayer, N., Lützgendort, N., Seth, A. C., Böker, T., Kamann, S., Leaman, R., van de Ven, G., Bianchini, F., Watkins, L. L., & Lyubenova, M. (2019). A Deep View into the Nucleus of the Sagittarius Dwarf Spheroidal Galaxy with MUSE. I. Data and Stellar Population Characterization. *The Astrophysical Journal*, *886*(1), 57. https://doi.org/10.3847/1538-4357/ab1b2c

Anand, G. S., Lee, J. C., Van Dyk, S. D., Leroy, A. K., Rosolowsky, E., Schinnerer, E., Larson, K., Kourkchi, E., Kreckel, K., Scheuermann, F., Rizzi, L., Thilker, D., Tully, R. B., Bigiel, F., Blanc, G. A., Boquien, M., Chandar, R., Dale, D., Emsellem, E., . . . Whitmore, B. (2021). Distances to PHANGS galaxies: New tip of the red giant branch measurements and adopted distances. *Monthly Notices of the Royal Astronomical Society*, *501*(3), 3621–3639. https://doi.org/10.1093/\mnras/staa3668

Andersson, E. P., Mac Low, M.-M., Agertz, O., Renaud, F., & Li, H. (2024). Pre-supernova feedback sets the star cluster mass function to a power law and reduces the cluster formation efficiency. *Astronomy & Astrophysics*, *681*, A28. https://doi.org/10.1051/0004-6361/202347792

Angulo, R. E., & Hilbert, S. (2015). Cosmological constraints from the DFHTLenS shear measurements using a new, accurate, and felible way of predicting non-linear mass clustering. *Monthly Notices of the Royal Astronomical Society*, *448*(1), 364–375. https://doi.org/10.1093/\mnras/stv050

Angulo, R. E., & White, S. D. M. (2010). One simulation to fit them all - changing the background parameters of a cosmological N-body simulation. *Monthly Notices of the Royal Astronomical Society*, *405*(1), 143–154. https://doi.org/10.1111/j.1365-2966.2010.16459.x

Annibali, F., Tosi, M., Aloisi, A., & van der Marel, R. P. (2011). The Cluster Population of the Irregular Galaxy NGC 4449 as Seen by the Hubble Advanced Camera for Surveys. *The Astronomical Journal*, *142*(4), 129. https://doi.org/10.1088/0004-6256/142/4/129

Annibali, F., Tosi, M., Monelli, M., Sirianni, M., Montegriffo, P., Aloisi, A., & Greggio, L. (2009). Young Stellar Populations and Star Clusters in NGC 1705. *The Astronomical Journal*, *138*(1), 169–183. https://doi.org/10.1088/0004-6256/138/1/169

Antonini, F. (2013). Origin and Growth of Nuclear Star Clusters around Massive Black Holes. *The Astrophysical Journal*, *763*(1), 62. https://doi.org/10.1088/0004-637X/763/1/62

Antonini, F. (2014). On the Distribution of Stellar Remnants around Massive Black Holes: Slow Mass Segragation, Star Cluster Inspirals, and Correlated Orbits. *The Astrophysical Journal*, *794*(2), 106. https://doi.org/10.1088/0004-637X/794/2/106

Antonini, F., Barausse, E., & Silk, J. (2015). The Coevolution of Nuclear Star Clusters, Massive Black Holes, and Their Host Galaxies. *The Astrophysical Journal*, *812*(1), 72. https://doi.org/10.1088/0004-637X/812/1/72

Antonini, F., Capuzzo-Dolcetta, R., Mastrobuono-Battisti, A., & Merritt, D. (2012). Dissipationless Formation and Evolution of the Milky Way Nuclear Star Cluster. *The Astrophysical Journal*, *750*(2), 111. https://doi.org/10.1088/0004-637X/750/2/111

Arca Sedda, M. (2020). Birth, Life, and Death of Black Hole Binaries around Supermassive Black Holes: Dynamical Evolution of Gravitational Wave Sources. *The Astrophysical Journal*, *891*(1), 47. https://doi.org/10.3847/1538-4357/ab723b

Arca Sedda, M., & Capuzzo-Dolcetta, R. (2014). The globular cluster migratory origin of nuclear star clusters. *Monthly Notices of the Royal Astronomical Society*, *444*(4), 3738–3755. https://doi.org/10.1093/\mnras/stu1683

Arca Sedda, M., & Gualandris, A. (2018). Gravitational wave sources from inspiralling globular clusters in the Galactic Centre and similar environments. *Monthly Notices of the Royal Astronomical Society*, *477*(4), 4423–4442. https://doi.org/10.1093/\mnras/sty922

Arca Sedda, M., Gualandris, A., Do, T., Feldmeier-Krause, A., Neumayer, N., & Erkal, D. (2020). On the Origin of a Rotating Metal-poor Stellar Population in the Milky Way Nuclear Cluster. *The Astrophysical Journal Letters*, *901*(2), L29. https://doi.org/10.3847/2041-8213/abb245

Arca Sedda, M., Kocsis, B., & Brandt, T. D. (2018). Gamma-ray and X-ray emission from the Galactic centre: hints on the nuclear star cluster formation history. *Monthly Notices of the Royal Astronomical Society*, *479*(1), 900–916. https://doi.org/10.1093/\mnras/sty1454

Arca-Sedda, M., & Capuzzo-Dolcetta, R. (2017). The MEGaN project - I. Missing formation of massive nuclear clusters and tidal disruption events by star clusters-massive black hole interactions. *Monthly Notices of the Royal Astronomical Society*, *471*(1), 478–490. https://doi.org/10.1093/\mnras/stx1586

Arca-Sedda, M., Capuzzo-Dolcetta, R., Antonini, F., & Seth, A. (2015). Henize 2-10: The Ongoing Formation of a Nuclear Star Cluster around a Massive Black Hole. *The Astrophysical Journal*, *806*(2), 220. https://doi.org/10.1088/0004-637X/806/2/220

Arcodia, R., Liu, Z., Merloni, A., Malyali, A., Rau, A., Chakraborty, J., Goodwin, A., Buckley, D., Brink, J., Gromadzki, M., Arzoumanian, Z., Buchner, J., Kara, E., Nandra, K., Ponti, G., Salvato, M., Anderson, G., Baldini, P., Grotova, I., . . . Ramos-Ceja, M. E. (2024a). The more the merrier: SRG/eROSITA discovers two further galaxies showing X-ray quasi-periodic eruptions. *Astronomy & Astrophysics*, *684*, A64. https://doi.org/10.1051/0004-6361/202348881

Arcodia, R., Merloni, A., Comparat, J., Dwelly, T., Seppi, R., Zhang, Y., Buchner, J., Georgakakis, A., Haberl, F., Igo, Z., Kyritsis, E., Liu, T., Nandra, K., Ni, Q., Ponti, G., Salvato, M., Ward, C., Wolf, J., & Zezas, A. (2024b). O Corona, where art thou? eROSITA's view of UV-optical-IR variability-selected massive black holes in low-mass galaxies. *Astronomy & Astrophysics*, *681*, A97. https://doi.org/10.1051/0004-6361/202347531

Arjona-Gálvez, E., Di Cintio, A., & Grand, R. J. J. (2024). The role of active galactic nucleus feedback on the evolution of dwarf galaxies from cosmological simulations: Supermassive black holes suppress star formation in low-mass galaxies. *Astronomy & Astrophysics*, *690*, A286. https://doi.org/10.1051/0004-6361/202449439

Arnaud, K., Borkowski, K. J., & Harrington, J. P. (1996). X-Ray Emission from the Wind-blown Bubble in the Planetary Nebula BD+30 degrees 3639. *The Astrophysical Journal Letters*, *462*, L75. https://doi.org/10.1086/310037

Ashok, A., Seth, A., Erwin, P., Debattista, V. P., de Lorenzo-Cáceres, A., Gadotti, D. A., Méndez-Abreu, J., Beckman, J. E., bender, R., Drory, N., Fisher, D., Hopp, U., Kluge, M., Kolcu, T., Maciejewski, W., Mehrgan, K., Parikh, T., Saglia, R., Seidel, M., & Thomas, J. (2023). Composite Bulges – III. A Study of Nuclear Star Clusters in Nearby Spiral Galaxies. *The Astrophysical Journal*, *958*(1), 100. https://doi.org/10.3847/1538-4357/ace341

Asmus, D., Gandhi, P., Hönig, S. F., Smette, A., & Duschl, W. J. (2015). The subarcsecond mid-infrared view of local active galactic nuclei - II. The mid-infrared-X-ray correlation. *Monthly Notices of the Royal Astronomical Society*, *454*(1), 766–803. https://doi.org/10.1093/\mnras/stv1950

Asplund, M., Grevesse, N., Sauval, A. J., & Scott, P. (2009). The Chemical Composition of the Sun. *Annual Review of Astronomy & Astrophysics*, *47*(1), 481–522. https://doi.org/10.1146/annurev.astro.46.060407.145222

Atallah, D., Trani, A. A., Kremer, K., Weatherford, N. C., Fragione, G., Spera, M., & Rasio, F. A. (2023). Growing black holes through successive mergers in galactic nuclei - I. Methods and first results. *Monthly Notices of the Royal Astronomical Society*, *523*(3), 4227–4250. https://doi.org/10.1093/mnras/stad1634

Atkinson, J. W., Collett, J. L., Marconi, A., Axon, D. J., Alonso-Herrero, A., Batcheldor, D., Binney, J. J., Capetti, A., Carollo, C. M., Dressel, L., Ford, H., Gerssen, J., Hughes, M. A., Macchetto, D., Maciejewski, W., Merrifield, M. R., Scarlata, C., Sparks, W., Stiavelli, W., . . . van der Marel, R. P. (2005). Supermassive black hole mass measurements for NGC 1300 and NGC 2748 based on Hubble Space Telescope emission-line gas kinematics. *Monthly Notices of the Royal Astronomical Society*, *359*(2), 504–520. https://doi.org/10.1111/j.1365-2966.2005.08904.x

Ayromlou, M., Kauffmann, G., Yates, R. M., Nelson, D., & White, S. D. M. (2021). Galaxy formation with L-GALAXIES: modelling the environment dependency of galaxy evolution and comparing with observations. *Monthly Notices of the Royal Astronomical Society*, *505*(1), 492–514. https://doi.org/10.1093/\mnras/stab1245

Bacon, R., Copin, Y., Monnet, G., Miller, B. W., Allington-Smith, J. R., Bureau, M., Carollo, C. M., Davies, R. L., Emsellem, E., Kuntschner, H., Peletier, R. F., Verolme, E. K., & de Zeeuw, P. T. (2001a). The SAURON project - I. The panoramic integral-field spectrograph. *Monthly Notices of the Royal Astronomical Society*, *326*(1), 23–35. https://doi.org/10.1046/j.1365-8711.2001.04612.x

Bacon, R., Emsellem, E., Combes, F., Copin, Y., Monnet, G., & Martin, P. (2001b). The M 31 double nucleus probed with OASIS. A natural $m = 1$ mode? *Astronomy & Astrophysics*, *371*, 409–428. https://doi.org/10.1051/0004-6361:20010317

Bacon, R., Emsellem, E., Monnet, G., & Nieto, J. L. (1994). Sub-arcsecond 2D photometry and Spectroscopy of the nucleus of M 31: the supermassive black hole revisited. *Astronomy & Astrophysics*, *281*, 691–717. https://doi.org/10.48550/arXiv.astro-ph/9309008

Bajkova, A. T., Smirnov, A. A., & Bobylev, V. V. (2023). The Influence of the Bar on the Dynamics of Globular Clusters in the Central Region of the Milky Way. Frequency Analysis of Orbits According to Gaia EDR3 Data. *Astrophysical Bulletin*, *78*(4), 499–513. https://doi.org/10.1134/S199034132360028X

Baldassare, V. F., Gallo, E., Miller, B. P., Plotkin, R. M., Treu, T., Valluri, M., & Woo, J.-H. (2014). AMUSE-Field. II. Nucleation of Early-type Galaxies in the Field versus Cluster Environment. *The Astrophysical Journal*, *791*(2), 133–145. https://doi.org/10.1088/0004-637X/791/2/133

Baldassare, V. F., geha, M., & Greene, J. (2018). Identifying AGNs in Low-mass Galaxies via Long-term Optical Variability. *The Astrophysical Journal*, *868*(2), 152. https://doi.org/10.3847/1538-4357/aae6cf

Baldassare, V. F., Stone, N. C., Foord, A., Gallo, E., & Ostriker, J. P. (2022). Massive Black Hole Formation in Dense Stellar Environments: Enhanced X-Ray Detection Rates in High-Velocity Dispersion Nuclear Star Clusters. *The Astrophysical Journal*, *929*(1), 84. https://doi.org/10.3847/1538-4357/ac5f51

Balick, B., & Brown, R. L. (1974). Intense sub-arcsecond structure in the galactic center. *The Astrophysical Journal*, *194*, 265–270. https://doi.org/10.1086/153242

Bañados, E., Venemans, B. P., Mazzucchelli, C., Farina, E. P., Walter, F., Wang, F., Decarli, R., Stern, D., Fan, X., Davies, F. B., Hennawi, J. F., Simcoe, R. A., Turner, M. L., Rix, H.-W., Yang, J., Kelson, D., Rudie, G. C., & Winters, J. M. (2018). An 800-million-solar-mass black hole in a significantly neutral Universe at a redshift of 7.5. *Nature*, *553*(7689), 473–476. https://doi.org/10.1038/nature25180

Banerjee, S. (2017). Stellar-mass black holes in young massive and open stellar clusters and their role in gravitational-wave generation. *Monthly Notices of the Royal Astronomical Society*, *467*(1), 524–539. https://doi.org/10.1093/mnras/stw3392

Banerjee, S., & Kroupa, P. (2017). How can young massive clusters reach their present-day sizes? *Astronomy & Astrophysics*, *597*, A28. https://doi.org/10.1051/0004-6361/201526928

Barmby, P., & Huchra, J. P. (2001). M 31 Globular Clusters in the Hubble Space Telescope Archive. I. Cluster Detection and Completeness. *The Astronomical Journal*, *122*(5), 2458–2468. https://doi.org/10.1086/323457

Barmby, P., Huchra, J. P., Brodie, J. P., Forbes, D. A., Schroder, L. L., & Grillmair, C. J. (2000). M 31 Globular Clusters: Colors and Metallicities. *The Astronomical*

Journal, *119*(2), 727–747. https://doi.org/10.1086/301213

Barrera, M., Springel, V., White, S. D. M., Hernández-Aguayo, C., hernquit, L., Frenk, C., Pakmor, R., Ferlito, F., Hadzhiyska, B., Delgado, A. M., Kannan, R., & Bose, S. (2023). The MillenniumTNG Project: semi-analytic galaxy formation models on past lightcones. *Monthly Notices of the Royal Astronomical Society*, *525*(4), 6312–6335. https://doi.org/10.1093/mnras/stad2688

Barth, A. J., Ho, L. C., Filippenko, A. V., & Sargent, W. L. (1995). Hubble Space Telescope Observations of Circumnuclear Star-Forming Rings in NGC 1097 and NGC 6951. *The Astronomical Journal*, *110*, 1009. https://doi.org/10.1086/117580

Barth, A. J., Strigari, L. E., Bentz, M. C., Greene, J. E., & Ho, L. C. (2009). Dynamical Constraints on the Masses of the Nuclear Star Cluster and Black Hole in Late-Type Spiral Galaxy NGC 3621. *The Astrophysical Journal*, *690*(1), 1031–1044. https://doi.org/10.1088/0004-637X/690/1/1031

Bassino, L. P., & Caso, J. P. (2017). The merger remnant NGC 3610 and its globular cluster system: a large-scale study. *Monthly Notices of the Royal Astronomical Society*, *466*(4), 4259–4271. https://doi.org/10.1093/mnras/stw3390

Bastian, N. (2008). On the star formation rate - brightest cluster relation: estimating the peak star formation rate in post-merger galaxies. *Monthly Notices of the Royal Astronomical Society*, *390*(2), 759–768. https://doi.org/10.1111/j.1365-2966.2008.13775.x

Bastian, N., Adamo, A., Gieles, M., Silva-Villa, E., Lamers, H. J. G. L. M., Larsen, S. S., Smith, L. J., Konstantopoulos, I. S., & Zackrisson, E. (2012). Stellar clusters in M 83: formation, evolution, disruption and the influence of the environment. *Monthly Notices of the Royal Astronomical Society*, *419*(3), 2606–2622. https://doi.org/10.1111/j.1365-2966.2011.19909.x

Bastian, N., & Lardo, C. (2018). Multiple Stellar Populations in Globular Clusters. *Annual Review of Astronomy and Astrophysics*, *56*, 83–136. https://doi.org/10.1146/annurev-astro-081817-051839

Bastian, N., Pfeffer, J., Kruijssen, J. M. D., Crain, R. A., Trujillo-Gomez, S., & Reina-Campos, M. (2020). The globular cluster system mass-halo mass relation in the E-MOSAICS simulations. *Monthly Notices of the Royal Astronomical Society*, *498*(1), 1050–1061. https://doi.org/10.1093/mnras/staa2453

Baugh, C. M. (2006). A primer on hierarchical galaxy formation: the semi-analytical approach. *Reports on Progress in Physics*, *69*(12), 3101–3156. https://doi.org/10.1088/0034-4885/69/12/R02

Baumgardt, H., & Hilker, M. (2018). A catalogue of masses, structural parameters, and velocity dispersion profiles of 112 Milky Way globular clusters. *Monthly Notices of the Royal Astronomical Society*, *478*(2), 1520–1557. https://doi.org/10.1093/\mnras/sty1057

Beasley, M. A., Bridges, T., Peng, E., Harris, W. E., Harris, G. L. H., Forbes, D. A., & Mackie, G. (2008). A 2dF spectroscopic study of globular clusters in NGC 5128: probing the formation history of the nearest giant elliptical. *Monthly Notices of the Royal Astronomical Society*, *386*(3), 1443–1463. https://doi.org/10.1111/j.1365-2966.2008.13123.x

Beasley, M. A., Leaman, R., Gallart, C., Larsen, S. S., Battaglia, G., Monelli, M., & Pedreros, M. H. (2019). An old, metal-poor globular cluster in Sextans A and the metallicity floor of globular cluster systems. *Monthly Notices of the Royal Astronomical Society*, *487*(2), 1986–1993. https://doi.org/10.1093/\mnras/stz1349

Becklin, E. E., & Neugebauer, G. (1968). Infrared Observations of the Galactic Center. *The Astrophysical Journal*, *151*, 145. https://doi.org/10.1086/149425

Beckmann, R. S., Dubois, Y., Volonteri, M., Dong-Páez, C. A., Trebitsch, M., Devriendt, J., Kaviraj, S., Kimm, T., & Peirani, S. (2023). Population statistics of intermediate-mass black holes in dwarf galaxies using the newhorizon simulation. *Monthly Notices of the Royal Astronomical Society*, 16. https://doi.org/10.1093/\mnras/stad1544

Bekki, K. (2007). The Formation of Stellar Galactic Nuclei through Dissipative Gas Dynamics. *Publications of the Astronomical Society of Australia*, *24*(2), 77–94. https://doi.org/10.1071/AS07008

Bekki, K., Couch, W. J., & Shioya, Y. (2006). Dissipative Transformation of Nonnucleated Dwarf Galaxies into Nucleated Systems. *The Astrophysical Journal Letters*, *642*(2), L133–L136. https://doi.org/10.1086/504588

Bekki, K., & Graham, A. W. (2010). On the Transition from Nuclear-cluster- to Black-hole-dominated Galaxy Cores. *The Astrophysical Journal Letters*, *714*(2), L313–L317. https://doi.org/10.1088/2041-8205/714/2/L313

Bell, E. F., McIntosh, D. H., Katz, N., & Weinberg, M. D. (2003). The Optical and Near-Infrared Properties of Galaxies. I. Luminosity and Stellar Mass Functions. *The Astrophysical Journal Series*, *149*(2), 289–312. https://doi.org/10.1086/378847

Bellazzini, M., Annibali, F., Tosi, M., Mucciarelli, A., Cignoni, M., Beccari, G., Nipoti, C., & Pascale, R. (2020). The strange case of the peculiar spiral galaxy NGC 5474. New pieces of a galactic puzzle. *Astronomy & Astrophysics*, *634*, A124. https://doi.org/10.1051/0004-6361/201937284

Bellovary, J., Volonteri, M., Governato, F., Shen, S., Quinn, T., & Wadsley, J. (2011). The First Massive Black Hole Seeds and Their Hosts. *The Astrophysical Journal*, *742*(1), 13. https://doi.org/10.1088/0004-637X/742/1/13

Bender, R., Kormendy, J., Bower, G., Green, R., Thomas, J., Danks, A. C., Gull, T., Hutchings, J. B., Joseph, C. L., Kaiser, M. E., Lauer, T. R., Nelson, C. H., Richstone, D., Weistrop, D., & Woodgate, B. (2005). HST STIS Spectroscopy of the Triple Nucleus of M 31: Two Nested Disks in Keplerian Rotation around a Supermassive Black Hole. *The Astrophysical Journal*, *631*(1), 280–300. https://doi.org/10.1086/432434

Bender, R., Kormendy, J., & Dehnen, W. (1996). Improved Evidence for a $3 \times 10^6 M_\odot$ Black Hole in M 32: Canada-France-Hawaii Telescope Spectroscopy with $FWHM = 0.47''$ Resolution. *The Astrophysical Journal Letters*, *464*, L123. https://doi.org/10.1086/310098

Bertin, G., & Romeo, A. B. (1988). Global spiral modes in stellar disks containing gas. *Astronomy & Astrophysics*, *195*, 105–113. https://ui.adsabs.harvard.edu/abs/1988A&A...195..105B

Bertola, F., Cinzano, P., Corsini, E. M., Pizzella, A., Persic, M., & Salucci, P. (1996). Counterrotating Stellar Disks in Early-Type Spirals: NGC 3593. *The Astrophysical Journal Letters*, *458*, L67. https://doi.org/10.1086/309924

Bertoldi, F., & McKee, C. F. (1992). Pressure-confined Clumps in Magnetized Molecular Clouds. *The Astrophysical Journal*, *395*, 140–157. https://doi.org/10.1086/171638

Bik, A., Lamers, H. J. G. L. M., Bastian, N., Panagia, N., & Romaniello, M. (2003). Clusters in the inner spiral arms of M 51: The cluster IMF and the formation history. *Astronomy & Astrophysics*, *397*, 473–486. https://doi.org/10.1051/0004-6361:20021384

Binggeli, B., Sandage, A., & Tammann, G. A. (1985). Studies of the Virgo cluster. II. A catalog of 2096 galaxies in the Virgo cluster area. *The Astronomical Journal*, *90*, 1681–1758. https://doi.org/10.1086/113874

Binggeli, B., Tammann, G. A., & Sandage, A. (1987). Studies of the Virgo Cluster. VI. Morphological and Kinematical Structure of the Virgo Cluster. *The Astronomical Journal*, *94*(2), 251–277. https://doi.org/10.1086/114467

Binney, J., Gerhard, O. E., Stark, A. A., Bally, J., & Uchida, K. I. (1991). Understanding the kinematics of Galactic Centre gas. *Monthly Notices of the Royal Astronomical Society*, *252*(2), 210. https://doi.org/10.1093/mnras/252.2.210

Binney, J., & Tremaine, S. (2008). *Galactic dynamics: Second edition*. Princeton University Press. http://www.jstor.org/stable/j.ctvc778ff

Birchall, K. L., Watson, M. G., & Aird, J. (2020). X-ray detected AGN in SDSS dwarf galaxies. *Monthly Notices of the Royal Astronomical Society*, *492*(2), 2268–2284. https://doi.org/10.1093/\mnras/staa040

Bittner, A., Sánchez-Blázquez, P., Gadotti, D. A., Neumann, J., Fragkoudi, F., Coelho, P., de Lorenzo-Cáceres, A., Falcón-Barroso, J., Kim, T., Leaman, R., Martín-Navarro, I., Méndez-Abreu, J., Pérez, I., Querejeta, M., Seidel, M. K., & van de Ven, G. (2020). Inside-out formation of nuclear discs and the absence of old central spheroids in barred galaxie sof the TIMER survey. *Astronomy & Astrophysics*, *643*, A65. https://doi.org/10.1051/0004-6361/202038450

Blakeslee, J. P. (1999). Globular Clusters in Dense Clusters of Galaxies. *The Astronomical Journal*, *118*(4), 1506–1525. https://doi.org/10.1086.301052

Blom, C., Spitler, L. R., & Forbes, D. A. (2012). Wide-field imaging of NGC 4365's globular cluster system: the third subpopulation revisited. *Monthly Notices of the Royal Astronomical Society*, *420*(1), 37–60. https://doi.org/10.1111/j.1365-2966.2011.19963.x

Bluck, A. F. L., Mendel, T. J., Ellison, S. L., Patton, D. R., Simard, S., Henriques, B. M. B., Torrey, P., Teimoorinia, H., Moreno, J., & Starkenburg, E. (2016). The impact of galactic properties and environment on the quenching of central and satellite galaxies: a comparison between SDSS, Illustris and L-Galaxies. *Monthly Notices of the Royal Astronomical Society*, *462*(3), 2559–2586. https://doi.org/10.1093/mnras/stw1665

Boggs, P. T., & Rogers, J. E. (1990, January). Orthogonal Distance Regression. In *Statistical analysis of measurement error models and applications: proceedings of the AMS-IMS-SIAM joint summer research conference held June 10-16 1989* (p. 186). Contemporary Mathematics. https://archive.org/details/orthogonaldistan8941bogg

Böker, T., Calzetti, D., Sparks, W., Axon, D., Bergeron, L. E., Bushouse, H., Colina, L., Daou, D., Gilmore, D., Holfeltz, S., MacKenty, J., Mazzuca, L., Monroe, B., Najita, J., Noll, K., Nota, A., Ritchie, C., Schultz, A., Sosey, M., . . . STScI NICMOS Group. (1999a). The NICMOS Snapshot Survey of Nearby Galaxies. *The Astrophysical Journal Series*, *124*(1), 95–126. https://doi.org/10.1086/313253

Böker, T., Laine, S., van der Marel, R. P., Sarzi, M., Rix, H.-W., Ho, L. C., & Shields, J. C. (2002). A Hubble Space Telescope Census of Nuclear Star Clusters in Late-Type Spiral Galaxies. I. Observations and Image Analysis. *The Astronomical Journal*, *123*(3), 1389–1410. https://doi.org/10.1086/339025

Böker, T., van der Marel, R. P., & Vacca, W. D. (1999b). CO Band Head Spectroscopy of IC 342: Mass and Age of the Nuclear Star Cluster. *The Astronomical Journal*, *118*(2), 831–842. https://doi.org/10.1086/300985

Bolatto, A. D., Wolfire, M., & Leroy, A. K. (2013). The CO-to-H_2 Conversion Factor. *Annual Review of Astronomy and Astrophysics*, *51*(1), 207–268. https://doi.org/10.1146/annurev-astro-082812-140944

Bonoli, S., Marulli, F., Springel, V., White, S. D. M., Branchini, E., & Moscardini, L. (2009). Modelling the cosmological co-evolution of supermassive black holes and galaxies - II. The clustering of quasars and their dark environment. *Monthly Notices of the Royal Astronomical Society*, *396*(1), 423–438. https://doi.org/10.1111/j.1365-2966.2009.14701.x

Bonoli, S., Mayer, L., & Callegari, S. (2014). Massive black hole seeds born via direct collapse in galaxy mergers: their properties, statistics and environments. *Monthly Notices of the Royal Astronomical Society*, *437*(2), 1576–1592. https://doi.org/10.1093/mnras/stt1990

Boquien, M., Burgarella, D., Roehlly, Y., Buat, V., Ciesla, L., Corre, D., Inoue, A. K., & Salas, H. (2019). CIGALE: a python Code Investigating GALaxy Emission. *Astronomy & Astrophysics*, *622*, A103. https://doi.org/10.1051/0004-6361/201834156

Bottema, R. (1993). The stellar kinematics of galactic disks. *Astronomy & Astrophysics*, *275*, 16–36. https://ui.adsabs.harvard.edu/abs/1993A&A...275...16B

Boulade, O., Charlot, X., Abbon, P., Aune, S., Borgeaud, P., Carton, P.-H., Carty, M., Da Costa, J., Deschamps, H., Desforge, D., Eppellé, D., Gallais, P., Gosset, L., Granelli, R., Gros, M., de Kat, J., Loiseau, D., Ritou, J., Roussé, J. Y., . . . Vigroux, L. G. (2003, March). MegaCam: the new Canada-France-Hawaii Telescope wide-field imaging camera. In M. Iye & A. F. M. Moorwood (Eds.), *Instrument Design and Performance for Optical/Infrared Ground-based Telescopes* (pp. 72–81, Vol. 4841). SPIE. https://www.spiedigitallibrary.org/conference-proceedings-of-spie/4841/1/Megacam--the-new-Canada-France-Hawaii-Telescope-wide-field/10.1117/12.459890.full?SSO=1

Boyer, M. L., Anderson, J., Gennaro, M., Geha, M., Wingfield McQuinn, K. B., Tollerud, E., Correnti, M., Brenner Newman, M. J., Cohen, R. E., Kallivayalil, N., Beaton, R., Cole, A. A., Dolphin, A., Kalirai, J. S., Sandstrom, K. M., Savino, A., Skillman, E. D., Weisz, D. R., & Williams, B. F. (2022). The JWST Resolved Stellar Populations Early Release Science Program. I. NIRCam Flux Calibration. *Research Notes of the American Astronomical Society*, *6*(9), 191. https://doi.org/10.3847/2515-5172/ac923a

Boylan-Kolchin, M., Springel, V., White, S. D. M., Jenkins, A., & Lemson, G. (2009). Resolving cosmic structure formation with the Millennium-II Simulation. *Monthly Notices of the Royal Astronomical Society*, *398*(3), 1150–1164. https://doi.org/10.1111/j.1365-2966.2009.15191.x

Bradley, L. D., Adamo, A., Vanzella, E., Sharon, K., Brammer, G., Coe, D., Diego, J. M., Kokorev, V., Mahler, G., Oguri, M., Abdurro'uf, Bhatawdekar, R., Christensen, L., Fujimoto, S., Hasimoto, T., Hsiao, T. Y.-Y., Inoue, A. K., Jiménez-Teja, Y., Messa, M., . . . Zitrin, A. (2024). Unveiling the Cosmic Gems Arc at $z \sim 10.2$ with JWST. *The Astrophysical Journal*, 22. https://doi.org/10.48550/arXiv.2404.10770

Brammer, G. (2022). *Preliminary updates to the NIRCam photometric calibration*. Zenodo. https://doi.org/10.5281/zenodo.7143382

Bressan, A., Marigo, P., Girardi, L., Salasnich, B., Dal Cero, C., Rubele, S., & Nanni, A. (2012). PARSEC: stellar tracks and isochrones with the PAdova and TRieste Stellar Evolution Code. *Monthly Notices of the Royal Astronomical Society*, *427*(1), 127–145. https://doi.org/10.1111/j.1365-2966.2012.21948.x

Briggs, F. H., Wolfe, A. M., Krumm, N., & Salpeter, E. E. (1980). First results of a sensitive search for HI envelopes in a complete sample of spiral galaxies: extensive HI near the isolated SCI NGC 628. *The Astrophysical Journal*, *238*, 510–523. https://doi.org/10.1086/158007

Brodie, J. P., & Strader, J. (2006). Extragalactic Globular Clusters and Galaxy Formation. *Annual Review of Astronomy & Astrophysics*, *44*(1), 193–267. https://doi.org/10.1146/annurev.astro.44.051905.092441

Brodie, J. P., Usher, C., Conroy, C., Strader, J., Arnold, J. A., Forbes, D. A., & Romanowsky, A. J. (2012). The SLUGGS Survey: NGC 3155, A Critical Test Case for Metallicity Bimodality in Globular Cluster Systems. *The Astrophysical Journal Letters*, *759*(2), L33. https://doi.org/10.1088/2041-8205/759/2/L33

Brogaard, K., VandenBerg, D. A., Bruntt, H., Grundahl, F., Frandsen, S., Bedin, L. R., Milone, A. P., Dotter, A., Feiden, G. A., Stetson, P. B., Sandquist, E., Miglio, A., Stello, D., & Jessen-Hansen, J. (2012). Age and helium content of the open cluster NGC 6791 from multiple eclipsing binary members. II. Age dependencies and new insights. *Astronomy & Astrophysics*, *543*, A106. https://doi.org/10.1051/0004-6361/201219196

Brown, G., & Gnedin, O. Y. (2021). Radii of young star clusters in nearby galaxies. *Monthly Notices of the Royal Astronomical Society*, *508*(4), 5935–5953. https://doi.org/10.1093/mnras/stab2907

Brown, G., & Gnedin, O. Y. (2022). Testing feedback from star clusters in simulations of the Milky Way formation. *Monthly Notices of the Royal Astronomical Society*, *514*(1), 280–301. https://doi.org/10.1093/\mnras/stac1164

Brunner, H., Liu, T., Lamer, G., Georgakakis, A., Merloni, A., Brusa, M., Bulbul, E., Dennerl, K., Friedrich, S., Liu, A., Maitra, C., Nandra, K., Ramos-Ceja, M. E., Sanders, J. S., Stewart, I. M., Boler, T., Buchner, J., Clerc, N., Comparat, J., . . . Wilms, J. (2022). The eROSITA Final Equatorial Depth Survey (eFEDS). X-ray catalogue. *Astronomy & Astrophysics*, *661*, A1. https://doi.org/10.1051/0004-6361/202141266

Bruzual, G., & Charlot, S. (2003). Stellar population synthesis at the resolution of 2003. *Monthly Notices of the Royal Astronomical Society*, *344*(4), 1000–1028. https://doi.org/10.1046/j.1365-8711.2003.06897.x

Buchner, J. (2019). Collaborative Nested Sampling: Big Data versus Complex Physical Models. *Publications of the Astronomical Society of the Pacific*, *131*(1004), 108005. https://doi.org/10.1088/1538-3873/aae7fc

Buchner, J. (2021). UltraNest - a robust, general purpose Bayesian inference ngine. *The Journal of Open Source Software*, *6*(60), 3001. https://doi.org/10.21105/joss.03001

Buchner, J., georgakakis, A., Nandra, K., hsu, L., Rangel, C., Brightman, M., Merloni, A., Salvato, M., Donley, J., & Kocevski, D. (2014). X-ray spectral modelling of the AGN obscuring region in the CDFS: Bayesian model selection and catalogue. *Astronomy & Astrophysics*, *564*, A125. https://doi.org/10.1051/0004-6361/201322971

Burgarella, D., Buat, V., & Iglesias-Páramo, J. (2005). Star formation and dust attenuation properties in galaxies from a statistical ultraviolet-to-far-infrared analysis. *Monthly Notices of the Royal Astronomical Society*, *360*(4), 1413–1425. https://doi.org/10.1111/j.1365-2966.2005.09131.x

Burkert, A., & Forbes, D. A. (2020). High-precision Dark Halo Virial Masses from Globular Cluster Numbers: Implications for Globular Cluster Formation and Galaxy Assembly. *The Astronomical Journal*, *159*(2), 56. https://doi.org/10.3847/1538-3881/ab5b0e

Burkhart, B. (2018). The Star Formation Rate in the Gravoturbulent Interstellar Medium. *The Astrophysical Journal*, *863*(2), 118. https://doi.org/10.3847/1538-4357/aad002

Bustamente-Rosell, M. J., Noyola, E., Gebhardt, K., Fabricius, M. H., Mazzalay, X., Thomas, J., & Zeimann, G. (2021). Dynamical Analysis of the Dark Matter and Central Black Hole Mass in the Dwarf Spheroidal Leo I. *The Astrophysical Journal*, *921*(2), 107. https://doi.org/10.3847/1538-4357/ac0c79

Butler, D. J., & Martínez-Delgado, D. (2005). On the Stellar Populations in NGC 185 and NGC 205 and the Nuclear Star Cluster in NGC 205 from Hubble Space Telescope Observations. *The Astronomical Journal*, *129*(5), 2217–2231. https://doi.org/10.1086/429524

Caldwell, N. (1983). Structure and stellar content of dwarf elliptical galaxies. *The Astronomical Journal*, *88*, 804–812. https://doi.org/10.1086/113367

Caldwell, N., & Romanowsky, A. J. (2016). Star Clusters in M 31. VII. Global Kinematics and Metallicity Sub-populations of the Globular Clusters. *The Astrophysical Journal*, *824*(1), 42. https://doi.org/10.3847/0004-637X/824/1/42

Callingham, T. M., Cautun, M., Deason, A. J., Frenk, C. S., Grand, R. J. J., & Marinacci, F. (2022). The chemo-dynamical groups of Galactic globular clusters. *Monthly Notices of the Royal Astronomical Society*, *513*(3), 4107–4129. https://doi.org/10.1093/mnras/stac1145

Calura, F., Pascale, R., Agertz, O., Andersson, E., Lacchin, E., Lupi, A., Meneghetti, M., Nipoti, C., Ragagnin, A., Rosdahl, J., Vanzella, E., Vesperini, E., & Zanella, A. (2024). SIEGE III. The formation of dense stellar clusters in sub-parsec resolution cosmological simulations with individual star feedback. *arXiv e-prints*, arXiv:2411.02502. https://doi.org/10.48550/arXiv.2411.02502

Calzetti, D., Lee, J. C., Sabbi, E., Adamo, A., Smith, L. J., Andrews, J. E., Ubeda, L., Bright, S. N., Thilker, D., Aloisi, A., Brown, T. M., Chandar, R., Christian, C., Cignoni, M., Clayton, G. C., da Silva, R., de Mink, S. E., Dobbs, C., Elmegreen, B. G., . . . Wofford, A. (2015). Legacy Extragalactic UV Survey (LEGUS) With the Hubble Space Telescope. I. Survey Description. *The Astronomical Journal*, *149*(2), 51. https://doi.org/10.1088/0004-6256/149/2/51

Cameron, E. (2011). On the Estimation of Confidence Intervals for Binomical Populations in Astronomy: The Simplicity and Superiority of the Bayesian Approach. *Publications of the Astronomical Society of Australia*, *28*(2), 128–139. https://doi.org/10.1071/AS10046

Cann, J. M., Weaver, K. A., Pfeifle, R. W., Secrest, N. J., Satyapal, S., & Gliozzi, M. (2024). Exploring X-ray Propeties of Low-metallicity Dwarf Galaxies. *The Astrophysical Journal*, *961*(2), 178. https://doi.org/10.3847/1538-4357/ad0a6b

Cantiello, M., Capaccioli, M., Napolitano, N., Grado, A., Limatola, L., Paolillo, M., Iodice, E., Romanowsky, A. J., Forbes, D. A., Raimondo, G., Spavone, M., La Barbera, F., Puzia, T. H., & Schipani, P. (2015). VEGAS-SSS. A VST early-type galaxy survey: analysis of small stellar systems. Testing the methodology on the globular cluster system in NGC 3115. *Astronomy & Astrophysics*, *576*, A14. https://doi.org/10.1051/0004-6361/201425165

Capaccioli, M. (1989). Photometry of early-type galaxies and the $r^{1/4}$ law. In H. G. Corwin & L. Bottinelli (Eds.), *World of Galaxies (Le Monde des Galaxies)* (pp. 208–227). https://ui.adsabs.harvard.edu/abs/1989woga.conf..208C

Cappellari, M. (2020). Efficient solution of the anisotropic spherically aligned axisymmetric Jeans equations of stellar hydrodynamics for galactic dynamics. *Monthly Notices of the Royal Astronomical Society*, *494*(4), 4819–4837. https://doi.org/10.1093/\mnras/staa959

Cappellari, M., & Emsellem, E. (2004). Parametric Recovery of Line-of-Sight Velocity Distributions from Absorption-Line Spectra of Galaxies via Penalized Likelihood. *The Publications of the Astronomical Society of the Pacific*, *116*(816), 138–147. https://doi.org/10.1086/381875

Capuzzo-Dolcetta, R. (1993). The Evolution of the Globular Cluster System in a Triaxial Galaxy: Can a Galactic Nucleus Form by Globular Cluster Capture? *The Astrophysical Journal*, *415*, 616. https://doi.org/10.1086/173189

Capuzzo-Dolcetta, R., & Mastrobuono-Battisti, A. (2009). Globular cluster system erosion in elliptical galaxies. *Astronomy & Astrophysics*, *507*(1), 193–193. https://doi.org/10.1051/0004-6361/200912255

Capuzzo-Dolcetta, R., & Tosta e Melo, I. (2017). On the relation between the mass of Compact Massive Objects and their host galaxies. *Monthly Notices of the Royal Astronomical Society*, *472*(4), 4013–4023. https://doi.org/10.1093/\mnras/stx2246

Cardelli, J. A., Clayton, G. C., & Mathis, J. S. (1989). The Relationship between Infrared, Optical, and Ultraviolet Extinction. *The Astrophysical Journal*, *345*, 245–256. https://doi.org/10.1086/167900

Carlsten, S. G., Greco, J. P., Beaton, R. L., & Greene, J. E. (2020). Wide-field Survey of Dwarf Satellite Systems around 10 Hosts in the Local Volume. *The Astrophysical Journal*, *891*(2), 144–173. https://doi.org/10.3847/1538-4357/ab7758

Carlsten, S. G., Greene, J. E., Beaton, R. L., & Greco, J. P. (2022). ELVES II: Globular Clusters and Nuclear Star Clusters of Dwarf Galaxies: the Importance of Environment. *The Astrophysical Journal*, *927*(1), 44. https://doi.org/10.3847/1538-4357/ac457e

Carollo, C. M., & Stiavelli, M. (1998). Spiral Galaxies with WFPC2. III. Nuclear Cusp Slopes. *The Astronomical Journal*, *115*(6), 2306–2319. https://doi.org/10.1086/300373

Carollo, C. M., Stiavelli, M., de Zeeuw, P. T., & Mack, J. (1997). Spiral Galaxies with WFPC2. I. Nuclear Morphology, Bulges, Star Clusters, and Surface Brightness Profiles. *The Astronomical Journal*, *114*(6), 2366–2380. https://doi.org/10.1086/118654

Carollo, C. M., Stiavelli, M., & Mack, J. (1998). Spiral Galaxies with WFPC2. II. The Nuclear Properties of 40 Objects. *The Astronomical Journal*, *116*(1), 68–84. https://doi.org/10.1086/300407

Carollo, C. M., Stiavelli, M., Massimo, S., Seigar, M., de Zeeuw, P. T., & Dejonghe, H. (2002). Spiral Galaxies with HST/NICMOS. I. Nuclear Morphologies, Color Maps, and Distinct Nuclei. *The Astronomical Journal*, *123*(1), 159–183. https://doi.org/10.1086/324725

Carretta, E., Gratton, R. G., Clementini, G., & Fusi Pecci, F. (2000). Distances, Ages, and Epoch of Formation of Globular Clusters. *The Astrophysical Journal*, *533*(1), 215–235. https://doi.org/10.1086/308629

Carson, D. J., Barth, A. J., Seth, A. C., den Brok, M., Cappellari, M., Greene, J. E., Ho, L. C., & Neumayer, N. (2015). The Strructure of Nuclear Star Clusters in Nearby Late-type Spiral Galaxies from Hubble Space Telescope Wide Field Camera 3 Imaging. *The Astronomical Journal*, *149*(5), 149–170. https://doi.org/10.1088/0004-6256/149/5/170

Cavanagh, M. K., Bekki, K., Groves, B. A., & Pfeffer, J. (2022). The evolution of barred galaxies in the EAGLE simulation. *Monthly Notices of the Royal Astronomical Society*, *510*(4), 5164–5178. https://doi.org/10.1093/\mnras/stab3786

Chabrier, G. (2003). Galactic Stellar and Substellar Initial Mass Function. *The Publications of the Astronomical Society of the Pacific*, *115*(809), 763–795. https://doi.org/10.1086/376392

Chandrasekhar, S. (1943). Dynamical Friction. I. General Considerations: the Coefficient of Dynamical Friction. *The Astrophysical Journal*, *97*, 255. https://doi.org/10.1086/144517

Chattopadhyay, D., Hurley, J., Stevenson, S., & Raidani, A. (2022). Dynamical double black holes and their host cluster properties. *Monthly Notices of the Royal Astronomical Society*, *513*(3), 4527–4555. https://doi.org/10.1093/mnras/stac1163

Chen, Y., Bressan, A., Girardi, L., Marigo, P., Kong, X., & Lanza, A. (2015). PARSEC evolutionary tracks of massive stars up to 350 $M_{\odot}$ at metallicities $0.0001 \leq Z \leq 0.04$. *Monthly Notices of the Royal Astronomical Society*, *452*(1), 1068–1080. https://doi.org/10.1093/\mnras/stv1281

Chen, Y., Girardi, L., Bressan, A., Marigo, P., Barbieri, M., & Kong, X. (2014). Improving PARSEC models for very low mass stars. *Monthly Notices of the Royal Astronomical Society*, *444*(3), 2525–2543. https://doi.org/10.1093/\mnras/stu1605

Chen, Z., Do, T., Ghez, A. M., Hosek, M., Feldmeier-Krause, A., Chu, D., Bentley, R., Lu, J. R., & Morris, M. R. (2022). The Star Formation History of the Milky Way's Nuclear Star Cluster, 37. https://arxiv.org/abs/2212.01397

Chen, Z., Do, T., Ghez, A. M., Hosek, M. W., Feldmeier-Krause, A., Chu, D. S., Bentley, R. O., Lu, J. R., & Morris, M. R. (2023). The Star Formation History of the Milky Way's Nuclear Star Cluster. *The Astrophysical Journal*, *944*(1), 79. https://doi.org/10.3847/1538-4357/aca8ad

Cheng, Z., Li, Z., Xu, X., & Li, X. (2018). A Chandra Survey of Milky Way Globular Clusters. I. Emissivity and Abundance of Weak X-ray Sources. *The Astrophysical Journal*, *858*(1), 33. https://doi.org/10.3847/1538-4357/aaba16

Chevance, M., Kruijssen, J. M. D., Hygate, A. P. S., Schruba, A., Longmore, S. N., Groves, B., Henshaw, J. D., Herrera, C. N., Hughes, A., Jeffreson, S. M. R., Lang, P., Leroy, A. K., Meidt, S. E., Pety, J., Razza, A., Rosolowsky, E., Schinnerer, E., Bigiel, F., Blanc, G. A., . . . Utomo, D. (2020). The lifecycle of molecular clouds in nearby star-forming disc galaxies. *Monthly Notices of the Royal Astronomical Society*, *493*(2), 2872–2909. https://doi.org/10.1093/\mnras/stz3525

Choksi, N., Behroozi, P., Volonteri, M., Schneider, R., Ma, C.-P., Silk, J., & Moster, B. (2017). Recoiling supermassive black hole escape velocities from dark matter haloes. *Monthly Notices of the Royal Astronomical Society*, *472*(2), 1526–1537. https://doi.org/10.1093/\mnras/stx2113

Choksi, N., & Gnedin, O. Y. (2019). Formation of globular cluster systems - II. Impact of the cut-off of the cluster initial mass function. *Monthly Notices of the Royal Astronomical Society*, *486*(1), 331–343. https://doi.org/10.1093/\mnras/stz811

Choksi, N., & Kruijssen, J. M. D. (2021). On the initial mass-radius relation of stellar clusters. *Monthly Notices of the Royal Astronomical Society*, *507*(4), 5492–5506. https://doi.org/10.1093/\mnras/stab2514

Claeyssens, A., Adamo, A., Richard, J., Mahler, G., Messa, M., & Dessauges-Zavadsky, M. (2023). Star formation at the smallest scales: A jwst study of the clump populations in smacs0723. *Monthly Notices of the Royal Astronomical Society*, *520*(2), 2180–2203. https://doi.org/10.1093/mnras/stac3791

Clark, G. W. (1975). X-ray binaries in globular clusters. *The Astrophysical Journal Letters*, *199*, L143–L145. https://doi.org/10.1086/181869

Clontz, C., Seth, A. C., Dotter, A., Häberle, M., Nitschai, M. S., Neumayer, N., Feldmeier-Krause, A., Latour, M., Wang, Z., Souza, S. O., Kacharov, N., Bellini, A., Libralato, M., Pechetti, R., van de Ven, G., & Alfaro-Cuello, M. (2024). oMEGACat. IV. Constraining the Ages of Omega Centauri Subgiant Branch Stars with HST and MUSE. *The Astrophysical Journal*, *977*(1), 14. https://doi.org/10.3847/1538-4357/ad8621

Cohen, J. G., Blakeslee, J. P., & Ryzhov, A. (1998). The Ages and Abundances of a Large Sample of M 87 Globular Clusters. *The Astrophysical Journal*, *496*(2), 808–826. https://doi.org/10.1086/305429

Colbert, E. J. M., Heckman, T. M., Ptak, A. F., Strickland, D. K., & Weaver, K. A. (2004). Old and Young X-Ray Point Source Populations in Nearby Galaxies. *The Astrophysical Journal*, *602*(1), 231–248. https://doi.org/10.1086/380899

Colombo, D., Hughes, A., Schinnerer, E., Meidt, S. E., Leroy, A. K., Pety, J., Dobbs, C. L., García-Burillo, S., Dumas, G., Thompson, T. A., Schuster, K. F., & Kramer, C. (2014). The PdBI Arcsecond Whirpool Survey (PAWS): Environmental Dependence of Giant Molecular Cloud Properties in M 51. *The Astrophysical Journal*, *784*(1), 3. https://doi.org/10.1088/0004-637X/784/1/3

Comparat, J., Luo, W., Merloni, A., More, S., Salvato, M., Krumpe, M., Miyaji, T., Brandt, W., Georgakakis, A., Akiyama, M., Buchner, J., Dwelly, T., Kawaguchi, T., Liu, T., Nagao, T., Nandra, K., Silverman, J., Toba, Y., Anderson, S. F., & Kollmeier, J. (2023). The cosmic web of X-ray active galactic nuclei seen through the eROSITA Final Equatorial Depth Survey (eFEDS). *Astronomy & Astrophysics*, *673*, A122. https://doi.org/10.1051/0004-6361/202245726

Comparat, J., Truong, N., Merloni, A., Pillepich, A., Ponti, G., Driver, S., Bellstedt, S., Liske, J., Aird, J., Brüggen, M., Bulbul, E., Davies, L., Villalba, J. A. G., Georgakakis, A., Haberl, F., Liu, T., Maitra, C., Nandra, K., Popesso, P., . . . Zhang, Y. (2022). The eROSITA Final Equatorial Depth Survey (eFEDS). X-ray emission around star-forming and quiescent galaxies t $0.05 < z < 0.3$. *Astronomy & Astrophysics*, *666*, A156. https://doi.org/10.1051/0004-6361/202243101

Condon, J. J. (1987). A 1.49 GHz Atlas of Spiral Galaxies with $B_T \leq +12$ and $\delta \geq -45°$. *The Astrophysical Journal Supplement Series*, *65*, 485–541. https://doi.org/10.1086/191234

Conroy, C., & Gunn, J. E. (2010, October a). *FSPS: Flexible Stellar Population Synthesis*. http://ascl.net/1010.043

Conroy, C., & Gunn, J. E. (2010b). The Propagation of Uncertainties in Stellar Population Synthesis Modeling. III. Model Calibration, Comparison, and Evaluation. *The Astrophysical Journal*, *712*(2), 833–857. https://doi.org/10.1088/0004-637X/712/2/833

Conroy, C., Gunn, J. E., & White, M. (2009). The Propagation of Uncertainties in Stellar Population Synthesis Modeling. I. The Relevance of Uncertain Aspects of Stellar Evolution and the Initial Mass Function to the Derived Physical Properties of Galaxies. *The Astrophysical Journal*, *699*(1), 486–506. https://doi.org/10.1088/0004-637X/699/1/486

Conroy, C., White, M., & Gunn, J. E. (2010). The Propagation of Uncertainties in Stellar Population Synthesis Modeling. II. The Challenge of Comparing Galaxy Evolution Models to Observations. *The Astrophysical Journal*, *708*(1), 58–70. https://doi.org/10.1088/0004-637X/708/1/58

Conselice, C. J., Grogin, N. A., Jogee, S., Lucas, R. A., Dahlen, T., de Mello, D., Gardner, J. P., Mobasher, B., & Ravindranath, S. (2004). Observing the Formation of the Hubble Sequence in the Great Observatories Origin Deep Survey. *The Astrophysical Journal Letters*, *600*(2), L139–L142. https://doi.org/10.1086/378556

Contenta, F., Balbinot, E., Petts, J. A., Read, J. I., Gieles, M., Collins, M. L. M., Peñarrubia, J., Delmore, M., & A, G. (2018). Probing dark matter with star clusters: a dark matter core in the ultra-faint dwarf Eridanus II. *Monthly Notices of the Royal Astronomical Society*, *476*(3), 3124–3136. https://doi.org/10.1093/mnras/sty424

Cook, D. O., Lee, J. C., Adamo, A., Calzetti, D., Chandar, R., Whitmore, B. C., Aloisi, A., Cignoni, M., Dale, D. A., Elmegreen, B. G., Fumagalli, M., Grasha, K., Johnson, K. E., Kennicutt, R. C., Kim, H., Linden, S. T., Messa, M., Östlin, G., Ryon, J. E., ... Wofford, A. (2023). Fraction of stars in clusters for the LEGUS dwarf galaxies. *Monthly Notices of the Royal Astronomical Society*, *519*(3), 3749–3775. https://doi.org/10.1093/mnras/stac3748

Cook, D. O., Seth, A. C., Dale, D. A., Johnson, L., Clifton, L., Weisz, D. R., Fouesneau, M., Olsen, K. A. G., Engelbracht, C. W., & Dalcanton, J. J. (2012). The ACS Nearby Galaxy Survey Treasury. X. Quantifying the Star Cluster Formation Efficiency of nearby Dwarf Galaxies. *The Astrophysical Journal*, *751*(2), 100. https://doi.org/10.1088/0004-637X/751/2/100

Correnti, M., Gennaro, M., Kalirai, J. S., Brown, T. M., & Calamida, A. (2016). Constraining Globular Cluster Age Unvertainties using the IR Color-Magnitude Diagram. *The Astrophysical Journal*, *823*(1), 18. https://doi.org/10.3847/0004-637X/823/1/18

Costa, A. H., Johnson, K. E., Indebetouw, R., Finn, M. K., Brogan, C. L., & Reines, A. (2021). Toward a More Complex Understanding of Natal Super Star Clusters with Multiwavelength Observations. *The Astrophysical Journal*, *918*(2), 76. https://doi.org/10.3847/1538-4357/ac0e93

Côté, P., Blakeslee, J. P., Ferrarese, L., Jordán, A., Mei, S., Merritt, D., Milosavljević, M., Peng, E. W., Tonry, J. L., & West, M. J. (2004). The ACS Virgo Cluster Survey. I. Introduction to the Survey. *The Astrophysical Journal Supplement Series*, *153*(1), 223–242. https://doi.org/10.1086/421490

Côté, P., Piatek, S., Ferrarese, L., Jordán, A., Merritt, D., Peng, E. W., Haşegan, M., Blakeslee, J. P., Mei, S., West, M. J., Milosavljević, M., & Tonry, J. L. (2006). The ACS Virgo Cluster Survey. VIII. The Nuclei of Early-Type Galaxies. *The Astrophysical Journal Supplement Series*, *165*(1), 57–94. https://doi.org/10.1086/504042

Crain, R. A., Schaye, J., Bower, R. G., Furlong, M., Schaller, M., Theuns, T., Dalla Vecchia, C., Frenk, C. S., McCarthy, I. G., Helly, J. C., Jenkins, A., Rosas-Guevara, Y. M., White, S. D. M., & Trayford, J. W. (2015). The EAGLE simulations of galaxy formation: calibration of subgrid physics and model variations. *Monthly Notices of the Royal Astronomical Society*, *450*(2), 1937–1961. https://doi.org/10.1093/\mnras/stv725

Cresci, G., Vanzi, L., Lanzuisi, G., Brusa, M., Mingozzi, M., Sauvage, M., & Johnson, K. (2017). The MUSE view of the He 2-10: No AGN ionization but a sparkling starburst. *Astronomy & Astrophysics*, *604*, A101. https://doi.org/10.1051/0004-6361/201730876

Cresci, G., Vanzi, L., Sauvage, M., Santangelo, G., & van der Werf, P. (2010). Integral-field near-infrared spectroscopy of the two blue dwarf galaxies: NGC 5253 and He 2-10. *Astronomy & Astrophysics*, *520*, A82. https://doi.org/10.1051/0004-6361/201014864

Crnojević, D., Sand, D. J., Zaritsky, D., Spekkens, K., Willman, B., & Hargis, J. R. (2016). Deep Imaging of Eridanus II and Its Lone Star Cluster. *The Astrophysical Journal Letters*, *824*(1), L14. https://doi.org/10.3847/2041-8205/824/1/L14

Croton, D. J. (2006). Evolution in the black hole mass-bulge mass relation: a theoretical perspective. *Monthly Notices of the Royal Astronomical Society*, *369*(4), 1808–1812. https://doi.org/10.1111/j.1365-2966.2006.10429.x

Croton, D. J., Springel, V., White, S. D. M., De Lucia, G., Frenk, C. S., Gao, L., Jenkins, A., Kauffmann, G., Navarro, J. F., & Yoshida, N. (2006). The many lives of active galactic nuclei: cooling flows, black holes and the luminosities and colours of galaxies. *Monthly Notices of the Royal Astronomical Society*, *365*(1), 11–28. https://doi.org/10.1111/j.1365-2966.2005.09675.x

Cutri, R. M., Wright, E. L., Conrow, T., Fowler, J. W., Eisenhardt, P. R. M., Grillmair, C., Kirkpatrick, J. D., Masci, F., McCallon, H. L., Wheelock, S. L., Fajardo-Acosta, S., Yan, L., benford, D., Harbut, M., Jarrett, T., Lake, S., Leisawitz, D., Ressler, M. E., Stanford, S. A., ... Wittman, M. (2013). Explanatory Supplement to the AllWISE Data Release Products. https://wise2.ipac.caltech.edu/docs/release/allwise/expsup/index.html

da Silva, R. L., Fumagalli, M., & Krumholz, M. (2012). SLUG–Stochastically Lighting Up Galaxies. I. Methods and Validating Tests. *The Astrophysical Journal*, *745*(2), 145. https://doi.org/10.1088/0004-637X/745/2/145

da Silva, R. L., Fumagalli, M., & Krumholz, M. (2014). SLUG–Stochastically Lighting Up Galaxies. II. Quantifying the effects of stochasticity on star formation rate indicators. *Monthly Notices of the Royal Astronomical*

Society, *444*(4), 3275–3287. https://doi.org/10.1093/\mnras/stu1688

Dashyan, G., Silk, J., Mamon, G. A., Dubois, Y., & Hartwig, T. (2018). AGN feedback in dwarf galaxies? *Monthly Notices of the Royal Astronomical Society*, *473*(4), 5698–5703. https://doi.org/10.1093/mnras/stx2716

Davies, B., de La Fuente, D., Najarro, F., Hinton, J. A., Trombley, C., Figer, D. F., & Puga, E. (2012). A newly discovered young massive star cluster at the far end of the Galactic Bar. *Monthly Notices of the Royal Astronomical Society*, *419*(3), 1860–1870. https://doi.org/10.1111/j.1365-2966.2011.19840.x

Davis, A. B., Nierenberg, A. M., Peter, A. H. G., garling, C. T., Greco, J. P., Kochanek, C. S., Utomo, D., Casey, K. J., Pogge, R. W., Roberts, D. M., Sand, D. J., & Sardone, A. (2021). The LBT satellites of Nearby Galaxies Survey (LBT-SONG): the satellite population of NGC 628. *Monthly Notices of the Royal Astronomical Society*, *500*(3), 3854–3869. https://doi.org/10.1093/\mnras/staa3246

Davis, M., Efstathiou, G., Frenk, C. S., & White, S. D. M. (1985). The evolution of large-scale structure in a universe dominated by cold dark matter. *The Astrophysical Journal*, *292*, 371–394. https://doi.org/10.1086/163168

de Grijs, R., Ma, C., Jia, S., Ho, L. C., & Anders, P. (2017). Young star clusters in circumnuclear starburst rings. *Monthly Notices of the Royal Astronomical Society*, *465*(3), 2820–2832. https://doi.org/10.1093/mnras/stw2806

De Lucia, G., & Blaizot, J. (2007). The hierarchical formation of the brightest cluster galaxies. *Monthly Notices of the Royal Astronomical Society*, *375*(1), 2–14. https://doi.org/10.1111/j.1365-2966.2006.11287.x

De Lucia, G., Kruijssen, J. M. D., Trujillo-Gomez, S., Hirschmann, M., & Xie, L. (2024). On the origin of globular clusters in a hierarchical universe. *Monthly Notices of the Royal Astronomical Society*, *530*(3), 2760–2777. https://doi.org/10.1093/mnras/stae1006

De Lucia, G., Tornatore, L., Frenk, C. S., Helmi, A., Navarro, J. F., & White, S. D. M. (2014). Elemental abundances in Milky Way-like galaxies from a hierarchical galaxy formation model. *Monthly Notices of the Royal Astronomical Society*, *445*(1), 970–987. https://doi.org/10.1093/mnras/stu1752

Decin, L. (2021). Evolution and Mass Loss of Cool Agein Stars: a Daedalean Story. *Annual Review of Astronomy and Astrophysics*, *59*, 337–389. https://doi.org/10.1146/annurev-astro-090120-033712

Dehnen, W. (2005). Phase-space mixing and the merging of cusps. *Monthly Notices of the Royal Astronomical Society*, *360*(3), 892–900. https://doi.org/10.1111/j.1365-2966.2005.09099.x

del P. Lagos, C., Bravo, M., Tobar, R., Obreschkow, D., Power, C., Robotham, A. S. G., Proctor, K. L., Hansen, S., Chandro-Gómez, Á., & Carrivick, J. (2024). Quenching massive galaxies across cosmic time with the semi-analytical model SHARK V2.0. *Monthly Notices of the Royal Astronomical Society*, *531*(3), 3551–3578. https://doi.org/10.1093/mnras/stae1024

den Brok, J. S., Chatzigiannakis, D., Bigiel, F., Pischnig, J., Barnes, A. T., Leroy, A. K., Jiménez-Donaire, M. J., Usero, A., Schinnerer, E., Rosolovsky, E., Faesi, C. M., Grasha, K., Hughes, A., Kruijssen, J. M. D., Liu, D., Neumann, L., Pety, J., Querejeta, M., Saito, T., . . . Stuber, S. (2021). New constraints on the ^{12}CO(2-1)/(1-0) line ratio across nearby disc galaxies. *Monthly Notices of the Royal Astronomical Society*, *504*(3), 3221–3245. https://doi.org/10.1093/\mnras/stab859

den Brok, M., Peletier, R. F., Seth, A. C., Balcells, M., Dominguez, L., Graham, A. W., Carter, D., Erwin, P., Ferguson, H. C., Goudfrooij, P., Guzmán, R., Hoyos, C., Jogee, S., Lucey, J., Phillipps, S., Puzia, T., Valentijn, E., Verdoes Kleijn, G., & Weinzirl, T. (2014). The HST/ACS Coma Cluster Survey - X. Nuclear star clusters in low-mass early-type galaxies: scaling relations. *Monthly Notices of the Royal Astronomical Society*, *445*(3), 2385–2403. https://doi.org/10.1093/\mnras/stu1906

Devereux, N., Ford, H., Tsvetanov, Z., & Jacoby, G. (2003). STIS Spectroscopy of the Central 10 Parsecs of M 81: Evidence for a Massive Black Hole. *The Astronomical Journal*, *125*(3), 1226–1235. https://doi.org/10.1086/367595

Dillamore, A. M., Monty, S., Belokurov, V., & Evans, N. W. (2024). Trojan Globular CLusters: Radial Migration via Trapping in Bar Resonances. *The Astrophysical Journal Letters*, *971*(1), L4. https://doi.org/10.3847/2041-8213/ad60c8

Do, T., Ghez, A. M., Morris, M. R., Lu, J. R., Matthews, K., Yelda, S., & Larkin, J. (2009). High Angular Resolution Integral-Field Spectroscopy of the Galaxy's Nuclear Cluster: A Missing Stellar Cusp? *The Astrophysical Journal*, *703*(2), 1323–1337. https://doi.org/10.1088/0004-637X/703/2/1323

Do, T., Kerzendorf, W., Winsor, N., Støstad, M., Morris, M. R., Lu, J. R., & Ghez, A. M. (2015). Discovery of Low-metallicity Stars in the Central Parsec of the Milky Way. *The Astrophysical Journal*, *809*(2), 143. https://doi.org/10.1088/0004-637X/809/2/143

Dobbs, C. L., Burkert, A., & Pringle, J. E. (2011). The properties of the interstellar medium in disc galaxies with stellar feedback. *Monthly Notices of the Royal Astronomical Society*, *417*(2), 1318–1334. https://doi.org/10.1111/j.1365-2966.2011.19346.x

Dolag, K., Borgani, S., Murante, G., & Springel, V. (2009). Substructures in hydrodynamical cluster simulations. *Monthly Notices of the Royal Astronomical Society*, *399*(2), 497–514. https://doi.org/10.1111/j.1365-2966.2009.15034.x

Dolfi, A., Pfeffer, J., Forbes, D. A., Couch, W. J., Bekki, K., Brodie, J. P., Romanowsky, A. J., & Kruijssen, J. M. D. (2022). The present-day globular cluster kinematics of lenticular galaxies from the E-MOSAICS simulations and their relation to the galaxy assembly histories. *Monthly Notices of the Royal Astronomical Society*, *511*(3), 3179–3197. https://doi.org/10.1093/mnras/stac258

Dolphin, A. E. (2009). A Revised Characterization of the WFPC2 CTE Loss. *Publications of the Astronomical Society of the Pacific*, *121*(880), 655. https://doi.org/10.1086/600028

Dong, X. Y., & De Robertis, M. M. (2006). Low-Luminosity Active Galaxies and Their Central Black

Holes. *The Astronomical Journal*, *131*(3), 1236–1252. https://doi.org/10.1086/499334

Downes, D., & Solomon, P. M. (1998). Rotating Nuclear Rings and Extreme Starbursts in Ultraluminous Galaxies. *The Astrophysical Journal*, *507*(2), 615–654. https://doi.org/10.1086/306339

Downing, J. M. B. (2012). Is there a size difference between red and blue globular clusters? *Monthly Notices of the Royal Astronomical Society*, *425*(3), 2234–2243. https://doi.org/10.1111/j.1365-2966.2012.21680.x

Drinkwater, M. J., Jones, J. B., Grerr, M. D., & Phillipps, S. (2000). Compact Stellar Systems in the Fornax Cluster: Super-massive Star Clusters or Extremely Compact Dwarf Galaxies? *Publications of the Astronomical Society of Australia*, *17*(3), 227–233. https://doi.org/10.1071/AS00034

Du, W., Cheng, C., Zheng, Z., & Wu, H. (2020). Stellar Mass and Stellar Mass-to-light Ratio-Color Relations for Low Surface Brightness Galaxies. *The Astronomical Journal*, *159*(4), 138. https://doi.org/10.3847/1538-3881/ab6efb

Dullo, B. T., Knapen, J. H., Baldi, R. D., Williams, D. R. A., Beswick, R. J., McHardy, I. M., Green, D. A., Gil de Paz, A., Aalto, S., Alberdi, A., Argo, M. K., Gallagher, J. S., Klöckner, H.-R., Miltie, I. M., Saikia, D. J., Saikia, P., Stevens, I. R., & Torrejón, S. (2024). LeMMINGs. Multiwavelength constraints on the co-existence of nuclear star clusters and AGN in nucleated galaxies. *Monthly Notices of the Royal Astronomical Society*, *532*(4), 4729–4751. https://doi.org/10.1093/mnras/stae1732

Dumont, A., Seth, A. C., Strader, J., Voggel, K., Sand, D. J., Hughes, A. K., Caldwell, N., Crnojević, D., Mateo, M., Bailey, J. I., & Forbes, D. A. (2022). A Population of Luminous Globular Clusters and Stripped Nuclei with Elevated Mass to Light Ratios around NGC 5128. *The Astrophysical Journal*, *929*(2), 147. https://doi.org/10.3847/1538-4357/ac551c

Duras, F., Bongiorno, A., Ricci, F., Piconcelli, E., Shankar, F., Lusso, E., Bianchini, S., Fiore, F., Maiolino, R., Marconi, A., Onori, F., Santi, E., Schneider, R., Vignali, C., & La Franca, F. (2020). Universal bolometric corrections for active galactic nuclei over seven luminosity decades. *Astronomy & Astrophysics*, *636*, A73. https://doi.org/10.1051/0004-6361/201936817

Dutil, Y., & Roy, J.-R. (1999). Chemical Evidence for Morphological Evolution of Spiral Galaxies. *The Astrophysical Journal*, *516*(1), 62–76. https://doi.org/10.1086/307100

Dutton, A. A., & Macció, A. V. (2014). Cold dark matter haloes in the Planck era: evolution of structural parameters for Einasto and NFW profiles. *Monthly Notices of the Royal Astronomical Society*, *441*(4), 3359–3374. https://doi.org/10.1093/\mnras/stu742

Eigenthaler, P., Puzia, T. H., Taylor, M. A., Ordenes-Briceño, Y., Muñoz, R. P., Ribbeck, K. X., Alamo-Martínez, K. A., Zhang, H., Ángel, S., Capaccioli, M., Côté, P., Ferrarese, L., Galaz, G., Grebel, E. K., Hempel, M., Hilker, M., Lançon, A., Mieske, S., Miller, B., . . . Spengler, C. (2018). The Next Generation Fornax Survey (NGFS). II. The Central Dwarf Galaxy Population. *The Astrophysical Journal*, *855*(2), 142. https://doi.org/10.3847/1538-4357/aaab60

Ekström, S., Georgy, C., Eggenberger, P., Meynet, G., Mowlavi, N., Wyttenbach, A., Granada, A., Decressin, T., Hirschi, R., Frischknecht, U., Charbonnel, C., & Maeder, A. (2012). Grids of stellar models with rotation. I. Models from 0.8 to 120 $M_\odot$ at solar metallicity ($Z = 0.014$). *Astronomy & Astrophysics*, *537*, A146. https://doi.org/10.1051/0004-6361/201117751

El-Badry, K., Quataert, E., Weisz, D. R., Choksi, N., & Boylan-Kolchin, M. (2019). The formation and hierarchical assembly of globular cluster populations. *Monthly Notices of the Royal Astronomical Society*, *482*(4), 4528–4552. https://doi.org/10.1093/\mnras/sty3007

Elmegreen, B., & Lahén, N. (2024). Spatial segregation of massive clusters in a simulation of colliding dwarf galaxies. *The Open Journal of Astrophysics*, *7*, 68. https://doi.org/10.33232/001c.122504

Elmegreen, D. M., & Elmegreen, B. G. (1984). Blue and near-infrared surface photometry of spiral strucutre in 34 nonbarred grand design and flocculent galaxies. *The Astrophysical Journal Supplement Series*, *54*, 127–149. https://doi.org/10.1086/190922

Elmegreen, D. M., Elmegreen, B. G., Ravindranath, S., & Coe, D. A. (2007). Resolved Galaxies in the Hubble Ultra Deep Field: Star Formation in Disks at High Redshift. *The Astrophysical Journal*, *658*(2), 763–777. https://doi.org/10.1068/511667

Emig, K. L., Bolatto, A. D., Leroy, A. K., Mills, E. A. C., Jiménez Donaire, M. J., Tielens, A. G. G. M., Ginsburg, A., Gorski, M., Krieger, N., Levy, R. C., Meier, D. S., Ott, J., Rosolowsky, E., Thompson, T. A., & Veilleux, S. (2020). Super Star Clusters in the Central Starburst of NGC 4945. *The Astrophysical Journal*, *903*(1), 50. https://doi.org/10.3847/1538-4357/abb67d

Emsellem, E., Schinnerer, E., Santoro, F., Belfiore, F., Pessa, I., McElroy, R., Blanc, G. A., Congiu, E., Groves, B., Ho, I.-T., Kreckel, K., Razza, A., Sanchez-Blazquez, P., Egorov, O., Faesi, C., Klessen, R. S., Leroy, A. K., Meidt, S., Querejeta, M., . . . Williams, T. G. (2022). The PHANGS-MUSE survey. Probing the chemo-dynamical evolution of disc galaxies. *Astronomy & Astrophysics*, *659*, A191. https://doi.org/10.1051/0004-6361/202141727

Emsellem, E., & van de Ven, G. (2008). Formation of Central Massive Objects via Tidal Compression. *The Astrophysical Journal*, *674*(2), 653–659. https://doi.org/10.1086/524720

Erwin, P. (2015). IMFIT: A Fast, Flexible New Program for Astronomicla Image Fitting. *The Astrophysical Journal*, *799*(2), 226–251. https://doi.org/10.1088/0004-637X/799/2/226

Erwin, P., & Gadotti, D. A. (2012). Do Nuclear Star Clusters and Supermassive Black Holes Follow the Same Host-Galaxy Correlations? *Advances in Astronomy*, *2012*, 946368. https://doi.org/10.1155/2012/946368

Escala, A., Larson, R. B., Coppi, P. S., & Mardones, D. (2004). The Role of Gas in the Merging of Massive Black Holes in Galactic Nuclei. I. Black Hole Merging in a Spherical Gas Cloud. *The Astrophysical Journal*, *607*(2), 765–777. https://doi.org/10.1086/386278

Escudero, C. G., Faifer, F. R., Bassino, L. P., Calderón, J. P., & Caso, J. P. (2015). The extremely populated globular cluster system of the lenticular galaxy NGC 6861. *Monthly Notices of the Royal Astronomical Society*, *449*(1), 612–628. https://doi.org/10.1093/mnras/stv283

Esquej, P., Saxton, R. D., Komossa, S., Read, A. M., Freyberg, M. J., Hasinger, G., García-Hernández, D. A., Lu, H., Rodriguez Zaurín, J., Sánchez-Portal, M., & Zhou, H. (2008). Evolution of tidal disruption candidates discovered by XMM-Newton. *Astronomy & Astrophysics*, *489*(2), 543–554. https://doi.org/10.1051/0004-6361:200810110

Euclid Collaboration. (2024a). Euclid: Early Release Observations – Dwarf galaxies in the Perseus galaxy cluster. *arXiv e-prints*, arXiv:2405.13502. https://doi.org/10.48550/arXiv.2405.13502

Euclid Collaboration. (2024b). Euclid: Early Release Observations – The intracluster light and intracluster globular clusters of the Perseus cluster. *arXiv e-prints*, arXiv:2405.13503. https://doi.org/10.48550/arXiv.2405.13503

Euclid Collaboration. (2024c). Euclid: Early Release Observations – Unveiling the morphology of two Milky Way globular clusters out to their periphery. *arXiv e-prints*, arXiv:2405.13498. https://doi.org/10.48550/arXiv.2405.13498

Euclid Collaboration. (2024d). Euclid. I. Overview of the Euclid mission. *arXiv e-prints*, arXiv:2405.13491. https://doi.org/10.48550/arXiv.2405.13491

Euclid Collaboration. (2024e). Euclid. II. The VIS Instrument. *arXiv e-prints*, arXiv:2405.13492. https://doi.org/10.48550/arXiv.2405.13492

Euclid Collaboration. (2024f). Eulicd: Early Release Observations – Globular clusters in the Fornax galaxy cluster, from dwarf galaxies to the intracluster field. *arXiv e-prints*, arXiv:2405.13500. https://doi.org/10.48550/arXiv.2405.134500

Euclid Collaboration. (2025a). Euclid preparation: LVIII. Detecting extragalactic globular clusters in the Euclid survey. *Astronomy & Asrophysics*, *693*, A251. https://doi.org/10.1051/0004-6361/202450851

Euclid Collaboration. (2025b). Euclid Quick Data Release (Q1) - Data release overview. *arXiv e-prints*, arXiv:2503.15302. https://doi.org/10.48550/arXiv.2503.15302

Euclid Collaboration. (2025c). Euclid: Quick Data Release (Q1) – A census of dwarf galaxies across a range of distances and environments. *arXiv e-prints*, arXiv:2503.15335. https://doi.org/10.48550/arXiv.2503.15335

Evans, I. N., Primini, F. A., Glotfelty, K. J., Anderson, C. S., Bonaventura, N. R., Chen, J. C., Davis, J. E., Doe, S. M., Evans, J. D., Fabbiano, G., Galle, E. C., Gibbs, D. G., Grier, J. D., Hain, R. M., Hall, D. M., Harbo, P. N., Xe, X. H., Houck, J. C., Karovska, M., . . . Zogfrafou, P. (2010). The Chandra Source Catalog. *The Astrophysical Journal Supplement Series*, *189*(1), 37–82. https://doi.org/10.1088/0067-0049/189/1/37

Evans, P. A., Nixon, C. J., Campana, S., Charalampopoulos, P., Perley, D. A., Breeveld, A. A., Page, K. L., Oates, S. R., Eyles-Ferris, R. A. J., Malesani, D. B., Izzo, L., Goad, M. R., O'Brien, P., Osborne, J. P., & Sbarufatti, B. (2023). Monthly quasi-periodic eruptions from repeated stellar disruption by a massive black hole. *Nature Astronomy*, *7*, 1368–1375. https://doi.org/10.1038/s41550-023-02073-y

Fahrion, K., Böker, T., Perna, M., Beck, T. L., Maiolino, R., Arribas, S., Bunker, A. J., Charlot, S., Ceci, M., Cresci, G., De Marchi, G., Lützgendorf, N., & Ulivi, L. (2024). Growing a nuclear star cluster from star formation and cluster mgerers: The JWST NIRSpec view of NGC 4654. *Astronomy & Astrophysics*, *687*, A83. https://doi.org/10.1051/0004-6361/202449629

Fahrion, K., Bulichi, T.-E., Hilker, M., Leaman, R., Lyubenova, M., Müller, O., Neumayer, N., Pinna, F., Rejkuba, M., & van de Ven, G. (2022a). Nuclear star cluster formation in star-forming dwarf galaxies. *Astronomy & Astrophysics*, *667*, A101. https://doi.org/10.1051/0004-6361/202244932

Fahrion, K., Leaman, R., Lyubenova, M., & van de Ven, G. (2022b). Disentangling the formation mechanisms of nuclear star clusters. *Astronomy & Astrophysics*, *658*, A172. https://doi.org/10.1051/0004-6361/202039778

Fahrion, K., Lyubenova, M., Hilker, M., van de Ven, G., Falcón-Barroso, J., Leaman, R., Martín-Navarro, I., Bittner, A., Coccato, L., Corsini, E. M., Gadotti, D. A., Iodice, E., McDermid, R. M., Pinna, F., Sarzi, M., Viaene, S., de Zeeuw, P. T., & Zhu, L. (2020a). The Fornax 3D project: Globular clusters tracing kinematics and metallicities. *Astronomy & Astrophysics*, *637*, A26. https://doi.org/10.1051/0004-6361/202037685

Fahrion, K., Lyubenova, M., van de Ven, G., Hilker, M., Leaman, R., Falcó-Barroso, J., Bittner, A., Coccato, L., Corsini, E. M., Gadotti, D. A., Iodice, E., McDermid, R. M., Martín-Navarro, I., Pinna, F., Poci, A., Sarzi, M., de Zeeuw, P. T., & Zhu, L. (2021). Diversity of nuclear star cluster formation mechanisms revealed by their star formation histories. *Astronomy & Astrophysics*, *650*, A137. https://doi.org/10.1051/0004-6361/202140644

Fahrion, K., Lyubenova, M., van de Ven, G., Leaman, R., Hilker, M., Martín-Navarro, I., Zhu, L., Alfaro-Cuello, M., Coccato, L., Corsini, E. M., Falcón-Barroso, J., Iodice, E., McDermid, R. M., Sarzi, M., & de Zeeuw, T. (2019). Constraining nuclear star cluster formation using MUSE-AO observations of the early-type galaxy FCC 47. *Asronomy & Astrophysics*, *628*, A92. https://doi.org/10.1051/0004-6361/201935832

Fahrion, K., Müller, O., Rejkuba, M., Hilker, M., Lyubenova, M., van de Ven, G., Georgiev, I. Y., Lelli, F., Pawlowski, M. S., & Jerjen, H. (2020b). Metal-poor nuclear star clusters in two dwarf galaxies near Centaurus A suggestion formation from the in-spiraling of globular clusters. *Astronomy & Astrophysics*, *634*, A53. https://doi.org/10.1051/0004-6361/201937120

Fathi, K., Backman, J. E., Zurita, A., Relaño, M., Knapen, J. H., Daigle, O., Hernandez, O., & Carignan, C. (2007). Evolution of structure in late-type spiral galaxies. I. Ionized gas kinematics in NGC 628. *Astronomy & Astrophysics*, *466*(3), 905–916. https://doi.org/10.1051/0004-6361:20066990

Feldmeier, A., Neumayer, N., Seth, A., Schödel, R., Lützgendorf, N., de Zeeuw, P. T., Kissler-Patig, M., Nishiyama, S., & Walcher, C. J. (2014). Large scale kinematics and dynamical modelling of the Milky Way nuclear star cluster. *Astronomy & Astrophysics*, *570*, A2. https://doi.org/10.1051/0004-6361/201423777

Feldmeier-Krause, A., Kerzendorf, W., Do, T., Nogueras-Lara, F., Neumayer, N., Walcher, C. J., Seth, A. C., Schödel, R., de Zeeuw, P. T., Hilker, M., Lützgendorf, N., Kuntschner, H., & Kissler-Patig, M. (2020). Asymmetric spatial distribution of subsolar metallicity stars in the Milky Way nuclear star cluster. *Monthly Notices of the Royal Astronomical Society*, *494*(1), 396–410. https://doi.org/10.1093/\mnras/staa703

Feldmeier-Krause, A., Kerzendorf, W., Neumayer, N., Schödel, R., Nogueras-Lara, F., Do, T., de Zeeuw, P. T., & Kuntschner, H. (2017a). KMOWS view of the Galacitc Centre – II. Metallicity distribution of late-type stars. *Monthly Notices of the Royal Astronomical Society*, *464*(1), 194–209. https://doi.org/10.1093/\mnras/stw2339

Feldmeier-Krause, A., Neumayer, N., Schödel, R., Seth, A. C., Hilker, M., de Zeeuw, P. T., Kuntschner, H., Walcher, C. J., Lützgendorf, N., & Kissler-Patig, M. (2015). KMOS view of the Galactic centre. I. Young stars are centrally concentrated. *Astronomy & Astrophysics*, *584*, A2. https://doi.org/10.1051/0004-6361/201526336

Feldmeier-Krause, A., Zhu, L., Neumayer, N., van de Ven, G., de Zeeuw, P. T., & Schödel, R. (2017b). Triaxial orbit-based modelling of the Milky Way Nuclear Star Cluster. *Monthly Notices of the Royal Astronomical Society*, *466*(4), 4040–4052. https://doi.org/10.1093/\mnras/stw3377

Fellhauer, M., & Kroupa, P. (2002). The formation of ultracompact dwarf galaxies. *Monthly Notices of the Royal Astronomical Society*, *330*(3), 642–650. https://doi.org/10.1046/j.1365-8711.2002.05087.x

Fellhauer, M., & Kroupa, P. (2005). A possible formation scenario for the ultramassive cluster W3 in NGC 7252. *Monthly Notices of the Royal Astronomical Society*, *359*(1), 223–227. https://doi.org/10.1111/j.1365-2966.2005.08891.x

Feng, C.-C., Lin, L.-H., Wang, H.-H., & Taam, R. E. (2014). Spiral density waves in m 81. i. stellar spiral density waves. *The Astrophysical Journal*, *785*(2), 103. https://doi.org/10.1088/0004-637X/785/2/103

Fensch, J., van der Burg, R. F. J., Jeřábková, T., Emsellem, E., Zanella, A., Agnello, A., Hilker, M., Müller, O., Rejkuba, M., Duc, P.-A., Durrell, P., Habas, R., Lim, S., Marleau, F. R., Peng, E. W., & Sánchez-Janssen, R. (2019). The ultra-diffuse galaxy NGC 1052-DF2 with MUSE. II. The population of DF2: stars, clusters, and planetary nebulae. *Astronomy & Astrophysics*, *625*, A77. https://doi.org/10.1051/0004-6361/201834911

Ferrarese, L., Côté, P., Cuillandre, J.-C., Gwyn, S. D. J., Peng, E. W., MacArthur, L. A., Duc, P.-A., Boselli, A., Mei, S., Erben, T., McConnachie, A. W., Durrell, P. R., Mihos, J. C., Jordán, A., Lançon, A., Puzia, T. H., Emsellem, E., Balogh, M. L., Blakeslee, J. P., . . . Manset, N. (2012). The Next Generation Virgo Cluster Survey (NGVS). I. Introduction to the Survey. *The Astrophysical Journal Series*, *200*(1), 4. https://doi.org/10.1088/0067-0049/200/1/4

Ferrarese, L., Côté, P., Dalla Bontá, E., Peng, E. W., Merritt, D., Jordán, A., Blakeslee, J. P., Haşegan, M., Mei, S., Piatek, S., Tonry, J. L., & West, M. J. (2006). A Fundamental Relation between Compact Stellar Nuclei, Supermassive Black Holes, and Their Host Galaxies. *The Astronomical Journal*, *644*(1), L21–L24. https://doi.org/10.1086/505388

Ferrarese, L., Côté, P., MacArthur, L. A., Durrell, P. R., Gwyn, S. D. J., Duc, P.-A., Sánchez-Janssen, R., Santos, M., Blakeslee, J. P., Boselli, A., Boyer, F., Cantiello, M., Courteau, S., Cuillandre, J.-C., Emsellem, E., Erben, T., Gavazzi, G., Guhathakurta, P., Huertas-Company, M., . . . Zhang, H. (2020). The Next Generation Virgo CLuster Survey (NGVS). XIV. The Discovery of Low-mass Galaxies and a New Galaxy Catalog in the Core of the Virgo Cluster. *The Astrophysical Journal*, *890*(2), 128–235. https://doi.org/10.3847/1538-4357/ab339f

Filion, C., McClure, R. L., Weinberg, M. D., D'Onghia, E., & Daniel, K. J. (2023). The Non-Axisymmetric Influence: Radius- and Angle-Dependent Trends in a Barred Galaxy. *Monthly Notices of the Royal Astronomical Society*, *524*(1), 276–287. https://doi.org/10.1093/mnras/stad1832

Filippenko, A. V., & Ho, L. C. (2003). A Low-Mass Central Black Hole in the Bulgeless Seyfert 1 Galaxy NGC 4395. *The Astrophysical Journal Letters*, *588*(1), L13–L16. https://doi.org/10.1086/375361

Fitzpatrick, E. L. (1999). Correcting for the Effects of Interstellar Extinction. *The Publication of the Astronomical Society of the Pacific*, *111*(755), 63–75. https://doi.org/10.1086/316293

Flynn, C., Holmberg, J., Portinari, L., Fuchs, B., & Jahreiß, H. (2006). On the mass-to-light ratio of the local Galactic disc and the optical luminosity of the Galaxy. *Monthly Notices of the Royal Astronomical Society*, *372*(3), 1149–1160. https://doi.org/10.1111/j.1365-2966.2006.10911.x

Foord, A., Gallo, E., Hodges-Kluck, E., Miller, B. P., Baldassare, V. F., Gültekin, K., & Gnedin, O. Y. (2017). AGN Activity in Nucleated Galaxies as Measured by Chandra. *The Astrophysical Journal*, *841*(1), 51. https://doi.org/10.3847/1538-4357/aa6d63

Forbes, D. A., Bastian, N., Gieles, M., Crain, R. A., Kruijssen, J. M. D., Larsen, S. S., Ploeckinger, S., Agertz, O., Trenti, M., Ferguson, A. M. N., Pfeffer, J., & Gnedin, O. Y. (2018). Globular cluster formation and evolution in the context of cosmological galaxy assembly: open questions. *Proceedings of the Royal Society of London Series A*, *474*(2210), 20170616. https://doi.org/10.1098/rspa.2017.0616

Forbes, D. A., & Bridges, T. (2010). Accreted versus in situ Milky Way globular clusters. *Monthly Notices of the Royal Astronomical Society*, *404*(3), 1203–1214. https://doi.org/10.1111/j.1365-2966.2010.16373.x

Forbes, D. A., & Romanowsky, A. J. (2023). Reconstructing the genesis of a globular cluster system at a look-back time of 9.1 Gyr with the *JWST*. *Monthly Notices of the Royal Astronomical Society*, *520*(1), L58–L62. https://doi.org/10.1093/mnrasl/slac162

Förster Schreiber, N. M., Shapley, A. E., Erb, D. K., Genzel, R., Steidel, C. C., Bouché, N., Cresci, G., & Davies, R. (2011). Constraints on the Assembly and Dynamics of Galaxies. I. Detailed Rest-frame Optical Morphologies on Kiloparsec Scale of $z \sim 2$ Star-

forming Galaxies. *The Astrophysical Journal*, *731*(1), 65. https://doi.org/10.1088/0004-637X/731/1/65
Fragione, G. (2022). Mergers of Supermassive and Intermediate-mass Black Holes in Galactic Nuclei from Disruptions of Star Clusters. *The Astrophysical Journal*, *939*(2), 97. https://doi.org/10.3847/1538-4357/ac98b6
Fragione, G., Antonini, F., & Gnedin, O. Y. (2018). Disrupted globular clusters and the gamma-ray excess in the Galactic Centre. *Monthly Notices of the Royal Astronomical Society*, *475*(4), 5313–5321. https://doi.org/10.1093/mnras/sty183
Fragione, G., Loeb, A., Kocsis, B., & Rasio, F. A. (2022). Merger Rates of Intermediate-mass Black Hole Binaries in Nuclear Star Clusters. *The Astrophysical Journal*, *933*(2), 170. https://doi.org/10.3847/1538-4357/ac75d0
Fragkoudi, F., Athanassoula, E., & Bosma, A. (2016). A close look at secular evolution: boxy/peanut bulges reduce gas inflow to the central kiloparsecs. *Monthly Notices of the Royal Astronomical Society*, *462*(1), L41–L45. https://doi.org/10.1093/mnrasl/slw120
Freeman, K. C. (1970). On the Disks of Spiral and S0 Galaxies. *The Astrophysical Journal*, *160*, 811. https://doi.org/10.1086/150474
Friedli, D., & Benz, W. (1995). Secular evolution of isolated barred galaxies. II. Coupling between stars and interstellar medium via star formation. *Astronomy & Astrophysics*, *301*(1), 649–665. https://ui.adsabs.harvard.edu/abs/1995A%5C%2526A...301..649F
Fritz, T. K., Chatzopoulos, S., Gerhard, O., Gillessen, S., Genzel, R., Pfuhl, O., Tacchella, S., Eisenhauer, F., & Ott, T. (2016). The Nuclear Cluster of the Milky Way: Total Mass and Luminosity. *The Astrophysical Journal*, *821*(1), 44. https://doi.org/10.3847/0004-637X/821/1/44
Fruchter, A. S., Hack, W., Dencheva, N., Droettboom, M., & Greenfield, P. (2010, July 21–23). BetaDrizzle: A Redesign of the MultiDrizzle Package. In S. Deustua & C. Oliveira (Eds.), *STScI Calibration Workshop* (pp. 376–381). Space Telescope Science Institute. https://ui.adsabs.harvard.edu/abs/2010bdrz.conf..382F
Fruchter, A. S., & Hook, R. N. (1997). Novel image reconstruction method applied to deep Hubble space telescope images. In A. G. Tescher (Ed.), *Applications of Digital Image Processing XX* (pp. 120–125, Vol. 3164). https://doi.org/10.1117/12.292751
Fu, J., Guo, Q., Kauffmann, G., & Krumholz, M. R. (2010). The atomic-to-molecular transition and its relation to the scaling properties of galaxy discs in the local Universe. *Monthly Notices of the Royal Astronomical Society*, *409*(2), 515–530. https://doi.org/10.1111/j.1365-2966.2010.17342.x
Fu, J., Kauffmann, G., Huang, M.-L., yates, R. M., Moran, S., Heckman, T. M., Davé, R., Guo, Q., & Henriques, B. M. B. (2013). Star formation and emtallicity gradients in semi-analytic models of disc galaxy formation. *Monthly Notices of the Royal Astronomical Society*, *434*(2), 1531–1548. https://doi.org/10.1093/mnras/stt1117
Fu, J., Kauffmann, G., Li, C., & Qi, G. (2012). The effect of star formation on the redshift evolution of interstellar metals, atomic and molecular gas in galaxies. *Monthly Notices of the Royal Astronomical Society*, *424*(4), 2701–2714. https://doi.org/10.1111/j.1365-2966.2012.21356.x
Fukui, Y., Ohama, A., Hanaoka, N., Furukawa, N., Torii, K., Dawson, J. R., Mizuno, N., Hasegawa, K., Fukuda, T., Soga, S., Moribe, N., Kuroda, Y., Hayakawa, T., Kawamura, A., Kuwahara, T., Yamamoto, H., Okuda, T., Onishi, T., Maezawa, H., & Mizuno, A. (2014). Molecular Clouds toward the Super Star Cluster NGC 3603. Possible Evidence for a Cloud-Cloud Collision in Triggering the Cluster Formation. *The Astrophysical Journal*, *780*(1), 36. https://doi.org/10.1088/0004-637X/780/1/36
Gabrielpillai, A., Somerville, R. S., Genel, S., Rodriguez-Gomez, V., Pandya, V., Yung, L. Y. A., & Hernquist, L. (2022). Galaxy formation in the Santa Cruz semi-analytic model compared with IllustrisTNG - I. Galaxy scaling relations, dispersions, and residuals at $z = 0$. *Monthly Notices of the Royal Astronomical Society*, *517*(4), 6091–6111. https://doi.org/10.1093/mnras/stac2297
Gadotti, D. A., Sánchez-Blázquez, P., Falcón-Barroso, J., Huseman, B., Seidel, M. K., Pérez, I., de Lorenzo-Cáceres, A., Martinez-Valpuesta, I., Fragkoudi, F., Leung, G., van de Ven, G., Leaman, R., Coelho, P., Martig, M., Kim, T., Neumann, J., & Querejeta, M. (2019). Time Inference with MUSE in Extragalactic Rings (TIMER): properties of the survey and high-level data products. *Monthly Notices of the Royal Astronomical Society*, *482*(1), 506–529. https://doi.org/10.1093/mnras/sty2666
Gaete, B., Schleicher, D. R. G., Lupi, A., Reinoso, B., Fellhauer, M., & Vergara, M. C. (2024). Supermassive black hole formation via collisions in black hole clusters. *Astronomy & Astrophysics*, *690*, A378. https://doi.org/10.1051/0004-6361/202450770
Gallagher, J. S., Goad, J. W., & Mould, J. (1982). Structure of the M 33 nucleus. *The Astrophysical Journal*, *263*, 263. https://doi.org/10.1086/160484
Gallego-Cano, E., Schödel, R., Nogueras-Lara, F., Dong, H., Shahzamanian, B., Fritz, T. K., Gallego-Calvente, A. T., & Neumayer, N. (2020). New constraints on the structure of the nuclear stellar cluster of the Milky Way from star counts and MIR imaging. *Astronomy & Astrophysics*, *634*, A71. https://doi.org/10.1051/0004-6361/201935303
Galleti, S., Bellazzini, M., Federici, L., Buzzoni, A., & Fusi Pecci, F. (2007). An updated survey of globular clusters in M 31. II. Newly discovered bright and remove clusters. *Astronomy & Astrophysics*, *471*(1), 127–136. https://doi.org/10.1051/0004-6361:20077788
Galleti, S., Federici, L., Bellazzini, M., Fusi Pecci, F., & Macrina, S. (2004). 2MASS NIR photometry for 693 candidate globular clusters in M 31 and the Revised Bologna Catalogue. *Astronomy & Astrophysics*, *416*, 917–924. https://doi.org/10.1051/0004-6361:20035632
Gao, Y., Li, H., Zhang, X., Su, M., & Ng, S. C. Y. (2024). Globular clusters contribute to the nuclear star clusters and galaxy centre γ-ray excess, moderated by galaxy assembly history. *Monthly Notices of*

the Royal Astronomical Society, *527*(3), 7731–7742. https://doi.org/10.1093/mnras/stad3585

Garcia, F. A. B., Ricotti, M., Sugimura, K., & Park, J. (2023). Star cluster formation and survival in the first galaxies. *Monthly Notices of the Royal Astronomical Society*, *522*(2), 2495–2515. https://doi.org/10.1093/mnras/stad1092

Garro, E. R., Minniti, D., & Fernández-Trincado, J. G. (2024). Over 200 globular cluters in the Milky Way and still none with super-Solar metallicity. *Astronomy & Astrophysics*, *687*, A214. https://doi.org/10.1051/0004-6361/202347389

Gebhardt, K., Richstone, D., Tremaine, S., Lauer, T. R., Bender, R., Bower, G., Dressler, A., Faber, S. M., Filippenko, A. V., Green, R., Grillmair, C., Ho, L. C., Kormendy, J., Magorrian, J., & Pinkney, J. (2003). Axisymmetric Dynamical Models of the Central Regions of Galaxies. *The Astrophysical Journal*, *583*(1), 92–115. https://doi.org/10.1086/345081

Genzel, R., Eckart, A., Ott, T., & Eisenhauer, F. (1997). On the nature of the dark mass in the centre of the Milky Way. *Monthly Notices of the Royal Astronomical Society*, *291*(1), 219–234. https://doi.org/10.1093/mnras/291.1.219

Genzel, R., Eisenhauer, F., & Gillessen, S. (2010). The Galactic Center massive black hole and nuclear star cluster. *Reviews of Modern Physics*, *82*(4), 3121–3195. https://doi.org/10.1103/RevModPhys.82.3121

Genzel, R., Newman, S., Jones, T., Förster Schreiber, N. M., Shapiro, K., Genel, S., Lilly, S. J., Renzini, A., Tacconi, L. J., Bouché, N., Burkert, A., Cresci, G., Buschkamp, P., Carollo, C. M., Ceverino, D., Davies, R., Dekel, A., Eisenhauer, F., Hicks, E., . . . Zamorani, G. (2011). The Sins Survey of $z \sim 2$ Galaxy Kinematics: Properties of the Giant Star-forming Clumps. *The Astrophysical Journal*, *733*(2), 101. https://doi.org/10.1088/0004-637X/733/2/101

Genzel, R., Pichon, C., Eckart, A., Gerhard, O. E., & Ott, T. (2000). Stellar dynamics in the Galactic Centre: proper motions and anisotropy. *Monthly Notices of the Royal Astronomical Society*, *317*(2), 348–374. https://doi.org/10.1046/j.1365-8711.2000.03582.x

Georgiev, I. Y., & Böker, T. (2014). Nuclear star clusters in 228 spiral galaxies in the HST/WFPC2 archive: catalogue and comparison to other stellar systems. *Monthly Notices of the Royal Astronomical Society*, *441*(4), 3570–3590. https://doi.org/10.1093/\mnras/stu797

Georgiev, I. Y., Böker, T., Leigh, N., Lützgendorf, N., & Neumayer, N. (2016). Masses and scaling relations for nuclear star clusters, and their co-existence with central black holes. *Monthly Notices of the Royal Astronomical Society*, *457*(2), 2122–2138. https://doi.org/10.1093/\mnras/stw093

Georgiev, I. Y., Hilker, M., Puzia, T. H., Goudfrooij, P., & Baumgardt, H. (2009a). Globular cluster systems in nearby dwarf galaxies - II. Nuclear star clusters and their relation to massive Galactic globular clusters. *Monthly Notices of the Royal Astronomical Society*, *396*(2), 1075–1085. https://doi.org/10.1111/j.1365-2966.2009.14776.x

Georgiev, I. Y., Neumayer, N., Gässler, W., Rabien, S., Busoni, L., Bonaglia, M., Ziegleder, J., Orban de Xivry, G., Peter, D., Kulas, M., Borelli, J., Rahmer, G., Lefebvre, M., & Baumgardt, H. (2019). The Milky Way like galaxy NGC 6384 and its nuclear star cluster at high NIR spatial resolution using LBT/ARGOS commissioning data. *Monthly Notices of the Royal Astronomical Society*, *484*(3), 3356–3375. https://doi.org/10.1093/\mnras/stz227

Georgiev, I. Y., Puzia, T. H., Hilker, M., & Goudfrooij, P. (2009b). Globular cluster systems in nearby dwarf galaxies - I. HST/ACS observations and dynamical properties of globular clusters at low environmental density. *Monthly Notices of the Royal Astronomical Society*, *392*(2), 879–893. https://doi.org/10.1111/j.1365-2966.2008.14104.x

Georgy, C., Ekström, S., Eggenberger, P., Meynet, G., Haemmerlé, L., Maeder, A., Granada, A., Groh, J. H., Hirschi, R., Mowlavi, N., Yusof, N., Charbonnel, C., Decressin, T., & Barblan, F. (2013). Grids of stellar models with rotation. III. Models from 0.8 to 120 $M_\odot$ at a metallicity $Z = 0.002$. *Astronomy & Astrophysics*, *558*, A103. https://doi.org/10.1051/0004-6361/201322178

Ghez, A. M., Klein, B. L., Morris, M., & Becklin, E. E. (1998). High Proper-Motion Stars in the Vicinity of Sagittarius A*: Evidence for a Supermassive Black Hole at the Center of Our Galaxy. *The Astrophysical Journal*, *509*(2), 678–686. https://doi.org/10.1086/306528

Gieles, M., Erkal, D., Antonini, F., Balbinot, E., & Peñarrubia, J. (2021). A supra-massive population of stellar-mass black holes in the globular cluster Palomar 5. *Nature Astronomy*, *5*, 957–966. https://doi.org/10.1038/s41550-021-01392-2

Gieles, M., & Gnedin, O. Y. (2023). The mass-loss rates of star clusters with stellar-mass black holes: implications for the globular cluster mass function. *Monthly Notices of the Royal Astronomical Society*, *522*(4), 5340–5357. https://doi.org/10.1093/\mnras/stad1287

Gieles, M., Heggie, D. C., & Zhao, H. (2011). The life cycle of star clusters in a tidal field. *Monthly Notices of the Royal Astronomical Society*, *413*(4), 2509–2524. https://doi.org/10.1111/j.1365-2966.2011.18320.x

Gieles, M., & Renaud, F. (2016). If it doe snot kill them, it makes them stronger: collisional evolution of star clusters with tidal shocks. *Monthly Notices of the Royal Astronomical Society*, *463*(1), L103–L107. https://doi.org/10.1093/\mnras/slw163

Giersz, M., Askar, A., Wang, L., Hzpki, A., Leveque, A., & Spurzem, R. (2019). MOCCA survey data base - I. Dissolution of tidally filling star clusters harbouring black hole subsystems. *Monthly Notices of the Royal Astronomical Society*, *487*(2), 2412–2423. https://doi.org/10.1093/mnras/stz1460

Giersz, M., & Heggie, D. C. (1994). Statistics of N-Body Simulations - Part One - Equal Masses Before Core Collapse. *Monthly Notices of the Royal Astronomical Society*, *268*(1), 257. https://doi.org/10.1093/\mnras/268.1.257

Gilfanov, M. (2004). Low-mass X-ray binaries as a stellar mass indicator for the host galaxy. *Monthly Notices of the Royal Astronomical Society*, *349*(1), 146–168. https://doi.org/10.1111/j.1365-2966.2004.07473.x

Gillessen, S., Eisenhauer, F., Tripper, S., Alexander, T., Genzel, R., Martins, F., & Ott, T. (2009). Monitoring Stellar Orbits Around the Massive Black Hole in the Galactic Center. *The Astrophysical Journal*, *692*(2), 1075–1109. https://doi.org/10.1088/0004-637X/62/2/1075

Gnedin, O. Y., Ostriker, J. P., & Tremaine, S. (2014). Co-evolution of galactic nuclei and globular cluster systems. *The Astrophysical Journal*, *785*(1), 71–86. https://doi.org/10.1088/0004-637X/785/1/71

Goddard, Q. E., Bastian, N., & Kennicutt, R. C. (2010). On the fraction of star clusters surviving the embedded phase. *Monthly Notices of the Royal Astronomical Society*, *405*(2), 857–869. https://doi.org/10.1111/j.1365-2966.2010.16511.x

Gonzaga, S., Hack, W., Fruchter, A., & Mack, J. (2012). *The DrizzlePac Handbook*. https://ui.adsabs.harvard.edu/abs/2012drzp.book.....G

Graham, A. W. (2012). Extending the M_{bh}-σ diagram with dense nuclear star clusters. *Monthly Notices of the Royal Astronomical Society*, *422*(2), 1586–1591. https://doi.org/10.1111/j.1365-2966.2012.20734.x

Graham, A. W., & Driver, S. P. (2005). A Concise Reference to (Projected) Sérsic $R^{1/n}$ Quantities, Including Concentration, Profile Slopes, Petrosian Indices, and Kron Magnitudes. *Publications of the Astronomical Society of Australia*, *22*(2), 118–127. https://doi.org/10.1071/AS05001

Graham, A. W., & Soria, R. (2019). Expected intermediate-mass black holes in the Virgo cluster - I. Early-type galaxies. *Monthly Notices of the Royal Astronomical Society*, *484*(1), 794–813. https://doi.org/10.1093/\mnras/sty3398

Graham, A. W., & Spitler, L. R. (2009). Quantifying the coexistence of massive black holes and dense nuclear star clusters. *Monthly Notices of the Royal Astronomical Society*, *397*(4), 2148–2162. https://doi.org/10.1111/j.1365-2966.2009.15118.x

Grasha, K., Calzetti, D., Adamo, A., Kim, H., Elmegreen, B. G., Gouliermis, D. A., Aloisi, A., Bright, S. N., Christian, C., Cignoni, M., Dale, D. A., Dobbs, D., Elmegreen, D. M., Fumagalli, M., Gallagher, J. S., Grebel, E. K., Johnson, K. E., Lee, J. C., Messa, M., ... Wofford, A. (2015). The Spatial Distribution of the Young Stellar Clusters in the Star-forming Galaxy NGC 628. *The Astrophysical Journal*, *815*(2), 93–109. https://doi.org/10.1088/0004-637X/815/2/93

Gray, E. I., Read, J. I., Taylor, E., Orkney, M. D. A., Rey, M. P., yates, R. M., Kim, S. Y., Noël, N. E. D., Agertz, O., Andersson, E., & Pontzen, A. (2024). EDGE: A new model for Nuclear Star Cluster formation in dwarf galaxies. *arXiv e-prints*, arXiv:2405.19286. https://doi.org/10.48550/arXiv.2405.19286

Green, A. W., Glazebrook, K., McGregor, P. J., I.Damjanov, Wisnioski, E., Abraham, R. G., Colless, M., Sharp, R. G., Crain, R. A., Poole, G. B., & McCarthy, P. J. (2014). DYNAMO - I. A sample of Hα-luminous galaxies with resolved kinematics. *Monthly Notices of the Royal Astronomical Society*, *437*(2), 1070–1095. https://doi.org/10.1093/mnras/stt1882

Greene, J. E., Strader, J., & Ho, L. C. (2020). Intermediate-Mass Black Holes. *Annual Review of Astronomy and Astrophysics*, *58*, 257–312. https://doi.org/10.1146/annurev-astro-032620-021835

Grimm, H.-J., Gilfanov, M., & Sunyaev, R. (2003). High-mass X-ray binaries as a star formation rate indicator in distant galaxies. *Monthly Notices of the Royal Astronomical Society*, *339*(3), 793–809. https://doi.org/10.1046/j.1365-8711.2003.06224.x

Groenewegen, M. A. T. (2006). The mid- and far-infrared colours of AGB and post-AGB stars. *Astronomy & Astrophysics*, *448*(1), 181–187. https://doi.org/10.1051/0004-6361:20054163

Guillard, N., Emsellem, E., & Renaud, F. (2016). New insights on the formation of nuclear star clusters. *Monthly Notices of the Royal Astronomical Society*, *461*(4), 3620–3629. https://doi.org/10.1093/\mnras/stw1570

Gültekin, K., Richstone, D. O., Gebhardt, K., Lauer, T. R., Pinkney, J., Aller, M. C., Bender, R., Dressler, A., Faber, S. M., Filippenko, A. V., Green, R., Ho, L. C., Kormendy, J., & Siopis, C. (2009). A Quintet of Black Hole Mass Determinations. *The Astrophysical Journal*, *695*(2), 1577–1590. https://doi.org/10.1088/0004-637X/695/2/1577

Guo, Q., White, S., Boylan-Kolchin, M., De Lucia, G., Kauffmann, G., Lemson, G., Li, C., Springel, V., & Weinmann, S. (2011). From dwarf spheroidals to cD galaxies: simulating the galaxy population in a ΛCDM cosmology. *Monthly Notices of the Royal Astronomical Society*, *413*(1), 101–131. https://doi.org/10.1111/j.1365-2966.2010.18114.x

Guo, S., & Qi, Z. (2023). Oort Constants and Local Stellar Kinematics from GCNS. *Universe*, *9*(6), 252. https://doi.org/10.3390/universe9060252

Guolo, M., Pasham, D. R., Zajaček, M., Coughlin, E. R., Gezari, S., Suková, P., Wevers, T., Witzany, V., Tombesi, F., van Velzen, S., Alexander, K. D., Yao, Y., Arcodia, R., Karas, V., Miller-Jones, J. C. A., Remillard, R., Gendreau, K., & Ferrara, E. C. (2024). X-ray eruptions every 22 days from the nucleus of a nearby galaxy. *Nature Astronomy*, *8*, 347–358. https://doi.org/10.1038/s41550-023-02178-4

Gustafsson, B., Church, R. P., Davies, M. B., & Rickman, H. (2016). Gravitational scattering of stars and clusters and the heating of the Galactic disk. *Astronomy & Astrophysics*, *593*, A85. https://doi.org/10.1051/0004-6361/201423916

Habas, R., Marleau, F. R., Duc, P.-A., Durrell, P. R., Paudel, S., Poulain, M., Sánchez-Janssen, R., Sreejith, S., Ramasawmy, J., Stemock, B., Leach, C., Cuillandre, J.-C., Gwyn, S., Agnello, A., Bílek, M., Fensch, J., Müller, O., Peng, E. W., & van der Burg, R. F. J. (2020). Newly discovered dwarf galaxies in the MATLAS low-density fields. *Monthly Notices of the Royal Astronomical Society*, *491*(2), 1901–1919. https://doi.org/10.1093/\mnras/stz3045

Häberle, M., Neumayer, N., Seth, A., Bellini, A., Libralato, M., Baumgardt, H., Whitaker, M., Dumont, A., Alfaro Cuello, M., Anderson, J., Clontz, C., Kacharov, N., Kamann, S., Feldmeier-Krause, A., Milone, A., Nitschai, M. S., Pechetti, R., & van de Ven, G. (2024). Fast-moving stars around an intermediate-mass black hole in Omega Centauri. *Nature*, 33. https://arxiv.org/abs/2405.06015

Habouzit, M., Volonteri, M., & Dubois, Y. (2017). Blossoms from black hole seeds: properties and early growth regulated by supernova feedback. *Monthly Notices of the Royal Astronomical Society*, *468*(4), 3935–3948. https://doi.org/10.1093/\mnras/stx666

Hackshaw, Z., Hawkins, K., Filion, C., Horta, D., Laporte, C. F. P., Carr, C., & Price-Whelan, A. M. (2024). [X/Fe] Marks the Spot: Mapping Chemical Azimuthal Variations in the Galactic Disk with APOGEE. *The Astrophysical Journal*, 19. https://doi.org/10.48550/arXiv.2405.18120

Haidar, H., Habouzit, M., Volonteri, M., Mezcua, M., Greene, J. E., Neumayer, N., Anglés-Alcázar, D., Martin-Navarro, I., Hoyer, N., Dubois, Y., & Davé, R. (2022). The black hole population in low-mass galaxies in large-scale cosmological simulations. *Monthly Notices of the Royal Astronomical Society*, *514*(4), 4912–4931. https://doi.org/10.1093/\mnras/stac1659

Hammer, F., Li, H., Mamon, G. A., Pawlowski, M. S., Bonifacio, P., Jiao, Y., Wang, H., Wang, J., & Yang, Y. (2023). The accretion history of the Milky Way - I. How it shapes globular clusters and dwarf galaxies. *Monthly Notices of the Royal Astronomical Society*, *519*(4), 5059–5075. https://doi.org/10.1093/mnras/stac3758

Hammer, F., Wang, J., Mamon, G. A., Pawlowski, M. S., Yang, Y., Jiao, Y., Li, H., Bonifacio, P., Caffau, E., & Wang, H. (2024). The accretion history of the Milky Way - II. Internal kinematics of globular clusters and of dwarf galaxies. *Monthly Notices of the Royal Astronomical Society*, *527*(2), 2718–2733. https://doi.org/10.1093/mnras/stad2922

Hannah, C. H., Seth, A. C., Nguyen, D. D., Dumont, A., Kacharov, N., Neumayer, N., & den Brok, M. (2021). Spatially Resolving the Star Formation Histories of Three Nearby Nuclear Star Clusters. *The Astronomical Journal*, *162*(6), 281. https://doi.org/10.3847/1538-3881/ac282e

Hannah, C. H., Seth, A. C., Stone, N. C., & van Velzen, S. (2024). Counting the Unseen. I. Nuclear Density Scaling Relations for Nucleated Galaxies. *The Astronomical Journal*, *168*(3), 137. https://doi.org/10.3847/1538-3881/ad630a

Hao, C.-N., Kennicutt, R. C., Johnson, B. D., Calzetti, D., Dale, D. A., & Moustakas, J. (2011). Dust-corrected Star Formation Rates of Galaxies. II. Combinations of Ultraviolet and Infrared Tracers. *The Astrophysical Journal*, *741*(2), 124. https://doi.org/10.1088/0004-637X/741/2/124

Harris, W. E. (1996). A Catalog of Parameters for Globular Clusters in the Milky Way. *The Astronomical Journal*, *112*(4), 1487–1488. https://doi.org/10.1086/118116

Harris, W. E., Ciccone, S. M., Eadie, G. M., Gnedin, O. Y., Geisler, D., Rothberg, B., & Bailin, J. (2017). Globular Cluster Systems in Brightest Cluster Galaxies. III: Beyond Bimodality. *The Astrophysical Journal*, *835*(1), 101. https://doi.org/10.3847/1538-4357/835/1/101

Hartmann, M., Debattista, V. P., Seth, A. C., Cappellari, M., & Quinn, T. R. (2011). Constraining the role of star cluster mergers in nuclear star cluster formation: simulations confront integral-field data. *Monthly Notices of the Royal Astronomical Society*, *418*(4), 2697–2714. https://doi.org/10.1111/j.1365-2966.2011.19659.x

Hassani, H., Rosolowsky, E., Leroy, A. K., Boquien, M., Lee, J. C., Barnes, A. T., Belfiore, F., Bigiel, F., Cao, Y., Chevance, M., Dale, D. A., Egorov, O. V., Emsellem, E., Faesi, C. M., Grasha, K., Kim, J., Klessen, R. S., Kreckel, K., Kruijssen, J. M. D., . . . Williams, T. G. (2023). PHANGS-JWST First Results: The 21 μm Compact Source Population. *The Astrophysical Journal Letters*, *944*(2), L21. https://doi.org/10.3847/2041-8213/aca8ab

Hawkins, K. (2023). Chemical cartography with LAMOST and Gaia reveal azimuthal and spiral structure in the Galactic disc. *Monthly Notices of the Royal Astronomical Society*, *525*(3), 3318–3329. https://doi.org/10.1093/mnras/stad1244

Heiter, U., Soubiran, C., Netopil, M., & Paunzen, E. (2014). On the metallicity of open clusters. II. Spectroscopy. *Astronomy & Astrophysics*, *561*, A93. https://doi.org/10.1051/0004-6361/201322559

Hénon, M. (1961). Sur l'évolution dynamique des amas globulaires. *Annales d'Astrophysique*, *24*, 369. https://ui.adsabs.harvard.edu/abs/1961AnAp...24..369H

Henriques, B. M. B., White, S. D. M., Thomas, P. A., Angulo, R., Guo, Q., Lemson, G., Springel, V., & Overzier, R. (2015). Galaxy formation in the Planck cosmology - I. Matching the observed evolution of star formation rates, colours and stellar masses. *Monthly Notices of the Royal Astronomical Society*, *451*(3), 2663–2680. https://doi.org/10.1093/\mnras/stv705

Henriques, B. M. B., Yates, R. M., Fu, J., Guo, Q., Kauffmann, G., Srisawat, C., Thomas, P. A., & White, S. D. M. (2020). L-GALAXIES 2020: Spatially resolved cold gas phases, star formation, and chemical enrichment in galactic discs. *Monthly Notices of the Royal Astronomical Society*, *491*(4), 5795–5814. https://doi.org/10.1093/\mnras/stz3233

Henshaw, J. D., Barnes, A. T., Battersby, C., Ginsburg, A., Sormani, M. C., & Walker, D. L. (2022). Star Formation in the Central Molecular Zone of the Milky Way. https://arxiv.org/abs/2203.11223

Heyer, M., Krawczyk, C., Duval, J., & Jackson, J. M. (2009). Re-Examining Larson's Scaling Relationships in Galactic Molecular Clouds. *The Astrophysical Journal*, *699*(2), 1092–1103. https://doi.org/10.1088/0004-637X/699/2/1092

Heyer, M. H., Corbelli, E., Schneider, S. E., & Young, J. S. (2004). The Molecular Gas Distribution and Schmidt Law in M33. *The Astrophysical Journal*, *602*(2), 723–729. https://doi.org/10.1086/381196

HI4PI Collaboration, Ben Bekhti, N., Flöer, L., Keller, R., Kerp, J., Lenz, D., Winkel, B., Bailin, J., Calabretta, M. R., Dedes, L., Ford, H. A., Gibson, B. K., Haud, U., Janowiecki, S., Kalberla, P. M. W., Lockman, F. J., McClure-Griffifts, N. N., Murphy, T., Nakaishi, H., . . . Staveley-Smith, L. (2016). HI4PI: A full-sky H I survey based on EBHIS and GASS. *Astronomy & Astrophysics*, *594*, A116. https://doi.org/10.1051/0004-6361/201629178

Hilker, M., Infante, L., Vieira, G., Kissler-Patig, M., & Richtler, T. (1999). The central region of the Fornax cluster. II. Spectroscopy and radial velocities of member and background galaxies. *Astronomy & Astrophysics*

Supplement Series, *134*, 75–86. https://doi.org/10.1051/aas:1999434

Hirschmann, M., De Lucia, G., & Fontanot, F. (2016). Galaxy assembly, stellar feedback and metal enrichment: the view from the GAEA model. *Monthly Notices of the Royal Astronomical Society*, *461*(2), 1760–1785. https://doi.org/10.1093/mnras/stw1318

Hislop, J. M., Naab, T., Steinwandel, U. P., Lahén, N., Irodotou, D., Johansson, P. H., & Walch, S. (2022). The challenge of simulating the star cluster population of dwarf galaxies with resolved interstellar medium. *Monthly Notices of the Royal Astronomical Society*, *509*(4), 5938–5954. https://doi.org/10.1093/\mnras/stab3347

Hixenbaugh, K., Chandar, P., & Mok, A. (2022). The Ancient Globular Clusters of NGC 1291. *The Astronomical Journal*, *163*(6), 271. https://doi.org/10.3847/1538-3881/ac680d

Ho, I.-T., Kreckel, K., Meidt, S. E., Groves, B., Blanc, G. A., Bigiel, F., Dale, D. A., Emsellem, E., Glover, S. C. O., Grasha, K., Kewley, L. J., Kruijssen, J. M. D., Lang, P., McElroy, R., Kudritzki, R.-P., Sanchez-Blazquez, P., Sandstrom, K., Santoro, F., Schinnerer, E., & Schruba, A. (2019). Mapping Electron Temperature Variations across a Spiral Arim in NGC 1672. *The Astrophysical Journal Letters*, *885*(2), L31. https://doi.org/10.3847/2041-8213/ab4feb

Ho, I.-T., Seibert, M., Meidt, S. E., Kudritzki, R.-P., Kobayashi, C., Groves, B. A., Kewley, L. J., Madore, B. F., Rich, J. A., Schinnerer, E., D'Agostino, J., & Poetrodjojo, H. (2017). The Chemical Evolution Carousel of Spiral Galaxies: Azimuthal Variations of Oxygen Abundance in NGC 1365. *The Astrophysical Journal*, *846*, 39. https://doi.org/10.3847/1538-4357/aa8460

Hopkins, P. F., & Quataert, E. (2010). How do massive black holes get their gas? *Monthly Notices of the Royal Astronomical Society*, *407*(3), 1529–1564. https://doi.org/10.1111/j.1365-2966.2010.17064.x

Hopkins, P. F., Quataert, E., & Murray, N. (2012). The structure of the interstellar medium of star-forming galaxies. *Monthly Notices of the Royal Astronomical Society*, *421*(4), 3488–3521. https://doi.org/10.1111/j.1365-2966.2012.20578.x

Horta, D., Hughes, M. E., Pfeffer, J. L., Bastian, N., Kruijssen, J. M. D., Reina-Campos, M., & Crain, R. A. (2011). Linking globular cluster formation at low and high redshift through the age-metallicity relation in E-MOSAICS. *Monthly Notices of the Royal Astronomical Society*, *500*(4), 4768–4778. https://doi.org/10.1093/\mnras/staa3522

Hoyer, N., Arcodia, R., Bonoli, S., Merloni, A., Neumayer, N., Zhang, Y., & Comparat, J. (2024). Massive black holes in nuclear star clusters. Investigation with *SRG/eROSITA* X-ray data. *Astronomy & Astrophysics*, *682*, A36. https://doi.org/10.1051/0004-6361/202347665

Hoyer, N., Bonoli, S., Bastian, N., Herrero Carrión, D., Neumayer, N., Izquierdo-Villalba, D., Spinosos, D., Yates, R., Polkas, M., & Artale, M. C. (2025). Massive Star Clusters in the Semi-Analytical Galaxy Formation Model L-Galaxies 2020. *Astronomy & Astrophysics*, 24. https://arxiv.org/abs/2504.12079

Hoyer, N., Neumayer, N., Georgiev, I. Y., Seth, A. C., & Greene, J. E. (2021). The nucleation fraction of local volume galaxies. *Monthly Notices of the Royal Astronomical Society*, *507*(3), 3246–3266. https://doi.org/10.1093/\mnras/stab2277

Hoyer, N., Neumayer, N., Seth, A. C., Georgiev, I. Y., & Greene, J. E. (2023a). Photometric and Structural Parameters of Newly Discovered Nuclear Star Clusters in Local Volume Galaxies. *Monthly Notices of the Royal Astronomical Society*, *520*(3), 4664–4682. https://doi.org/10.1093/\mnras/stad220

Hoyer, N., Pinna, F., Kamlah, A. W. H., Nogueras-Lara, F., Feldmeier-Krause, A., Neumayer, N., Sormani, M. C., Boquien, M., Emsellem, E., Seth, A. C., Klessen, R. S., Williams, T. G., Schinnerer, E., Barnes, A. T., Leroy, A. K., Bonoli, S., Kruijssen, J. M. D., Neumann, J., Sánchez-Blázquez, P., ... Hassani, H. (2023b). PHANGS–JWST First Results: A combined *HST* and *JWST* analysis of the nuclear star cluster in NGC 628. *The Astrophysical Journal Letters*, *944*(2), L25. https://doi.org/10.3847/2041-8213/aca53e

Hsieh, P.-Y., Koch, P. M., Kim, W.-T., Martín, S., Yen, H.-W., Carpenter, J. M., Harada, N., Turner, J. L., Ho, P. T. P., Tang, Y.-W., & Beck, S. (2021). The Circumnuclear Disk Revealed by ALMA. I. Dense Clouds and Tides in the Galactic Center. *The Astrophysical Journal*, *913*(2), 94. https://doi.org/10.3847/1538-4357/abf4cd

Huchra, J. P., Brodie, J. P., & Kent, S. M. (1991). Extragalactic Globular Clusters. II. The M 31 Globular Cluster System. *The Astrophysical Journal*, *370*, 495–504. https://doi.org/10.1086/169836

Hudson, M. J., Harris, G. L., & Harris, W. E. (2014). Dark Matter Halos in Galaxies and Globular Cluster Populations. *The Astrphysical Journal Letters*, *787*(1), L5. https://doi.org/10.1088/2041-8205/787/1/L5

Huertas-Company, M., Iyer, K. G., Angeloudi, E., Bagley, M. B., Finkelstein, S. L., Kartaltepe, J., McGarth, E. J., Sarmiento, R., Vega-Ferrero, J., Arrabal Haro, P., Behroozi, P., Buitrago, F., Cheng, Y., Constantin, L., Dekel, A., Dickinson, M., Elbaz, D., Grogin, N. A., Hathi, N. P., ... Yung, L. Y. A. (2024). Galaxy morphology from $z \sim 6$ through the lens of JWST. *Astronomy & Astrophysics*, *685*, A48. https://doi.org/10.1051/0004-6361/202346800

Hughes, M. E., Pfeffer, J., Martig, M., Bastian, N., Crain, R. A., Kruijssen, J. M. D., & Reina-Campos, M. (2019). Fossil stellar streams and their globular cluster populations in the E-MOSAICS simulations. *Monthly Notices of the Royal Astronomical Society*, *482*(2), 2795–2806. https://doi.org/10.1093/mnras/sty2889

Hughes, M. E., Pfeffer, J. L., Bastian, N., Martig, M., Kruijssen, J. M. D., Crain, R. A., Reina-Campos, M., & Trujillo-Gomez, S. (2022). The physics governing the upper truncation mass of the globular cluster mass function. *Monthly Notices of the Royal Astronomical Society*, *510*(4), 6190–6200. https://doi.org/10.1093/mnras/stab3597

Hughes, M. E., Pfeffer, J. L., Martig, M., Reina-Campos, M., Bastian, N., Crain, R. A., & Kruijssen, J. M. D. (2020). The [α/Fe]-[Fe/H] relation in the E-MOSAICS simulations: its connection to the birth place of globular clusters and the fraction of globular cluster field stars in the bulge. *Monthly Notices of the Royal Astronomical Society*, *491*(3), 4012–4022. https://doi.org/10.1093/mnras/staz3341

Hunt, E. L., & Reffert, S. (2023). Improving the open cluster census. II. An all-sky cluster catalogue with Gaia DR3. *Astronomy & Astrophysics*, *673*, A114. https://doi.org/10.1051/0004-6361/202346285

Hunter, D. A., Elmegreen, B. G., Dupuy, T. J., & Mortonson, M. (2003). Cluster Mass Functions in the Large and Small Magellanic Clouds: Fading and Size-of-Sample Effects. *The Astronomical Journal*, *126*(4), 1836–1848. https://doi.org/10.1086/378056

Huxor, A. P., Mackey, A. D., Ferguson, A. M. N., Irwin, M. J., Martin, N. F., Tanvir, N. R., Veljanoski, J., McConnachie, A., Fishlock, C. K., Ibata, R., & Lewis, G. F. (2014). The outer halo globular cluster system of M 31 - I. The final PAndAS catalogue. *Monthly Notices of the Royal Astronomical Society*, *442*(3), 2165–2187. https://doi.org/10.1093/\mnras/stu771

Huxor, A. P., Tanvir, N. R., Ferguson, A. M. N., Irwin, M. J., Ibata, R., Bridges, T., & Lewis, G. F. (2008). Globular clusters in the outer halo of M 31: the survey. *Monthly Notices of the Royal Astronomical Society*, *385*(4), 1989–1997. https://doi.org/10.1111/j.1365-2966.2008.12882.x

Hwang, H.-C., Barrera-Ballesteros, J. K., Heckman, T. M., Rowlands, K., Lin, L., Rodriguez-Gomez, V., Pan, H.-A., Hsieh, B.-C., Sánchez, S., Bizyaev, D., Sánchez Almeida, J., Thilker, D. A., Lotz, J. M., Jones, A., Nair, P., Andrews, B. H., & Drory, N. (2019). Anomalously Low-metallicity Regions in MaNGA Star-forming Galaxies: Accretion Caught in Action? *The Astrophysical Journal*, *872*(2), 144. https://doi.org/10.3847/1538-4357/aaf7a3

Ines Ennis, A., Caso, J. P., & Bassino, L. P. (2024). Imprints of interaction processes in the globular cluster system if NGC 3640. *The Open Journal of Astrophysics*, 12. https://doi.org/10.48550/arXiv.2403.00065

Inoue, S. (2009). The test for suppressed dynamical friction in a constant density core of dwarf galaxies. *Monthly Notices of the Royal Astronomical Society*, *397*(2), 709–716. https://doi.org/10.1111/j.1365-2966.2009.15066.x

Into, T., & Portinari, L. (2013). New colour-mass-to-light relations: the role of the asymptotic giant branch phase and of interstellar dust. *Monthly Notices of the Royal Astronomical Society*, *430*(4), 2715–2731. https://doi.org/10.1093/\mnras/stt071

Irodotou, D., Thomas, P. A., Henriques, B. M. B., Sargent, M. T., & Hislop, J. M. (2019). Morphological evolution and galactic sizes in the L-Galaxies SA model. *Monthly Notices of the Royal Astronomical Society*, *489*(3), 3609–3624. https://doi.org/10.1093/\mnras/stz2365

Irwin, J. A. (2005). The Birthplace of Low-Mass X-Ray Binaries: Field Versus Globular Cluster Populations. *The Astrophysical Journal*, *631*(1), 511–517. https://doi.org/10.1086/432611

Iwasawa, K., Sanders, D. B., Evans, A. S., Mazzarella, J. M., Armus, L., & Surace, J. A. (2009). High-Ionization Fe K Emission from Luminous Infrared Galaxies. *The Astrophysical Journal Letters*, *695*(1), L103–L106. https://doi.org/10.1088/0004-637X/695/1/L103

Izquierdo-Villalba, D., Bonoli, S., Dotti, M., Sesana, A., Rosas-Guevara, Y., & Spinoso, D. (2020). From galactic nuclei to the halo outskirts: tracing supermassive black holes across cosmic history and environments. *Monthly Notices of the Royal Astronomical Society*, *495*(4), 4681–4706. https://doi.org/10.1093/\mnras/staa1399

Izquierdo-Villalba, D., Bonoli, S., Spinoso, D., Rosas-Guevara, Y., Henriques, B. M. B., & Hernández-Monteagudo, C. (2019). The build-up of pseudo-bulges in a hierarchical universe. *Monthly Notices of the Royal Astronomical Society*, *488*(1), 609–632. https://doi.org/10.1093/\mnras/stz1694

Izquierdo-Villalba, D., Sesana, A., Bonoli, S., & Colpi, M. (2022). Massive black hole evolution models confronting the nHz amplitude of the stochastic gravitational wave background. *Monthly Notices of the Royal Astronomical Society*, *509*(3), 3488–3503. https://doi.org/10.1093/mnras/stab3239

Jaffe, W. (1983). A simple model for the distribution of light in spherical galaxies. *Monthly Notices of the Royal Astronomical Society*, *202*(4), 995–999. https://doi.org/10.1093/\mnras/202.4.995

Janz, J., Norris, M. A., Forbes, D. A., Huxor, A., Romanowsky, A. J., frank, M. J., Escudero, C. G., abd J. C. Forte, F. R. F., Kannappan, S. J., Maraston, C., Brodie, J. P., Strader, J., & Thompson, B. R. (2016). The AIMSS Project - III. The stellar populations of compact stellar systems. *Monthly Notices of the Royal Astronomical Society*, *456*(1), 617–632. https://doi.org/10.1093/mnras/stv2636

Jennings, Z. G., Romanowsky, A. J., Brodie, J. P., Janz, J., Norris, M. A., Forbes, D. A., Martinez-Delgado, D., Fagioli, M., & Penny, S. J. (2015). NGC 3628-UCD 1: A Possible ω Cen Anaog Embedded in a Stellar Stream. *The Astrophysical Journal Letters*, *812*(1), L10. https://doi.org/10.1088/2041-8205/812/1/L10

Johnson, B., Foreman-Mackey, D., Sick, J., Leja, J., Walmsley, M., Tollerud, E., Leung, H., Scott, S., & Park, M. (2023). *python-fsps*. https://doi.org/10.5281/zenodo.10026684

Johnson, K. E., Leitherer, C., Vacca, W. D., & Conti, P. S. (2000). Hubble Space Telescope Observations of HE 2-10: Outflows and Young Super-Star Clusters. *The Astronomical Journal*, *120*(3), 1273–1288. https://doi.org/10.1086/301541

Jordán, A., Côté, P., Blakeslee, J. P., Ferrarese, L., McLaughlin, D. E., Mei, S., Peng, E. W., Tonry, J. L., Merritt, D., Milosavljević, M., Sarazin, C. L., Sivakoff, G. R., & West, M. J. (2005). The ACS Virgo Cluster Survey. X. Half-Light Radii of Globular Clusters in Early-Type Galaxies: Environmental Dependencies and a Standard Ruler for Distance Estimation. *The Astrophysical Journal*, *634*(2), 1002–1019. https://doi.org/10.1086/497092

Jordán, A., McLaughlin, D. E., Côté, P., Ferrarese, L., Peng, E. W., Mei, S., Villegas, D., Merritt, D., Tonry, J. L., & West, M. J. (2007a). The ACS Virgo Cluster Survey. XII. The Luminosity Function of Globular Clusters in Early-Type Galaxies. *The Astrophysical*

Journal Supplement Series, *171*(1), 101–145. https://doi.org/10.1086/516840
Jordán, A., Sivakoff, G. R., McLaughlin, D. E., Blakeslee, J. P., Evans, D. A., Kraft, R. P., Hardcastle, M. J., Peng, E. W., Côté, P., Croston, J. H., Juett, A. M., Minniti, D., Raychaudhury, S., Sarazin, C. L., Worrall, D. M., Harris, W. E., Woodley, K. A., Birkinshaw, M., Brassington, N. J., ... Murray, S. S. (2007b). Low-Mass X-Ray Binaries and Globular Clusters in Centaurus A. *The Astrophysical Journal Letters*, *671*(2), L117–L120. https://doi.org/10.1086/525524
Kacharov, N., Neumayer, N., Seth, A. C., Cappellari, M., McDermid, R., Walcher, C. J., & Böker, T. (2018). Stellar populations and star formation histories of the nuclear star clusters in six nearby galaxies. *Monthly Notices of the Royal Astronomical Society*, *480*(2), 1973–1998. https://doi.org/10.1093/\mnras/sty1985
Kamlah, A. W. H., Spruzem, R., Berczik, P., Arca Sedda, M., Flammini Dotti, F., Neumayer, N., Pang, X., Shu, Q., Tanikawa, A., & Giersz, M. (2022). The impact of stellar evolution on rotating star clusters: the gravothermal-gravogyro catastrophe and the formation of a bar of black holes. *Monthly Notices of the Royal Astronomical Society*, *516*(3), 3266–3283. https://doi.org/10.1093/\mnras/stac2281
Kamphuis, J., & Briggs, F. (1992). Kinematics of the extended HI disk of NGC 628. High velocity gas and deviations from circular rotation. *Astronomy & Astrophysics*, *253*, 335–348. https://ui.adsabs.harvard.edu/abs/1992A%5C&A...253..335K
Karachentsev, I. D., Makarov, D. I., & Kaisina, E. I. (2013). Updated Nearby Galaxy Catalog. *The Astronomical Journal*, *145*(4), 101–123. https://doi.org/10.1088/0004-6256/145/4/101
Karam, J., & Sills, A. (2022). Modelling star cluster formation: mergers. *Monthly Notices of the Royal Astronomical Society*, *513*(4), 6095–6104. https://doi.org/10.1093/\mnras/stac1298
Karam, J., & Sills, A. (2023). Modelling star cluster formation: Gas accretion. *Monthly Notices of the Royal Astronomical Society*, *521*(4), 5557–5569. https://doi.org/10.1093/mnras/stad850
Kataria, S. K., & Vivek, M. (2024). How does the presence of a bar affects the fueling of supermassive black holes? An IllustrisTNG 100 perspective. *Monthly Notices of the Royal Astronomical Society*, *527*(2), 3366–3380. https://doi.org/10.1093/mnras/stad3383
Katz, H., & Ricotti, M. (2013). Two epochs of globular cluster formation from deep field luminosity functions: implications for reionization and the Milky Way satellites. *Monthly Notices of the Royal Astronomical Society*, *432*(4), 3250–3261. https://doi.org/10.1093/mnras/stt676
Katz, H., Sijacki, D., & Haehnelt, M. G. (2015). Seeding high-redshift QSOs by collisional runaway in primordial star clusters. *Monthly Notices of the Royal Astronomical Society*, *451*(3), 2352–2369. https://doi.org/10.1093/mnras/stv1048
Kauffmann, G., & Haehnelt, M. (2000). A unified model for the evolution of galaxies and quasars. *Monthly Notices of the Royal Astronomical Society*, *311*(3), 576–588. https://doi.org/10.1046/j.1365-8711.2000.03077.x
Kauffmann, G., Heckman, T. M., Tremonti, C., Brinchmann, J., Charlot, S., White, S. D. M., Ridgway, S. E., Brinkmann, J., Fukugita, M., Hall, P. B., Ivezić, Ž., Richards, G. T., & Schneider, D. P. (2003). The host galaxies of active galactic nuclei. *Monthly Notices of the Royal Astronomical Society*, *346*(4), 1055–1077. https://doi.org/10.1111/j.1365-2966.2003.07154.x
Kaviraj, S., Ferreras, I., Yoon, S.-J., & Yi, S. K. (2005). On the globular cluster formation history of NGC 5128. *Astronomy & Astrophysics*, *439*(3), 913–919. https://doi.org/10.1051/0004-6361:20041328
Keller, B. W., Kruijssen, J. M. D., Pfeffer, J., Reina-Campos, M., Bastian, N., Trujillo-Gomez, S., Hughes, M. E., & Crain, R. A. (2020). Where did the globular clusters of the Milky Way form? Insights from the E-MOSAICS simulations. *Monthly Notices of the Royal Astronomical Society*, *495*(4), 4248–4267. https://doi.org/10.1086/313233
Kenney, J. D. P., & Lord, S. D. (1991). Orbit Crowding of Molecular Gas at a Bar-Spiral Arm Transition Zone in M 83. *The Astrophysical Journal*, *381*, 118. https://doi.org/10.1086/170634
Kennicutt, R. C. (1998). Star Formation in Galaxies Along the Hubble Sequence. *Annual Review of Astronomy and Astrophysics*, *36*, 189–232. https://doi.org/10.1146/annurev.astro.36.1.189
Kennicutt, R. C., & Evans, N. J. (2012). Star Formation in the Milky Way and Nearby Galaxies. *Annual Review of Astronomy and Astrophysics*, *50*, 531–608. https://doi.org/10.1146/annurev-astro-081811-125610
Kewley, L. J., & Ellison, S. L. (2008). Metallicity Calibrations and the Mass-Metallicity Relation for Star-forming Galaxies. *The Astrophysical Journal*, *681*(2), 1183–1204. https://doi.org/10.1086/423264
Khim, D. J., Zaritsky, D., Lambert, M., & Donnerstein, R. (2024). Properties of Nuclear Star Clusters in Low Surface Brightness Galaxies. *The Astronomical Journal*, *168*(1), 45. https://doi.org/10.3847/1538-3881/ad4ed3
Khim, D. J., Zaritsky, D., Sandoval Ascencio, L., Cooper, M. C., & Donnerstein, R. (2025). A Closer Look at an Unusual Ultra-Diffuse Galaxy. *arXiv e-prints*, arXiv:2502.19465. https://doi.org/10.48550/arXiv.2502.19465
Kikuchihara, S., Ouchi, M., Ono, Y., Mawatari, K., Chevallard, J., Harikane, Y., Kojima, T., Oguri, M., Bruzual, G., & Charlot, S. (2020). Early low-mass Galaxies and Star-cluster Candidates at $z \sim 6$-9 Identified by the Gravitational-lensing Technique and Deep Optical/Near-infrared Imaging. *The Astrophysical Journal*, *893*(1), 60. https://doi.org/10.3847/1538-4357/ab7dbe
King, I. (1962). The structure of star clusters. I. an empirical density law. *The Astronomical Journal*, *67*(8), 471–485. https://doi.org/10.1086/108756
King, I. R. (1966). The structure of star clusters. III. Some simple dynamical models. *The Astronomical Journal*, *71*, 64. https://doi.org/10.1086/109857
Kıroğlu, F., Kremer, K., Biscoveanu, S., González Prieto, E., & Rasio, F. A. (2025). Black Hole Accretion and Spin-up through Stellar Collisions in Dense Star

Clusters. *The Astrophysical Journal*, *979*(2), 237. https://doi.org/10.3847/1538-4357/ada26b
Klessen, R. S., & Glover, S. C. O. (2016). Physical Processes in the Interstellar Medium. *Saas-Fee Advanced Course*, *43*, 85. https://doi.org/10.1007/978-3-662-47890-5_2
Knapen, J. H., Laine, S., & Relaño, M. (1999). Circumnuclear Star-Forming Regions in Barred Galaxies. *Astrophysics and Space Science*, *269–270*, 605–608. https://doi.org/10.1023/A:1017004121535
Koleva, M., de Rijcke, S., Prugniel, P., Zeilinger, W. W., & Michielsen, D. (2009). Formation and evolution of dwarf elliptical galaxies - II. Spatially resolved star formation histories. *Monthly Notices of the Royal Astronomical Society*, *396*(4), 2133–2151. https://doi.org/10.1111/j.1365-2966.2009.14820.x
Komossa, S., & Bade, N. (1999). The giant X-ray outbursts in NGC 5905 and IC 3599: Follow-up observations and outburst scenarios. *Astronomy & Astrophysics*, *343*, 775–787. https://doi.org/10.48550/arXiv.astro-ph/9901141
Kormendy, J. (1985). Brightness profiles of the cores of bulges and elliptical galaxies. *The Astrophysical Journal Letters*, *292*, L9–L13. https://doi.org/10.1086/184463
Kormendy, J., & Bender, R. (1999). The Double Nucleus and Central Black Hole of M 31. *The Astrophysical Journal*, *522*(2), 772–792. https://doi.org/10.1086/307665
Kormendy, J., Bender, R., Magorrian, J., Tremaine, S., Gebhardt, K., Richstone, D., Dressler, A., Faber, S. M., Grillmair, C., & Lauer, T. R. (1997). Spectroscopic Evidence for a Supermassive Black Hole in NGC 4486B. *The Astrophysical Journal Letters*, *482*(2), L139–L142. https://doi.org/10.1086/310720
Kormendy, J., & Djorgovski, S. (1989). Surface photometry and the structure of elliptical galaxies. *Annual Review of Astronomy and Astrophysics*, *27*, 235–277. https://doi.org/10.1146/annurev.aa.27.090189.001315
Kormendy, J., Drory, N., Bender, R., & Cornell, M. E. (2010). Bulgeless Giant Galaxies Challenge Our Picture of Galaxy Formation by Hierarchical Clustering. *The Astrophysical Journal*, *723*(1), 54–80. https://doi.org/10.1088/0004-637X/723/1/54
Kormendy, J., & Ho, L. C. (2013). Coevolution (Or Not) of Supermassive Black Holes and Host Galaxies. *Annual Review of Astronomy and Astrophysics*, *51*(1), 511–653. https://doi.org/10.1146/annurev-astro-082708-101811
Kormendy, J., & Richstone, D. (1995). Inward Bound—The Search For Supermassive Black Holes In Galactic Nuclei. *Annual Review of Astronomy and Astrophysics*, *33*, 581. https://doi.org/10.1146/annurev.aa.33.090195.003053
Krauss, L. M., & Chaboyer, B. (2003). Age Estimates of Globular Clusters in the Milky Way: Constraints on Cosmology. *Science*, *229*(5603), 65–70. https://doi.org/10.1126/science.1075631
Kravtsov, A. V., & Gnedin, O. Y. (2005). Formation of Globular Clusters in Hierarchical Cosmology. *The Astrophysical Journal*, *623*(2), 650–665. https://doi.org/10.1086/428636
Kreckel, K., Faesi, C., Kruijssen, J. M. D., Schruba, A., Groves, B., Leroy, A. K., Bigiel, F., Blanc, G. A., Chevance, M., Herrera, C., Hughes, A., McElroy, R., Pety, J., Querejeta, M., Rosolowsky, E., Schinnerer, E., Sun, J., Usero, A., & Utomo, D. (2018). A 50 pc Scale View of Star Formation Efficiency across NGC 628. *The Astrophysical Journal Letters*, *863*(2), L21–L27. https://doi.org/10.3847/2041-8213/aad77d
Kreckel, K., Ho, I.-T., Blanc, G. A., Groves, B., Santoro, F., Schinnerer, E., Bigiel, F., Chevance, M., Congiu, E., Emsellem, E., Faesi, C., Glover, S. C. O., Grasha, K., Kruijssen, J. M. D., Lang, P., Leroy, A. K., Meidt, S. E., McElroy, R., Pety, J., . . . Schruba, A. (2019). Mapping Metallicity Variations across Nearby Galaxy Disks. *The Astrophysical Journal*, *887*(1), 80. https://doi.org/10.3847/1538-4357/ab5115
Krist, J. (1993). Tiny Tim : an HST PSF Simulator. In R. J. Hanisch, R. J. V. Brissenden, & J. Barnes (Eds.), *Astronomical Data Analysis Software and Systems II* (p. 536, Vol. 52). https://ui.adsabs.harvard.edu/abs/1993ASPC...52..536K
Krist, J. (1995). Simulation of HST PSFs using Tiny Tim. In R. A. Shaw, H. E. Payne, & J. J. E. Hayes (Eds.), *Astronomical Data Analysis Software and Systems IV* (p. 349, Vol. 77). https://adass.org/adass/proceedings/adass94/kristj.html
Kritos, K., Berti, E., & Silk, J. (2023). Massive black hole assembly in nuclear star clusters. *Physical Review D*, *108*(8), 083012. https://doi.org/10.1103/PhysRevD.108.083012
Kritsuk, A. G., Norman, M. L., Padoan, P., & Wagner, R. (2007). The Statistics of Supersoniv Isothermal Turbulence. *The Astrophysical Journal*, *665*(1), 416–431. https://doi.org/10.1086/519443
Kritsuk, A. G., Ustyugov, S. D., & Norman, M. L. (2017). The structure and statistics of interstellar turbulence. *New Journal of Physics*, *19*(6), 065003. https://doi.org/10.1088/1367-2630/aa7156
Kroupa, P. (2001). On the variation of the initial mass function. *Monthly Notices of the Royal Astronomical Society*, *322*(2), 231–246. https://doi.org/10.1046/j.1365-8711.2001.04022.x
Kruijssen, J. M. D. (2012). On the fraction of star formation occurring in bound stellar clusters. *Monthly Notices of the Royal Astronomical Society*, *426*(4), 3008–3040. https://doi.org/10.1111/j.1365-2966.2012.21923.x
Kruijssen, J. M. D. (2014). Globular cluster formation in the context of galaxy formation and evolution. *Classical and Quantum Gravity*, *31*(24), 244006. https://doi.org/10.1088/0264-9381/31/24/244006
Kruijssen, J. M. D. (2015). Globular clusters as the relics of regular star formation in 'normal' high-redshift galaxies. *Monthly Notices of the Royal Astronomical Society*, *454*(2), 1658–1686. https://doi.org/10.1093/\mnras/stv2026
Kruijssen, J. M. D., & Cooper, A. P. (2012). The initial mass spectrum of old globular clusters in dwarf galaxies. *Monthly Notices of the Royal Astronomical Society*, *420*(1), 340–345. https://doi.org/10.1111/j.1365-2966.2011.20037.x

Kruijssen, J. M. D., Pfeffer, J. L., Chevance, M., Bonaca, A., Trujillo-Gomez, S., Bastian, N., Reina-Campos, M., Crain, R. A., & Hughes, M. E. (2020a). Kraken reveals itself - the merger history of the Milky Way reconstructed with the E-MOSAICS simulations. *Monthly Notices of the Royal Astronomical Society*, *498*(2), 2472–2491. https://doi.org/10.1093/\mnras/staa2452

Kruijssen, J. M. D., Pfeffer, J. L., Chevance, M., Bonaca, A., Trujillo-Gomez, S., Bastian, N., Reina-Campos, M., Crain, R. A., & Hughes, M. E. (2020b). Kraken reveals itself - the merger history of the Milky Way reconstructed with the E-MOSAICS simulations. *Monthly Notices of the Royal Astronomical Society*, *498*(2), 2472–2491. https://doi.org/10.1093/mnras/staa2452

Kruijssen, J. M. D., Pfeffer, J. L., Crain, R. A., & Bastian, N. (2019a). The E-MOSAICS project: tracing galaxy formation and assembly with the age-metallicity distribution of globular clusters. *Monthly Notices of the Royal Astronomical Society*, *486*(3), 3134–3179. https://doi.org/10.1093/mnras/stz968

Kruijssen, J. M. D., Pfeffer, J. L., Reina-Campos, M., Crain, R. A., & Bastian, N. (2019b). The formation and assembly history of the Milky Way revleaed by its globular cluster population. *Monthly Notices of the Royal Astronomical Society*, *486*(3), 3180–3202. https://doi.org/10.1093/\mnras/sty1609

Krumholz, M. R., & Burkhart, B. (2016). Is turbulence in the interstellar medium driven by feedback or gravity? An observational test. *Monthly Notices of the Royal Astronomical Society*, *458*(2), 1671–1677. https://doi.org/10.1093/mnras/stw434

Krumholz, M. R., Burkhart, B., Forbes, J. C., & Crocker, R. M. (2018). A unified model for galactic discs: star formation, turbulence driving, and mass transport. *Monthly Notices of the Royal Astronomical Society*, *477*(2), 2716–2740. https://doi.org/10.1093/mnras/sty852

Krumholz, M. R., Fumagalli, M., da Silva, R. L., Rendahl, T., & Parra, J. (2015). SLUG–Stochastically Lighting Up Galaxies. III. A suite of tools for simulated photometry, spectroscopy, and Bayesian inference with stochastic stellar populations. *Monthly Notices of the Royal Astronomical Society*, *452*(2), 1447–1467. https://doi.org/10.1093/\mnras/stv1374

Krumholz, M. R., & Kruijssen, J. M. D. (2015). A dynamical model for the formation of gas rings and episodic starbursts near galactic centres. *Monthly Notices of the Royal Astronomical Society*, *453*(1), 739–757. https://doi.org/10.1093/\mnras/stv1670

Krumholz, M. R., & McKee, C. F. (2005). A General Theory of Turbulence-regulated Star Formation, from Spirals to Ultraluminous Infrared Galaxies. *The Astrophysical Journal*, *630*(1), 260–268. https://doi.org/10.1086/431734

Krumholz, M. R., McKee, C. F., & Tumlinson, J. (2009). The Atomic-to-Molecular Transition in Galaxies. II: H I and H_2 Column Densities. *The Astrophysical Journal*, *693*(1), 216–235. https://doi.org/10.1088/0004-637X/693/1/216

Kuijken, K., & Gilmore, G. (1989). The mass dstribution in the galactic disc. I - A technique to determine the integral surface mass density of the disc near the sun. *Monthly Notices of the Royal Astronomical Society*, *239*(2), 571–603. https://doi.org/10.1093/mnras/239.2.571

Kundu, A., Maccarone, T. J., & Zepf, S. E. (2002). The Low-Mass X-Ray Binary-Globular Cluster Connection in NGC 4472. *The Astrophysical Journal Letters*, *574*(1), L5–L9. https://doi.org/10.1086/342353

Kundu, A., & Whitmore, B. C. (2001). New Insights from HST Studies of Globular Cluster Systems. I. Colors, Distances, and Specific Frequencies of 28 Elliptical Galaxies. *The Astronomical Journal*, *121*(6), 2950–2973. https://doi.org/10.1086/321073

Kuo, C. Y., Braatz, J. A., Condon, J. J., Impellizzeri, C. M. V., Lo, K. Y., zaw, I., Schenker, M., Henkel, C., Reid, M. J., & Greene, J. E. (2011). The megamaser Cosmology Project. III. Accurate Masses of Seven Supermassive Black Holes in Active Galaxies with Circumnuclear Megamaser Disks. *The Astrophysical Journal*, *727*(1), 20. https://doi.org/10.1088/0004-637X/727/1/20

Lahén, N., Naab, T., Johansson, P. H., Elmegreen, B., Hu, C.-Y., Walch, S., Steinwandel, U. P., & Moster, B. P. (2020). The GRIFFIN Project—Formation of Star Clusters with Individual Massive Stars in a Simulated Dwarf Galaxy Starburst. *The Astrophysical Journal*, *891*(1), 2. https://doi.org/10.3847/1538-4357/ab7190

Lahén, N., Naab, T., Kauffmann, G., Szécsi, D., Hislop, J. M., Rantala, A., Kozyreva, A., Walch, S., & Hu, C.-Y. (2023). Formation of star clusters and enrichment by massive stars in simulations of low-metallicity galaxies with a fully sampled initial stellar mass function. *Monthly Notices of the Royal Astronomical Society*, *522*(2), 3092–3116. https://doi.org/10.1093/mnras/stad1147

Lahén, N., Naab, T., & Szécsi, D. (2024a). Star clusters forming in a low-metallicity starburst - rapid self-enrichment by (very) massive stars. *Monthly Notices of the Royal Astronomical Society*, *530*(1), 645–667. https://doi.org/10.1093/mnras/stae904

Lahén, N., Rantala, A., Naab, T., Partmann, C., Johansson, P. H., & Hislop, J. M. (2024b). The formation, evolution and disruption of star clusters with improved gravitational dynamics in simulated dwarf galaxies. *arXiv e-prints*, arXiv:2410.01891. https://doi.org/10.48550/arXiv.2410.01891

Lake, W., Naoz, S., Marinacci, F., Burkhart, B., Vogelsberger, M., Williams, C. E., Chiou, Y. S., Chiaki, G., Nakazato, Y., & Yoshida, N. (2023). The Supersonic Project: Star Formation in Early Star Clusters without Dark Matter. *The Astrophysical Journal Letters*, *956*(1), L7. https://doi.org/10.3847/2041-8213/acfa9b

Lake, W., Noaz, S., Chiou, Y. S., Burkhart, B., Marinacci, F., Vogelsberger, M., & Kremer, K. (2021). The Supersonic Project: SIGOs, A Proposed Progenitor to Globular Clusters, and Their Connections to Gravitational-wave Anisotropies. *The Astrophysical Journal*, *922*(1), 86. https://doi.org/10.3847/1538-4357/ac20d0

Lambert, M., Khim, D. J., Zaritsky, D., & Donnerstein, R. (2024). Systematically Measuring Ultra-diffuse Galaxies (SMUDGes). VI. Nuclear Star Clusters. *The Astro-*

nomical Journal, *167*(2), 61. https://doi.org/10.3847/1538-3881/ad0f25

Lamers, H. J. G. L. M., Gieles, M., & Portegies Zwart, S. F. (2005). Disruption time scales of star clusters in different galaxies. *Astronomy & Astrophysics*, *429*, 173–179. https://doi.org/10.1051/0004-6361:20041476

Lang, P., Meidt, S. E., Rosolowsky, E., Nofech, J., Schinnerer, E., Leroy, A. K., Emsellem, E., Pessa, I., Glover, S. C. O., Groves, B., Hughes, A., Kruijssen, J. M. D., Querejeta, M., Schruba, A., Bigiel, F., Blanc, G. A., Chevance, M., Colombo, D., Faesi, C., . . . Usero, A. (2020). PHANGS CO Kinematics: Disk Orientations and Rotation Curves at 150 pc Resolution. *The Astrophysical Journal*, *897*(2), 122. https://doi.org/10.3847/1538-4357/ab9953

Larsen, S. S. (1999). Young massive star clusters in nearby galaxies. II. Software tools, data reductions and clusters sizes. *Astronomy and Astrophysics Supplement*, *139*, 393–415. https://doi.org/10.1051/aas:1999509

Larsen, S. S. (2002). The Luminosity Function of Star Clusters in Spiral Galaxies. *The Astronomical Journal*, *124*(3), 1393–1409. https://doi.org/10.1086/342381

Larsen, S. S. (2010). Young and intermediate-age massive star clusters. *Philosophical Transactions of the Royal Society of London Series A*, *368*(1913), 867–887. https://doi.org/10.1098/rsta.2009.0255

Larsen, S. S., Romanowsky, A. J., Brodie, J. P., & Wasserman, A. (2020). An extremelt metal-deficient globular cluster in the Andromeda Galaxy. *Science*, *370*(6519), 970–973. https://doi.org/10.1126/science.abb1970

Larson, R. B. (1981). Turbulence and star formation in molecular clouds. *Monthly Notices of the Royal Astronomical Society*, *194*, 809–826. https://doi.org/10.1093/mnras/194.4.809

Lau, R. M., Herter, T. L., Morris, M. R., Becklin, E. E., & Adams, J. D. (2013). SOFIA/FORCAST Imaging of the Circumnuclear Ring at the Galactic Center. *The Astrophysical Journal*, *775*(1), 37. https://doi.org/10.1088/0004-637X/775/1/37

Lauer, T. R. (1985). High-resolution surface photometry of elliptical galaxies. *The Astrophysical Journal*, *57*, 473–502. https://doi.org/10.1086/191011

Lauer, T. R., Faber, S. M., Gebhardt, K., Richstone, D., Tremaine, S., Ajhar, E. A., Aller, M. C., Bender, R., Dressler, A., Filippenko, A. V., Green, R., Grillmair, C. J., Ho, L. C., Kormendy, J., Magorrian, J., Pinkney, J., & Siopis, C. (2005). The Centers of Early-Type Galaxies with Hubble Space Telescope. V. New WFPC2 Photometry. *The Astronomical Journal*, *129*(5), 2138–2185. https://doi.org/10.1086/429565

Lauer, T. R., Faber, S. M., Groth, E. J., Shaya, E. J., Campbell, B., Code, A., Currie, D. G., Baum, W. A., Ewald, S. P., Hester, J. J., Holtzman, J. A., Kristian, J., Light, R. M., Ligynds, C. R., O'Neil, E. J., & Westphal, J. A. (1993). Planetary Camera Observations of the Double Nucleus of M 31. *The Astronomical Journal*, *106*, 1436. https://doi.org/10.1086/116737

Launhardt, R., Zylka, R., & Mezger, P. G. (2002). The nuclear bulge of the Galaxy. III. Large-scale physical characteristics of stars and interstellar matter. *Astronomy & Astrophysics*, *384*, 112–139. https://doi.org/10.1051/0004-6361:20020017

Le, M. N., & Cooper, A. P. (2024). Globular cluster counts around 700 nearby galaxies. *The Astrophysical Journal*, 26. https://doi.org/10.48550/arXiv.2408.07124

Leaman, R., Ruiz-Lara, T., Cole, A. A., Beasley, M. A., Boecker, A., Fahrion, K., Bianchini, P., Falcóm-Barroso, J., Webb, J., Sills, A., Mastrobuono-Battisti, A., Neumayer, N., & Sippel, A. C. (2020). Globular cluster ejection, infall, and the host dark matter halo of the Pegasus dwarf galaxy. *Monthly Notices of the Royal Astronomical Society*, *492*(4), 5102–5120. https://doi.org/10.1093/\mnras/staa004

Leaman, R., & van de Ven, G. (2022). On the link between nuclear star cluster and globular cluster system mass, nucleation fraction, and environment. *Monthly Notices of the Royal Astronomical Society*, *516*(4), 4691–4715. https://doi.org/10.1093/\mnras/stab1966

Leaman, R., VandenBerg, D. A., & Mendel, J. T. (2013). The bifurcated age-metallicity relation of Milky Way globular clusters and its implications for the accretion history of the galaxy. *Monthly Notices of the Royal Astronomical Society*, *436*(1), 122–135. https://doi.org/10.1093/mnras/stt1540

Lee, J. C., Sandstrom, K. M., Leroy, A. K., Thilker, D. A., Schinnerer, E., Rosolowsky, E., Larson, K. L., Egorov, O. V., Williams, T. G., Schmidt, J., Emsellem, E., Anand, G. S., Barnes, A. T., Belfiore, F., Bešlić, I., Bigiel, F., Blanc, G. A., Bolatto, A. D., Boquien, M., . . . Razza, A. (2023). The PHANGS-JWST Treasury Survey: Star Formation, Feedback, and Dust Physics at High Angular resolution in Nearby GalaxieS. *The Astrophysical Journal Letters*, *944*(2), L17. https://doi.org/10.3847/2041-8213/acaaae

Lee, J. C., Whitmore, B. C., Thilker, D. A., Deger, S., Larson, K. L., Ubeda, L., Anand, G. S., Boquien, M., Chandar, R., Dale, D. A., Emsellem, E., Leroy, A. K., Rosolowsky, E., Schinnerer, E., Schmidt, J., Lilly, J., Turner, J., van Dyk, S., White, R. L., . . . Williams, T. G. (2022). The PHANGS-HST Survey: Physics at High Angular Resolution in Nearby Galaxies with the Hubble Space Telescope. *The Astrophysical Journal Series*, *258*(1), 10. https://doi.org/10.3847/1538-4365/ac1fe5

Lee, M. G. (2003). On the Formation of Giant Elliptical Galaxies and Globular Clusters. *Journal of Korean Astronomical Society*, *36*(3), 189–212. https://doi.org/10.5303/JKAS.2003.36.3.189

Lehmer, B. D., Alexander, D. M., Bauer, F. E., Brandt, W. N., Goulding, A. D., Jenkins, L. P., Ptak, A., & Roberts, T. P. (2010). A Chandra Perspective on Galaxy-wide X-ray Binary Emission and its Correlation with Star Formation Rate and Stellar Mass: New Results from Luminous Infrared Galaxies. *The Astrophysical Journal*, *724*(1), 559–571. https://doi.org/10.1088/0004-637X/724/1/559

Lehmer, B. D., Berkeley, M., Zezas, A., Alexander, D. M., Basu-Zych, A., Bauer, F. E., Brandt, W. N., Fragos, T., Hornschemeier, A. E., Kalogera, V., Ptak, A., Sivakoff, G. R., Tzanavaris, P., & Yukita, M. (2014). The X-Ray Luminosity Functions of Field Low-mass X-Ray Binaries in Early-type Galaxies: Evidence for a Stellar Age Dependence. *The Astrophysical Journal*, *789*(1), 52. https://doi.org/10.1088/0004-637X/789/1/52

Lehmer, B. D., Eufrasio, R. T., Tzanavaris, P., Basu-Zych, A., Fragos, T., Prestwich, A., Yukita, M., Zezas, A., Hornschemeier, A. E., & Ptak, A. (2019). X-Ray Binary Luminosity Function Scaling Relations for Local Galaxoes Based on Subgalactic Modeling. *The Astrophysical Journal Supplement Series*, *243*(1), 3. https://doi.org/10.3847/1538-4365/ab22a8

Lehmer, B. D., Ferrell, A. P., Doore, K., Eufrasio, R. T., Monson, E. B., Alexander, D. M., Basu-Zych, A., Brandt, W. N., Sivakoff, G. R., Tzanavaris, P., Yukita, M., Fragos, T., & Ptak, A. (2020). X-Ray Binary Luminosity Function Scaling Relations in Elliptical Galaxies: Evidence for Globular Cluster Seeding of Low-mass X-Ray Binaries in Galactic Fields. *The Astrophysical Journal Supplement Series*, *248*, 31. https://doi.org/10.3847/1538-4365/ab9175

Lehnert, M. D., Nesvadba, N. P. H., Le Tiran, L., Di Matteo, P., van Driel, W., Douglas, L. S., Chemin, L., & Bournaud, F. (2009). Physical Conditions in the Interstellar Medium of Intensely Star-Forming Galaxies at Redshift ~ 2. *The Astrophysical Journal*, *699*(2), 1660–1678. https://doi.org/10.1088/0004-637X/699/2/1660

Leigh, N., Böker, T., & Knigge, C. (2012). Nuclear star clusters and the stellar spheroids of their host galaxies. *Monthly Notices of the Royal Astronomical Society*, *424*(3), 2130–2138. https://doi.org/10.1111/j.1365-2966.2012.21365.x

Leroy, A. K., Sandstrom, K., Rosolowsky, E., Belfiore, F., Bolatto, A. D., Cao, Y., Koch, E. W., Schinnerer, E., Barnes, A. T., Bešlić, I., Bigiel, F., Blanc, G. A., Chastenet, J., Mayker Chen, N., Chevance, M., Chown, R., Congiu, E., Dale, D. A., Egorov, O. V., . . . Williams, T. G. (2023). PHANGS-JWST First Results: Mid-infrared Emission Traces Both Gas Column Densit and Heating at 100 pc Scales. *The Astrophysical Journal Letters*, *944*(2), L9. https://doi.org/10.3847/2041-8213/acaf85

Leroy, A. K., Schinnerer, E., Hughes, A., Rosolowsky, E., Pety, J., Schruba, A., Usero, A., Blanc, G. A., Chevance, M., Emsellem, E., Faesi, C. M., Herrera, C. N., Liu, D., Meidt, S. E., Querejeta, M., Saito, T., Sandstrom, K. M., Sun, J., Williams, T. G., . . . Whitmore, B. (2021). PHANGS-ALMA: Arcsecond CO(2-1) Imaging of Nearby Star-forming Galaxies. *The Astrophysical Journal Series*, *257*(2), 43. https://doi.org/10.3847/1538-4365/ac17f3

Leroy, A. K., Walter, F., Brinks, E., Bigiel, F., de Blok, W. J. G., Madore, B., & Thornley, M. D. (2008). The Star Formation Efficiency in Nearby Galaxies: Measuring Where Gas Forms Stars Effectively. *The Astronomical Journal*, *136*(6), 2782–2845. https://doi.org/10.1088/0004-6256/136/6/2782

Lesch, H., Biermann, P. L., Crusius, A., Reuter, H. P., Dahlem, M., Barteldrees, A., & Wielebinski, R. (1990). The formation of molecular gas rings in galactic central regions. *Monthly Notices of the Royal Astronomical Society*, *242*, 194–199. https://doi.org/10.1093/\mnras/242.2.194

Leveque, A., Giersz, M., Banerjee, S., Vesperini, E., Hong, J., & Portegies Zwart, S. (2022). A Monte Carlo study of early gas expulsion and evolution of star clusters: new simulations with the MOCCA code in the AMUSE framework. *Monthly Notices of the Royal Astronomical Society*, *514*(4), 5739–5750. https://doi.org/10.1093/\mnras/stac1690

Levy, R. C., Bolatto, A. D., Mayya, D., Cuevas-Otahola, B., Tarantino, E., Boyer, M. L., Boogaard, L. A., Böker, T., Cronin, S. A., Dale, D. A., Donaghue, K., Emig, K. L., Fisher, D. B., Glover, S. C. O., Herrera-Camus, R., Jiménez-Donaire, M. J., Klessen, R. S., Lenkić, L., Leroy, A. K., . . . van der Werf, P. P. (2024). JWST Observations of Starbursts: Massive Star Clusters in the Central Starburst of M 82. *The Astrophysical Journal Letters*, 16. https://doi.org/10.48550/arXiv.2408.04135

Li, H., & Gnedin, O. Y. (2019). Star cluster formation in cosmological simulations - III. Dynamical and chemical evolution. *Monthly Notices of the Royal Astronomical Society*, *486*(3), 4030–4043. https://doi.org/10.1093/mnras/stz1114

Li, H., Gnedin, O. Y., & Gnedin, N. Y. (2018). Star Cluster Formation in Cosmological Simulations. II. Effects of Star Formation Efficiency and Stellar Feedback. *The Astrophysical Journal*, *861*(2), 107. https://doi.org/10.3847/1538-4357/aac9b8

Li, H., Gnedin, O. Y., Gnedin, N. Y., Meng, X., Semenov, V. A., & Kravtsov, A. V. (2017). Star Cluster Formation in Cosmological Simulations. I. Properties of Young Clusters. *The Astrophysical Journal*, *834*(1), 69. https://doi.org/10.3847/1538-4357/834/1/69

Li, H., Vogelberger, M., Bryan, G. L., Marinacci, F., Sales, L. V., & Torrey, P. (2022). Formation and evolution of young massive clusters in galaxy mergers: the SMUGGLE view. *Monthly Notices of the Royal Astronomical Society*, *514*(1), 265–279. https://doi.org/10.1093/\mnras/stac1136

Light, E. S., Danielson, R. E., & Schwarzschild, M. (1974). The nucleus of M 31. *The Astrophysical Journal*, *194*, 257–263. https://doi.org/10.1086/153241

Lim, S., & Lee, M. G. (2015). The Star Cluster System in the Local Group Starburst Galaxy IC 10. *The Astrophysical Journal*, *804*(2), 123. https://doi.org/10.1088/0004-637X/804/2/123

Lin, C. C., & Shu, F. H. (1966). On the Spiral Structure of Disk Galaxies, II. Outline of a Theory of Density Waves. *Proceedings of the National Academy of Science*, *55*(2), 229–234. https://doi.org/10.1073/pnas.55.2.229

Linial, I., & Metzger, B. D. (2024a). Coupled Disk-Star Evolution in Galactic Nuclei and the Lifetimes of QPE Sources. *The Astrophysical Journal*, 24. https://doi.org/10.48550/arXiv.2404.12421

Linial, I., & Metzger, B. D. (2024b). Ultraviolet Quasiperiodic Eruptions from Star-Disk Collisions in Galactic Nuclei. *The Astrophysical Journal Letters*, *963*(1), L1. https://doi.org/10.3847/2041-8213/ad2464

Linial, I., & Quataert, E. (2024). Period evolution of repeating transients in galactic nuclei. *Monthly Notices of the Royal Astronomical Society*, *527*(2), 4317–4329. https://doi.org/10.1093/mnras/stad3470

Liu, B., & Bromm, V. (2021). Gravitational waves from the remnants of the first stars in nuclear star clusters. *Monthly Notices of the Royal Astronomical Society*, *506*(4), 5451–5467. https://doi.org/10.1093/mnras/stab2028

Liu, S., Wang, L., Hu, Y.-M., Tanikawa, A., & Trani, A. A. (2024). Merging hierarchical triple black hole systems with intermediate-mass black holes in population III star clusters. *Monthly Notices of the Royal Astronomical Society*, *533*(2), 2262–2281. https://doi.org/10.1093/mnras/stae1946

Liu, Y., Peng, E. W., Jordán, A., Blakeslee, J. P., Côté, P., Ferrarese, L., & Puzia, T. H. (2019). The ACS Fornax Cluster Survey. III. Globular Cluster Specific Frequencies of Early-type Galaxies. *The Astrophysical Journal*, *875*(2), 156. https://doi.org/10.3847/1538-4357/ab12d9

Lomelí-Núñez, L., Mayya, Y. D., Rodríguez-Merino, L. H., Ovando, P. A., Alzate, J. A., Rosa-González, D., Cuevas-Otahola, B., Bruzual, G., Cortesi, A., Gómez-González, V. M. A., & Escudero, C. G. (2024). Ages and metallicities of globular clusters in M 81 using GTC/OSIRIS spectra. *Monthly Notices of the Royal Astronomical Society*, *528*(2), 1445–1459. https://doi.org/10.1093/mnras/stae051

Loose, H. H., Kruegel, E., & Tutukov, A. (1982). Bursts of star formation in the galactic centre. *Astronomy & Astrophysics*, *105*(2), 342–350. https://ui.adsabs.harvard.edu/abs/1982A&A...105..342L

Lotz, J. M., Telford, R., Ferguson, H. C., Miller, B. W., Stiavelli, M., & Mack, J. (2001). Dynamical Friction in DE Globular Cluster Systems. *The Astrophysical Journal*, *552*(2), 572–581. https://doi.org/10.1086/320545

Loup, C., Zijlstra, A. A., Waters, L. B. F. M., & Groenewegen, M. A. T. (1997). Obscured AGB stars in the Magellanic Clouds. I. IRAS candidates. *Astronomy & Astrophysics Supplement series*, *125*, 419–437. https://doi.org/10.1051/aas:1997377

Lu, J. R., Ghez, A. M., Hornstein, S. D., Morris, M. R., Becklin, E. E., & Matthews, K. (2009). A Disk of Young Stars at the Galactic Center as Determined by Individual Stellar Orbits. *The Astrophysical Journal*, *690*(2), 1463–1487. https://doi.org/10.1088/0004-637X/690/2/1463

Lynden-Bell, D., & Pringle, J. E. (1974). The evolution of viscous discs and the origin of the nebular variables. *Monthly Notices of the Royal Astronomical Society*, *168*, 603–637. https://academic.oup.com/%5Cmnras/article/168/3/603/990948

Lyu, W., Zhang, H.-X., Paudel, S., Li, T., Tang, Y., Chen, G., Kong, X., & Peng, E. W. (2025). Dependence of Metal Enrichment of Nuclear Star Clusters on Galaxy Stellar Mass. *The Astrophysical Journal*, *979*(1), 85. https://doi.org/10.3847/1538-4357/ad9b0d

Lyubenova, M., & Tsatsi, A. (2019). Nuclear angular momentum of early-type galaxies hosting nuclear star clusters. *Astronomy & Astrophysics*, *629*, A44. https://doi.org/10.1051/0004-6361/201833954

Lyubenova, M., van den Bosch, R. C. E., Côté, P., Kuntschner, H., van de Ven, G., Ferrarese, L., Jordán, A., Infante, L., & Peng, E. W. (2013). The complex nature of the nuclear star cluster in FCC 277. *Monthly Notices of the Royal Astronomical Society*, *431*(4), 3364–3372. https://doi.org/10.1093/\mnras/stt414

Mackey, A. D., Wilkinson, M. I., Davies, M. B., & Gilmore, G. F. (2008). Black holes and core expansion in massive star clusters. *Monthly Notices of the Royal Astronomical Society*, *386*(1), 65–95. https://doi.org/10.1111/j.1365-2966.2008.13052.x

Maggorian, J., Tremaine, S., Richstone, D., Bender, R., Bower, G., Dressler, A., Faber, S. M., Gebhardt, K., Green, R., Grillmair, C., Kormendy, J., & Lauer, T. (1998). The Demogrpahy of Massive Dark Objects in Galaxy Centers. *The Astronomical Journal*, *115*(6), 2285–2305. https://doi.org/10.1086/300353

Mai, Y., Croom, S. M., Wisnioski, E., Vaughan, S. P., Varidel, M. R., Battisti, A. J., Medel, J. T., Mun, M., Tsukui, T., Foster, C., Harborne, K. E., Lagos, C. D. P., Wang, D., Bellstedt, S., Bland-Hawthorn, J., Colless, M., D'Eugenio, F., Grasha, K., Peng, Y., . . . Ziegler, B. (2024). The MAGPI Survey: the evolution and drivers of gas turbulence in intermediate-redshift galaxies. *Monthly Notices of the Royal Astronomical Society*, 15. https://doi.org/https://doi.org/10.48550/arXiv.2408.12224

Maji, M., Zhu, Q., Li, Y., Charlton, J., Hernquist, L., & Knebe, A. (2017). The Formation and Evolution of Star Clusters in Interacting Galaxies. *The Astrophysical Journal*, *844*(2), 108. https://doi.org/10.3847/1538-4357/aa7aa1

Makarov, D., Prugniel, P., Terekhova, N., Courtois, H., & Vauglin, I. (2014). HyperLEDA. III. The catalogue of extragalactic distances. *Astronomy & Astrophysics*, *570*, A13. https://doi.org/10.1051/0004-6361/201423496

Maksym, W. P., Ulmer, M. P., & Eracleous, M. (2010). A Tidal Disruption Flare in A 1689 from an Archival X-ray survey of Galaxy Clusters. *The Astrophysical Journal*, *772*(2), 1035–1050. https://doi.org/10.1088/0004-637X/722/2/1035

Mapelli, M., & Bressan, A. (2013). Impact of metallicity on the evolution of young star clusters. *Monthly Notices of the Royal Astronomical Society*, *430*(4), 3120–3127. https://doi.org/10.1093/mnras/stt119

Mapelli, M., Dall'Amico, M., Bouffanais, Y., Giacobbo, N., Arca Sedda, M., Artale, M. C., Ballone, A., Di Carlo, U. N., Iorio, G., Santoloquido, F., & Torniamenti, S. (2021). Hierarchical black hole mergers in young, globular and nuclear star clusters: the effect of metallicity, spin and cluster properties. *Monthly Notices of the Royal Astronomical Society*, *505*(1), 339–358. https://doi.org/10.1093/mnras/stav1334

Maraston, C., Bastian, N., Saglia, R. P., Kissler-Patig, M., Schweizer, F., & Goudfrooij, P. (2004). The dynamical mass of the young cluster W3 in NGC 7252. Hearvy-weight globular cluster of ultra compact dwarf galaxy? *Astronomy & Astrophysics*, *416*, 467–473. https://doi.org/10.1051/0004-6361:20031604

Marconi, A., Capetti, A., Axon, D. J., Koekemoer, A., Macchetto, D., & Schreier, E. J. (2001). Pering through the Dust: Evidence for a Supermassive Black Hole at the Nucleus of the Centaurus A form VLT Infrared Spectroscopy. *The Astrophysical Journal*, *549*(2), 915–937. https://doi.org/10.1086/319445

Marigo, P., Girardi, L., Bressan, A., Rosenfield, P., Aringer, B., Chen, Y., Dussin, M., Nanni, A., Pastorelli, G., Rodrigues, T., Trabucchi, M., Bladh, S., Dalcanton, J., Groenewegen, M. A. T., Montalbán, J., & Wood, P. R. (2017). A New Generation of PARSEC-COLIBRI Stellar Isochrones Including the TP-AGB Phase. *The*

Astrophysical Journal, *835*(1), 77. https://doi.org/10.3847/1538-4357/835/1/77

Martin, N. F., Venn, K. A., Aguado, D. S., Starkenburg, E., González Hernández, J. I., Ibata, R. A., Bonifacio, P., Caffai, E., Sestito, F., Arentsen, A., Allende Prieto, C., Carlberg, R. G., Fabbro, S., Fouesneau, M., Hill, V., Jablonka, P., Kordopatis, G., Lardo, C., Malhan, K., . . . Mucciarelli, A. (2022). A stellar stream remnant of a globular cluster below the metallicity floor. *Nature*, *601*(7891), 45–48. https://doi.org/10.1038/s41586-021-04162-2

Martin, P. (1995). Quantitative Morphology of Bars in Spiral Galaxies. *The Astronomical Journal*, *109*(6), 2428–2443. https://doi.org/10.1086/117461

Maschmann, D., Lee, J. C., Thilker, D. A., Whitmore, B. C., Deger, S., Boquien, M., Chandar, R., Dale, D. A., Wofford, A., Hannon, S., Larson, K. L., Leroy, A. D., Schinnerer, E., Rosolowsky, E., Úbeda, L., Barnes, A. T., Emsellem, E., Grasha, K., Groves, B., . . . Williams, T. G. (2024). PHANGS-HST Catalogs for $\sim 100,000$ Star Clusters and Compact Associations in 38 Galaxies. I. Observed Properties. *The Astrophysical Journal Supplement Series*, *273*(1), 14. https://doi.org/10.3847/1538-4365/ad3cd3

Matthews, L. D., Gallagher, J. S., Krist, J. E., Watson, A. M., Burrows, C. J., Griffiths, R. E., Hester, J. J., Trauger, J. T., Ballester, G. E., Clarke, J. T., Crisp, D., Evans, R. W., Hoessel, J. G., Holtzman, J. A., Mould, J. R., Scowen, P. A., Stapelfeldt, K. R., & Westphal, J. A. (1999). WFPC2 Observations of Compact Star Cluster Nuclei in Low-Luminosity Spiral Galaxies. *The Astronomical Journal*, *118*(1), 208–235. https://doi.org/10.1086/300909

Matzner, C. D., & McKee, C. F. (2000). Efficiencies of low-mass star and star cluster formation. *The Astrophysical Journal*, *545*(1), 364–378. https://doi.org/10.1086/317785

Mayer, L., Kazantzidis, S., & Escala, A. (2008). Formation of Nuclear Disks and Supermassive Black Hole Bianries in Galaxy Mergers. *Memorie della Societá Astronomica Italiana*, *79*, 1284. https://doi.org/10.48550/arXiv.0807.3329

McCrady, N., & Graham, J. R. (2007). Super Star Cluster Velocity Dispersion and Virial Masses in the M 82 Nuclear Starburst. *The Astrophysical Journal*, *663*(2), 844–856. https://doi.org/10.1086/518357

McGaugh, S. S., & Schombert, J. M. (2014). Color-Mass-to-light-ratio Relations for Disk Galaxies. *The Astronomical Journal*, *148*(5), 77. https://doi.org/10.1088/0004-6256/148/5/77

McKee, C. F., & Krumholz, M. R. (2010). The Atomic-to-Molecular Transition in Galaxies. III. A New Method for Determining the Molecular Content of Primordial and Dusty Clouds. *The Astrophysical Journal*, *709*(1), 308–320. https://doi.org/10.1088/0004-637X/709/1/308

McKee, C. F., & Tan, J. C. (2003). The Formation of Massive Stars from Turbulent Cores. *The Astrophysical Journal*, *585*(2), 850–871. https://doi.org/10.1086/346149

McLaughlin, D. E., King, A. R., & Nayakshin, S. (2006). The M-σ Relation for Nucleated Galaxies. *The Astrophysical Journal Letters*, *650*(1), L37–L40. https://doi.org/10.1086/508627

McLaughlin, D. E., & van der Marel, R. P. (2005). Resolved Massive Star Clusters in the Milky Way and Its Satellites: Brightness Profiles and a Catalog of Fundamental Parameters. *The Astrophysical Journal Series*, *161*(2), 304–360. https://doi.org/10.1086/497429

McMaster, M., Biretta, J., Baggett, S., Bedin, L., Brammer, G., Burrows, C., Casertano, S., Chiaberge, M., Clampin, M., Dixon, V., Ferguson, H., Fruchter, A., Gilliland, R., Golimowski, D., Gonzaga, S., Griffiths, R., Heyer, I., Holtzman, J., Hulbert, S., . . . Whitmore, B. (2008). *Wide Field and Planetary Camera 2 Instrument Handbook v. 10.0*. Space Telescope Science Institude (STScI). Balitmore, USA.

McQuinn, K. B. W., Skillman, E. D., Dolphin, A. E., Berg, D., & Kennicutt, R. (2017). Accurate Distances to Important Spiral Galaxies: M 63, M 74, NGC 1291, NGC 4559, NGC 4625, and NGC 5398. *The Astronomical Journal*, *154*(2), 51–63. https://doi.org/10.3847/1538-3881/aa7aad

Meibom, S., Grundahl, F., Clausen, J. V., Mathieu, R. D., Frandsen, S., Pigulski, A., Narwid, A., Steslicki, M., & Lefever, K. (2009). Age and Distance for the Old Open Cluster NGC 188 from the Eclipsing Binary Member V 12. *The Astronomical Journal*, *137*(6), 5086–5098. https://doi.org/10.1088/0004-6256/137/6/5086

Merrell, K. A., Vasiliev, E., Bentz, M. C., Valluri, M., & Onken, C. A. (2023). The Mass of the Black Hole in NGC 5273 from Stellar Dynamical Modeling. *The Astrophysical Journal*, *949*(1), 13. https://doi.org/10.3847/1538-4357/acc4bc

Merritt, D., Mikkola, S., & Szell, A. (2007). Long-Term Evolution of Massive Black Hole Binaries. III. Binary Evolution in Collisional Nuclei. *The Astrophysical Journal*, *671*(1), 53–72. https://doi.org/10.1086/522691

Merritt, D., Piatek, S., Portegies Zwart, S., & Hemsendorf, M. (2004). Core Formation by a Population of Massive Remnants. *The Astrophysical Journal Letters*, *608*(1), L25–L28. https://doi.org/10.1086/422252

Metha, B., Trenti, M., Battisti, A., & Chu, T. (2024). A geostatistical analysis of multiscale metallicity varaitions in galaxies - III. Spatial resolution and data quality limits. *Monthly Notices of the Royal Astronomical Society*, *529*(1), 104–128. https://doi.org/10.1093/mnras/stae491

Metha, B., Trenti, M., & Chu, T. (2021). A geostatistical analysis of multiscale metallicity varaitions in galaxies - I. Introduction and comparison of high-resolution metallicity maps to an analytical metal transport model. *Monthly Notices of the Royal Astronomical Society*, *508*(1), 489–507. https://doi.org/10.1093/mnras/stab2554

Meynet, G., Maeder, A., Schaller, G., Schaerer, D., & Charbonnel, C. (1994). Grids of massive stars with high mass loss rates. V. From 12 to 120 $M_{\odot}$ at $Z = 0.001$, 0.004, 0.008, 0.020 and 0.040. *Astronomy & Astrophysics Supplement Series*, *103*, 97–105. https://ui.adsabs.harvard.edu/abs/1994A&AS..103...97M

Mezcua, M., & Domínguez Sánchez, H. (2020). Hidden AGNs in Dwarf Galaxies Revealed by MaNGA: Light Echoes, Off-nuclear Wanderers, and a New Broad-line

AGN. *The Astrophysical Journal Letters*, *898*(2), L30. https://doi.org/10.3847/2041-8213/aba199

Mezcua, M., Siudek, M., Suh, H., Valiante, R., Spinoso, D., & Bonoli, S. (2023). Overmassive Black Holes in Dwarf Galaxies Out to $z \sim 0.9$ in the VIPERS Survey. *The Astrophysical Journal Letters*, *943*(1), L5. https://doi.org/10.3847/2041-8213/acae25

Mieske, S., Frank, M. J., Baumgardt, H., Lützgendorf, N., Neumayer, N., & Hilker, M. (2013). On central black holes in ultra-compact dwarf galaxies. *Astronomy & Astrophysics*, *558*, A14. https://doi.org/10.1051/0004-6361/201322167

Mieske, S., Hilker, M., & Misgeld, I. (2012). The specific frequencies of ultra-compact dwarf galaxies. *Astronomy & Astrophysics*, *537*, A3. https://doi.org/10.1051/0004-6361/201117634

Mihos, J. C., & Hernquist, L. (1994). Dense Stellar Cores in Merger Remnants. *The Astrophysical Journal Letters*, *437*, L47. https://doi.org/10.1086/187679

Miller, B. P., Gallo, E., Greene, J. E., Kelly, B. C., Treu, T., Woo, J.-H., & Baldassare, V. (2015a). X-Ray Constraints on the Local Supermassive Black Hole Occupation Fraction. *The Astrophysical Journal*, *799*(1), 98. https://doi.org/10.1088/0004-637X/799/1/98

Miller, B. W., & Lotz, J. M. (2007). The Globular Cluster Luminosity Function and Specific Frequency in Dwarf Elliptical Galaxies. *The Astrophysical Journal*, *670*(2), 1074–1089. https://doi.org/10.1086/522323

Miller, J. M., Kaastra, J. S., Miller, M. C., Reynolds, M. T., Brown, G., Cenko, S. B., Drake, J. J., Gezari, S., Guillochon, J., Gultekin, K., Irwin, J., Levan, A., Maitra, D., Maksym, W. P., Mushotzky, R., O'Brien, P., Paerels, F., de Plaa, J., Ramirez-Ruiz, E., . . . Tanvir, N. (2015b). Flows of X-ray gas reveal the disruption of a star by a massive black hole. *Nature*, *526*(7574), 542–545. https://doi.org/10.1038/nature15708

Milosavljević, M. (2004). On the Origin of Nuclear Star Clusters in Late-Type Spiral Galaxies. *The Astrophysical Journal Letters*, *605*(1), L13–L16. https://doi.org/10.1086/420696

Milosavljević, M., & Merritt, D. (2001). Formation of Galactic Nuclei. *The Astrophysical Journal*, *563*(1), 34–62. https://doi.org/10.1086/323830

Minniti, D., Geisler, D., Alonso-García, J., Palma, T., Beamín, J. C., Borissova, J., Catelan, M., Clariá, J. J., Cohen, R. E., Contreras Ramos, R., Dias, B., Fernández-Trincado, J. G., Gómez, M., Hempel, M., Ivanov, V. D., Kurtev, R., Lucas, P. W., Moni-Bidin, C., Pullen, J., . . . Valenti, E. (2017). New VVV Survey Globular Cluster Candidates in the Milky Way Bulge. *The Astrophysical Journal Letters*, *849*(2), L24. https://doi.org/10.3847/2041-8213/aa95b8

Mockler, B., Guillochon, J., & Ramirez-Ruiz, E. (2019). Weighing Blakc Holes Using Tidal Disruption Events. *The Astrophysical Journal*, *872*(2), 151. https://doi.org/10.3847/1538-4357/ab010f

Mockler, B., Melchor, D., Naoz, S., & Ramirez-Ruiz, E. (2023). Uncovering Hidden Massive Black Hole Companions with Tidal Disruption Events. *The Astrophysical Journal*, 18. https://doi.org/10.48550/arXiv.2306.05510

Modak, S., Danieli, S., & Greene, J. E. (2023). Distinguishing Dark Matter Cusps from Cores Using Globular Clusters. *The Astrophysical Journal*, *950*(2), 178. https://doi.org/10.3847/1538-4357/accc2d

Monaco, P., Fontanot, F., & Taffoni, G. (2007). The MORGANA model for the rise of galaxies and active nuclei. *Monthly Notices of the Royal Astronomical Society*, *375*(4), 1189–1219. https://doi.org/10.1111/j.1365-2966.2006.11253.x

Morrissey, P., Conrow, T., Barlow, T. A., Small, T., Seibert, M., Wyder, T. K., Budaári, T., Arnouts, S., Friedman, P. G., Forster, K., Martin, D. C., Neff, S. G., Schiminovich, D., Bianchi, L., Donas, J., Heckman, T. M., Lee, Y.-W., Madore, B. F., Milliard, B., . . . Yi, S. K. (2007). The Calibration and Data Products of GALEX. *The Astrophysical Journal Supplement Series*, *173*(2), 682–697. https://doi.org/10.1086/520512

Mowla, L., Iyer, K., Asada, Y., Desprez, G., Tan, V. Y. Y., Martis, N., Sarrouh, G., Strait, V., Abraham, R., Bradač, M., Brammer, G., Muzzin, A., Pacifici, C., Ravindranath, S., Sawicki, M., Willott, C., Estrada-Carpenter, V., Jahan, N., Noirot, G., . . . Zabl, J. (2024). The Firefly Sparkle: The Earliest Stages of the Assembly of A Milky Way-type Galaxy in a 600 Myr Old Universe. *arXiv e-prints*, arXiv:2402.08696. https://doi.org/10.48550/arXiv.2402.08696

Mowla, L., Iyer, K. G., Desprez, G., Estrada-Carpenter, V., Martis, N. S., Noirot, G., Sarrouh, G. T., Strait, V., Asada, Y., Abraham, R. G., Brammer, G., Sawicki, M., Willott, C. J., Bradac, M., Doyon, R., Muzzin, A., Pacifici, C., Ravinranath, S., & Zabl, J. (2022). The sparkler: Evolved high-redshift globular cluster candidates captured by jwst. *The Astrophysical Journal Letters*, *937*(2), L35. https://doi.org/10.3847/2041-8213/ac90ca

Mukherjee, D., Zhu, Q., Ogiza, G., Rodriguez, C. L., & Trac, H. (2023). Evolution of massive black hole binaries in collisionally relaxed nuclear star clusters - Impact of mass segregation. *Monthly Notices of the Royal Astronomical Society*, *518*(4), 4801–4817. https://doi.org/10.1093/mnras/stac3390

Mulcahy, D. D., Beck, R., & Heald, G. H. (2017). Resolved magnetic structures in the disk-halo interface of NGC 628. *Astronomy & Astrophysics*, *600*, A6. https://doi.org/10.1051/0004-6361/201629907

Muñoz, R. P., Eigenthaler, P., Puzia, T. H., Taylor, M. A., Ordenes-Briceño, Y., Alamo-Martínez, K., Ribbeck, K. X., Ángel, S., Capaccioli, M., Côté, P., Ferrarese, L., Galaz, G., Hempel, M., Hilker, M., Jordán, A., Lançon, A., Mieske, S., Paolillo, M., Richtler, T., . . . Zhang, H. (2015). Unveiling a Rich System of Faint Dwarf Galaxies in the Next Generation Fornax Survey. *The Astrophysical Journal Letters*, *813*(1), L15. https://doi.org/10.1088/2041-8205/813/1/L15

Muratov, A. L., & Gnedin, O. Y. (2010). Modeling the Metallicity Distribution of Globular Clusters. *The Astrophysical Journal*, *718*(2), 1266–1288. https://doi.org/10.1088/0004-637X/718/2/1266

Murphy, G. G., Yates, R. M., & Mohamed, S. S. (2022). L-GALAXIES 2020: the formation and chemical evolution of stellar haloes in Milky Way analogues and galaxy clusters. *Monthly Notices of the Royal Astro-*

nomical Society, *510*(2), 1945–1963. https://doi.org/10.1093/\mnras/stab3568

Myeong, G. C., Evans, N. W., Belokurov, V., Sanders, L. J., & Koposov, S. E. (2018). The Sausage Globular Clusters. *The Astrophysical Journal Letters*, *863*(2), L28. https://doi.org/10.3847/2041-8213/aad7f7

Myers, P. C., & Goodman, A. A. (1988). Magnetic Molecular Clouds: Indirect Evidence for Magnetic Support and Ambipolar Diffusion. *The Astrophysical Journal*, *329*, 392–405. https://doi.org/10.1086/166385

Naiman, J. P., Ramirez-Ruiz, E., Debuhr, J., & Ma, C.-P. (2015). The Role of Nuclear Star Clusters in Enhancing Supermassive Black Hole Feeding Rates During Galaxy Mergers. *The Astrophysical Journal*, *803*(2), 81. https://doi.org/10.1088/0004-637X/803/2/81

Nandra, K., Barret, D., Barcons, X., Fabian, A., den Herder, J.-W., Piro, L., Watson, M., Adai, C., Aird, J., Afonsi, J. M., Alexander, D., Argiroffi, C., Amati, L., Arnaud, M., Atteia, J.-L., Audard, M., Badenes, C., Ballet, J., Ballo, L., . . . Yhuravleva, I. (2013). The Hot and Energetic Universe: A White Paper presenting the science theme motivating the Athena+ mission. *arXiv e-prints*, 19. https://doi.org/10.48550/arXiv.1306.2307

Nardiello, D., Bedin, L. R., Burgasser, A., Salaris, M., Cassisi, S., Griggio, M., & Scalco, M. (2022). Photometry and astrometry with JWST - I. NIRCam Point Spread Functions and the first JWST colour-magnitude diagrams of a globular cluster. *Monthly Notices of the Royal Astronomical Society*. https://doi.org/10.1093/\mnras/stac2659

Navarro, J. F., Frenk, C. S., & White, S. D. M. (1996). The Structure of Cold Dark Matter Halos. *The Astrophysical Journal*, *462*, 563. https://doi.org/10.1086/177173

Neumayer, N., Seth, A. C., & Böker, T. (2020). Nuclear star clusters. *The Astronomy and Astrophysics Review*, *28*(1), 75. https://doi.org/10.1007/s00159-020-00125-0

Neumayer, N., Walcher, C. J., Andersen, D., Sánchez, S. F., Böker, T., & Rix, H.-W. (2011). Two-dimensional Hα kinematics of bulgeless disc galaxies. *Monthly Notices of the Royal Astronomical Society*, *413*(3), 1875–1888. https://doi.org/10.1111/j.1365-2966.2011.18266.x

Newton, O., Davies, J. J., Pfeffer, J., Crain, R. A., Kruijssen, J. M. D., Pontzen, A., & Bastian, N. (2024). The formation and disruption of globular cluster populations in simulations of present-day $L^\star$ galaxies with controlled assembly histories. *arXiv*, 17. https://doi.org/10.48550/arXiv.2409.04516

Nguyen, D. D., Bureau, M., Thater, S., Nyland, K., den Brok, M., Cappellari, M., Davis, T. A., Greene, J. E., Neumayer, N., Imanishi, M., Izumi, T., Kawamuro, T., Baba, S., Nguyen, P. M., Iguchi, S., Tsukui, T., Lam, T. N., & Ho, T. (2022). The MBHBM* Project - II. Molecular gas kinematics in the lenticular galaxy NGC 3593 reveal a supermassive black hole. *Monthly Notices of the Royal Astronomical Society*, *509*(2), 2920–2939. https://doi.org/10.1093/\mnras/stab3016

Nguyen, D. D., Seth, A. C., den Brok, M., Neumayer, N., Cappellari, M., Barth, A. J., Caldwell, N., Williams, B. F., & Binder, B. (2017). Improved Dynamical Constraints on the Mass of the Central Black Hole in NGC 404. *The Astrophysical Journal*, *836*(2), 237. https://doi.org/10.3847/1538-4357/aa5cb4

Nguyen, D. D., Seth, A. C., Neumayer, N., Iguchi, S., Cappellari, M., Strader, J., Chomiuk, L., Tremou, E., Pacucci, F., Nakanishi, K., Bahramian, A., Nguyen, P. M., den Brok, M., Ahn, C. C., Voggel, K. T., Kachariv, N., tsukui, T., Ly, C. K., Dumont, A., & Pechetti, R. (2019). Improved Dynamical Constraints on the Masses of the Central Black Holes in Nearby Low-mass Early-type Galactic Nuclei and the First Black Hole Determination for NGC 205. *The Astrophysical Journal*, *872*(1), 104. https://doi.org/10.3847/1538-4357/aafe7a

Nguyen, D. D., Seth, A. C., Neumayer, N., Kamann, S., Voggel, K. T., Cappellari, M., Picotti, A., Nguyen, P. M., Böker, T., Debattista, V., Caldwell, N., McDermid, R., Bastian, N., Ahn, C. C., & Pechetti, R. (2018). Nearby Early-type Galacitc Nuclei at High Resolution: Dynamical Black Hole and Nuclear Star Cluster Mass Measurements. *The Astrophysical Journal*, *858*(2), 118–147. https://doi.org/10.3847/1538-4357/aabe2

Nguyen, D. D., Seth, A. C., Reines, A. E., den Brok, M., Sand, D., & McLeod, B. (2014). Extended Structure and Fate fo the Nucleus in Henize 2-10. *The Astrophysical Journal*, *794*(1), 34. https://doi.org/10.1088/0004-637X/794/1/34

Nieto, J.-L., & Auriere, M. (1982). Optical structure of the nucleus of M 33. *Astronomy & Astrophysics*, *108*(2), 334–338. https://ui.adsabs.harvard.edu/abs/1982A&A..108..334N

Nitschai, M. S., Neumayer, N., Häberle, M., Clontz, C., Seth, A. C., Milone, A. P., Alfaro-Cuello, M., Bellini, A., Dreizler, S., Feldmeier-Krause, A., Husser, T.-O., Kacharov, N., Kamann, S., Latour, M., Libralato, M., van de Ven, G., Voggel, K., & Wang, Z. (2024). oMEGACat III. Multi-band photometry and metallicities reveal spatially well-mixed populations within ω Centauri's half-light radius. *The Astrophysical Journal*, 22. https://doi.org/10.48550/arXiv.2406.01688

Nogueras-Lara, F. (2022). Kinematic data rebuild the Nuclear star cluster as the most metal rich region of the Galaxy. *Astronomy & Astrophysics*, *666*, A72. https://doi.org/10.1051/0004-6361/202244411

Nogueras-Lara, F., Feldmeier-Krause, A., Schödel, R., Sormani, M. C., de Lorenzo-Cáceres, A., Mastrobuono-Battisti, A., Schultheis, M., Neumayer, N., Rich, R. M., & Nieuwmunster, N. (2023). Smooth kinematic and metallicity gradients reveal that the Milky Way's nuclear star cluster and disc might be part of the same structure. *Astronomy and Astrophysics*, *680*, A75. https://doi.org/10.1051/0004-6361/202347421

Nogueras-Lara, F., Schödel, R., Gallego-Calvente, A. T., Gallego-Cano, E., Shahzamanian, B., Dong, H., Neumayer, N., Hilker, M., Najarro, F., Nishiyama, S., Feldmeier-Krause, A., Girard, J. H. V., & Cassisi, S. (2020). Early formation and recent starburst activity in the nuclear disk of the Milky Way. *Nature Astronomy*, *4*, 377–381. https://doi.org/10.1038/s41550-019-0967-9

Nogueras-Lara, F., Schödel, R., & Neumayer, N. (2019). The Nuclear Star Cluster and Nuclear Stellar Disk of the Milky Way: Different Stellar Populations and Star Formation Histories. *The Astrophysical Journal*, *920*(2), 97. https://doi.org/10.3847/1538-4357/ac185e

Noll, S., Burgarella, D., Giovannoli, E., Buat, V., Marcillac, D., & Muñoz-Mateos, J. C. (2009). Analysis of galaxy spectral energy distributions from far-UV to far-IR with CIGALE: studying a SINGS test sample. *Astronomy & Astrophysics*, *507*(3), 1793–1813. https://doi.org/10.1051/0004-6361/200912497

Nordlund, Å., & Padoan, P. (1999). The Density PDFs of Supersonic Random Flows. In J. Franco & A. Carraminana (Eds.), *Interstellar Turbulence* (p. 218). https://arxiv.org/abs/astro-ph/9810074

Norris, M. A., Escudero, C. G., Faifer, F. R., Kannappan, S. J., Forte, J. C., & van den Bosch, R. C. E. (2015). An extended star formation history in an ultra-compact dwarf. *Monthly Notices of the Royal Astronomical Society*, *451*(4), 3615–3626. https://doi.org/10.1093/mnras/stv1221

Norris, M. A., Kannappan, S. J., Forbes, D. A., Romanowsky, A. J., Brodie, J. P., Faifer, F. R., Huxor, A., Maraston, C., Moffett, A. J., Penny, S. J., Pota, V., Smith-Castelli, A., Strader, J., Bradley, D., Eckert, K. D., Fohring, D., McBride, J., Stark, D. V., & Vaduvescu, O. (2014). The AIMSS Project - I. Bridging the star cluster-galaxy divide. *Monthly Notices of the Royal Astronomical Society*, *443*(2), 1151–1172. https://doi.org/10.1093/\mnras/stu1186

Norris, M. A., van de Ven, G., Kannappan, S. J., Schinnerer, E., & Leaman, R. (2019). Is there a fundamental upper limit to the mass of a star cluster? *Monthly Notices of the Royal Astronomical Society*, *488*(4), 5400–5408. https://doi.org/10.1093/mnras/stz2096

Nowak, N., Saglia, R. P., Thomas, J., bender, R., Davies, R. I., & Gebhardt, K. (2008). The supermassive black hole of Fornax A. *Monthly Notices of the Royal Astronomical Society*, *391*(4), 1629–1649. https://doi.org/10.1111/j.1365-2966.2008.13960.x

O'Connell, R. W. (1983). Star formation in the semistellar nucleus of M 33. *The Astrophysical Journal*, *267*, 80–92. https://doi.org/10.1086/160846

O'Donnell, J. E. (1994). R_V-dependent Optical and Near-Ultraviolet Extinction. *The Astrophysical Journal*, *422*, 158–163. https://doi.org/10.1086/173713

Oh, K. S., & Lin, D. N. C. (2000). Nucleation of Dwarf Galaxies in the Virgo Cluster. *The Astrophysical Journal*, *543*(2), 620–633. https://doi.org/10.1086/317118

Ohlson, D., Seth, A. C., Gallo, E., Baldassare, V. F., & Greene, J. E. (2023). The 50 Mpc Galaxy Catalog (50MGC): Consistent and Homogeneous Masses, Distances, Colors, and Morphologies. *The Astronomical Journal*, 23. https://doi.org/10.48550/arXiv.2309.05701

Oklopčić, A., Hopkins, P. F., Feldmann, R., Kereš, D., Faucher-Giguére, C.-A., & Murray, N. (2017). Giant clumps in the FIRE simulations: a case study of a massive high-redshift galaxy. *Monthly Notices of the Royal Astronomical Society*, *465*(1), 952–969. https://doi.org/10.1093/mnras/stw2754

Önehag, A., Gustafsson, B., & Korn, A. (2014). Abundances and possible diffusion of elements in M 67 stars. *Astronomy & Astrophysics*, *562*, A102. https://doi.org/10.1051/0004-6361/201322663

Ono, Y., Ouchi, M., Harikane, Y., Yajima, H., Nakajima, K., Fujimoto, S., Nakane, M., & Xu, Y. (2025). Morphological Demographics of Galaxies at $z \sim$ 10-16: Log-Normal Size Distribution and Exponential Profiles Consistent with the Disk Formation Scenario. *arXiv e-prints*, 24. https://doi.org/10.48550/arXiv.2502.08885

Ordenes-Briceño, Y., Puzia, T. H., Eigenthaler, P., Taylor, M. A., Muñoz, R. P., Zhang, H., Alamo-Matrínez, K., Ribbeck, K. X., Grebel, E. K., Ángel, S., Côté, P., Ferrarese, L., Hilker, M., Lançon, A., Mieske, S., Miller, B. W., Rong, Y., & Sánchez-Janssen, R. (2018). The Next Generation Fornax Survey (NGFS). IV. Mass and Age Bimodality of Nuclear Clusters in the Fornax Core Region. *The Astrophysical Journal*, *860*(1), 4. https://doi.org/10.3847/1538-4357/aac1b8

Ostriker, E. C. (1999). Dynamical Friction in a Gaseous Medium. *The Astrophysical Journal*, *513*(1), 252–258. https://doi.org/10.1086/306858

Ostriker, E. C., Stone, J. M., & Gammie, C. F. (2001). Density, Velocity, and Magnetic Field Structure in Turbulent Molecular Cloud Models. *The Astrophysical Journal*, *546*(2), 980–1005. https://doi.org/10.1086/318290

Pace, A. B. (2024). The Local Volume Database: a library of the observed properties of nearby dwarf galaxies and star clusters. *arXiv e-prints*, arXiv:2411.07424. https://doi.org/10.48550/arXiv.2411.07424

Padoan, P., Jimenez, R., & Jones, B. (1997). On star formation in primordial protoglobular clouds. *Monthly Notices of the Royal Astronomical Society*, *185*(4), 711–717. https://doi.org/10.1093/mnras/285.4.711

Padoan, P., & Nordlund, Å. (2002). The stellar initial mass function from turbulent fragmentation. *The Astrophysical Journal*, *576*(2), 870–879. https://doi.org/10.1086/341790

Padoan, P., & Nordlund, Å. (2011). The Star Formation Rate of Supersonic Magnetohydrodynamic Turbulence. *The Astrophysical Journal*, *730*(1), 40. https://doi.org/10.1088/0004-637X/730/1/40

Pak, M., Paudel, S., Lee, Y., & Kim, S. C. (2016). MCG+08-22-082: A Double Core and Boxy Appearance Dwarf Lenticular Galaxy Suspected to be a Merger Remnant. *The Astronomical Journal*, *151*(6), 141. https://doi.org/10.3847/0004-6256/151/6/141

Parente, M., Ragone-Figueroa, C., Granato, G. L., & Lapi, A. (2023). The $z \lesssim 1$ drop of cosmic dust abundance in a semi-analytic framework. *Monthly Notices of the Royal Astronomical Society*, *521*(4), 6105–6123. https://doi.org/10.1093/mnras/stad907

Parente, M., Ragone-Figueroa, C., López, P., Martínez, H., Ruiz, A., Ceccarelli, L., Coenda, V., Rodriguez, F., Granato, G. L., Lapi, A., & van de Weygaert, R. (2024). Star Formation and Dust in the Cosmic Web. *The Astrophysical Journal*, *966*(2), 154. https://doi.org/10.3847/1538-4357/ad320e

Parmentier, G., & Gilmore, G. (2007). The origin of the Gaussian initial mass function of old globular cluster systems. *Monthly Notices of the Royal Astronomical Society*, *377*(1), 352–372. https://doi.org/10.1111/j.1365-2966.2007.11611.x

Partmann, C., Naab, T., Lahén, N., Rantala, A., Hirschmann, M., Hislop, J. M., Petersson, J., & Johansson, P. H. (2024). The importance of nuclear star clusters for massive black hole growth and nuclear star formation in simulated low-mass galaxies. *arXiv* *e-prints*, arXiv:2409.18096. https://doi.org/10.48550/arXiv.2409.18096

Pasquali, A., Bik, A., Zibetti, S., Ageorges, N., Seifert, W., Brandner, W., Rix, H.-W., Jütte, M., Knierim, V., Buschkamp, P., Feiz, C., Femperlein, H., Germeroth, A., Hofmann, R., Laun, W., Lederer, R., Lehmitz, M., Lenzen, R., Mall, U., . . . Weiser, P. (2011). Infrared Narrowband Tomography of the Local Starburst NGC 1569 with the Large Binocular Telescope/LUCIFER. *The Astronomical Journal*, *141*(4), 132. https://doi.org/10.1088/0004-6256/141/4/132

Pastorelli, G., Marigo, P., Girardi, L., Aringer, B., Chen, Y., Rubele, S., Trabucchi, M., Bladh, S., Boyer, M. L., Bressan, A., Dalcanton, J. J., Groenewegen, M. A. T., Lebzelter, T., Mowlavi, N., Chubb, K. L., Cioni, M.-R. L., de Grijs, R., Ivanov, V. D., Nanni, A., . . . Zaggia, S. (2020). Constraining the thermally pulsing asymptotic giant branch phase with resolved stellar populations in the Large Magellanic Cloud. *Monthly Notices of the Royal Astronomical Society*, *498*(3), 3283–3301. https://doi.org/10.1093/\mnras/staa2565

Pastorelli, G., Marigo, P., Girardi, L., Chen, Y., Rubele, S., Trabucchi, M., Aringer, B., Bladh, S., Bressan, A., Montalbán, J., Boyer, M. L., Dalcanton, J. J., Eriksson, K., Groenewegen, M. A. T., Höfner, S., Lebzelter, T., Nanni, A., Rosenfield, P., Wood, P. R., & Cioni, M.-R. L. (2019). Constraining the thermally pulsing asymptotic giant branch phase with resolved stellar populations in the Small Magellanic Cloud. *Monthly Notices of the Royal Astronomical Society*, *485*(4), 5666–5692. https://doi.org/10.1093/\mnras/stz725

Pastorello, N., Forbes, D. A., Usher, C., Brodie, J. P., Romanowsky, A. J., Strader, J., Spitler, L. R., Alabi, A. B., Foster, C., Jennings, Z. G., Kartha, S. S., & Pota, V. (2015). The SLUGGS survey: combining stellar and globular cluster metallicities in the outer regions of early-type galaxies. *Monthly Notices of the Royal Astronomical Society*, *451*(3), 2625–2639. https://doi.org/10.1093/mnras/stv1131

Paudel, S., Duc, P.-A., Lim, S., Poulain, M., Marleau, F. R., Müller, O., Sánchez-Janssen, R., Habas, R., Durrell, P. R., Heesters, N., Chhatkuli, D. N., & Yoon, S.-J. (2023). The creation of a massive UCD by tidal threshing from NGC 936. *Monthly Notices of the Royal Astronomical Society*, *526*(1), L136–L142. https://doi.org/10.1093/mnrasl/slad126

Paudel, S., Lisker, T., & Kuntschner, H. (2011). Nuclei of early-type dwarf galaxies: insights from stellar populations. *Monthly Notices of the Royal Astronomical Society*, *413*(3), 1764–1776. https://doi.org/10.1111/j.1365-2966.2011.18256.x

Paudel, S., & Yoon, S.-J. (2020). Starbursting Nuclei in Old Dwarf Galaxies. *The Astrophysical Journal Letters*, *898*(2), L47. https://doi.org/10.3847/2041-8213/aba6ed

Paumard, T., Genzel, R., Martins, F., Nayakshin, S., Beloborodov, A. M., Levin, Y., Trippe, S., Eisenhauer, F., Ott, T., Gillessen, S., Abuter, R., Cuadra, J., Alexander, T., & Sternberg, A. (2006). The Two Young Star Disks in the Central Parsec of the Galaxy: Properties, Dynamics, and Formation. *The Astrophysical Journal*, *643*(2), 1011–1035. https://doi.org/10.1086/503273

Paunzen, E., & Netopil, M. (2006). On the current status of open-cluster parameters. *Monthly Notices of the Royal Astronomical Society*, *371*(4), 1641–1647. https://doi.org/10.1111/j.1365-2966.2006.10783.x

Peacock, M. B., Maccarone, T. J., Waters, C. Z., Kundu, A., Zepf, S. E., Knigge, C., & Zurek, D. R. (2009). Wide Field Camera survey of M 31 globular clusters: low-mass X-ray binaries. *Monthly Notices of the Royal Astronomical Society*, *392*(1), L55–L59. https://doi.org/10.1111/j.1745-3933.2008.00588.x

Pechetti, R., Seth, A., Kamann, S., Caldwell, N., Strader, J., den Brok, M., Lützgendorf, N., Neumayer, N., & Voggel, K. (2022). Detection of a 100000 $M_\odot$ black hole in M 31's Most Massive Globular Cluster: A Tidally Stripped Nucleus. *The Astrophysical Journal*, *924*(2), 48–50. https://doi.org/10.3847/1538-4357/ac339f

Pechetti, R., Seth, A. C., Neumayer, N., Georgiev, I. Y., Kacharov, N., & den Brok, M. (2020). Luminosity Models and Density Profiles for Nuclear Star Clusters for a Nearby Volume-limited Sample of 29 Galaxies. *The Astrophysical Journal*, *900*(1), 32–50. https://doi.org/10.3847/1538-4357/abaaa7

Peng, E. W., Jordán, A., Côté, P., Blakeslee, J. P., Ferrarese, L., Mei, S., West, M. J., Merritt, D., Milosavljević, M., & Tonry, J. L. (2006). The ACS Virgo Cluster Survey. IX. The Color Distribution of Globular Cluster Systems in Early-Type Galaxies. *The Astrophysical Journal*, *639*(1), 95–119. https://doi.org/10.1086/498210

Peng, E. W., Jordán, A., Côté, P., Takamiya, M., West, M. J., Blakeslee, J. P., Chen, C.-W., Ferrarese, L., Mei, S., Tonry, J. L., & West, A. A. (2008). The ACS Virgo Cluster Survey. XV. The Formation Efficiencies of Globular Clusters in Early-Type Galaxies: The Effects of Mass and Environment. *The Astrophysical Journal*, *681*(1), 197–224. https://doi.org/10.1086/587951

Pérez, E., Márquez, I., Marrero, I., Durret, F., González Delgado, R. M., Masegosa, J., Maza, J., & Moles, M. (2000). Circumnuclear structure and kinematics in the active galaxy NGC 6951. *Astronomy & Astrophysics*, *353*, 893–909. https://doi.org/10.48550/arXiv.astro-ph/9909495

Perrett, K. M., Bridges, T. J., Hanes, D. A., Irwin, M. J., Brodie, J. P., Carter, D., Huchra, J. P., & Watson, F. G. (2002). The Kinematics and Metallicity of the M 31 Globular Cluster System. *The Astronomical Journal*, *123*(5), 2490–2510. https://doi.org/10.1086/340186

Perrin, M. D., Sivaramakrishnan, A., Lajoie, C.-P., Elliott, E., Pueyo, L., Ravindranath, S., & Albert, L. (2014). Updated point spread function simulations for JWST with WebbPSF. In J. M. Oschmann, M. Clampin, G. G. Fazio, & H. A. MacEwen (Eds.), *Space Telescopes and Instrumentation 2014: Optical, Infrared, and Millimeter Wave* (p. 91433X, Vol. 9143). https://doi.org/10.1117/12.2056689

Perrin, M. D., Soummer, R., Elliott, E. M., Lallo, M. D., & Sivaramakrishnan, A. (2012). Simulating point spread functions for the James Webb Space Telescope with WebbPSF. In M. C. Clampin, G. G. Fazio, H. A. MacEwen, & J. M. Oschmann (Eds.), *Space Telescopes and Instrumentation 2012: Optical, Infrared,* *and Millimeter Wave* (p. 84423D, Vol. 8442). https://doi.org/10.1117/12.925230

Petersson, J., Hirschmann, M., Tress, R. G., Farcy, M., Glover, S. C. O., Klessen, R. S., Naab, T., Partmann, C., & Whitworth, D. J. (2025). The NOCTUA Suite of Simulations - The Difficulty of Growing Massive Black Holes in Low-Mass Dwarf Galaxies. *arXiv*, 25. https://doi.org/10.48550/arXiv.2504.08035

Pfahl, E., Rappaport, S., & Podsiadlowski, P. (2003). The Galactic Population of Low- and Intermediate-Mass X-Ray Binaries. *The Astrophysical Journal*, *597*(2), 1036–1048. https://doi.org/10.1086/378632

Pfeffer, J., Bastian, N., Crain, R. A., Kruijssen, J. M. D., Hughes, M. E., & Reina-Campos, M. (2019a). The evolution of the UV luminosity function of globular clusters in the E-MOSAICS simulations. *Monthly Notices of the Royal Astronomical Society*, *487*(4), 4550–4564. https://doi.org/10.1093/mnras/stz1592

Pfeffer, J., Bastian, N., Kruijssen, J. M. D., Reina-Campos, M., Crain, R. A., & Usher, C. (2019b). Young star cluster populations in the E-MOSAICS simulations. *Monthly Notices of the Royal Astronomical Society*, *490*(2), 1714–1733. https://doi.org/10.1093/\mnras/stz2721

Pfeffer, J., Forbes, D. A., Romanowsky, A. J., Bastian, N., Crain, R. A., Kruijssen, J. M. D., Bekki, K., Brodie, J. P., Chevance, M., Couch, W. J., & Gannon, J. S. (2024a). Comparing E-MOSAICS predictions of high-redshift proto-globular clusters with JWST observations in lensed galaxies. *arXiv e-prints*, arXiv:2410.07498. https://doi.org/10.48550/arXiv.2410.07498

Pfeffer, J., Hilker, M., Baumgardt, H., & Griffen, B. F. (2016). Constraining ultracompact dwarf galaxy formation with galaxy clusters in the local universe. *Monthly Notices of the Royal Astronomical Society*, *458*(3), 2492–2508. https://doi.org/10.1093/\mnras/stw498

Pfeffer, J., Janssens, S. R., Buzzo, M. L., Gannon, J. S., Bastian, N., Bekki, K., Brodie, J. P., Couch, W. J., Crain, R. A., Forbes, D. A., Kruijssen, J. M. D., & Romanowsky, A. J. (2024b). Origin of the correlation between stellar kinematics and globular cluster system richness in ultradiffuse galaxies. *Monthly Notices of the Royal Astronomical Society*, *429*(4), 4914–4928. https://doi.org/10.1083/mnras/stae850

Pfeffer, J., Kruijssen, J. M. D., Bastian, N., Crain, R. A., & Trujillo-Gomez, S. (2023). Globular cluster metallicity distributions in the E-MOSAICS simulations. *Monthly Notices of the Royal Astronomical Society*, *519*(4), 5384–5401. https://doi.org/10.1093/mnras/stad044

Pfeffer, J., Kruijssen, J. M. D., Crain, R. A., & Bastian, N. (2018). The E-MOSAICS project: simulating the formation and co-evolution of galaxies and their star cluster populations. *Monthly Notices of the Royal Astronomical Society*, *475*(4), 4309–4346. https://doi.org/10.1093/\mnras/stx3124

Pfister, H., Volonteri, M., Dai, J. L., & Colpi, M. (2020). Enhancement of the tidal disruption event rate in galaxies with a nuclear star cluster: from dwarfs to ellipticals. *Monthly Notices of the Royal Astronomical Society*, *497*(2), 2276–2285. https://doi.org/10.1093/\mnras/staa1962

Phillipps, S., Drinkwater, M. J., Gregg, M. D., & Jones, J. B. (2001). Ultracompact Dwarf Galaxies in the Fornax Cluster. *The Astrophysical Journal*, *560*(1), 201–206. https://doi.org/10.1086/322517

Piner, B. G., Stone, J. M., & Teuben, P. J. (1995). Nuclear Rings and Mass Inflow in Hydrodynamic Simulations of Barred Galaxies. *The Astrophysical Journal*, *449*, 508. https://doi.org/10.1086/176075

Pinna, F., Neumayer, N., Seth, A. C., Emsellem, E., Nguyen, D. D., Böker, T., Cappellari, M., McDermind, R. M., Voggel, K., & Walcher, C. J. (2021). Resolved Nuclear Kinematics Link the Formation and Growth of Nuclear Star Clusters with the Evolution of Their Early- and Late-type Hosts. *The Astrophysical Journal*, *921*(1), 8. https://doi.org/10.3847/1538-4357/ac158f

Pizzella, A., Corsini, E. M., Morelli, L., Sarzi, M., Scarlata, C., Stiavelli, M., & Bertola, F. (2002). Nuclear Stellar Disks in Spiral Galaxies. *The Astrophysical Journal*, *573*(1), 131–137. https://doi.org/10.1086/340486

Planck Collaboration. (2014). Planck 2013 results. XVI. Cosmological parameters. *Astronomy & Astrophysics*, *571*, A16. https://doi.org/10.1051/0004-6361/201321591

Plummer, H. C. (1911). On the problem of distribution in globular star clusters. *Monthly Notices of the Royal Astronomical Society*, *71*(5), 460–470. https://doi.org/10.1093/\mnras/71.5.460

Poggio, E., Recio-Blano, A., Palicio, P. A., Re Fiorentin, P., de Laverny, P., Drimmel, R., Kordopatis, G., Lattanzi, M. G., Schultheis, M., Spagna, A., & Spitoni, E. (2022). The chemical signature of the Galactic spiral arms revealed by Gaia DR3. *Astronomy & Astrophysics*, *666*, L4. https://doi.org/10.1051/0004-6361/202244361

Polkas, M., Bonoli, S., Bortolas, E., Izquierdo-Villalba, D., Sesana, A., Broggi, L., Hoyer, N., & Spinoso, D. (2024). Demographics of Tidal Disruption Events with L-Galaxies: I. Volumetric TDE rates and the abundance of nuclear star clusters. *Astronomy & Astrophysics*, *689*, A204. https://doi.org/10.1051/0004-6361/202449470

Portegies Zwart, S. F., Makino, J., McMillan, S. L. W., & Hut, P. (2001). How Many Young Star Clusters Exist in the Galactic Center? *The Astrophysical Journal Letters*, *546*(2), L101–L104. https://doi.org/10.1086/318869

Portegies Zwart, S. F., Makino, J., McMillan, S. L. W., & Hut, P. (2002). The Lives and Deaths of Star Clusters near the Galactic Center. *The Astrophysical Journal*, *565*(1), 265–279. https://doi.org/10.1086/324141

Portegies Zwart, S. F., McMillan, S. L. W., & Gieles, M. (2010). Young Massive Star Clusters. *Annual Review of Astronomy and Astrophysics*, *48*, 431–493. https://doi.org/10.1146/annurev-astro-081309-130834

Portinari, L., Sommer-Larsen, J., & Tantalo, R. (2004). On the mass-to-light ratio and the initial mass function in disc galaxies. *Monthly Notices of the Royal Astronomical Society*, *347*(3), 691–719. https://doi.org/10.1111/j.1365-2966.2004.07207.x

Poulain, M., Marleau, F. R., Habas, R., Duc, P.-A., Sánchez-Janssen, R., Durrell, P. R., Paudel, S., Ahad, S. L., Chougule, A., Müller, O., Lim, S., Bílek, M., & Fensch, J. (2021). Structure and morphology of the MATLAS dwarf galaxies and their central nuclei. *Monthly Notices* *of the Royal Astronomical Society*, *506*(4), 5494–5511. https://doi.org/10.1093/\mnras/stab2092

Poulain, M., Smith, R., Duc, P.-A., Marleau, F. R., Habas, R., Durrell, P. R., Fensch, J., Lim, S., Müller, O., Paudel, S., & Sánchez-Janssen, R. (2025). Evidence of star cluster migration and merger in dwarf galaxies. *arXiv*, 19. https://doi.org/10.48550/arXiv.2504.06749

Predehl, P., Andritschke, R., Arefiev, V., Babyshkin, V., Batanov, O., Becker, W., Böhringer, H., Bogomolov, A., Boller, T., Borm, K., Bornemann, W., Bräuninger, H., Brüggen, M., Brunner, H., Brusa, M., Bulbul, E., Buntov, M., Burwitz, V., Burkert, W., . . . Yaroshenko, V. (2021). The eROSITA X-ray telescope on SRG. *Astronomy & Astrophysics*, *647*, A1. https://doi.org/10.1051/0004-6361/202039313

Prieto, J. L., & Gnedin, O. Y. (2008). Dynamical Evolution of Globular Clusters in Hierarchical Cosmology. *The Astrophysical Journal*, *689*(2), 919–935. https://doi.org/10.1086/591777

Puzia, T. H., Paolillo, M., Goudfrooij, P., Maccarone, T. J., Fabbiano, G., & Angelini, L. (2014). Wide-field Hubble Space Telescope Observations of the Globular Cluster System in NGC 1399. *The Astrophysical Journal*, *786*(2), 78. https://doi.org/10.1088/0004-637X/786/2/78

Querejeta, M., Schinnerer, E., Meidt, S., Sun, J., Leroy, A. K., Emsellem, E., Klessen, R. S., Muñoz-Mateos, J. C., Salo, H., Laurikainen, E., Bešlić, I., Blanc, G. A., Chevance, M., Dale, D. A., Eibensteiner, C., Faesi, C., García-Rodríguez, A., Glover, S. C. O., Grasha, K., . . . Williams, T. G. (2021). Stellar structures, molecular gas, and star formation across the PHANGS sample of nearby galaxies. *Astronomy & Astrophysics*, *656*, A133. https://doi.org/10.1051/0004-6361/202140695

Quinlan, G. D., & Hernquist, L. (1997). The dynamical evolution of massive black hole binaries – II. Self-consistent N-body integrations. *New Astronomy*, *2*(6), 553–554. https://doi.org/10.1016/S1384-1076(97)00039-0

Rafelski, M., & Zaritsky, D. (2005). The Star Cluster of the Small Magellanic Cloud: Age Distribution. *The Astronomical Journal*, *129*(6), 2701–2713. https://doi.org/10.1086/424938

Rafikov, R. R. (2001). The local axisymmetric instability criterion in a thin, rotating, multicomponent disc. *Monthly Notices of the Royal Astronomical Society*, *323*(2), 445–452. https://doi.org/10.1046/j.1365-8711.2001.04201.x

Ramírez-Alegría, S., Borissova, J., Chené, A. B., O'Leary, E., Amigo, P., Minniti, D., Saito, R. K., Geisler, D., Kurtev, R., Hempel, M., Gromadzki, M., Clarke, J. R. A., Negueruela, I., Marco, A., Fierro, C., Bonatto, C., & Catelan, M. (2014). Massive open star clusters using the VVV survey. III. A young massive cluster at the far edge of the Galactic bar. *Astronomy & Astrophysics*, *564*, L9. https://doi.org/10.1051/0004-6361/201322619

Randriamanakoto, Z., Väisänen, P., Ryder, S. D., & Ranaivomanana, P. (2019). Young massive clusters in the interacting LIRG Arp 299: evidence for the dependence of star cluster formation and evolution on environment. *Monthly Notices of the Royal Astronomical Society*, *482*(2), 2530–2554. https://doi.org/10.1093/mnras/sty2837

Read, J. I., Goerdt, T., Moore, B., Pontzen, A. P., Stadel, J., & Lake, G. (2006). Dynamical friction in constant density cores: a failure of the Chandrasekhar formula. *Monthly Notices of the Royal Astronomical Society*, *373*(4), 1451–1460. https://doi.org/10.1111/j.1365-2966.2006.11022.x

Reaves, G. (1983). A catalog of dwarf galaxies in Virgo. *The Astrophysical Journal Supplement Series*, *53*, 375–395. https://doi.org/10.1086/190895

Rees, M. J. (1988). Tidal disruption of stars by black holes of 10^6-10^8 solar masses in nearby galaxies. *Nature*, *333*(6173), 523–528. https://doi.org/10.1038/333523a0

Regan, J. A., Pacucci, F., & Bustamente-Rosell, M. J. (2023). Observational signatures of massive black hole progenitor pathways: could Leo I be a smoking gun? *Monthly Notices of the Royal Astronomical Society*, *518*(4), 5997–6003. https://doi.org/10.1093/\mnras/stac3463

Reina-Campos, M., Gnedin, O. Y., Sills, A., & Li, H. (2024). The Star Clusters As Links between galaxy Evolution and Star formation (SCALES) project I: Numerical methods. *arXiv e-prints*, arXiv:2408.04694. https://doi.org/10.48550/arXiv.2408.04694

Reina-Campos, M., Hughes, M. E., Kruijssen, J. M. D., Pfeffer, J. L., Bastian, N., Crain, R. A., Koch, A., & Grebel, E. K. (2020). The mass fraction of halo stars contributed by the disruption of globular clusters in the E-MOSAICS simulations. *Monthly Notices of the Royal Astronomical Society*, *493*(3), 3422–3428. https://doi.org/10.1093/\mnras/staa483

Reina-Campos, M., Keller, B. W., Kruijssen, J. M. D., Gensior, J., Trujillo-Gomez, S., Jeffreson, S. M. R., Pfeffer, J. L., & Sills, A. (2022a). Introducing EMP-Pathfinder: modelling the simultaneous formation and evolution of stellar clusters in their host galaxies. *Monthly Notices of the Royal Astronomical Society*, *517*(3), 3144–3180. https://doi.org/10.1093/\mnras/stac1934

Reina-Campos, M., & Kruijssen, J. M. D. (2017). A unified model for the maximum mass scales of molecular clouds, stellar clusters and high-redshift clumps. *Monthly Notices of the Royal Astronomical Society*, *469*(2), 1282–1298. https://doi.org/10.1093/mnras/stx790

Reina-Campos, M., Kruijssen, J. M. D., Pfeffer, J. L., Bastian, N., & Crain, R. A. (2019). Formation histories of stars, clusters, and globular clusters in the E-MOSAICS simulations. *Monthly Notices of the Royal Astronomical Society*, *486*(4), 5838–5852. https://doi.org/10.1093/\mnras/stz1236

Reina-Campos, M., Sills, A., & Bichon, G. (2023a). Initial sizes of star clusters: implications for cluster dissolution during galaxy evolution. *Monthly Notices of the Royal Astronomical Society*, *524*(1), 968–980. https://doi.org/10.1093/mnras/stad1879

Reina-Campos, M., Trujillo-Gomez, S., Deason, A. J., Kruijssen, J. M. D., Pfeffer, J. L., Crain, R. A., Bastian, N., & Hughes, M. E. (2022b). Radial distributions of globular clusters trace their host dark matter halo: insights from the E-MOSAICS simulations. *Monthly*

Notices of the Royal Astronomical Society, *513*(3), 3925–3945. https://doi.org/10.1093/\mnras/stac1126

Reina-Campos, M., Trujillo-Gomez, S., Pfeffer, J. L., Sills, A., Deason, A. J., Crain, R. A., & Kruijssen, J. M. D. (2023b). Constraining the shape of dark matter haloes with globular clusters and diffuse stellar light in the E-MOSAICS simulations. *Monthly Notices of the Royal Astronomical Society*, *521*(4), 6368–6382. https://doi.org/10.1093/mnras/stad920

Reines, A. E., & Volonteri, M. (2015). Relations between Central Black Hole Mass and Total Galaxy Stellar Mass in the Local Universe. *The Astrophysical Journal*, *813*(2), 82. https://doi.org/10.1088/0004-637X/813/2/82

Renaud, F. (2018). Star clusters in evolving galaxies. *New Astronomy Reviews*, *81*, 1–38. https://doi.org/10.1016/j.newar.2018.03.001

Renaud, F., Gieles, M., & Boily, C. M. (2011). Evolution of star clusters in arbitrary tidal fields. *Monthly Notices of the Royal Astronomical Society*, *418*(2), 759–769. https://doi.org/10.1111/j.1365-2966.2011.19531.x

Requena-Torres, M. A., Güsten, R., Weiss, A., Harris, A. I., Martín-Pintado, J., Stutzki, J., Klein, B., Heyminck, S., & Risacher, C. (2012). GREAT confirms transient nature of the circum-nuclear disk. *Astromomy & Astrophysics*, *542*, L21. https://doi.org/10.1051/0004-6361/201219068

Riccio, G., Paolillo, M., Cantiello, M., D'Abrusco, R., Jin, X., Li, Z., Puzia, T., Mieske, S., Prole, D. J., Iodice, E., D'Ago, G., Gatto, M., & Spavone, M. (2022). Properties of intra-cluster low-mass X-ray binaries in Fornax globular clusters. *Astronomy & Astrophysics*, *664*, A41. https://doi.org/10.1051/0004-6361/202142894

Riccio, G., Yang, G., Ma lek, K., Boquien, M., Junais, S., Pistis, F., Hamed, M., Grespan, M., Paolillo, M., & Torbaniuk, O. (2023). X-ray luminosity-star formation rate scaling relation: Constraints from the eROSITA Final Equatorial Depth Survey (eFEDS). *Astronomy & Astrophysics*, *678*, A164. https://doi.org/10.1051/0004-6361/202346857

Rieke, G. H., Young, E. T., Engelbracht, C. W., Kelly, D. M., Low, F. J., Haller, E. E., Beeman, J. W., Gordon, K. D., Stansberry, J. A., Misselt, K. A., Cadien, J., Morrison, J. E., Rivlis, G., Latter, W. B., Noriega-Crespo, A., Padgett, D. L., Stapelfeldt, K. R., Hines, D. C., Egami, E., . . . Richards, P. L. (2004). The Multiband Imaging Photometer for Spitzer (MIPS). *The Astrophysical Journal Supplement Series*, *154*(1), 25–29. https://doi.org/10.1086/422717

Rodruck, M., Charlton, J., Borthakur, S., Chitre, A., Durrell, P. R., Elmegreen, D., English, J., Gallagher, S. C., Gronwall, C., Knierman, K., Konstantopoulos, I., Li, Y., Maji, M., Bullan, B., Trancho, G., & Vacca, W. (2023). Star clusters in tidal debris. *Monthly Notices of the Royal Astronomical Society*, *526*(2), 2341–2364. https://doi.org/10.1093/\mnras/stad2886

Roediger, J. C., & Courteau, S. (2015). On the uncertainties of stellar mass estimates via colour measurements. *Monthly Notices of the Royal Astronomical Society*, *452*(3), 3209–3225. https://doi.org/10.1093/\mnras/stv1499

Rom, B., & Sari, R. (2025). Segregation in Nuclear Stellar Clusters: Rates and Mass Distributions of TDEs, QPEs, Plunges, and EMRIs. *arXiv e-prints*, arXiv:2502.13209. https://doi.org/10.48550/arXiv.2502.13209

Román, J., Sánchez-Alarcón, P. M., Knapen, J. H., & Peletier, R. (2023). Evidence for globular cluster collapse after a dwarf-dwarf merger: A potential nuclear star cluster in formation. *Astronomy & Astrophysics*, *671*, L7. https://doi.org/10.1051/0004-6361/202345928

Romeo, A. B., & Wiegert, J. (2011). The effective stability parameter for two-component galactic discs: is $Q^{-1} \approx Q_{stars}^{-1} + Q_{gas}^{-1}$? *Monthly Notices of the Royal Astronomical Society*, *416*(2), 1191–1196. https://doi.org/10.1111/j.1365-2966.2011.19120.x

Rosolowsky, E., & Blitz, L. (2005). Giant Molecular Clouds in M 64. *The Astrophysical Journal*, *623*(2), 826–845. https://doi.org/10.1086/428897

Rossa, J., van der Marel, R. P., Böker, T., Gerssen, J., Ho, L. C., Rix, H.-W., Shields, J. C., & Walcher, C.-J. (2006). Hubble Space Telescope STIS Spectra of Nuclear Star Clusters in Spiral Galaxies: Dependence of Age and Mass on Hubble Type. *The Astronomical Journal*, *132*(3), 1074–1099. https://doi.org/10.1086/505968

Rostami-Shirazi, A., Zonoozi, A. H., Haghi, H., & Rabiee, M. (2024). Origin of the metal-rich versus metal-poor globular clusters dichotomies in the Milky Way: a sign of low black hole natal kicks. *Monthly Notices of the Royal Astronomical Society*, *535*(4), 3489–3499. https://doi.org/10.1093/mnras/stae2365

Rusli, S. P., Thomas, J., Erwin, P., Saglia, R. P., Nowak, N., & Bender, R. (2011). The central black hole mass of the high-σ but low-bulge-luminosity lenticular galaxy NGC 1332. *Monthly Notices of the Royal Astronomical Society*, *410*(2), 1223–1236. https://doi.org/10.1111/j.1365-2966.2010.17610.x

Ryon, J. E., Adamo, A., Bastian, N., Smith, L. J., Gallagher, J. S., Konstantopoulos, I. S., Larsen, S., Silva-Villa, E., & Zackrisson, E. (2014). The Snapshot Hubble U-Band Cluster Survey (SHUCS). II. The Star Cluster Population of NGC 2997. *The Astronomical Journal*, *148*(2), 33. https://doi.org/10.1088/0004-6256/148/2/33

Ryon, J. E., Bastian, N., Adamo, A., Konstantopoulos, I. S., Gallagher, J. S., Larsen, S., Hollyhead, K., Silva-Villa, E., & Smith, L. J. (2015). Sizes and shapes of young star cluster light profiles in M 83. *Monthly Notices of the Royal Astronomical Society*, *452*(1), 525–539. https://doi.org/10.1093/mnras/stv1282

Ryon, J. E., Gallagher, J. S., Smith, L. J., Adamo, A., Calzetti, D., Bright, S. N., Cignoni, M., Cook, D. O., Dale, D. A., Elmegreen, B. E., Fumagalli, M., Gouliermis, D. A., Grasha, K., Grebel, E. K., Kim, H., Messa, M., Thilker, D., & Ubeda, L. (2017). Effective Radii of Young, Massive Star Clusters in Two LEGUS Galaxies. *The Astrophysical Journal*, *841*(2), 92. https://doi.org/10.3847/1538-4357/aa719e

Ryon, J. E., Grogin, N., Anderson, J., Avila, R., Bellini, A., Bohlin, R., Chiaberge, M., Desjardins, T., Deustua, S., Hathi, N., Hoffmann, S., Lucas, R., Miles, N., & Olaes, M. (2019). *Advanced Camera for Surveys Instru-*

ment Handbook for Cycle 27. Space Telescope Science Institude (STScI). Balitmore, USA.

Safronov, V. S. (1960). On the gravitational instability in flattened systems with axial symmetry and non-uniform rotation. *Annales d'Astrophysique*, *23*, 979. https://ui.adsabs.harvard.edu/abs/1960AnAp...23..979S

Saglia, R. P., Opitsch, M., Erwin, P., Thomas, J., Beifiori, A., Fabricius, M., Mazzalay, X., Nowak, N., Rusli, S. P., & Bender, R. (2016). The SINFONI Black Hole Survey: The Black Hole FUndamental Plane Revisited and the Paths of (Co)evolution of Supermassive Black Holes and Bulges. *The Astrophysical Journal*, *818*(1), 47. https://doi.org/10.3847/0004-637X/818/1/47

Saha, K., tseng, Y.-H., & Taam, R. E. (2010). The Effect of Bars and Transient Spirals on the Vertical Heating in Disk Galaxies. *The Astrophysical Journal*, *721*(2), 1878–1890. https://doi.org/10.1088/0004-637X/721/2/1878

Sakamoto, K., Okumura, S. K., Ishitzuki, S., & Scoville, N. Z. (1999). Bar-driven Transport of Molecular Gas to Galactic Centers and Its Consequences. *The Astrophysical Journal*, *525*(2), 691–701. https://doi.org/10.1086/307910

Sakurai, Y., Yoshida, N., Fujii, M. S., & Hirano, S. (2017). Formation of intermediate-mass black holes through runaway collisions in the first star clusters. *Monthly Notices of the Royal Astronomical Society*, *472*(2), 1677–1684. https://doi.org/10.1093/mnras/stx2044

Salmon, B., Coe, D., Bradley, L., Bradač, M., Strait, V., Paterno-Mahler, R., Huang, K.-H., Oesch, P. A., Zitrin, A., Acebron, A., Cibirka, N., Kikuchihara, S., Oguri, M., Brammer, G. B., Sharon, K., Trenti, M., Avila, R. J., Ogaz, S., Andrade-Santos, F., . . . Umetsu, K. (2018). RELICS: A Candidate $z \sim 10$ Galaxy Strongly Lensed into a Spatially Resolved Arc. *The Astrophysical Journal Letters*, *864*(1), L22. https://doi.org/10.3847/2041-8213/aadc10

Salpeter, E. E. (1955). The Luminosity Function and Stellar Evolution. *The Astrophysical Journal*, *121*, 161. https://doi.org/10.1086/145971

Sánchez, S. F., Rosales-Ortega, F. F., Kennicutt, R. C., Johnson, B. D., Diaz, A. I., Pasquali, A., & Hao, C. N. (2011). PPAK Wide-field Integral Field Spectroscopy of NGC 628 - I. The largest spectroscopic mosaic on a single galaxy. *Monthly Notices of the Royal Astronomical Society*, *410*(1), 313–340. https://doi.org/10.1111/j.1365-2966.2010.17444.x

Sánchez-Blázquez, P., Rosales-Ortega, F., Diaz, A., & Sánchez, S. F. (2014). PPAK Wide field Integral Field Spectroscopy of NGC 628 - III. Stellar population properties. *Monthly Notices of the Royal Astronomical Society*, *437*(2), 1534–1548. https://doi.org/10.1093/\mnras/stt1984

Sánchez-Janssen, R., Côté, P., Ferrarese, L., Peng, E. W., Roediger, J., Blakeslee, J. P., Emsellem, E., Puzia, T. H., Spengler, C., Tayloer, J., Álamo-Martínez, K. A., Boselli, A., Cantiello, M., Cuillandre, J.-C., Duc, P.-A., Durrell, P., Gwyn, S., MacArthur, L., Lançon, A., . . . Toloba, E. (2019a). The Next Generation Virgo Cluster Survey. XXIII. Fundamentals of Nuclear Star Clusters over Seven Decades in Galaxy Mass. *The Astrophysical Journal*, *878*(1), 18–32. https://doi.org/10.3847/1538-4357/aaf4fd

Sánchez-Janssen, R., Puzia, T. H., Ferrarese, L., Côté, P., Eigenthaler, P., Miller, B., Ordenes-Briceño, Y., Peng, E. W., Ribbeck, K. X., Roediger, J., Spengler, C., & Taylor, M. A. (2019b). How nucleation and luminosity shape faint dwarf galaxies. *Monthly Notices of the Royal Astronomical Society*, *486*(1), L1–L5. https://doi.org/10.1093/\mnrasl/slz008

Sánchez-Menguiano, L., Sánchez, S. F., Kawata, D., Chemin, L., Pérez, I., Ruiz-Lara, T., Sánchez-Blázquez, P., Galbany, L., Anderson, J. P., Grand, R. J. J., Minchev, I., & Gómez, F. A. (2016). Evidence of Ongoing Radial Migration in NGC 6754: Azimuthal Variations of the Gas Properties. *The Astrophysical Journal Letters*, *830*(2), L40. https://doi.org/10.3847/2041-8205/830/2/L40

Sánchez-Menguiano, L., Sánchez, S. F., Pérez, I., Ruiz-Lara, T., Galbany, L., Anderson, J. P., Krühler, T., Kuncarayakti, H., & Lyman, J. D. (2018). The shape of oxygen abundance profiles explored with MUSE: evidence for widespread deviations from single gradients. *Astronomy & Astrophysics*, *609*, A119. https://doi.org/10.1051/0004-6361/201731486

Sanders, R. L., Shapley, A. E., Jones, T., Reddy, N. A., Kriek, M., Siana, B., Coil, A. L., Mobasher, B., Shivaei, I., Davé, R., Azadi, M., Price, S. H., Leung, G., Freeman, W. R., Fetherolf, T., de Groot, L., Zick, T., & Barro, G. (2021). The MOSDEF Survey: The Evolution of the Mass-Metallicity Relation from $z = 0$ to $z \sim 3.3$. *The Astrophysical Journal*, *914*(1), 19. https://doi.org/10.3847/1538-4357/abf4c1

Sattari, Z., Mobasher, B., Chartab, N., Kelson, D. D., Teplitz, H. I., Rafelski, M., Grogin, N. A., Koekemoer, A. M., Wang, X., Windhorst, R. A., Alavi, A., Prichard, L., Sunnquist, B., Gardner, J. P., Gawiser, E., Hathi, N. P., Hayes, M. J., Ji, Z., Mehta, V., . . . Ravindranath, S. (2023). Fraction of Clumpy Star-forming Galaxies at $0.5 \leq z \leq 3$ in UVCANDELS: Dependence on Stellar Mass and Environment. *The Astrophysical Journal*, *951*(2), 147. https://doi.org/10.3847/1538-4357/acd5d6

Saulder, C., van Kampen, E., Chilingarian, I. V., Mieske, S., & Zeilinger, W. W. (2016). The matter distribution in the local Universe as derived from galaxy groups in SDSS DR12 and 2MRS. *Asronomy & Astrophysics*, *596*, A14. https://doi.org/10.1051/0004-6361/201526711

Scarano, S., & Lépine, J. R. D. (2013). Radial metallicity distribution breaks at corotation radius in spiral galaxies. *Monthly Notices of the Royal Astronomical Society*, *428*(1), 625–640. https://doi.org/10.1093/\mnras/sts048

Schaller, G., Schaerer, D., Meynet, G., & Maeder, A. (1992). New Grids of Stellar Models from 0.8 Solar Masses to 120 Solar Masses at $Z = 0.020$ and $Z = 0.001$. *Astronomy & Astrophysics Supplement Series*, *96*, 269–331. https://ui.adsabs.harvard.edu/abs/1992A&AS...96..269S

Schaye, J., Crain, R. A., Bower, R. G., Furlong, M., Schaller, M., Theuns, T., Dalla Vecchia, C., Frenk, C. S., McCarthy, I. G., Helly, J. C., Jenkins, A., Rosas-

Guevara, Y. M., White, S. D. M., Baes, M., Booth, C. M., Camps, P., Navarro, J. F., Qu, Y., Rahmati, A., . . . Trayford, J. (2015). The EAGLE project: simulating the evolution and assembly of galaxies and their environments. *Monthly Notices of the Royal Asronomical Society*, *446*(1), 521–554. https://doi.org/10.1093/\mnras/stu2058

Schinnerer, E., Hughes, A., Leroy, A., Groves, B., Guillermo, A., Kreckel, K., Bigiel, F., Chevance, M., Dale, D., Emsellem, E., Faesi, C., Glover, S., Grasha, K., Henshaw, J., Hygate, A., Kruijssen, J. M. D., Meidt, S., Pety, J., Querejeta, M., . . . Utomo, D. (2019). The Gas-Star Formation Cycle in Nearby Star-forming Galaxies. I. Assessment of Multi-scale Variations. *The Astrophysical Journal*, *887*(1), 49. https://doi.org/10.3847/1538-4357/ab50c2

Schlafly, E. F., & Finkbeiner, D. P. (2011). Measuring Reddening with Sloan Digital Sky Survey Stellar Spectra and Recalibrating SFD. *The Astrophysical Journal*, *737*(2), 103–115. https://doi.org/10.1088/0004-637X/737/2/103

Schlegel, D. J., Finkbeiner, D. P., & Davis, M. (1998). Maps of Dust Infrared Emission for Use in Estimation of Reddening and Cosmic Microwave Background Radiation Foregrounds. *The Astrophysical Journal*, *500*(2), 525–5537. https://doi.org/10.1086/305772

Schleicher, D. R. G., Reinoso, B., Latif, M., Klessen, R. S., Vergara, M. Z. C., Das, A., Alister, P., Díaz, V. B., & Solar, P. A. (2022). Origin of supermassive black holes in massive metal-poor protoclusters. *Monthly Notices of the Royal Astronomical Society*, *512*(4), 6192–6200. https://doi.org/10.1093/\mnras/stac926

Schödel, R., Feldmeier, A., Kunneriath, D., Stolovy, S., Neumayer, N., Amaro-Seoane, P., & Nishiyama, S. (2014a). Surface brightness profile of the Milky Way's nuclear star cluster. *Astronomy & Astrophysics*, *566*, A47. https://doi.org/10.1051/0004-6361/201423481

Schödel, R., Feldmeier, A., Kunneriath, D., Stolovy, S., Neumayer, N., Amaro-Seoane, P., & Nishiyama, S. (2014b). Surface brightness profile of the Milky Way's nuclear star cluster. *Astronomy & Astrophysics*, *566*, A47. https://doi.org/10.1051/0004-6361/201423481

Schödel, R., Nogueras-Lara, F., Gallego-Cano, E., Shahzamanian, B., Gallego-Calvente, A. T., & Gardini, A. (2020). The Milky Way's nuclear star cluster: Old, metal-rich, and cuspy. Structure and star formation history from deep imaging. *Astronomy & Astrophysics*, *641*, A102. https://doi.org/10.1051/0004-6361/201936688

Schultheis, M., Fritz, T. K., Nandakumar, G., Rojas-Arriagada, A., Nogueras-Lara, F., Feldmeier-Krause, A., Gerhard, O., Neumayer, N., Patrick, L. R., Prieto, M. A., Schödel, R., Mastrobuono-Battisti, A., & Sormani, M. C. (2021). The nuclear stellar disc of the Milky Way: A dynamically cool and metal-rich component possibly formed from the central molecular zone. *Astronomy & Astrophysics*, *650*, A191. https://doi.org/10.1051/0004-6361/202140499

Schuster, K. F., Kramer, C., Hitschfeld, M., Garcia-Burillo, S., & Mookerjea, B. (2007). A complete ^{12}CO 2-1 map of M 51 with HERA. I. Radial averages of CO, H I, and radio continuum. *Astronomy & Astrophysics*, *461*(1), 143–151. https://doi.org/10.1051/0004-6361:20065579

Schwarz, G. (1978). Estimating the Dimension of a Model. *Annals of Statistics*, *6*(2), 461–464. https://ui.adsabs.harvard.edu/link_gateway/1978AnSta...6..461S

Scott, N., & Graham, A. W. (2013). Updated Mass Scaling Relations for Nuclear Star Clusters and a Comparison to Supermassive Black Holes. *The Astrophysical Journal*, *763*(2), 76. https://doi.org/10.1088/0004-637X/763/2/76

Seigar, M. S. (2002). Is Messier 74 a barred spiral galaxy? Near-infrared imaging of M 74. *Astronomy & Astrophysics*, *393*, 499–502. https://doi.org/10.1051/0004-6361:20021060

Sérsic, J. L. (1968). *Atlas de Galaxias Australes*. Universidad Nacional de Cordoba. https://ui.adsabs.harvard.edu/abs/1968adga.book.....S

Sesana, A., Haardt, F., & Madau, P. (2008). Interaction of Massive Black Hole Binaries with Their Stellar Environments. III. Scattering of Bound Stars. *The Astrophysical Journal*, *686*(1), 432–447. https://doi.org/10.1086/590651

Sesto, L. A., Faifer, F. R., Smith Castelli, A. V., Forte, J. C., & Escudero, C. G. (2018). Young globular clusters in NGC 1316. *Monthly Notices of the Royal Astronomical Society*, *479*(1), 478–494. https://doi.org/10.1093/mnras/srx1416

Seth, A., Agüeros, M., Lee, D., & Basu-Zych, A. (2008a). The Coincidence of Nuclear Star Clusters and Active Galactic Nuclei. *The Astrophysical Journal*, *678*(1), 116–130. https://doi.org/10.1086/528955

Seth, A. C., Blum, R., Bastian, N., Caldwell, N., & Debattista, V. P. (2008b). The Rotating Nuclear Star Cluster in NGC 4244. *The Astrophysical Journal*, *687*(2), 997–1003. https://doi.org/10.1086/591935

Seth, A. C., Cappellari, M., Neumayer, N., Caldwell, N., Bastian, N., Olsen, K., Blum, R. D., Debattista, V. P., McDermid, R., Puzia, T., & Stephens, A. (2010). The NGC 404 Nucleus: Star Cluster and Possible Intermediate-mass Black Hole. *The Astrophysical Journal*, *714*(1), 713–731. https://doi.org/10.1088/0004-637X/714/1/713

Seth, A. C., Dalcanton, J. J., Hodge, P. W., & Debattista, V. P. (2006). Clues to Nuclear Star Cluster Formation from Edge-on Spirals. *The Astronomical Journal*, *132*(6), 2539–2555. https://doi.org/10.1086/508994

Seth, A. C., van den Bosch, R., Mieske, S., Baumgardt, H., den Brok, M., Strader, J., Neumayer, N., Chilingarian, I., Hilker, M., McDermid, R., Spitler, L., Brodie, J., Frank, M. J., & Walsh, J. L. (2014). A supermassive black hole in an ultra-compact dwarf galaxy. *Nature*, *513*(7518), 398–400. https://doi.org/10.1038/nature13762

Shakura, N. I., & Sunyaev, R. A. (1973). Black holes in binary systems. Observational appearance. *Astronomy & Astrophysics*, *24*, 337–355. https://ui.adsabs.harvard.edu/abs/1973A%5C&A....24..337S

Sharma, R. S., Brooks, A. M., Tremmel, M., Bellovary, J., Ricarte, A., & Quinn, T. R. (2022). iA Hidden Population of Massive Black Holes in Simulated Dwarf Galaxies. *The Astrophysical Journal*, *936*(1), 82. https://doi.org/10.3847/1538-4357/ac8664

She, R., Ho, L. C., & Feng, H. (2017). Chandra Survey of Nearby Galaxies: The Catalog. *The Astrophysical Journal*, *835*(2), 223. https://doi.org/10.3847/1538-4357/835/2/223

Sheth, K., Vogel, S. N., Regan, M. W., Thornley, M. D., & Teuben, P. J. (2005). Secular Evolution via Bar-driven Gas Inflow: Results from BIMA SONG. *The Astrophysical Journal*, *632*(1), 217–226. https://doi.org/10.1086/432409

Shibuya, T., Ouchi, M., Kubo, M., & Harikane, Y. (2016). Morphologies of 190 000 Galaxies at z = 0-10 Revealed with HST Legacy Data. II. Evolution of Clumpy Galaxies. *The Astrophysical Journal*, *821*(2), 72. https://doi.org/10.3847/0004-637X/821/2/72

Shields, J. C., Böker, T., Ho, L. C., Rix, H.-W., van der Marel, R. P., & Walcher, C. J. (2012). Chandra Observations of the Nuclear Star Cluster and Ultraluminous X-Ray Sources in NGC 2139. *The Astronomical Journal*, *144*(1), 12. https://doi.org/10.1088/0004-6256/144/1/12

Shlosman, I., Begelman, M. C., & Frank, J. (1990). The fuelling of active galactic nuclei. *Nature*, *345*(6277), 679–686. https://doi.org/10.1038/345679a0

Sil'chenko, O. K., & Moiseev, A. V. (2006). Nature of Nuclear Rings in Unbarred Galaxies: NGC 7742 and NGC 7217. *The Astronomical Journal*, *131*(3), 1336–1346. https://doi.org/10.1086/499945

Silk, J. (2017). Feedback by Massive Black Holes in Gas-rich Dwarf Galaxies. *The Astrophysical Journal Letters*, *839*(1), L13. https://doi.org/10.3847/2041-8213/aa67da

Silva-Villa, E., & Larsen, S. S. (2011). The star cluster - field star connection in nearby spiral galaxies. II. Field star and cluster formation histories and their relation. *Astronomy & Astrophysics*, *529*, A25. https://doi.org/10.1051/0004-6361/201016206

Sirianni, M., Lee, M. J., Benítez, N., Blakeslee, J. P., Martel, A. R., Meurer, G., Clampin, M., De Marchi, G., Ford, H. C., Gilliland, R., Hartig, G. F., Illingworth, G. D., Mack, J., & McCann, W. J. (2005). The Photometric Performance and Calibration of the Hubble Space Telescope Advanced Camera for Surveys. *The Publications of the Astronomical Society of the Pacific*, *117*(836), 1049–1112. https://doi.org/10.1086/444553

Sivakoff, G. R., Jordán, A., Sarazin, C. L., Blakeslee, J. P., Côté, P., Ferrarese, L., Juett, A. M., Mei, S., & Peng, E. W. (2007). The Low-Mass X-ray Binary and Globular Cluster Connection in Virgo Cluster Early-Type Galaxies: Optical Properties. *The Astrophysical Journal*, *660*(2), 1246–1263. https://doi.org/10.1086/513094

Smith, R., Choi, H., Lee, J., Rhee, J., Sanchez-Janssen, R., & Yi, S. K. (2016). The Preferential Tidal Stripping of Dark Matter versus Stars in Galaxies. *The Astrophysical Journal*, *833*(1), 109. https://doi.org/10.3847/1538-4357/833/1/109

Somalwar, J. J., Ravi, V., Yao, Y., Guolo, M., Graham, M., Hammerstein, E., Lu, W., Nicholl, M., Sharma, Y., Stein, R., & van Velzen, S. (2024). Fallback Rates in partial Tidal Disruptions of White Dwarfs by Intermediate-mass Black Holes. *The Astrophysical Journal*, *967*(2), 167. https://doi.org/10.3847/1538-4357/ad3dfa

Somerville, R. S., & Davé, R. (2015). Physical Models of Galaxy Formation in a Cosmological Framework. *Annual Review of Astronomy and Astrophysics*, *53*, 51–113. https://doi.org/10.1146/annurev-astro-082812-140951

Somerville, R. S., Hopkins, P. F., Cox, T. J., Robertson, B. E., & Hernquist, L. (2008). A semi-analytic model for the co-evolution of galaxies, black holes and active galactic nuclei. *Monthly Notices of the Royal Astronomical Society*, *391*(2), 481–506. https://doi.org/10.1111/j.1365-2966.2008.13805.x

Sormani, M. C., Binney, J., & Magorian, J. (2015). Gas flow in barred potentials. *Monthly Notices of the Royal Astronomical Society*, *449*(3), 2421–2435. https://doi.org/10.1093/\mnras/stv441

Sormani, M. C., & Li, Z. (2020). Do nuclear rings in barred galaxies form at the shear minimum of the rotation curve? *Monthly Notices of the Royal Astronomical Society*, *494*(4), 6030–6035. https://doi.org/10.1093/\mnras/staa1139

Sormani, M. C., Tress, R. G., Glover, S. C. O., dn C. D. Battersby, R. S. K., Clark, P. C., Hatchfield, H. P., & Smith, R. J. (2020). Simulations of the Milky Way's central molecular zone - II. Star formation. *Monthly Notices of the Royal Astronomical Society*, *497*(4), 5024–5040. https://doi.org/10.1093/\mnras/staa1999

Spengler, C., Côté, P., Roediger, J., Ferrarese, L., Sánchez-Janssen, R., Toloba, E., Liu, Y., Guhathakurta, P., Cuillandre, J.-C., Gwyn, S., Zirm, A., Muñoz, R., Puzia, T., Lançon, A., Peng, E. W., Mei, S., & Powalka, M. (2017). Virgo Redux: The Masses and Stellar Content of Nuclei in Early-type Galaxies from Multiband Photometry and Spectroscopy. *The Astrophysical Journal*, *849*(1), 55–89. https://doi.org/10.3847/1538-4357/aa8a78

Spina, L., Magrini, L., & Cunha, K. (2022). Mapping the Galactic Metallicity Gradient with Open Clusters: The State-of-the-Art and Future Challenges. *Universe*, *8*(2), 87. https://doi.org/10.3390/universe8020087

Spinoso, D., Bonoli, S., Dotti, M., Mayer, L., Madau, P., & Bellovary, J. (2017). Bar-driven evolution and quenching of spiral galaxies in cosmological simulations. *Monthly Notices of the Royal Asronomical Society*, *465*(3), 3729–3740. https://doi.org/10.1093/\mnras/stw2934

Spinoso, D., Bonoli, S., Valiante, R., Schneider, R., & Izquierdo-Villalba, D. (2023). Multiflavour SMBH seeding and evolution in cosmological environments. *Monthly Notices of the Royal Astronomical Society*, *518*(3), 4672–4692. https://doi.org/10.1093/\mnras/stac3169

Spitler, L. R., & Forbes, D. A. (2009). A new method for estimating dark matter halo masses using globular cluster systems. *Monthly Notices of the Royal Astronomical Society*, *392*(1), L1–L5. https://doi.org/10.1111/j.1745-3933.2008.00567.x

Spitzer, L. (1940). The stability of isolated clusters. *Monthly Notices of the Royal Astronomical Society*, *100*(5), 396. https://doi.org/10.1093/\mnras/100.5.396

Spitzer, L. (1987). *Dynamical evolution of globular clusters*.

Springel, V., White, S. D. M., Jenkins, A., Frenk, C. S., Yoshida, N., Gao, L., Navarro, J., Thacker, R., Croton, D., Helly, J., Peacock, J. A., Cole, S., Thomas, P., Couchman, H., Evrard, A., Colberg, J., & Pearce, F. (2005). Simulations of the formation, evolution and clustering of galaxies and quasars. *Nature*, *435*(7042), 629–636. https://doi.org/10.1038/nature03597

Springel, V., White, S. D. M., Tormen, G., & Kauffmann, G. (2001). Populating a cluster of galaxies - I. Results at $z = 0$. *Monthly Notices of the Royal Astronomical Society*, *328*(3), 726–750. https://doi.org/10.1046/j.1365-8711.2001.04912.x

Stahler, S. (2018). *The birth of star clusters*. Springer Cham. https://link.springer.com/book/10.1007/978-3-319-22801-3

Stone, N. C., Küpper, A. H. W., & Ostriker, J. P. (2017). Formation of massive black holes in galactic nuclei: runaway tidal encounters. *Monthly Notices of the Royal Astronomical Society*, *467*(4), 4180–4199. https://doi.org/10.1093/\mnras/stx097

Storchi-Bergmann, T., & Schnorr-Müller, A. (2019). Observational constraints on the feeding of supermassive black holes. *Nature Astronomy*, *3*, 48–61. https://doi.org/10.1038/s41550-018-0611-0

Storn, R., & Price, K. (1997). Differential Evolution - A Simple and Efficient Heuristic for global Optimization over Continuous Spaces. *Journal of Global Optimization*, *11*, 341–359. https://doi.org/10.1023/A:1008202821328

Strader, J., Brodie, J. P., Cenarro, A. J., Beasley, M. A., & Forbes, D. A. (2005). Extragalactic Globular Clusters: Old Spectroscopic Ages and New Views on Their Formation. *The Astronomical Journal*, *130*(4), 1315–1323. https://doi.org/10.1086/432717

Straižys, V., Maskoliūnas, M., Boyle, R. P., Zdanavičius, K., Zdanavičius, J., Laugalys, V., & Kazlauskas, A. (2014). The open cluster NGC 7142: interstellar extinction, distance and age. *Monthly Notices of the Royal Astronomical Society*, *437*(2), 1628–1635. https://doi.org/10.1093/mnras/stt1995

Su, A. H., Salo, H., Janz, J., Laurikainen, E., Venhola, A., Peletier, R. F., Iodice, E., Hilker, M., Cantiello, M., Napolitano, M., Spavone, M., Raj, M. A., van de Ven, G., Mieske, S., Paolillo, M., Capaccioli, M., Valentijn, E. A., & Watkins, A. E. (2021). The Fornax Deep Survey (FDS) with the VST. XI. The search for signs of preprocessing between the Fornax main cluster and Fornax A group. *Astronomy & Astrophysics*, *647*, A100. https://doi.org/10.1051/0004-6361/202039633

Su, A. H., Salo, H., Janz, J., Venhola, A., & Peletier, R. F. (2022). Photometric properties of nuclear star clusters and their host galaxies in the Fornax cluster. *Astronomy & Astrophysics*, *664*, A167. https://doi.org/10.1051/0004-6361/202142593

Sun, J., Leroy, A. K., Rosolowsky, E., Hughes, A., Schinnerer, E., Schruba, A., Koch, E. W., Blanc, G. A., Chiang, I.-D., Groves, B., Liu, D., Meidt, S., Pan, H.-A., Pety, J., Querejeta, M., Saito, T., Sandstrom, K., Sardone, A., Usero, A., . . . Thilker, D. A. (2022). Molecular Cloud Properties in the Context of Their Host Galaxy Environments: A Multiwavelength Perspective. *The Astronomical Journal*, *164*(2), 43. https://doi.org/10.3847/1538-3881/ac74bd

Sun, J., Leroy, A. K., Schruba, A., Rosolowsky, E., Hughes, A., Kruijssen, J. M. D., Meidt, S., Schinnerer, E., Blanc, G. A., Brigiel, F., Bolatto, A. D., Chevance, M., Groves, B., Herrera, C. N., Hygate, A. P. S., Pety, J., Querejeta, M., Usero, A., & Utomo, D. (2018). Cloud-scale Molecular Gas Properties in 15 Nearby Galaxies. *The Astrophysical Journal*, *860*(2), 172. https://doi.org/10.3847/1538-4357/aac326

Sun, Y., Lyu, J., Rieke, G. H., Ji, Z., Sun, F., Zhu, Y., Bunker, A. J., Cargile, P. A., Circosta, C., D'Eugenio, F., Egami, E., Hainline, K., Helton, J. M., Rinaldi, P., Robertson, B. E., Scholtz, S., Shivaei, I., Stone, M. A., Tacchella, S., . . . Willott, C. (2025). No evidence for a Significant Evolution of $M_\bullet$-$M_\star$ Relation in Massive Galaxies up to $z \sim 4$. *The Astrophysical Journal*, *978*(1), 98. https://doi.org/10.3847/1538-4357/ad973b

Sunyaev, R., Arefiev, V., Babyshkin, V., Bogomolov, A., Borisov, K., Buntov, M., Brunner, H., Burenin, R., Churayov, E., Coutinho, D., Eder, J., Eismont, N., Freyberg, M., Gilfanov, M., Gureyev, P., Hasinger, G., Khabibullin, I., Kolmykov, V., Komovkin, S., . . . Voron, V. (2021). SRG X-ray optical observator. Its telescopes and first scientific results. *Astronomy & Astrophysics*, *656*, A132. https://doi.org/10.1051/0004-6361/202141179

Symeonidis, M., Georgakakis, A., Seymour, N., Auld, R., Bock, J., Brisbin, D., Buat, V., Burgarella, D., Chanial, P., Clements, D. L., Cooray, A., Eales, S., Farrah, D., Franceschini, A., Glenn, J., Griffin, M., Hatziminaoglou, E., Ibar, E., Ivison, R. J., . . . Wright, G. (2011). Herschel/HerMES: the X-ray-infrared correlation for star-forming galaxies at $z \sim 1$. *Monthly Notices of the Royal Astronomical Society*, *417*(3), 2239–2252. https://doi.org/10.111/j.1365-2966.2011.19405.x

Tanaka, T., & Haiman, Z. (2009). The Assembly of Supermassive Black Holes at High Redshifts. *The Astrophysical Journal*, *696*(2), 1798–1822. https://doi.org/10.1088/0004-637X/696/2/1798

Tang, J., Bressan, A., Rosenfield, P., Slemer, A., Marigo, P., Girardi, L., & Bianchi, L. (2014). New PARSEC evolutionary tracks of massive stars at low metallicity: testing canonical stellar evolution in nearby star-forming dwarf galaxies. *Monthly Notices of the Royal Astronomical Society*, *445*(4), 4287–4305. https://doi.org/10.1093/\mnras/stu2029

Taylor, M. A., Tahmasebzadeh, B., Thompson, S., Vasiliev, E., Valluri, M., Drinkwater, M. J., Côté, P., Ferrarese, L., Roediger, J., Baumgardt, H., Bentz, M. C., Dage, K., Peng, E. W., Lapeer, D., Liu, C., Sumners, Z., Wang, K., Baldassare, V., Blakeslee, J. P., . . . Woods, T. E. (2025). A Supermassive Black Hole in a Diminutive Ultra-compact Dwarf Galaxy Discovered with JWST/NIRSpec+IFU. *arXiv e-prints*, arXiv:2503.00113. https://doi.org/10.48550/arXiv.2503.00113

Thater, S., Jethwa, P., Tahmasebzadeh, B., Zhu, L., den Brok, M., Santucci, G., Ding, Y., Poci, A., Lilley, E., de Zeeuw, T. P., Zocchi, A., Maindl, T. I., Rigamonti, F., Yang, M., Fahrion, K., & van de Ven, G. (2022a). Testing the robustness of DYNAMITE triaxial Schwarzschild modelling: The effects of correcting the orbit mirroring. *Astronomy & Astrophysics*, *667*, A51. https://doi.org/10.1051/0004-6361/202243926

Thater, S., Krajnović, D., Cappellari, M., Davis, T. A., de Zeeuw, P. T., McDermid, R. M., & Sarzi, M. (2019). Six new supermassive black hole mass determinations from adaptive-optics assisted SINFONI observations. *Astronomy & Astrophysics*, *625*, A62. https://doi.org/10.1051/0004-6361/201834808

Thater, S., Krajnović, D., Weilbacher, P. M., Nguyen, D. D., Bureau, M., Cappellari, M., Davis, T. A., Iguchi, S., McDermid, R., Onishi, K., Sarzi, M., & van de Ven, G. (2022b). Cross-checking SMBH mass estimates in NGC 6958 - I. Stellar dynamics from adaptive optics-assisted MUSE observations. *Monthly Notices of the Royal Astronomical Society*, *509*(4), 5416–5436. https://doi.org/10.1093/\mnras/stab3210

Thater, S., Lyubenova, M., Fahrion, K., Martín-Navarro, I., Jethwa, P., Nguyen, D. D., & van de Ven, G. (2023). Effect of the initial mass function on the dynamical SMBH mass estimate in the nucleated early-type galaxy FCC 47. https://doi.org/10.48550/arXiv.2304.13310

Tonini, C. (2013). The Metallicity Bimodality of Globular Cluster Systems: A Test of Galaxy Assembly and of the Evolution of the Galaxy Mass-Metallicity Relation. *The Astrophysical Journal*, *762*(1), 39. https://doi.org/10.1088/0004-637X/762/1/39

Tonry, J. L. (1984). Evidence for a central mass concentration in M 32. *The Astrophysical Journal Letters*, *283*, L27–L30. https://doi.org/10.1086/184326

Toomre, A. (1964). On the gravitational stability of a disk of stars. *The Astrophysical Journal*, *139*, 1217–1238. https://doi.org/10.1086/147861

Torniamenti, S., Mapelli, M., Périgois, C., Arca Sedda, M., Artale, M. C., Dall'Amico, M., & Vaccaro, M. P. (2024). Hierarchical binary black hole mergers in globular clusters: Mass function and evolution with redshift. *Astronomy & Astrophysics*, *688*(4), A148. https://doi.org/10.1051/0004-6361/202449272

Torrey, P., Vogelsberger, M., Marinacci, F., Pakmor, R., Springel, V., Nelson, D., Naiman, J., Pillepich, A., genel, S., Weinberger, R., & Hernquist, L. (2019). The evolution of the mass-metallicity relation and its scatter in IllustrisTNG. *Monthly Notices of the Royal Astronomical Society*, *484*(4), 5587–5607. https://doi.org/10.1093/mnras/stz243

Trabucchi, M., Wood, P. R., Mowlavi, N., Pastorelli, G., Marigo, P., Girardi, L., & Lebzelter, T. (2021). Modelling long-period variables - II. Fundamental mode pulsation in the non-linear regime. *Monthly Notices of the Royal Astronomical Society*, *500*(2), 1575–1591. https://doi.org/10.1093/\mnras/staa3356

Trani, A. A., Mapelli, M., & Ballone, A. (2018). Forming Circumnuclear Disks and Rings in Galactic Nuclei: A Competition Between Supermassive Black Hole and Nuclear Star Cluster. *The Astrophysical Journal*, *864*(1), 17. https://doi.org/10.3847/1538-4357/aad414

Tremaine, S., Gebhardt, K., Bender, R., Bower, G., Dressler, A., Faber, S. M., Filippenko, A. V., Green, R., Grillmair, C., Ho, L. C., Kormendy, J., Lauer, T. R., Maggorian, J., Pinkney, J., & Richstone, D. (2002). The Slope of the Black Hole Mass versus Velocity Dispersion Correlation. *The Astrophysical Journal*, *574*(2), 740–753. https://doi.org/10.1086/341002

Tremaine, S. D., Ostriker, J. P., & Spitzer, L. (1975). The formation of the nuclei of galaxies. I. M31. *The Astrophysical Journal*, *196*, 407–411. https://doi.org/10.1086/153422

Tremmel, M., Ricarte, A., Natarajan, P., Bellovary, J., Sharma, R., & Quinn, T. R. (2024). An Enhanced Massive Black Hole Occupation Fraction in Cluster Dwarf Galaxies. *Open Journal of Astrophysics*, *7*, 26. https://doi.org/10.33232/001c.116617

Tremonti, C. A., Heckman, T. M., Kauffmann, G., Brinchmann, J., Charlot, S., White, S. D. M., Seibert, M., Peng, E. W., Schlegel, D. J., Uomoto, A., Fukugita, M., & Brinkmann, J. (2004). The Origin of the Mass-Metallicity Relation: Insights from 53 000 Star-forming Galaxies in the Sloan Digital Sky Survey. *The Astrophysical Journal*, *613*(2), 898–913. https://doi.org/10.1086/423264

Tress, R. G., Sormani, M. C., Glover, S. C. O., Klessen, R. S., Battersby, C. D., Clark, P. C., Hatchfield, H. P., & Smith, R. J. (2020). Simulations of the Milky Way's central molecular zone - I. Gas dynamics. *Monthly Notices of the Royal Astronomical Society*, *499*(3), 4455–4478. https://doi.org/10.1093/\mnras/staa3120

Trujillo-Gomez, S., Kruijssen, J. M. D., Reina-Campos, M., Pfeffer, J. L., Keller, B. W., Crain, R. A., Bastian, N., & Hughes, M. E. (2021). The kinematics of globular cluster populations in the E-MOSAICS simulations and their implications for the assembly history of the Milky Way. *Monthly Notices of the Royal Astronomical Society*, *503*(1), 31–58. https://doi.org/10.1093/mnras/stab341

Trump, J. R., Sun, M., Zeimann, G. R., Luck, C., Bridge, J. S., Grier, C. J., Hagen, A., Huneau, S., Montero-Dorta, A., Rosario, D. J., Brandt, W. N., Ciardullo, R., & Schneider, D. P. (2015). The Biases of Optical Line-Ratio Selection for Active Galactic Nuclei and the Intrinsic Relationship between Black Hole Accretion and Galaxy Star Formation. *The Astrophysical Journal*, *811*(1), 26. https://doi.org/10.1088/0004-637X/811/1/26

Tsatsi, A., Mastrobuono-Battisti, A., van de Ven, G., Perets, H. B., Bianchini, P., & Neumayer, N. (2017). On the rotation of nuclear star clusters formed by cluster inspirals. *Monthly Notices of the Royal Astronomical Society*, *464*(3), 3720–3727. https://doi.org/10.1093/\mnras/stw2593

Turner, J. A., Dale, D. A., Lee, J. C., Boquien, M., Chandar, R., Deger, S., Larson, K. L., Mok, A., Thilker, D. A., Ubeda, L., Whitmore, B. C., Belfiore, F., Bigiel, F., Blanc, G. A., Emsellem, E., Grasha, K., Groves, B., Klessen, R. S., Kreckel, K., . . . Williams, T. G. (2021). PHANGS-HST: star cluster spectral energy distribution fitting with CIGALE. *Monthly Notices of the Royal Astronomical Society*, *502*(1), 1366–1385. https://doi.org/10.1093/\mnras/stab055

Turner, M. L., Côté, P., Ferrarese, L., Jordán, A., Blakeslee, J. P., Mei, S., Peng, E. W., & West, M. J. (2012). The ACS Fornax Cluster Survey. VI. The Nuclei of Early-type Galaxies in the Fornax Cluster. *The Astrophysical*

Journal Series, *203*(1), 5. https://doi.org/10.1088/0067-0049/203/1/5

Untzaga, J., Bonoli, S., Izquierdo-Villalba, D., Mezcua, M., & Spinoso, D. (2024). A link to the past: characterizing wandering black holes in Milky Way-type galaxies. *Monthly Notices of the Royal Astronomical Society*, 13. https://doi.org/https://doi.org/10.48550/arXiv.2404.12354

Usher, C., Caldwell, N., & Cabrera-Ziri, I. (2024). Measuring M 31 globular cluster ages and metallicities using both photometry and spectroscopy. *Monthly Notices of the Royal Astronomical Society*, *528*(4), 6010–6024. https://doi.org/10.1093/mnras/stae282

Usher, C., Forbes, D. A., Brodie, J. P., Foster, C., Spitler, L. R., Arnold, J. A., Romanowsky, A. J., Strader, J., & Pota, V. (2012). The SLUGGS survey: calcium triplet-based spectroscopic metallicities for over 900 globular clusters. *Monthly Notices of the Royal Astronomical Society*, *426*(2), 1475–1495. https://doi.org/10.1111/j.1365-2966.2012.21801.x

Usher, C., Forbes, D. A., Spitler, L. R., Brodie, J. P., Romanowsky, A. J., Strader, J., & Woodley, K. A. (2013). The SLUGGS Survey: wide field imaging of the globular cluster system of NGC 4278. *Monthly Notices of the Royal Astronomical Society*, *436*(2), 1172–1190. https://doi.org/10.1093/mnras/stt1637

van den Bosch, R. C. E., & de Zeeuw, P. T. (2010). Estimating black hole masses in triaxial galaxies. *Monthly Notices of the Royal Astronomical Society*, *401*(3), 1770–1780. https://doi.org/10.1111/j.1365-2966.2009.15832.x

van der Kruit, P. C., & Freeman, K. C. (2011). Galaxy Disks. *Annual Review of Astronomy and Astrophysics*, *49*(1), 301–371. https://doi.org/10.1146/annurev-astro-083109-153241

van Donkelaar, F., Mayer, L., Capelo, P. R., Tamfal, T., Quinn, T. R., & Madau, P. (2024). Stellar cluster formation in a Milky Way-sized galaxy at $z > 4$ - II. A hybrid formation scenario for the nuclear star cluster and its connection to the nuclear stellar ring. *Monthly Notices of the Royal Astronomical Society*, *529*(4), 4104–4116. https://doi.org/10.1093/mnras/stae804

van Loon, J. T., Zijlstra, A. A., Whitelock, P. A., te Lintel Hekkert, P., Chapman, J. M., Loup, C., Groenewegen, M. A. T., Waters, L. B. F. M., & Trams, N. R. (1998). Obscured Asymptotic Giant Branch stars in the Magellanic Coulds. IV. Carbon stars and OH/IR stars. *Astronomy & Astrophysics*, *329*, 169–185. https://ui.adsabs.harvard.edu/abs/1998A&A...329..169V

Vani, A., Ayromlou, M., Kauffmann, G., & Springel, V. (2025). Probing galaxy evolution from $z = 0$ to $z \simeq 10$ through galaxy scaling relations in three L-GALAXIES flavours. *Monthly Notices of the Royal Astronomical Society*, *536*(1), 777–806. https://doi.org/10.1093/mnras/stae2625

Vanzella, E., Calura, F., Meneghetti, M., Castellano, M., Caminha, G. B., Mercurio, A., Cupani, G., Rosati, P., Grillo, C., Gilli, R., Mignoli, M., Fiorentino, G., Arcidiacono, C., Lombini, M., & Cortecchia, F. (2019). Massive star cluster formation under the microscope at $z = 6$. *Monthly Notices of the Royal Astronomical Society*, *483*(3), 3618–3635. https://doi.org/10.1093/mnras/sty3311

Vanzella, E., Calura, F., Meneghetti, M., Mercurio, A., Castellano, M., Caminha, G. B., Balestra, I., Rosati, P., Tozzi, P., De Barros, S., Grazian, A., D'Ercole, A., Ciotti, L., Caputi, K., Grillo, C., Merlin, E., Pentericci, L., Fontana, A., Cristiani, S., & Coe, D. (2017). Paving the way for the JWST: witnessing globular cluster formation at $z > 3$. *Monthly Notices of the Royal Astronomical Society*, *467*(4), 4303–4321. https://doi.org/10.1093/mnras/stx351

Vanzella, E., Claeyssens, A., Welch, B., Adamo, A., Coe, D., Diego, J. M., Mahler, G., Khullar, G., Kokorev, V., Oguri, M., Ravindranath, S., Furtak, L. J., Hsiao, T. Y.-Y., Abdurro'uf, Mandelker, N., Brammer, G., Bradley, L. D., Bradač, M., Conselice, C. J., . . . Norman, C. (2023). Jwst/nircam probes young star clusters in the reionization era sunrise arc. *The Astrophysical Journal*, *945*(1), 53. https://doi.org/10.3847/1538-4357/acb59a

Vazquez-Semadeni, E. (1994). Hierarhical Structure in Nearly Pressureless Flows as a Consequence of Self-similar Statistics. *The Astrophysical Journal*, *423*, 681. https://doi.org/10.1086/173847

Vázquez-Semadeni, J. S. E., Chappell, D., & Passot, T. (1998). On the Probability Density Function of Galactic Gas. I. Numerical Simulations and the Significance of the Polytropic Index. *The Astrophysical Journal*, *504*(2), 835–853. https://doi.org/10.1086/306099

Veljanoski, J., Ferguson, A. M. N., Mackey, A. D., Huxor, A. P., Hurley, J. R., Bernard, E. J., Côté, P., Irwin, M. J., Martin, N. F., Burgtt, W. S., Chambers, K. C., Flewelling, H., Kudritzki, R., & Waters, C. (2015). The globular cluster system of NGC 6822. *Monthly Notices of the Royal Astronomical Society*, *452*(1), 320–332. https://doi.org/10.1093/mnras/stv1259

Venhola, A., Peletier, R., Laurikainen, E., Salo, H., Iodice, E., Mieske, S., Hilker, M., Wittmann, C., Lisker, T., Paolillo, M., Cantiello, M., Janz, J., pavone, M., D'Abrusco, R., van dde Ven, G., Napolitano, N., Ver does Kleijn, G., Maddox, N., Capaccioli, M., . . . Limatola, L. (2018). The Fornax Deep Survey with the VST. IV. A size and magnitude limited catalog of dwarf galaxies in the area of the Fornax cluster. *Astronomy & Astrophysics*, *620*, A165. https://doi.org/10.1051/0004-6361/201833933

Verbunt, F., & van den Heuvel, E. P. J. (1995). Formation and evolution of neutron stars and black holes in binaries. In *X-ray Binaries* (pp. 457–494). https://ui.adsabs.harvard.edu/abs/1995xrbi.nasa..457V

Vijayan, A. P., Scott, S. J., Thomas, P. A., Yates, R. M., Wilkins, S. M., & Henriques, B. M. (2019). Detailed dust modelling in the L-GALAXIES semi-analytic model of galaxy formation. *Monthly Notices of the Royal Astronomical Society*, *489*(3), 4072–4089. https://doi.org/10.1093/\mnras/stz1948

Vílchez, J. M., Relaño, M., Kennicutt, R., De Looze, I., Mollá, M., & Galametz, M. (2019). Metals and dust content across the galaxies M 101 and NGC 628. *Monthly Notices of the Royal Astronomical Society*, *483*(4), 4968–4983. https://doi.org/10.1093/\mnras/sty3455

Villaume, A., Romanowsky, A. J., Brodie, J., & Strader, J. (2019). New Constraints on Early-type Galaxy Assembly from Spectroscopic Metallicites of Globular Clusters in M 87. *The Astrophysical Journal*, *879*(1), 45. https://doi.org/10.3847/1538-4357/ab24d7

Voggel, K., Hilker, M., & Richtler, T. (2016). Globular cluster clustering and tidal features around ultra-compact dwarf galaxies in the halo of NGC 1399. *Astronomy & Astrophysics*, *586*, A102. https://doi.org/10.1051/0004-6361/201527070

Voggel, K. T., Seth, A. C., Baumgardt, H., Husemann, B., Neumayer, N., Hilker, M., Pechetti, R., Mieske, S., Dumont, A., & Georgiev, I. (2022). First direct dynamical detection of a dual supermassive black hole system at sub-kiloparsec separation. *Astronomy & Astrophysics*, *658*, A152. https://doi.org/10.1051/0004-6361/202140827

Volonteri, M., Madau, P., & Haardt, F. (2003). The Formation of Galaxy Stellar Cores by the Hierarchical Merging of Supermassive Black Holes. *The Astrophysical Journal*, *593*(2), 661–666. https://doi.org/10.1086/376722

Walcher, C. J., van der Marel, R. P., McLaughlin, D., Rix, H.-W., Böker, T., Häring, N., Ho, L. C., Sarzi, M., & Shields, J. C. (2005). Masses of Star Clusters in the Nuclei of Bulgeless Spiral Galaxies. *The Astrophysical Journal*, *618*(1), 237–246. https://doi.org/10.1086/425977

Walcher, C.-J., Böker, T., Charlot, S., Ho, L. C., Rix, H.-W., Rossa, J., Shields, J. C., & van der Marel, R. P. (2006). Stellar Populations in the Nuclei of Late-Type Spiral Galaxies. *The Astrophysical Journal*, *649*(2), 692–708. https://doi.org/10.1086/505166

Walsh, J. L., Barth, A. J., & Sarzi, M. (2010). The Supermassive Black Hole in M 84 Revisited. *The Astrophysical Journal*, *721*(1), 762–776. https://doi.org/10.1088/0004-637X/721/1/762

Walsh, J. L., van den Bosch, R. C. E., Barth, A. J., & Sarzi, M. (2012). A Stellar Dynamical Mass Measurement of the Black Hole in NGC 3998 from Keck Adaptive Optics Observations. *The Astrophysical Journal*, *753*(1), 79. https://doi.org/10.1088/0004-637X/753/1/79

Walton, D. J., Mackenzie, A. D. A., Gully, H., Patel, N. R., Roberts, T. P., Earnshaw, H. P., & Mateos, S. (2022). A multimission catalogue of ultraluminous X-ray source candidates. *Monthly Notices of the Royal Astronomical Society*, *509*(2), 1587–1604. https://doi.org/10.1093/\mnras/stab3001

Wang, E., Wang, H., Mo, H., van den Bosch, F. C., Lim, S. H., Wang, L., Yang, X., & Chen, S. (2018). The Dearth of Differences between Central and Satellite Galaxies. II. Comparison of Observations with L-GALAXIES and EAGLE in Star Formation Quenching. *The Astrophyiscal Journal*, *864*(1), 51. https://doi.org/10.3847/1538-4357/aad554

Wang, K., & Peng, Y. (2024). Testing galaxy formation models with the stellar mass-halo mass relations for star-forming and quiescent galaxies. *Astronomy & Astrophysics*, 12. https://doi.org/https://doi.org/10.48550/arXiv.2408.07743

Watson, G. N. (1944). *A treatise on the theory of bessel functions*. Cambridge University Press. https://www.cambridge.org/core/journals/mathematical-gazette/article/abs/treatise-on-the-theory-of-bessel-functions-by-g-n-watson-2nd-edition-pp-viii-804-60s-1944-cambridge-university-press/A61884BD1BD53516C81688CB553FD1CF

Webb, J. J., Harris, W. E., & Sills, A. (2012). The Size Difference between Red and Blue Globular Clusters is not due to Projection Effects. *The Astrophysical Journal Letters*, *759*(2), L39. https://doi.org/10.1088/2041-8205/759/2/L39

Wehner, E. H., & Harris, W. E. (2006). From Supermassive Black Holes to Dwarf Elliptical Nuclei: A Mass Continuum. *The Astrophysical Journal Letters*, *644*(1), L17–L20. https://doi.org/10.1086/505387

West, M. J., Côté, P., Jones, C., Forman, W., & Marzke, R. O. (1995). Intracluster Globular Clusters. *The Astrophysical Journal Letters*, *453*, L77. https://doi.org/10.1086/309748

West, M. J., Côté, P., Marzke, R. O., & Jordán, A. (2004). Reconstructing galaxy histories from globular clusters. *Nature*, *427*(6969), 31–35. https://doi.org/10.1038/nature02235

Westfall, K. B., Andersen, D. R., Bershady, M. A., Martinsson, T. P. K., Swaters, R. A., & Verheijen, M. A. W. (2014). The diskmass survey. viii. on the relationship between disk stability and star formation. *The Astrophysical Journal*, *785*(1), 43. https://doi.org/10.1088/0004-637X/785/1/43

White, S. D. M., & Frenk, C. S. (1991). Galaxy Formation through Hierarchical Clustering. *The Astrophysical Journal*, *379*, 52. https://doi.org/10.1086/170483

White, S. D. M., & Rees, M. J. (1978). Core condensation in heavy halos: a two-stage theory for galaxy formation and clustering. *Monthly Notices of the Royal Astronomical Society*, *183*, 341–358. https://doi.org/10.1093/mnras/183.3.341

Whitmore, B. C., Chandar, R., Bowers, A. S., Larsen, S., Lindsay, K., Ansari, A., & Evans, J. (2014). The Luminosity Function of Star Clusters in 20 Star-forming Galaxies Based in Hubble Legacy Archive Photometry. *The Astronomical Journal*, *147*(4), 78. https://doi.org/10.1088/0004-6256/147/4/78

Willmer, C. N. A. (2018). The Absolute Magnitude of the Sun in Several Filters. *The Astrophysical Journal Supplement*, *236*(2), 47. https://doi.org/10.3847/1538-4365/aabfdf

Wright, E. L., Eisenhardt, P. R. M., Mainzer, A. K., Ressler, M. E., Cutri, R. M., Jarrett, T., Krikpatrick, J. D., Padgett, D., McMillan, R. S., Skrutskie, M., Stanford, S. A., Cohen, M., Walker, R. G., Mather, J. C., Leisawith, D., Gautier, T. N., McLean, I., Benford, D., Lonsdale, C. J., . . . Tsai, C.-W. (2010). The Wide-field Infrared Survey Explorer (WISE): Mission Description and Initial On-orbit Performance. *The Astronomical Journal*, *140*(6), 1868–1881. https://doi.org/10.1088/0004-6256/140/6/1868

Yadav, J., Das, M., Patra, N. N., Dwarakanath, K. S., Rahna, P. T., McGaugh, S. S., Schombert, J., & Murthy, J. (2021). Comparing the Innter and Outer Star-forming Complexes in the Nearby Spiral Galaxies NGC 628, NGC 5457, and NGC 6946 Using UVIT Observations. *The Astrophysical Journal*, *914*(1), 54–70. https://doi.org/10.3847/1538-4357/abf8c1

Yang, G., Boquien, M., Brandt, W. N., Buat, V., Burgarella, D., Ciesla, L., Lehmer, B. D., Malek, K., Mountrichas, G., Papovich, C., Pons, E., Stalevski, M., Theulé, P., & Zhu, S. (2022). Fitting AGN/Galaxy X-Ray-to-radi SEDs with CIGALE and Improvement of the Code. *The Astrophysical Journal*, *927*(2), 192. https://doi.org/10.3847/1538-4357/ac4971

Yang, G., Boquien, M., Buat, V., Burgarella, D., Ciesla, L., Duras, F., Stalevski, M., Brandt, W. N., & Papovich, C. (2020). X-CIGALE: Fitting AGN/galaxy SEDs from X-ray to infrared. *Monthly Notices of the Royal Astronomical Society*, *491*(1), 740–757. https://doi.org/10.1093/\mnras/stz3001

Yao, Y., Ravi, V., Gezari, S., van Velzen, S., Lu, W., Schulze, S., Somalwar, J. J., Kulkarni, S. R., Hammerstein, E., Bicholl, M., Graham, M. J., Perley, D. A., Cenko, S. B., Stein, R., Ricarte, A., Chadayammuri, U., Quataert, E., Bellm, E. C., Bloom, J. S., . . . Yan, L. (2023). Tidal Disruption Event Demographics with the Zwicky Transient Facility: Volumetric Rates, Luminosity Function, and Implications for the Local Black Hole Mass Function. *The Astrophysical Journal Letters*, *955*(1), L6. https://doi.org/10.3847/2041-8213/acf216

Yates, R. M., Hendriks, D., Vijayan, A. P., Izzard, R. G., Thomas, P. A., & Das, P. (2024). The impact of binary stars on the dust and metal evolution of galaxies. *Monthly Notices of the Royal Astronomical Society*, *527*(3), 6292–6311. https://doi.org/10.1093/mnras/stad3419

Yates, R. M., Henriques, B. M. B., Fu, J., Kauffmann, G., Thomas, P. A., Guo, Q., White, S. D. M., & Schady, P. (2021). L-GALAXIES 2020: The evolution of radial metallicity profiles and global metallicites in disc galaxies. *Monthly Notices of the Royal Astronomical Society*, *503*(3), 4474–4495. https://doi.org/10.1093/\mnras/stab741

Yates, R. M., Henriques, B. M. B., Thomas, P. A., Kauffmann, G., Johansson, J., & White, S. D. M. (2013). Modelling element abundances in semi-analytical models of galaxy formation. *Monthly Notices of the Royal Astronomical Society*, *435*(4), 3500–3520. https://doi.org/10.1093/\mnras/stt1542

Yates, R. M., Thomas, P. A., & Henriques, B. M. B. (2017). Iron in galaxy groups and clusters: confronting galaxy evolution models with a newly homogenized data set. *Monthly Notices of the Royal Astronomical Society*, *464*(3), 3169–3193. https://doi.org/10.1093/mnras/stw2361

Zanatta, E., Sánchez-Janssen, R., Chies-Santos, A. L., de Souza, R. S., & Blakeslee, J. P. (2021). A high occurrence of nuclear star clusters in faint Coma galaxies, and the roles of mass and environment. *Monthly Notices of the Royal Astronomical Society*, *508*(1), 986–998. https://doi.org/10.1093/\mnras/stab2348

Zaragoza-Cardiel, J., Fritz, J., Aretxaga, I., Mayya, D., Rosa-González, D., Beckman, J. E., Bruzual, G., Charlot, S., & Lomelí-Núñez, L. (2019). Detection of the self-regulation of star formation in galaxy discs. *Monthly Notices of the Royal Astronomical Society*, *487*(1), L61–L66. https://doi.org/10.1093/\mnrasl/slz093

Zaritsky, D. (2022). Revisiting the relation between the number of globular clusters and galaxy mass for low-mass galaxies. *Monthly Notices of the Royal Astronomical Society*, *513*(2), 2609–2614. https://doi.org/10.1093/mnras/stac1072

Zentner, A. R., & Bullock, J. S. (2003). Halo Substructure and the Power Spectrum. *The Astrophysical Journal*, *598*(1), 49–72. https://doi.org/10.1086/378797

Zhang, H., Behroozi, P., Volonteri, M., Silk, J., Fan, X., Aird, J., Yang, J., Wang, F., Tee, W. L., & Hopkins, P. F. (2024). TRINITY IV: predictions for supermassive black holes at $z \gtrsim 6$. *Monthly Notices of the Royal Astronomical Society*, *531*(4), 4974–4989. https://doi.org/10.1093/mnras/stae1447

Zhang, Q., & Fall, S. M. (1999). The Mass Function of Young Star Clusters in the "Antennae" Galaxies. *The Astrophysical Journal Letters*, *527*(2), L81–L84. https://doi.org/10.1086/312412

Zhang, Y., Ouchi, M., Gebhardt, K., Liu, C., Harikane, Y., Cooper, E. M., Davis, D., Farrow, D. J., Gawiser, E., Hill, G. J., Kollatschny, W., Ono, Y., Schneider, D. P., Finkelstein, S. L., Gronwall, C., Jogee, S., & Krumpe, M. (2023). The Stellar Mass-Black Hole Mass Relation at $z \sim 2$ down to $M_{BH} \sim 10^7$ $M_\odot$ Determined by HETDEX. *The Astrophysical Journal*, *948*(2), 103. https://doi.org/10.3847/1538-4357/acc2c2

Zhong, W., Fu, J., Sharma, P., Shen, S., & Yates, R. M. (2023a). The hot gas distribution, X-ray luminosity, and baryon budget in the L-galaxies semi-analytic model of galaxy formation. *Monthly Notices of the Royal Astronomical Society*, *519*(3), 4344–4359. https://doi.org/10.1093/mnras/stac3735

Zhong, W., Fu, J., Shen, S., & Yuan, F. (2023b). Mock X-Ray Observations of Hot Gas with L-Galaxies Semi-analytic Models of Galaxy Formation. *Research in Astronomy & Astrophysics*, *23*(7), 075004. https://doi.org/10.1088/1674-4527/acd0e9

Zhou, L., Federrath, C., Yuan, T., Bian, F., Medling, A. M., Shi, Y., Bland-Hawthorn, J., Bryant, J. J., Brough, S., Catinella, B., Croom, S. M., Goodwin, M., Goldstein, G., Green, A. W., Konstatoloulos, I. S., Lawrence, J. S., Owers, M. S., Richards, S. N., & Sanchez, S. F. (2017). The sami galaxy survey: Energy sources of the turbulent velocity dispersion in spatially resolved local star-forming galaxies. *Monthly Notices of the Royal Astronomical Society*, *470*(4), 4573–4582. https://doi.org/10.1093/mnras/stx1504

Zibetti, S., Charlot, S., & Rix, H.-W. (2009). Resolved stellar mass maps of galaxies - I. Method and omplications for global mass estimates. *Monthly Notices of the Royal Astronomical Society*, *400*(3), 1181–1198. https://doi.org/10.1111/j.1365-2966.2009.15528.x